



**This electronic thesis or dissertation has been
downloaded from Explore Bristol Research,
<http://research-information.bristol.ac.uk>**

Author:
Naha, Shaini

Title:
Modelling hydrological responses of a large-scale river basin in India

General rights

Access to the thesis is subject to the Creative Commons Attribution - NonCommercial-No Derivatives 4.0 International Public License. A copy of this may be found at <https://creativecommons.org/licenses/by-nc-nd/4.0/legalcode>. This license sets out your rights and the restrictions that apply to your access to the thesis so it is important you read this before proceeding.

Take down policy

Some pages of this thesis may have been removed for copyright restrictions prior to having it been deposited in Explore Bristol Research. However, if you have discovered material within the thesis that you consider to be unlawful e.g. breaches of copyright (either yours or that of a third party) or any other law, including but not limited to those relating to patent, trademark, confidentiality, data protection, obscenity, defamation, libel, then please contact collections-metadata@bristol.ac.uk and include the following information in your message:

- Your contact details
- Bibliographic details for the item, including a URL
- An outline nature of the complaint

Your claim will be investigated and, where appropriate, the item in question will be removed from public view as soon as possible.



This electronic thesis or dissertation has been downloaded from Explore Bristol Research, <http://research-information.bristol.ac.uk>

Author:
Naha, Shaini

Title:
Modelling hydrological responses of a large-scale river basin in India

General rights

Access to the thesis is subject to the Creative Commons Attribution - NonCommercial-No Derivatives 4.0 International Public License. A copy of this may be found at <https://creativecommons.org/licenses/by-nc-nd/4.0/legalcode>. This license sets out your rights and the restrictions that apply to your access to the thesis so it is important you read this before proceeding.

Take down policy

Some pages of this thesis may have been removed for copyright restrictions prior to having it been deposited in Explore Bristol Research. However, if you have discovered material within the thesis that you consider to be unlawful e.g. breaches of copyright (either yours or that of a third party) or any other law, including but not limited to those relating to patent, trademark, confidentiality, data protection, obscenity, defamation, libel, then please contact collections-metadata@bristol.ac.uk and include the following information in your message:

- Your contact details
- Bibliographic details for the item, including a URL
- An outline nature of the complaint

Your claim will be investigated and, where appropriate, the item in question will be removed from public view as soon as possible.

*Modelling hydrological responses of a large-scale river basin in
India*

by

Shaini Naha



Department of Civil Engineering
University of Bristol

A dissertation submitted to the University of Bristol in accordance
with the requirements of the degree of DOCTOR OF
PHILOSOPHY in the Faculty of Engineering
November 2021

Word Count: 58539

Abstract

Global warming has led to the increase in average temperature and annual rainfall in most parts of India. The country has also faced a remarkable change in land cover in the past decades. These anthropogenic impacts can potentially have a serious impact on hydrology. The Mahanadi river basin is a large-scale river basin located in the eastern part of India. The basin has undergone severe environmental changes during the last decades resulting in serious threat of increased flows. Therefore, understanding how these environmental impacts affect the hydrological behaviour of the basin, especially on a regional scale, forms an important step towards water resources planning and management. Such impacts on the hydrological components are sometimes predicted using a single model realization in conjunction with different land use or climate scenarios. However, such impacts are associated with considerable uncertainties which can arise from model parameterisation, calibration procedures, and due to data availability at local to regional scale as opposed to global products. Little attention has been directed towards understanding these uncertainties while assessing the hydrological impacts of climate and land cover changes in India. In this thesis, we use the most recently released land cover and climate scenarios from Land Use Harmonisation, version 2 (LUH2) database and Climate Model Intercomparison Project, version 6 (CMIP6), respectively, to predict the hydrological responses of Mahanadi river basin to changing land cover and climate conditions. We accounted for the uncertainties associated with modelling those responses, through the sensitivity-guided model calibration performed within a Monte Carlo Framework. This will likely make the predictions more robust and reliable. We identified the important parameters that would have a major control in simulating the hydrological components thereby yielding good simulations on a daily scale for all subbasins, with median KGE ranging between 0.63 to 0.86 in calibration and 0.59 to 0.82 in validation across subcatchments. With regards to predicting the hydrological system in the Mahanadi basin, our findings suggests that a noticeable increase in the cropland at the expense of forest would cause a percent increase in the extreme flows of upto $347 \text{ m}^3\text{s}^{-1}$. The effects of projected increase in temperature and precipitation in the basin is however more pronounced, resulting in a significant increase in mean annual discharge and peak river discharge upto 29,776 and 2849 m^3s^{-1} respectively. Further, modelling hydrological responses in developing countries like India face additional challenges, because of acute shortages of in-situ hydro-meteorological data. In this respect, we seek to understand how reliable the hydrological model predictions in the region are when combinations of global datasets are used instead of locally available observations. Our results suggest, some global datasets (such as precipitation from Global Precipitation Measurements and soil from SoilGrids) could be used as a viable alternative to local observations in this river basin. Our modelled hydrological responses will be useful for water resource managers to mitigate future risks associated with climate and land use changes, and also would help in selection of the most robust combination of input datasets for the basin.

Dedication and acknowledgements

Undertaking this PhD has been truly a wonderful experience for me, and it is my pleasure to acknowledge the roles of several individuals who were instrumental for the completion of my PhD research.

Firstly, I would like to express my sincere gratitude to my supervisors, Miguel Rico-Ramirez, and Rafael Rosolem, who have guided me through this PhD, gave their valuable advice while supporting me at both professional and person level. You both created a research environment for me with those insightful discussions and constructive feedback, that stimulated original thinking and initiative. Your prompt feedback, numerous comments, and suggestions on my work, helped me navigate any potential obstacles along the way and achieve my objectives. I thank you for your enduring supervision, expert guidance, and every support during this process. I could not have imagined having better supervisors for my PhD research.

I also want to thank my internal reviewers, Thorsten Wagener and Francesca Pianosi for the discussions that we had and the useful suggestions during the review process.

Thanks to my colleagues from Woodland Road, especially my officemates Elisa and Pablo for the chats, laughs, Greek biscuits, and for being such a joyful daily company.

Thanks to everyone associated with Hodgkin house where I have stayed for these four years of my PhD. I had a chance to meet PhD researchers from around the world, have made some amazing friends and have wonderful memories. I specially thank my Indian group at the house for all the fun times, late night chats, special dinners on every occasion and most importantly being there for each other.

Most of all, I thank my parents and my sister for their never-ending support and belief that I could do this and always being there for me. I am sure my father would have been the proudest.

AUTHOR'S DECLARATION

I declare that the work in this dissertation was carried out in accordance with the requirements of the University's Regulations and Code of Practice for Research Degree Programmes and that it has not been submitted for any other academic award. Except where indicated by specific reference in the text, the work is the candidate's own work. Work done in collaboration with, or with the assistance of, others, is indicated as such. Any views expressed in the dissertation are those of the author.

SIGNED:

DATE:18/3/2022.....

Table of contents

List of tables	xi
List of figures	xiii
1. Introduction.....	2
1.1. Background and overview	2
1.1.1. Changing environment and its impact on hydrology	2
1.1.2. Modelling hydrological changes	8
1.2. Research objectives	12
2. Data and Methods	17
2.1. Study area	17
2.2. Data.....	21
2.2.1. Meteorological data.....	21
2.2.2. Ancillary data	27
2.2.3. Validation data.....	31
2.2.4. Summary of datasets used in each chapter.....	32
2.2.5. Comparisons between local, satellite and reanalysis meteorological observations	33
2.3. Variable Infiltration Capacity (VIC) model.....	38
2.3.1. Water balance processes	39
2.3.2. Routing model.....	41
2.3.3. Model parameterization	42
2.3.4. Model calibration and validation.....	46
2.3.5. Root depth and fraction estimation approach in VIC model.....	46
3. Sensitivity analysis and model calibration.....	49
3.1. Introduction.....	49
3.2. Model input datasets and uncertain parameters	52
3.3. Methods.....	56
3.3.1. Morris Sensitivity Analysis Method	56
3.3.2. Screening of input parameters	57

3.3.3.	Calibration strategy.....	58
3.4.	Results.....	60
3.4.1.	Morris screening	60
3.4.2.	Calibration and validation	65
3.5.	Discussions.....	71
3.6.	Conclusions.....	73
4.	Quantifying the impact of land cover changes on hydrological responses	74
4.1.	Context and Background	74
4.2.	Materials and Methods	77
4.2.1.	Model input datasets and parameters	77
4.2.2.	LULC scenarios	79
4.3.	Results.....	86
4.3.1.	Sensitivity Analysis, Model Calibration and Validation	86
4.3.2.	Baseline scenario performance	86
4.3.3.	LULC impacts and uncertainties.....	88
4.4.	Discussions.....	93
4.5.	Conclusions.....	96
5.	Assessing the impact of future climate changes on hydrological responses.....	97
5.1.	Context and background	97
5.2.	Materials and methods	100
5.2.2.	Model Input datasets and parameters.....	100
5.2.3.	Setting up climate scenarios impact study.....	102
5.3.	Results.....	110
5.3.1.	Model performance in historical period.....	110
5.3.2.	Impacts on peak flows and model parameter uncertainties	114
5.4.	Discussions.....	116
5.5.	Conclusions.....	120
6.	Assessing the impact of local versus global datasets on hydrological responses.....	122
6.1.	Introduction	122
6.2.	Data and Methods	125
6.2.1.	Model input datasets and parameters	125
6.2.2.	Experimental design and model evaluation	129

6.3.	Results.....	132
6.3.1.	Model performance of all experiments.....	132
6.3.2.	Factors causing changes in model performance due to different data sources 134	
6.4.	Discussion	139
6.5.	Conclusions.....	141
7.	Conclusions and future outlook	144
7.1.	Summary.....	144
7.2.	Overarching remarks	148
7.3.	Recommendations for future work.....	150
	Data availability.....	156
	BIBLIOGRAPHY	157
	Appendix A – Supporting information for chapter 6.....	177
	Appendix B – Supporting information for chapter 7	184
	Curriculum Vitae	185

List of tables

Table 2.1 CMIP6 GCMs considered for bias correction in Mishra et al., (2020a).....	24
Table 2.2. Description of the Scenarios used in this thesis (Gidden et al., 2019)	24
Table 2.3 LUH2 future scenarios and models used in the thesis. Description of the Scenarios can be found in Table 2.2.....	30
Table 2.4 Gauging stations and their descriptions	32
Table 2.5: Data information used in this thesis.	33
Table 2.6 Hydraulic properties of the dominant soil textures in Mahanadi river basin	43
Table 2.7 Soil parameters and equations used for estimation of these soil parameters	44
Table 2.8 Details of the vegetation parameters for the dominant vegetation types in Mahanadi River basin.....	45
Table 2.9: Coefficients a and b in vegetation root distribution for Eq 2.9 for the land cover types used in this study. The depth of the rooting zone z_t is also given (Zeng, 2002).....	48
Table 3.1: VIC and routing model parameters tested for sensitivity analysis and feasible ranges.	55
Table 4.1 LUH2 LULC classes remapped to VIC LULC cover classes.....	79
Table 4.2 Percent of each Land use type in NRSC2005 and LUH2005 in the entire Mahanadi river basin (WB – Water Body; ENF – Evergreen Needleleaf Forest; DBF – deciduous Broadleaf Forest; GL- Grassland; CL- Cropland; U – Urban).....	82
Table 4.3 Land cover area change across all subcatchments of Mahanadi river basin.....	85
Table 4.4 Range of KGE’S for the daily calibration and validation at all subcatchments.	88
Table 4.5 Ranges of percent change, change in flows, and uncertainty (i.e., difference between max. and min. predicted flow) in extreme and mean annual flows in all the scenarios with respect to the baseline scenario.....	92
Table 6.1: Summary of model input datasets used in this study.....	126

Table 6.2: Describing the experiments performed in this study131

List of figures

Figure1.1 (a) Bar chart showing change in LULC area estimates during 1985 to 1995, 1995 to 2005 and 2005 to 2025 for Mahanadi river basin in India (Behera et al., 2018). (b) Downstream of Mahanadi river and its tributaries submerged, as the excess water released from Hirakud dam, located at the upstream, Source: Times of India, August, 2020 (Mahanadi floods more downstream areas, situation expected to worsen | Bhubaneswar News - Times of India (indiatimes.com)).5

Figure1.2: Projected change in global flood frequency. Multi-model median return period (years) in future (2071– 2100) for discharge corresponding to a 100-year flood in the past (1971–2000), for CMIP6 models under the high emission scenario SSP5-8.5 (RCP8.5 and ssp585) (Hirabayashi et al., 2021)..... 6

Figure1.3: Summary of the thesis structure15

Figure 2.1 The Mahanadi river basin boundary and the analysed gauges and their catchments. Abbreviations for gauge names are Ba- Basantpur, Ka-Kantamal, Ke-Kesinga, Su- Sundergarh and Sa-Salebhata 18

Figure 2.2. (a) Seasonal rainfall pattern averaged for the time period 1990-2016 in Mahanadi river basin (b) Measured daily discharge at Kantamal (subbasin of Mahanadi river basin) for year 2008. 19

Figure 2.3. (a) Long term pattern of (a) mean annual rainfall (b) annual average temperature averaged over Mahanadi river basin of spatial area of 140,000 km², for the time period 1951-2016 obtained from Indian Meteorological Department (IMD) 19

Figure 2.4. Percent change in the LULC classes obtained from LULC map of 2013-2014 relative to the LULC map of year 2005-2006, obtained from the National Remote Sensing Centre (NRSC) 20

Figure 2.5 Projected (a) annual precipitation, (b) minimum and (c) maximum temperatures from 52 (13 models*4 scenarios) ensembles of CMIP6 (red) and the ensemble mean (blue), for Mahanadi river basin for the future period 2015-2100..... 26

Figure 2.6 (a) National soil map derived from National Bureau of Soil Survey and Land Use Planning (NBSSSLUP) with a spatial resolution of 500 metres and (b) Global soil map derived from SoilGrids with a spatial resolution 250 metres for the Mahanadi river basin. The spatial resolution of the maps shown here is 5km which is used by the VIC model to perform the simulations. 28

Figure 2.7 (a) National LULC map derived from National Remote Sensing centre (NRSC), India of year 2013-2014 of resolution 56 meters and (b) Global LULC map derived from ESA CCI of year 2014 of resolution 250 metres 29

Figure 2.8 Land cover changes and fractional area covered in all LUH2 scenarios mentioned in Table 2.3..... 31

Figure 2.9: Spatial distributions of mean annual rainfall over Mahanadi river basin averaged for the time period 2014-2016, derived from IMD gauge-based, IMERG, and ERA5-LAND precipitation datasets 34

Figure 2.10: Spatial distributions of (a) Correlation between GPM and IMD (b) Correlation between ERA5-Land and IMD (c) PBIAS of GPM against IMD (d) PBIAS of ERA5-Land and IMD daily rainfall over Mahanadi river for 2014-2016..... 35

Figure 2.11: Spatial distributions of mean daily maximum temperature derived from (a) IMD and (b) ERA5-LAND. Spatial distributions of mean daily minimum temperature derived from (c) IMD and (d) ERA5-Land. averaged for the time 2014-2016 37

Figure 2.12: Spatial distributions of (a) Correlation between maximum temperature from ERA5-Land and IMD (b) Correlation between minimum temperature from ERA5-Land and IMD (c) P-Bias between maximum temperature from ERA5-Land and IMD (d) P-Bias between maximum temperature from ERA5-Land and IMD, over Mahanadi river averaged for 2014-2016. 38

Figure 2.13: (a) Schematic diagram for Variable Infiltration Capacity (VIC) macroscale hydrological model (b) Schematic diagram of VIC river network routing model (Gao et al., 2010) 39

Figure 2.14: (left) Representation of rooting distributions in VIC-3L model. z_1 , z_2 and z_3 are the user-defined depths of three root zones, respectively. d_1 , d_2 , d_3 are the depths of three soil layers. f_1 , f_2 and f_3 are user-defined fractions of root in each zone, respectively. f_1' , f_2' and f_3' are fractions of root in each soil layer computed by VIC. (right) Our approach of representation of rooting distributions in VIC-3L model. z_t is the total root depth. 47

Figure 3.1: Sensitivity indices (Mean and Standard deviation) of Morris Method for VIC-3L parameters for (a-e) individual subbasins of Mahanadi river basin respectively (f) weighted average of all subcatchments. Parameters, top to bottom, listed on the right side are in ranking order, highest to lowest respectively, based on Mean of EEs. Red dashed vertical line is the screening threshold. Parameters that are Influential i.e., above the screening threshold are within the black dashed box. Rest of the parameters are non-influential..... 63

Figure 3.2: Convergence analysis with increasing sample size (expressed as number of simulations) for (a-e) all individual subcatchments respectively (f) weighted average of all subcatchments..... 64

Figure 3.3: Maximum width of the 95% bootstrap confidence interval of all parameters for all subbasins. Dotted red line is the *StatScreen* threshold, below which are the non-influential parameters that have converged.65

Figure 3.4: Boxplots showing (a) KGE and (b) PBIAS range for calibrated (black) and validated (grey) simulations, respectively.66

Figure 3.5: Simulated and observed discharge in the calibration and validation period for all subcatchments. Hydrographs are zoomed in to the monsoon season of the most wet year during the calibration and validation period; model performance is similar in other years. .68

Figure 3.6: Parallel coordinate plot representing VIC-3L behavioural parameterization for all subcatchments obtained during model calibration. Lines in black are simulations where KGE lies within top 2% i.e., behavioural simulations and lines in grey are non- behavioural simulations. Behavioural KGE at Ba, Ka, Ke, Su and Sa ranges from 0.83 to 0.88, 0.85-0.88; 0.81-0.84; 0.74-0.76 and 0.62 to 0.66 respectively. Parameters are defined in Tables 1.69

Figure 3.7: Plots of the water balance components (runoff and ET) resulting from the Monte Carlo simulation for all subcatchments. ‘Cal’ indicates calibration and ‘val’ indicates validation.70

Figure 4.1 (a) LULC map of Mahanadi River basin from NRSC of year 2005 (b) Comparison of LAI values from MODIS, averaged over the time period, 2000-2015 and GLDAS for the land cover classes shown in LULC map on (a).78

Figure 4.2 Forested areas in NRSC, ‘Potential Non-Forested areas’ in LUH2 and ‘potentially forested areas’ in LUH2. ‘Potential Non-Forested areas’ in LUH2 is comparable with the Forested areas in NRSC, through visual inspection. Therefore, both the ‘potentially forested area’ and ‘potentially non-forested area’ are combined and mapped as forest.80

Figure 4.3 Comparison of spatial patterns of land cover types from NRSC and LUH for the baseline year, 2005. All land cover classes shown here are resampled to the model grid resolution of 5km. The color bar represents the fraction of area covered by each land cover type.81

Figure 4.4: Top: Fraction of catchment area occupied by Land use classes for scenario RCP3.4 SSP4 Bottom: land cover scenarios from LUH (resolution- 25 km) for years 2015, 2050 and 2100 used in this study. LUH land cover classes shown here are resampled to the model grid resolution and only the predominant class is shown here for clarity. For actual model simulations VIC accounts for the individual proportion for each land cover type at each grid point.84

Figure 4.5 Box plot showing (a) KGE range and (b) PBIAS for calibrated, validated and baseline scenario simulations87

Figure 4.6: (a) Percent change in extreme flows (i.e., 95th percentile or higher) (right) (b) Change in extreme flows in m^3s^{-1} (c) Percent change in mean flows (d) Change in mean flows in m^3s^{-1} , averaged annually over the time 2001-2010 in the Near future (NF), Far future (FF),

Cropland (CL) and Forest (F) scenarios with respect to baseline scenario for all the subcatchments. Please note that the climate forcing is kept fixed for the period corresponding to year (2001-2010) The results are shown for the behavioural model simulations obtained through calibration.90

Figure 4.7: Percent change in (a) mean runoff (b) mean ET averaged annually over the time (2001-2010) in the Near future (NF), Far future (FF), Cropland (CL), Forest (F) scenarios with respect to baseline scenario for all the subcatchments. Please note that the climate forcing is kept fixed for the period corresponding to year (2001-2010). The results are shown for the behavioural model simulations obtained through calibration.....91

Figure 5.1. Comparison of monthly mean precipitation produced by IMD (blue) against thirteen CMIP6 models (red), spatially averaged for the entire Mahanadi River basin for the historical time 1990-2014 considered in this study.104

Figure 5.2. Comparison of monthly mean (a) maximum temperature and (b) minimum temperature produced by IMD (blue) against thirteen CMIP6 models (red), spatially averaged for the entire Mahanadi River basin for the historical time 1990-2014 considered in this study.104

Figure 5.3 (a) Different possible combinations of normalized differences for temperature ΔT ($^{\circ}\text{C}$) and precipitation ΔP (%) between the 3224 sets of 25-year periods from the 52 (13 models*4 scenarios) ensembles of CMIP6 against the 25-year Control Period from IMD, averaged over the entire Mahanadi river basin (b) Heat map showing the density of sample points lying within each grid of Figure 5.3 (a).106

Figure 5.4 Procedure to choose a climate sample point from a particular grid, where temperature (ΔT) varying from 1°C to 2°C and precipitation (ΔP) varying from 10% to 20%. (a) Choosing a scenario based on the maximum occurrences (i.e., computed from mode of the scenarios) (b) Choosing a time based on the median time. (c) choosing a model based on maximum occurrences (i.e., computed from mode of the models) (d) Choosing a future land cover map from LUH2 land cover scenarios, based on the scenario (a) and time chosen (b) for a particular grid. Marked in black are the climate samples chosen for this particular grid..109

Figure 5.5: Boxplots showing KGE and PBIAS range for 101 VIC model simulations for the subcatchments of Mahanadi river basin (Ba- Basantpur; Ka- Kantamal; Ke- Kesinga; Su- Sundergarh; Sa- Salebhata).....110

Figure 5.6 (A) Percentage change in mean annual flows (B) change in mean annual flows in m^3s^{-1} (C) Standard deviation in the percent change of mean annual flows resulted from 100 behavioral VIC models, representing the VIC model parameter uncertainty, at all subcatchments in the future period against the control case simulation in the historical period 1990-2015.113

Figure 6.1 (a) Cumulative daily precipitation of Subbasin Basantpur from IMD, GPM IMERG and ERA5-Land, for the period 2014–2016. (b) Daily minimum and maximum temperatures from IMD and ERA5-Land, for the period 2014–2016 of Subbasin Basantpur128

Figure 6.2: (top) Values of KGE calculated for prediction of discharge of all experiments at all subbasins. Boxplot of KGE values represents 250 behavioural models, meaning the uncertainties stemming from 250 model parameters sets (b) Bar charts representing the percent changes in datasets (precipitation, temperature, soil and land cover) obtained from global sources with respect to that of datasets from local source. In the legend, T, P, S and L are temperature, precipitation, soil and LULC respectively.134

Figure 6.3: Annual average of runoff and evapotranspiration at Basantpur for all experiments. In the legend, T, P, S and L are temperature, precipitation, soil and LULC respectively. Please note that the precipitation varies across experiments.136

Figure 6.4: Comparison of daily observed discharge and ensemble mean of simulated discharge of experiments at Basantpur using (a) precipitation from GPM, ERA5-land and IMD (reference) (b) temperature from ERA5-Land and IMD (reference) (c) soil from SoilGrids and local soil (reference) (d) LULC from ESA CCI and local LULC (reference) (e) all global datasets and all local datasets (reference), averaged for the years (2014-2016). In order to show the details of the hydrographs, they are zoomed in to the monsoon (wet) months; Results for other subcatchments are similar and can be found in the Appendix (Figures. A4–A7).....138

Figure A.1: (top) Values of KGE calculated for prediction of discharge of all experiments, ranked in order of their performance, at all subbasins. Boxplot of KGE values represents 250 behavioural models, meaning the uncertainties stemming from 250 model parameters sets (b) Bar charts representing the corresponding percent changes in datasets (precipitation, temperature, soil and land cover) obtained from global sources with respect to that of datasets from local source. In the legend, T, P, S and L are temperature, precipitation, soil and LULC respectively.177

Figure A.2: Annual average of runoff and evapotranspiration at Kantamal, Kesinga, Sundergarh and Salebhata, for all experiments. In the legend, T, P, S and L are temperature, precipitation, soil and LULC respectively. Please note that the precipitation varies across experiments.179

Figure A.3. Comparison of daily observed discharge and ensemble mean of simulated discharge of experiments at Kantamal, Kesinga, Sundergarh and Salebhata using (a) precipitation from GPM, ERA5-land and IMD (reference) (b) temperature from ERA5-Land and IMD (reference) (c) soil from SoilGrids and local soil (reference) (d) LULC from ESA CCI and local LULC (reference) (e) all global datasets and all local datasets (reference), averaged for the years (2014-2016). In order to show the details of the hydrographs, they are zoomed in to the monsoon (wet) months.....183

1. Introduction

1.1. Background and overview

1.1.1. Changing environment and its impact on hydrology

Environmental change is occurring globally, which includes land degradation, loss of biodiversity, changes in climate patterns and hydrology, resulting from the continuously increasing greenhouse emissions from the enhanced anthropogenic activities. About 41% of the global natural vegetation has been replaced by the anthropogenic land cover such as croplands or pasture (Sterling et al., 2013). The increasing anthropogenic activities is causing worrying levels of global warming which is also causing a constant rise in the global temperatures (Yaduvanshi et al., 2019). Under the warmer climate, global monsoon rainfall is likely to increase at the end of 21st century (Chen et al., 2020). The anthropogenic impacts, of both, emission driven climate change as well as human-intervened changes such as building river projects, water withdrawals and land use changes, have a serious impact on hydrology. These impacts includes changes, in local and regional water availability, quality and quantity of both surface and ground water (Dwarakish and Ganasri, 2015), magnitude and timing of streamflow, and frequency and intensity of hydrologic extremes such as floods and droughts (Bosmans et al., 2017; Jiang et al., 2007).

Change in climate affects the basic components of the water cycle such as precipitation, atmospheric water content and soil moisture. On the other hand, land cover changes alters water cycle by directly changing the timing and magnitudes of evapotranspiration (Sterling et al., 2013), thus affecting the runoff to evaporation ratio and also the interception and infiltration rates (Bosmans et al., 2017). Understanding these changes in hydrological behaviour due to the changes in land cover and climate forms an important step towards the water resources planning and management (Chawla and Mujumdar, 2015).

The interrelationships of LULC changes with various aspects of the hydrological processes remains a prominent topic of research around the world (Berihun et al., 2019; Costa et al., 2003; Legesse et al., 2003; Liu et al., 2011; Mishra et al., 2010; Tekleab et al., 2014). A significant increase is observed in the annual river discharge worldwide since 1900 (Sterling

et al., 2013), and the researchers suggest that about 50% of this increase is due to the LULC change (Kumar et al., 2017). Specifically, a remarkable increase in runoff due to cropland expansion is produced by Southern Asia, Eastern Europe, and Eastern South America while few regions, principally eastern part of North America have undergone reduction in crop area, consequently resulted in reduced runoff (Piao et al., 2007). Studies dealing with land cover change impacts on global hydrology generally find increased discharge through reduced evapotranspiration (Bosmans et al., 2017; Gordon et al., 2005; Piao et al., 2007; Rost et al., 2008). A recent study by Bosmans et al., (2017) showed that land cover change impacts from year 1800 to 2000, when globally averaged, resulted in reduced evapotranspiration through increased discharge.

Some studies investigating land cover impacts on a regional scale has reported large variability in the signs and magnitudes of changes, at different climate zones with a specific land cover change. For instance, Urban expansion resulted in significant increase in runoff in Midwestern United States having a humid continental climate (Wu et al., 2013), while this similar change in land cover has decreased surface runoff in a subtropical catchment in India (Kumar et al., 2018). There are also studies that have reported similar responses i.e., higher surface runoff and/or reduced evapotranspiration, due to conversion from natural vegetation to agricultural land in similar climate zones, for instance, in tropical and subtropical river basins (Abe et al., 2018a; Babar and Ramesh, 2015; Berihun et al., 2019; Costa et al., 2003; Gebremicael et al., 2019). However, different LULC changes in different river basins may produce significantly different hydrological responses hence land cover changes in one river basin cannot be superimposed onto a nearby basin to generate same hydrological responses as in previous basin. This is because discharge produced from river basins is dependent on many other factors such as soil, vegetation and spatial and temporal variation in climate (Kumar et al., 2018).

Changes in Land Use and Land Cover (LULC) is mostly noticeable over regions having high population density, agricultural heterogeneity, deforestation, and urbanization. India is the second most populous country in the world and is characterized by a wide range of climate, flora, fauna, land use and land cover, topography and socioeconomic conditions (Faostat, 2017) . In the past 140 years in India, there has been a remarkable change in the land use and land cover including cropland changes, deforestation, and urban expansion (Roy et al., 2015).

Specifically, the increases in the agricultural production have been notable over the last decades. The annual loss of forest cover recorded for the period between 1990 and 2000 is 380 km² (FAO,2000). It is observed that the launch of India's 'Green Revolution' to support a large population in terms of sustainable economic development and food security has led to expansion of agricultural land through extensive deforestation (Singh, 2000). These ongoing developmental activities in the country has impacted the LULC in each river basin in India (Garg et al., 2019).

Ganga river basin, a large-scale river basin in India, has undergone a substantial land cover change over the last four decades including an increase in the urban land (Behera et al., 2014) and agricultural land (Patidar and Behera, 2019) at the cost of natural vegetations and barren land. These changes have resulted in an increase in flows during monsoon. Tons River basin in semi-arid regions in India, has been facing drastic land cover change due to rapid increase in population (Kumar et al., 2018) which has predicted a decrease in surface flow and slight increment in groundwater flow in future. Similar changes were also observed in the river basins of Pune, a rapidly developing city in India (Wagner et al., 2013), where decrease in ET is reported. However, despite the substantial land cover changes in some of these basins, negligible impacts on runoff and ET are reported at the basin scale. In the last decades, Mahanadi river basin, a major peninsular river basin in east-central India have also undergone drastic reduction in forest areas due to agricultural expansions, dam constructions, industrialization, and urbanisation. A similar trend is also observed in future LULC prediction for year 2025 with a total decrease in forest areas of 1376 km² in the basin (Behera et al., 2018) (See Figure 1.1 a). Frequent occurrences of floods (example shown in Figure 1.1 b), droughts and cyclones in this basin in recent times suggests a shift in the hydrological response of the basin which might be attributed to landcover changes (Dadhwal et al., 2010). Few previous studies (Dadhwal et al., 2010; Das et al., 2018) reported an increase in runoff in this basin owing to these land cover changes. Moreover, a recent research at national scale in India suggests agricultural lands are likely to extend in the future to meet food demands, due to population growth and climate change, resulting in biodiversity losses (Hinz et al., 2020). This necessitates the need for investigating LULC impacts and its future prediction at basin scale which shall guide towards proper decision making and resource management. In this thesis, we will be focussing on Mahanadi River basin in India.

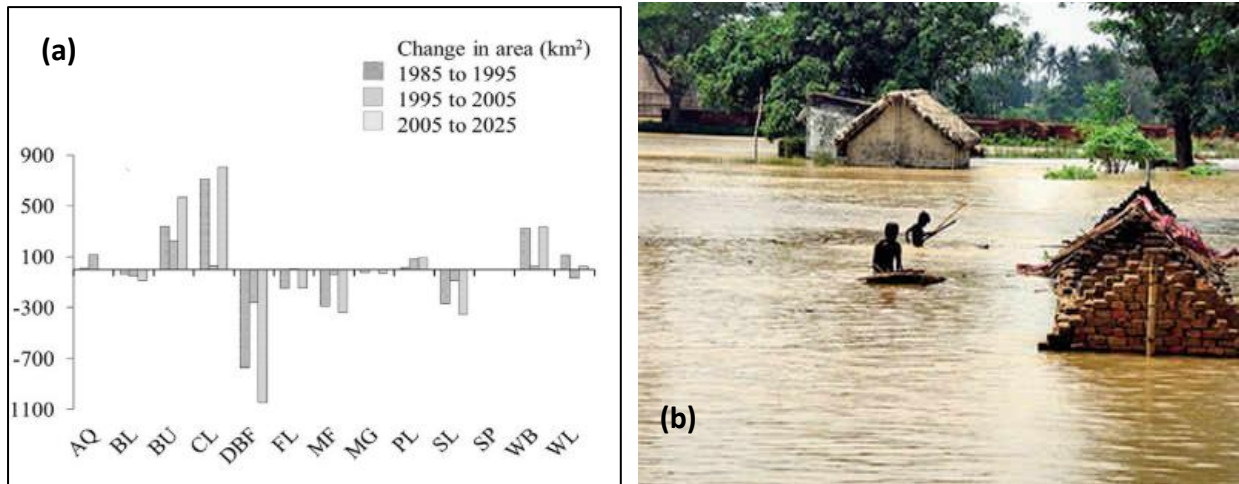


Figure 1.1 (a) Bar chart showing change in LULC area estimates during 1985 to 1995, 1995 to 2005 and 2005 to 2025 for Mahanadi river basin in India; AQ – Aquaculture; BL- Barren land; BU – Built up; CL – Cropland; DBF- Deciduous broadleaf forest; FL- Fallow land; MF- Mixed forest; MG- Mangrove; PL- Plantation; SL- Scrubland; SP- Saltpan; WB- Water body; WL- Waste land (Behera et al., 2018). (b) Downstream of Mahanadi river and its tributaries submerged (location: Khurda, 20.1863° N, 85.6223° E), as the excess water released from Hirakud dam, located at the upstream, Source: Times of India, August, 2020 ([Mahanadi floods more downstream areas, situation expected to worsen | Bhubaneswar News - Times of India \(indiatimes.com\)](https://timesofindia.indiatimes.com/Bhubaneswar-News-Mahanadi-floods-more-downstream-areas-situation-expected-to-worsen/Bhubaneswar-News-Times-of-India/indiatimes.com)).

The rise in temperature is expected to be causing changes in the intensity, frequency and duration of precipitation and most studies reported that higher air temperature may increase the chances of more recurrent and extreme precipitation events due to the increased water vapor content in the atmosphere (Stoffel et al., 2014). This, in turn can have significant impacts on the hydrological processes such as magnitudes of runoff, baseflow, evapotranspiration, groundwater recharge and sediment load (DeFries and Eshleman, 2004). Both global and regional hydrological cycles are greatly impacted by climate change in the past decades. Climate modelling on a global scale suggests that precipitation is projected to increase by the end of the 21st century across some middle and higher latitude regions while some regions including the Mediterranean region, Africa and Southern Australia will receive less precipitation (Hagemann et al., 2013). Future changes in runoff is predicted to follow the same pattern as the projected precipitation to a large extent (Hagemann et al., 2013) i.e. runoff is likely to increase in those regions where precipitation increases. Moreover, extreme

precipitation events are also expected to increase in most parts of the world under climate change (Groisman et al., 2005), which shall potentially lead to increase in the magnitude of extreme flows (Eccles et al., 2019). Despite a certain level of uncertainty in these climate projections, a great deal of scientific studies predict that, global warming will exceed by 2°C and may accelerate up to 6 °C by the year 2100 (Betts et al., 2016). New climate projections from Climate Model Intercomparison Project (CMIP6) indicated potential global exposure to flooding as a result of global warming in many regions of the world including South Asia (Hirabayashi et al., 2021) (See Figure 1.2).

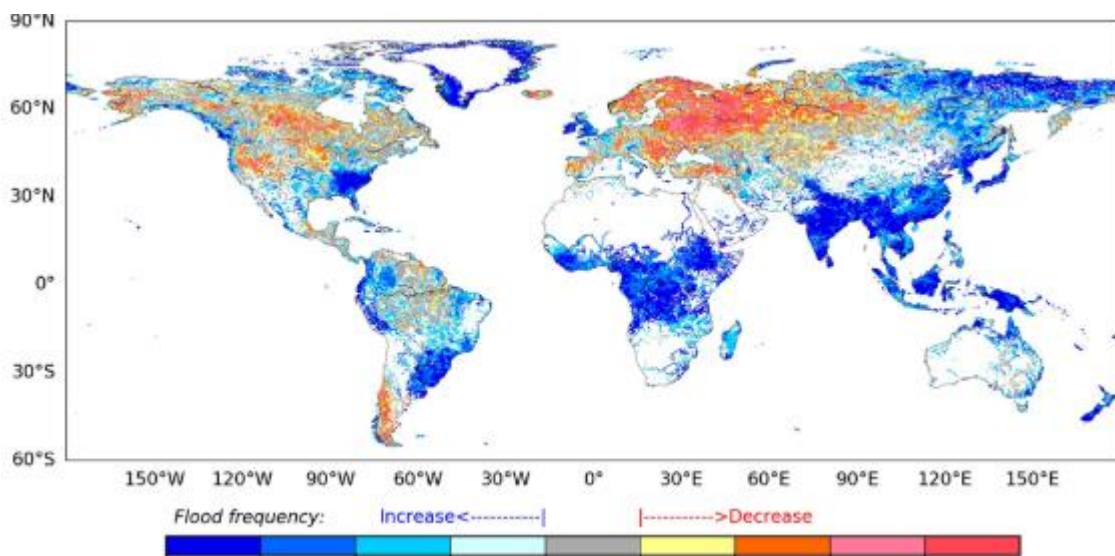


Figure 1.2: Projected change in global flood frequency. Multi-model median return period (years) in future (2071– 2100) for discharge corresponding to a 100-year flood in the past (1971–2000), for CMIP6 models under the high emission scenario SSP5-8.5 (RCP8.5 and ssp585) (Hirabayashi et al., 2021).

South Asia is among the global hot spots that are expected to face adverse impacts of climate change and pose threats on agriculture, infrastructure, water resources and livelihood of a huge population (Mishra et al., 2020a). Global advances in economy and higher living standards have led to a growing dependency on water resources (Legesse et al., 2003). This dependence is even more evident in India, as 70% of her population is dependent on agriculture (Jain et al., 2007) which is largely controlled by the southwest monsoon rainfall occurring during the months of June-Oct (Jin et al., 2018). The Indian monsoon is a complex oceanic-atmospheric-coupled mechanism of the tropics that is manifested with the development of low-pressure region in the north-western part of Indian landmass (Tibetan

plateau) due to seasonal migration of the inter-tropical convergence zone (ITCZ). This shift in ITCZ is caused due to differential heating of the Indian landmass, which leads to heavy precipitation during June, July, August, and September (Gusain et al., 2020). Studies related to Indian monsoon rainfall speculates that global teleconnections such El Niño Southern Oscillation (ENSO), Indian Ocean Dipole (IOD) Atlantic Multidecadal Oscillation (AMO), Atlantic zonal mode (AZO), Eurasian snow cover, equatorial Indian Ocean Oscillation, low pressure systems, and Madden-Julian Oscillation pose a notably strong influence on intraseasonal, interannual and multi-decadal variability of Indian monsoon (Gusain et al., 2020; Saha et al., 2014). Particularly, Mahanadi river basin is sensitive to ENSO and IOD because it is located adjacent to the Bay of Bengal (Maity and Nagesh Kumar, 2009). Panda et al., (2013) found a direct correspondence of the rainfall and streamflow series with the ENSO in the basin, which is contrary to the established inverse relationship over India.

India ranks 10th among highest climate risk countries in Asia based on extreme environment events (Global Sustainable Development Report 2015) (Yaduvanshi et al., 2019). Therefore, developing countries like India are likely to face severe impacts due to their agriculturally based rural economy (Jin et al., 2018). Various studies exist on the variability of Indian rainfall under warming conditions suggesting annual precipitation has significantly increased in the last century. Yaduvanshi et al., (2019) attempted to understand the implications of global rise in temperature by 1.5-2°C (IPCC, 2014) using global climate models on a regional scale across India. Findings of this study indicates rise in temperature between 0.5-4°C across states in India and increase in the annual rainfall in most parts, with maximum increase during the monsoon season (0-350 mm). An increasing trend in Indian monsoon rainfall is also found in Jin and Wang, (2017). The peak flood discharge, frequency of extreme floods and also tendency of expansion of flood prone areas are apparently on rise in India (Kapuria and Modak, 2019) that can be attributed to the significant increase in rainfall during the monsoons. Increased flooding under climate change is projected in various catchments in India (Eccles et al., 2019; Whitehead et al., 2018). Mahanadi river basin is a major large scale river basin in India and is predicted to face severe floods under the future climate change scenarios (Asokan and Dutta, 2008; Gosain et al., 2006; Jin et al., 2018). Similar hydrological responses are also reported for other major basins, Ganga river basin (Tsarouchi and Buytaert, 2018; Whitehead et al., 2015) and Brahmaputra river (Mohammed et al., 2017; Philip et al., 2018).

Climate models predict that intensification of monsoon rainfall in India and its annual variability would also result in an increased inter-annual variability in terms of droughts and floods (May, 2004; Rickards et al., 2020; Rupa Kumar et al., 2006). India experiences uneven distribution of available water resources over space and time that results in floods in some parts of the country and droughts in others. For instance, studies also predicted reduction in the occurrence of high flow events in parts of Mahanadi river basin, thereby resulting in increasing trend of extreme meteorological drought (Ghosh and Mujumdar, 2007b, 2007a; Mujumdar and Ghosh, 2008). During the dry season, many regions of India are likely to face critical levels of water scarcity due to the growing water demand due to rapid population growth, exacerbated by climate change, affecting food supply and livelihoods (Mall et al., 2006; Rickards et al., 2020; Saleth, 2011). These hydrological extremes have a direct effect on regional water storage and utilization (Mall et al., 2006).

With the scarcity in the water resources availability in some parts and increase in floods in other parts of the country, hydrologists are studying more about the role of land cover and climate in affecting these hydrological responses. India along with the state governments has pledged to address these climate change issues through its National Action Plan of Climate Change (NAPCC) (Yaduvanshi et al., 2019). The hydrological cycle is expected to be altered as a result of both, human induced land use activities such as deforestation and agricultural activities within the river basin (Babar and Ramesh, 2015), as well as the increase in temperature (Joseph et al., 2018). Simulating these hydrological consequences has received increased attention within the hydrological and land surface modelling communities (Xu et al., 2005). The study of these hydrological impacts especially on a regional scale is crucial for the management of water resources.

1.1.2. Modelling hydrological changes

Hydrologic models have become increasingly important tools for solving the hydrological problems and for the management of the water resources. Hydrologists agree that the relationship among the land use, climate and the hydrological processes can be best solved through a hydrological model that considers the spatio-temporal basin characteristics, enabling accurate estimation of dynamic water balance of a watershed (Costa et al., 2003; Dwarakish and Ganasri, 2015; Thanapakpawin et al., 2007).

Hydrological processes represented by hydrological models are 1. Soil-Vegetation-Atmosphere transfer processes such as evapotranspiration through vegetation canopies, rain and snow interception, snowmelt, and soil evaporation; 2. Soil moisture storage and runoff generation processes such as, infiltration, surface, and subsurface runoff. 3. Channel routing and 4. Other processes such as groundwater recharge, snow and glacial melt (Thanapakpawin et al., 2007).

Two major criteria for selecting a model for specific application are model functionality and complexity. The model functionality differs from one model to another in terms of different process representations, different equations used to represent those processes and model discretization. On the other hand, model complexity is based on the requirement of measured data, time, cost, resources for calibration and parameterization of a model and also experience needed to employ these models (Dwarakish and Ganasri, 2015).

Traditionally, the hydrological models can be classified based on their representations of hydrological processes such as empirical, conceptual and distributed (Bergström and Graham, 1998; Refsgaard et al., 1989). Empirical approaches are based on simple relationships derived from experiments, such as linear regressions. Priestley-Taylor method is an empirical approach for computing evapotranspiration (Gardelin and Lindström, 1997), used in HEC-HMS and HBV model. Conceptual modelling involves simplified assumptions to derive solutions for the governing equations which are used to describe conservation of mass, momentum, and/or energy (Cornelissen et al., 2013). An example is the Green-Ampt equation for partitioning of rainwater into infiltration and surface runoff (Li et al., 2009). In physically based models, partial differential equations are used to describe the conservation of mass, momentum and energy. A few examples are Penman Monteith equation for estimating evapotranspiration (Mao and Cherkauer, 2009), St. Venant's equation for channel routing (Lohmann et al., 1996) and Richard's equation for saturated zone flow (Gao et al., 2010). Another important aspect to consider while simulating land cover impacts, is the model's ability to spatially discretize the watershed as per different soil and vegetation types, to account for the vegetation heterogeneity. Also, temporal discretization, meaning the time steps at which simulations can be performed, must be considered. Running the model at different time steps may lead to different outputs.

These types of hydrologic models have their own advantages and disadvantages. Physical based distributed models are able to explicitly represent the spatial variability of the land surface characteristics (Legesse et al., 2003), thus, are more suited for complex catchments and predicting the hydrological responses to the dynamics of environmental changes (Beven, 2011). However, a physically based fully distributed models are quite data intensive i.e., need large number of input parameters to represent the surface and sub-surface hydrological processes, which makes the model calibration task extremely challenging. On the contrary, lumped conceptual models are less complex and typically have modest input data requirements, but generally fail to replicate the non-linear dynamics of catchment characteristic (Sivapalan et al., 2003).

In recent years, several attempts are made to understand the land cover and climate change impacts on land surface hydrologic responses, using hydrologic models ranging from conceptual to fully physically based distributed/semi-distributed models for various geographic locations (Ashagrie et al., 2006; Hundecha and Bárdossy, 2004; Hurkmans et al., 2009; Legesse et al., 2003; Liu et al., 2011; Patidar and Behera, 2019; Tekleab et al., 2014; Tsarouchi and Buytaert, 2018; Woldesenbet et al., 2017) including Indian river basins (Gosain et al., 2006; Joseph et al., 2018; Raje et al., 2014; Wilk and Hughes, 2002). Most of these studies use the traditional way of predicting hydrologic responses to land cover change which is done by (1) Setting up a hydrological model for a baseline land cover scenario, (2) calibrating and validating the model using the present meteorological conditions and (3) Finally, using a single calibrated model to run the model for different land use scenarios using same meteorological inputs. Climate change is a rather complex issue entailing interactions and feedbacks among atmosphere, oceans and the land surface. The traditional way of tackling the climate change problem is by using global climate models that solves large scale physical processes governing the climate system. Currently, Global Climate Models (GCM) are the most reliable models for providing information about the future global climate change by simulating the time series of climate variables (Jiang et al., 2007). However, GCMs are at very coarse resolution, hence it is not yet possible to obtain reliable predictions directly from the climate models, for regional hydrologic changes. Therefore, simulating climate change impacts on a regional scale involves (1) Obtaining time series of future climate variables using

GCMs (2) Downscaling the GCM climate outputs to the regional scale and using these as meteorological forcing in a hydrological model to simulate the hydrologic impacts.

The impact assessments, both in case of land cover and climate change is associated with considerable uncertainties that are involved in every step of modelling these changes (Beven, 2011; Hagemann et al., 2013; Seibert and van Meerveld, 2016). Hydroclimatic modelling involves uncertainties originating from climate projections, downscaling techniques, and hydrologic model structures and parameters (Xu, 1999). Similarly, hydrological modelling under changed land cover conditions are also subjected to wide range of uncertainties that are commonly from measured input data, model structures and parameters (Chen et al., 2019b; Ma et al., 2010).

The concept of equifinality is ignored in most of the studies. Equifinality means multiple parameter sets can result in equally good or acceptable model outputs. Although the impact of equifinality is considered substantial in hydrologic modelling (Her et al., 2019), little attention has been directed towards understanding the model parameter uncertainties associated with these hydrologic impacts. Notable exceptions are (Breuer et al., 2006; Chen et al., 2019, Bennett et al., 2018; Her et al., 2019; Joseph et al., 2018), which indicated that model parameters could exert significant influence on land cover and climate change impacts, and should not be overlooked in environmental impact assessment, especially for decision makers. Calibration approaches in these studies also involves sensitivity analysis, which has been acknowledged as a necessary modelling tool in hydrology to identify key processes and ways to reduce model parameter uncertainties (Beven and Binley, 1992; Muleta and Nicklow, 2005). Sensitivity analysis is carried out to divide the model parameters into two groups; influential and non-influential, so as to eliminate the non-influential parameters from the calibration space to reduce the uncertainties resulting from overparameterization (van Griensven et al., 2006). To allow consideration of equifinality or different parameter sets in hydrological modelling, Monte Carlo approaches (Breuer et al., 2006; Demaria et al., 2013; Yang, 2011) are typically employed which generates a large sample, by sampling across a specified parameter range, to run the models (Beven and Freer, 2001). Notice Monte Carlo approaches requires a large number of model runs.

Understanding the land surface hydrologic responses to the land cover and climate perturbations requires a sophisticated representation of detailed hydrologic processes within

a hydrologic or a land surface model (Van Den Hurk et al., 2011). This has encouraged the development and assessment of many high resolution hydrologic models for simulating the interactions between land and atmosphere over regional and global scales (Bierkens et al., 2015; Demaria et al., 2013; Wood et al., 2011). But the problem lies in the availability of the prerequisite datasets (high resolution meteorological and ancillary datasets) locally in developing countries (Lorenz and Kunstmann, 2012; Rodríguez et al., 2020), including India (Mujumdar, 2015). Either low density rain-gauge network, for instance in Amazonian basin (Zubieta et al., 2016), or data not being openly accessible for research purposes, such as in India (Beria et al., 2017; Mujumdar, 2015), limits the understanding of hydrological processes and modelling over the region. However, in the last two decades, high quality satellite products from the ever-expanding remote sensing activities, reanalysis products and other large data global datasets forms a motivation to be used as a viable alternative to the local datasets, especially in the data scarce region (Bierkens et al., 2015; Gao et al., 2020). Satellite based precipitation datasets such as from TRMM, GPM, TMPAV7, TMPA RT have been widely used for hydrometeorological applications in various regions of the world (Gilewski and Nawalany, 2018; Tang et al., 2020; Zubieta et al., 2016) including Indian river basins (Beria et al., 2017; Prakash et al., 2018). Similarly, precipitation and temperature from reanalysis products such as ERA-Interim, ERA5 etc. are also being tested for hydrologic applications (Dembélé et al., 2020; Gao et al., 2020; Mahto and Mishra, 2019). Both satellite and the numerical weather prediction system are continuously improving with the development of new data assimilation approaches and improvements in model parameterisations. Consequently, a comprehensive evaluation of the benefits and limitations of these recently released products is essential to understand their suitability for hydrological applications.

1.2. Research objectives

The overall aim of this thesis is to understand the hydrological responses of Mahanadi river basin in India, to the changing environment, including land cover and climate changes. In addition, the thesis investigates the hydrological responses to using various input datasets, including local or global data in a regional scale hydrological model. Mahanadi river basin is a large-scale (140,000 km²) river basin and is one of the twelve major river basins in India. This basin have undergone severe deforestation during last decades (Behera et al., 2018) and under the serious threat of increased flows during the wet period, which enhances the flood

potential (Jin et al., 2018; Raje et al., 2014). Several studies exist in this domain in various regions (Abe et al., 2018a; Eum et al., 2016a; Rodriguez and Tomasella, 2016), including river basins in India (Chawla and Mujumdar, 2015; Dadhwal et al., 2010; Das et al., 2018; Patidar and Behera, 2019). These studies have provided key insights into the mechanisms of environmental change impacts on hydrological responses; however, the uncertainty of these impacts is poorly understood (Chen et al., 2019b). These hydrological impacts are simulated using hydrological models in conjunction with different land cover or climate scenarios. However, hydrological models through their complex interactions among the model parameters to generate hydrological processes, can introduce significant uncertainties to the hydrological projections. The methodological approach for assessing the land cover and climate change impacts adopted in this study accounts for the uncertainties associated with modelling those hydrological responses, which shall possibly make the predictions more robust and reliable. Further, modelling hydrological responses in developing countries like India face challenges, because of acute shortages of in-situ hydro-meteorological data. However, recent advances in global data availability of the geophysical attributes, such as soil, vegetation and fine-scale meteorological data from the ever-expanding remote sensing activities, reanalysis products and other large data sets makes it a unique opportunity to evaluate such products in the region. The hydrological impacts in this thesis are modelled using a semi-distributed macroscale hydrological or a land surface model, known as Variable Infiltration Capacity model (VIC) (Nijssen et al., 1997). Prior to simulating these hydrological impacts, we performed a sensitivity guided model calibration to understand the important VIC model parameters across Mahanadi river basin, that would have a major control in simulating the hydrological components and analysed the performance of our calibration framework over the basin. Specifically, in this thesis we address the following main research questions: -

- 1) What are the sensitive VIC model parameters across Mahanadi river basin?
- 2) How does our calibration framework perform over the basin?
- 3) What are the expected impacts of LULC changes on the water balance components of the Mahanadi river basin?
- 4) What is the influence of future climate conditions on hydrological responses of Mahanadi river basin?

- 5) How reliable are the global datasets in producing a comparable hydrological model performance when compared against local observations?

Figure 1.3 outlines the content of the individual chapters of this thesis. Chapter 2 presents the descriptions of the research area and introduces all the input datasets (meteorological, soil and LULC) used in all research chapters and provides an overview of the VIC modelling including processes and parameterizations. The results of the thesis are described separately in the next four chapters. In Chapter 3, we address research question 1 and 2 where we design Monte Carlo experiments to perform a detailed sensitivity analysis of the VIC model parameters, calibrate, and validate the model at different subcatchments of Mahanadi river basin. Here, we intend to identify the behavioural parameter sets (behavioural models) for the research area to further model the impacts of environmental changes shown in the subsequent chapters. We address research question 3 in Chapter 4, where we implement these behavioural models, in conjunction with the land cover scenarios over Mahanadi river basin to assess the impacts on modelled discharge, and water balance components such as runoff and ET. Researchers formulate various land use or land cover change scenarios for the future and assess the hydrological impacts of those scenarios, such as based on socio-economic scenarios in Cornelissen et al., (2013), regional development plans in He and Hogue, (2012), hypothetical scenarios based on Oil-Sands development in Eum et al., (2016b) and extreme hypothetical scenarios, where entire river basin is replaced by predominating land use types in (Yang et al., 2014). The land cover scenarios that we used to address this question are most up-to-date scenarios, available from version 2 of the Land Use Harmonization (LUH2) dataset (Hurtt et al., 2018), which represents future changes in the LULC based on Shared Socioeconomic Pathways (SSPs) (O'Neill et al., 2016). We further explore the contribution of uncertainty from model parameterization to the hydrologic predictions due to LULC change.

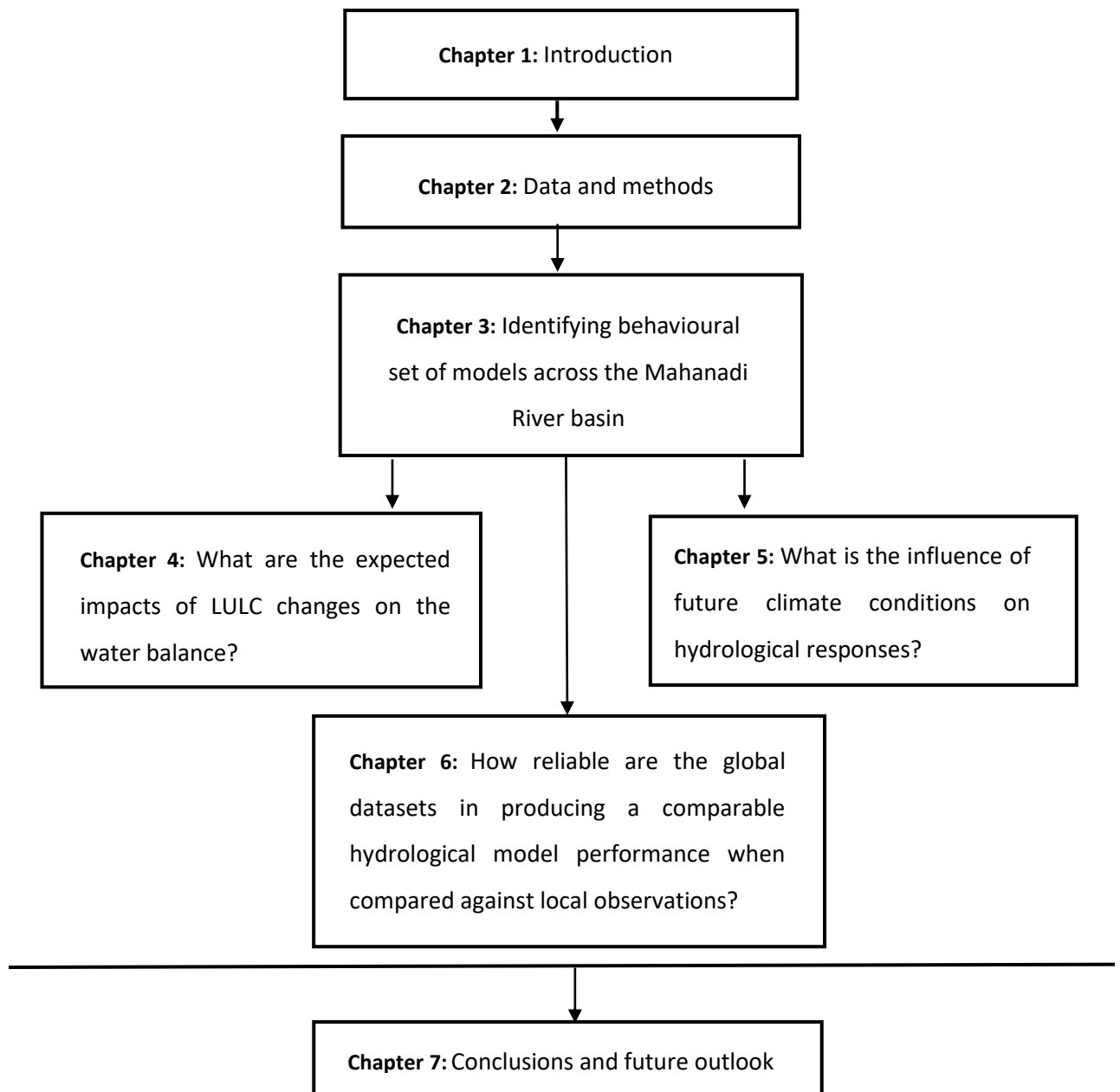


Figure 1.3: Summary of the thesis structure

We then address research question 4 in Chapter 5. We use the climate projections from latest global climate models from Coupled Model Intercomparison Project Phase 6 (CMIP6) (Mishra et al., 2020) and the behavioural hydrological models to assess the hydrological impacts in the basin. In chapter 6, we address research question 5. In this chapter, we evaluate the impacts of using global vs local datasets such as meteorological forcings, soil, and land use datasets, in a regional scale hydrological model, on discharge, runoff and ET. We identify critical input datasets which may have significant impacts on our model performance. Our intention here is to discern the hydrological impacts caused due to the changes in a model

input (local or global) or a combination of model inputs (local and global) in a data scarce region to provide a basis for relying on the global data in a regional scale hydrological model for future use.

2. Data and Methods

2.1. Study area

The Mahanadi river basin (Figure 2.1) is one of the major river basins located in eastern part of India draining an area of 141,589 km², which nearly accounts for 4.3% of the total geographical area of India. It extends from 80°28'E to 86°43 E and 19°8'N to 23°32' N. The river flows through the states of Chhattisgarh (53%) and Odisha (46.3%). The basin has a varying topography with its lowest elevated area (-17 m) lying in the coastal reaches and the highest elevated area (1323 m) in the northern hills. It ranks second after Godavari river basin in India in terms of water holding and flood producing capacity. Summer, Winter, monsoon and post monsoon are the 4 dominant seasons experienced by the river basin.

The basin is characterized by tropical climate zone and receives rainfall from southwest monsoons between June and October. The average annual rainfall is 1200 mm, with 90% of the total annual rainfall occurring during the monsoon months (Jin et al., 2018). The southwest monsoon is therefore the major controlling factor of river discharge in this basin. Figure 2.2a shows the seasonal rainfall pattern of the basin averaged for the time period 1951-2016. Figure 2.2b shows the daily discharge measured at Kantamal, a subbasin of Mahanadi, in a flood year, 2008. The uneven distribution of rainfall within the basin has resulted in recurrent floods in some parts of the basin such as at the eastern coast and drought in the central region of the basin (Dilley, 2005). The maximum temperature within the basin ranges between 39 and 45 °C and minimum temperatures varies between 4 and 12 °C. The long-term average annual rainfall and temperature trend in the basin is shown in Figure 2.3a and 2.3b. These trends are based on gridded rainfall datasets obtained from Indian Meteorological department (IMD).

The basin comprises of several water resource structures such as dams, weirs and barrages which stores the water for different purposes such as producing hydroelectric power, irrigation, supplying drinking water and regulating flood. Hirakud dam (shown in Figure 2.1)

with a length of 4800 m is the longest dam in the basin and is also considered as Asia’s largest dam with a catchment area of 83400 sq. km. This dam was constructed in the year 1957 mainly to alleviate the flood problems. Notice that about 65% of the basin is placed upstream of the Hirakud dam. Despite its significant storage capacity, the large flows from upstream of dam and middle reaches of the catchment causes devastating floods during the monsoon in the deltaic region of the basin (Jena et al., 2014). Please note as there is no major control structure located upstream of the Hirakud dam, the river discharge at the gauging stations (shown in Figure 2.1) are considered as unregulated, also followed in (Panda et al., 2013). The basin has been subjected to high floods frequently, exceeding $35000 \text{ m}^3\text{s}^{-1}$ in the past decades such as in the year 1980, 1982, 2001, 2003, 2006, 2008, and 2011, mainly due to the release of huge discharges from the Hirakud dam (Jena et al., 2014; Panda et al., 2013).

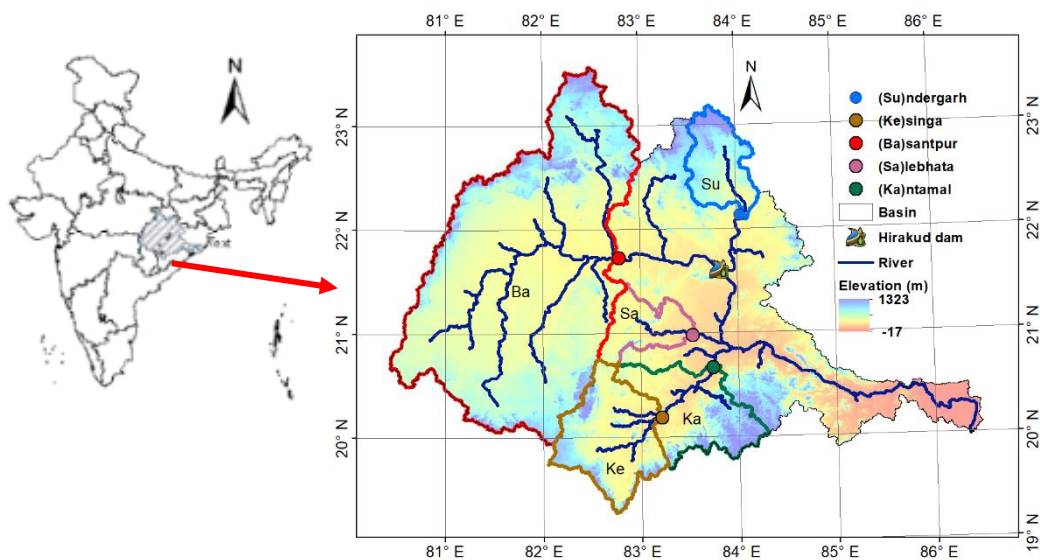


Figure 2.1 The Mahanadi river basin boundary and the analysed gauges and their catchments. Abbreviations for gauge names are Ba- Basantpur, Ka-Kantamal, Ke-Kesinga, Su- Sundergarh and Sa-Salebhata

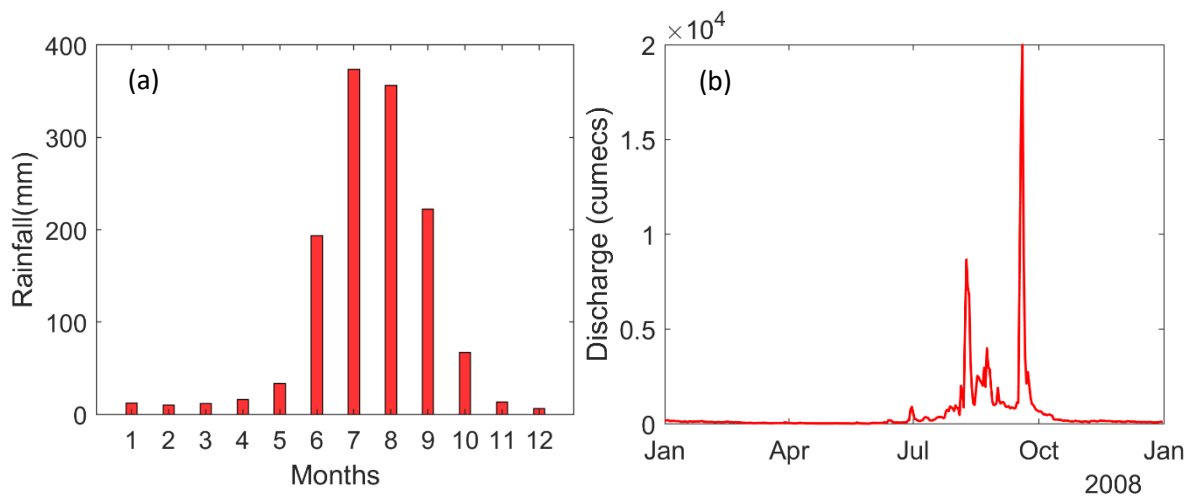


Figure 2.2. (a) Seasonal rainfall pattern averaged for the time period 1990-2016 in Mahanadi river basin (b) Measured daily discharge at Kantamal (subbasin of Mahanadi river basin) for year 2008.

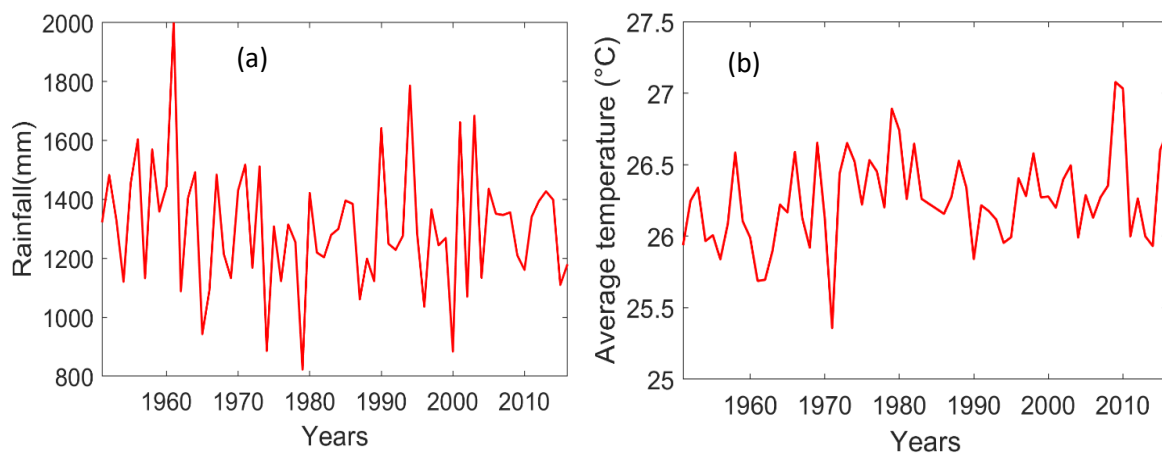


Figure 2.3. (a) Long term pattern of (a) mean annual rainfall (b) annual average temperature averaged over Mahanadi river basin of spatial area of 140,000 km², for the time period 1951-2016 obtained from Indian Meteorological Department (IMD)

The major vegetation types are forest and agriculture with approximately 30% and 48% of the basin area respectively. The Indian cropping season is classified into two main seasons 1) Kharif and 2) Rabi. 30% of the agricultural land is cropped during the kharif season, from July to October during the south-west monsoon and 3% during Rabi season from October to March during winter. Rest 15% of the agricultural land is under double or triple irrigation. Deciduous Broadleaved Forest (DBF) being dominant among other forest types, covers 25% of the basin area. Built up, plantation, grassland, shrubland, water bodies and other forest types constitute the rest 22 % of the basin area. Comparison of the LULC maps of 2005 and 2014, obtained from the National Remote Sensing Centre (NRSC), India shows an increase in

the agricultural land from about 43 to 48% at the expense of fallow land, built up areas and water bodies while changes in forest covers were insignificant. Figure 2.4 shows the percent change in the LULC classes obtained from LULC map of 2013-2014 relative to the LULC map of year 2005-2006. In addition, loamy and clayey are the major soil types covering roughly 53% and 42% respectively of the total basin area (NBBSS-LUP, India). Approximately 90% of the basin has moderately shallow to deep soil having depth greater than 50 cm. The population of Mahanadi river basin as per the census, 2001 is approximately 3 million out of which more than 1.49 million dwells in lower region of the basin.

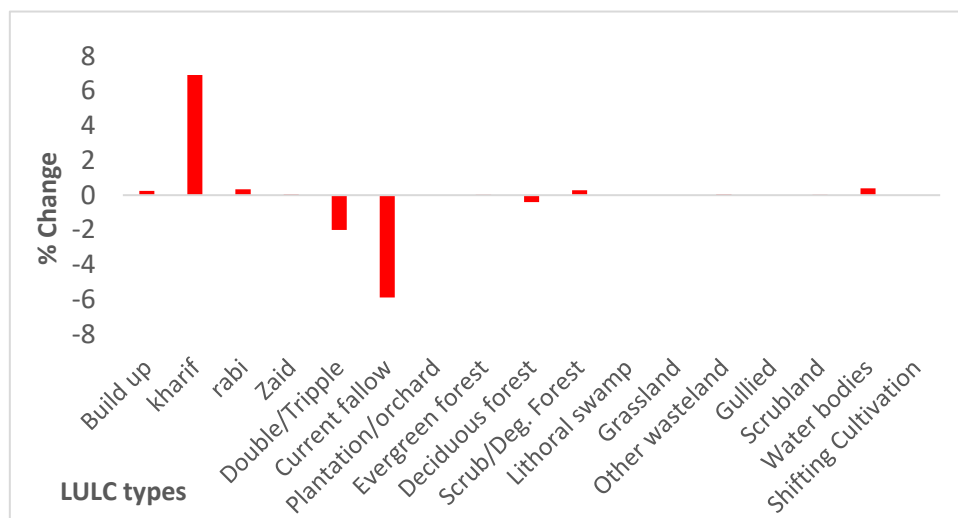


Figure 2.4. Percent change in the LULC classes obtained from LULC map of 2013-2014 relative to the LULC map of year 2005-2006, obtained from the National Remote Sensing Centre (NRSC)

Owing to the hydroclimatic sensitivity of this river basin (Panda et al., 2013), various researchers in the past have evaluated streamflow (including floods) change under the changing climate (Asokan and Dutta, 2008; Ghosh et al., 2010; Gosain et al., 2006; Jena et al., 2014; Jin et al., 2018; Panda et al., 2013; Raje et al., 2014). Mahanadi is a rain-fed river basin, mostly covered by agriculture and forest, however, have undergone severe deforestation during last decades mainly due to dam constructions, industrialization, urbanization and agricultural expansion (Behera et al., 2018). Studies assessing the LULC impacts on hydrology of this river basin also exists (Dadhwai et al., 2010; Das et al., 2018), however are limited compared to the climate impact studies.

2.2. Data

2.2.1. Meteorological data

2.2.1.1. Local gridded observations

The reference precipitation data set used is daily gridded precipitation product at a grid resolution, $0.25^\circ \times 0.25^\circ$, developed by the Indian Meteorological Department (IMD)(Pai et al., 2014) and archived at National Data Centre, IMD, Pune. The rain gauge observations are recorded from about 7000 rain gauges well-spread across India (A. K. Srivastava, 2009) and having 201 gauges within Mahanadi river basin. These rain gauge observations are interpolated using a modified version of the angular distance weighing algorithm, proposed by Shepard, (1968) to prepare the gridded rainfall dataset. Twelve years of records (January 1988–December 2016) for IMD are used for analysis in this study. This recently released dataset is an advancement over the previously used gridded rainfall dataset of 1° (Rajeevan et al., 2006, 2008) and 0.5° (A. K. Srivastava, 2009) from IMD and is comparable with other existing daily gauge based precipitation products (Pai et al., 2014). It is worth pointing out that other available gauge-based precipitation datasets use only a subset of rain gauge data sets over India (Prakash et al., 2018).

Daily gridded maximum and minimum temperature datasets are also obtained from IMD at a grid resolution, $1^\circ \times 1^\circ$. developed from 395 station observations across India using interpolation technique proposed by Shepard, (1968). There are 20 grids present within Mahanadi river basin (Srivastava et al., 2009). Temperature datasets from IMD are also found comparable with other existing datasets in the region.

Both rainfall and temperature datasets from IMD is extensively used in a variety of studies (Beria et al., 2017; Ghodichore et al., 2018; Mahto and Mishra, 2019; Mishra et al., 2020a; Prakash et al., 2016). All local gridded observations are re-gridded to spatial resolution of $0.05^\circ \times 0.05^\circ$ to be consistent with the VIC model grid resolution (See section 2.3) used in all the research chapters of this study.

2.2.1.2. Satellite observation

In this study, we used the recently released (June 2019) version (V06B) of Integrated Multi-Satellite Retrievals (IMERG) mission Early Run (Near real time product), with high spatial (0.1°)

and temporal (30 min) resolution (George et al., 2019). IMERG algorithm uses all available sensors of TRMM and GPM eras to provide high resolution global precipitation estimates. The latest version of this product, V06 is a retrospective processing of IMERG to TRMM era and uses new algorithm with several major improvements, which is believed to enhance the quality of the precipitation estimates (Tang et al., 2020). Since the reference gauge-based data set from IMD accumulates rainfall ending at 0300 UTC; we computed daily rainfall from half-hourly IMERG ending at the same time for being consistent. Precipitation products from IMERG are re-gridded to spatial resolution of $0.05^\circ \times 0.05^\circ$ to be consistent with the VIC model grid resolution used in all the research chapters of this study.

Several studies exist that assessed the quality of IMERG rainfall products and used this product (especially the previous versions) for hydrological applications worldwide (Gao et al., 2020; Gilewski and Nawalany, 2018; Sharifi et al., 2016; Sungmin et al., 2017; Tang et al., 2020; Zubieta et al., 2016), including in India (Beria et al., 2017; Prakash et al., 2016, 2018).

2.2.1.3. Reanalysis data

We derived hourly precipitation and temperature datasets from European Center for Medium-Range Weather Forecasts Reanalysis v5 (ERA5-Land) (Muñoz-Sabater et al., 2021). This is a recently released reanalysis product and replay of the land component of ERA5, which is also a new climate reanalysis dataset from ECMWF. ERA5-Land is based on several improvements and particularly an advancement over other recently released reanalysis product, such as having much finer spatial resolution of $\sim 9\text{km}$ compared to ERA5 (31 km) and ERA-Interim (80 km) and finer temporal resolution. In this study, we used the hourly temperatures to derive the daily maximum and minimum temperatures as required by the VIC model. Since the reference gauge-based data set from IMD accumulates rainfall ending at 0300 UTC; we computed daily rainfall from half-hourly ERA5-Land ending at the same time for being consistent. Both precipitation and temperature products are re-gridded to spatial resolution of $0.05^\circ \times 0.05^\circ$ to be consistent with the VIC model grid resolution used in all the research chapters of this study.

Local observations of daily wind speed are not available, hence were obtained from National Centers for Environmental Prediction (NCEP), and the National Center for Atmospheric Research (NCAR) reanalysis of resolution $1^\circ \times 1^\circ$ (Kalnay et al., 1996). This dataset is then further re-gridded to $0.05^\circ \times 0.05^\circ$ to be consistent with the VIC model grid resolution used in

all the research chapters of this study. Daily wind speed from NCEP-NCAR, in combination with precipitation and temperature extremes from IMD, has been tested for hydrological simulations of Indian river basins in previous studies (Hengade et al., 2018; Saha et al., 2014).

2.2.1.4. Historical and Future climate scenarios

Climate projections used in this study for Mahanadi river basin is derived from the recently released, bias corrected climate projections for South Asia from Coupled-Model intercomparison project-6 (Mishra et al., 2020a). The CMIP6 climate projections are produced with updated versions of climate models (than CMIP5) and are driven based on new future pathways of societal development, the Shared Socioeconomic Pathways (SSPs) scenarios and radiative concentration pathways (RCPs). These scenarios are produced with updated versions of integrated assessment models (IAMs) and recent emission trends (O'Neill et al., 2016).

These bias corrected data of precipitation, maximum temperatures and minimum temperatures are available at daily temporal and 0.25° spatial resolution for South Asian countries including 18 river basins in India. A total of thirteen GCMs (Table 2.1) are considered for bias correction based on the availability of all three climate variables and four scenarios, combining SSPs and RCPs at the end of 21st century (Gidden et al., 2019). These scenarios are SSP1-2.6, SSP2-4.5, SSP3-7.0, SSP5-8.5, explained in Table 2.2. For instance, SSP1-2.6 indicates SSP-1 and target radiative forcing of 2.6 Watt/m² at the end of the 21st century, which is a mitigation scenario (Gidden et al., 2019). More descriptions regarding these scenarios can be found in (Gidden et al., 2019).

Mishra et al., (2020a) employed Empirical Quantile Mapping (EQM) for the bias corrections of the historic (1951–2014) and projected (2015–2100) climate data. EQM is a statistical approach, based on the distribution and relationship between the observed and projected data for the historical period (Pierce et al., 2015). Observed daily gridded climate variables (gridded precipitation, maximum and minimum temperatures) from IMD (spatial resolution of 0.25°) is considered as a reference for the bias correction in Mishra et al., (2020a), as IMD datasets are widely used for hydroclimatic studies in India, and also station data is not available.

Table 2.1 CMIP6 GCMs considered for bias correction in Mishra et al., (2020a)

S. No.	Model name
1	ACCESS-CM2
2	ACCESS-ESM1-5
3	BCC-CSM2-MR
4	CanESM5
5	EC-Earth3
6	EC-Earth3-Veg
7	INM-CM4-8
8	INM-CM5-0
9	MPI-ESM1-2-HR
10	MPI-ESM1-2-LR
11	MRI-ESM2-0
12	NorESM2-LM
13	NorESM2-MM

Table 2. 2. Description of the Scenarios used in this thesis (Gidden et al., 2019)

Scenario Name	SSP	Target forcing level	Scenario type
		RCP (Wm^{-2})	
SSP126	1	2.6	Mitigation
SSP245	2	4.5	Mitigation
SSP370	3	7.0	Baseline
SSP434	4	3.4	Mitigation
SSP460	4	6.0	Mitigation
SSP585	5	8.5	Baseline

Figure 2.5 a-c shows the total annual precipitation, mean annual maximum and minimum temperatures, for the fifty-two ensembles (13 CMIP6 models*4 SSP based scenarios) (red colour) and the mean of the ensemble (blue colour) for the future period 2015-2100, for the entire Mahanadi river basin. The increase of both mean annual minimum and maximum temperature, based on the mean of the ensemble, is 0.3 °C per decade and mean annual rainfall shall increase with a rate about 42 mm per decade.

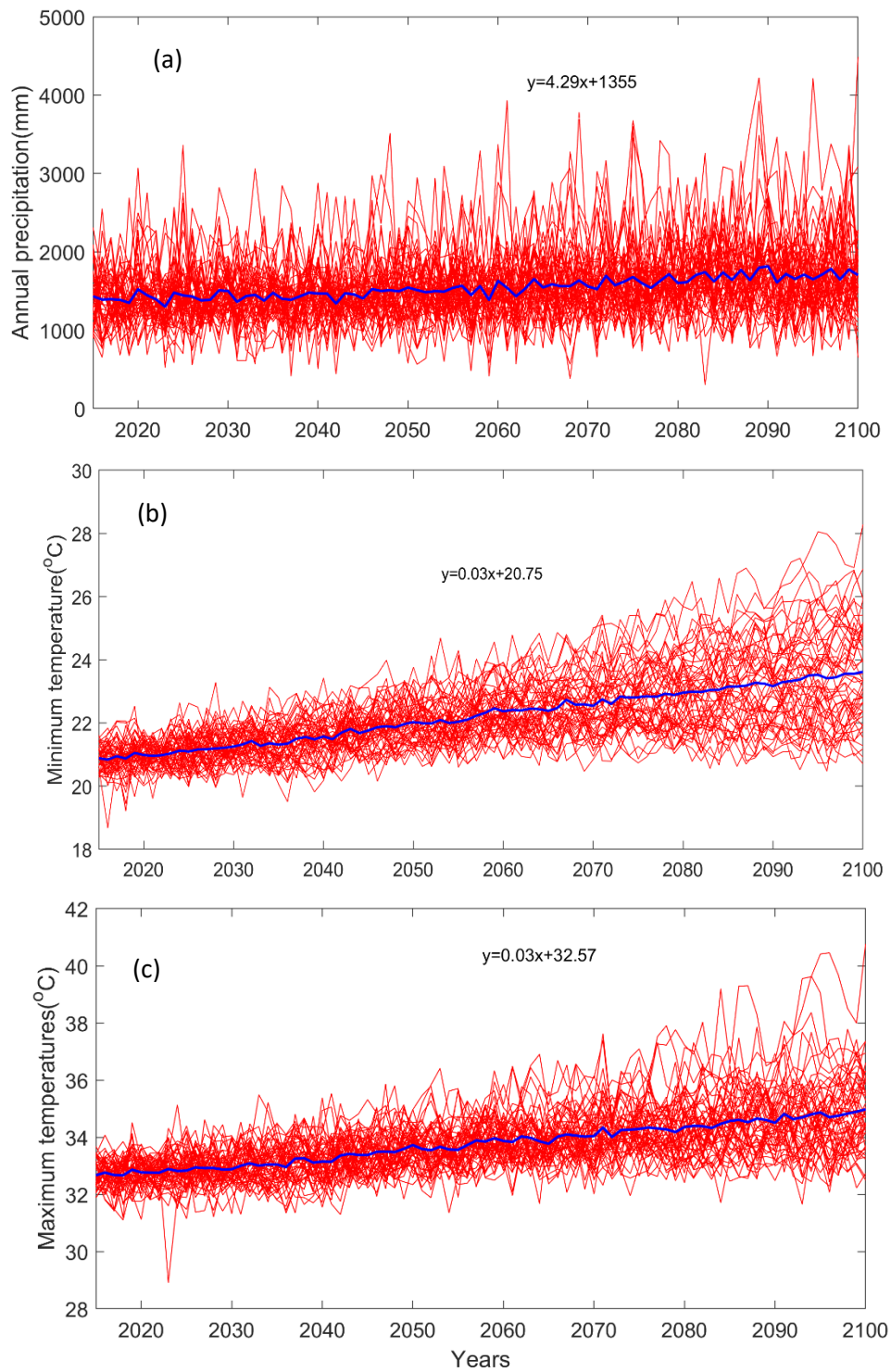


Figure 2.5 Projected (a) annual precipitation, (b) minimum and (c) maximum temperatures from 52 (13 models*4 scenarios) ensembles of CMIP6 (red) and the ensemble mean (blue), for Mahanadi river basin for the future period 2015-2100.

2.2.2. Ancillary data

2.2.2.1. Soil dataset

Local soil dataset

National or local level soil map (Figure 2.6 a) is derived from the digitized soil map as provided by National Bureau of Soil Survey and Land Use Planning (NBSSSLUP) of spatial resolution of 500 metres (Scale 1:250000). Loam and clay are the dominant soil textures within the basin. The local soil map is resampled to model grid size of 0.05°. X 0.05°.

Global soil dataset

Global gridded soil textures (Figure 2.6 b) are derived from SoilGrids (Hengl et al., 2017), recently released most detailed global soil dataset, of resolution 250 m. The soil texture fractions of clay, sand and silt in SoilGrids are mapped at 7 standard depths ranging from 0 to 200 cm. There were not many differences observed in the soil fractional maps at individual depths. We averaged soil fraction maps of 30, 60, 100 and 200 cm (typical VIC soil depths for individual soil layers respectively) and resampled to model grid size of 0.05°. X 0.05°. Next, zonal statistics of the soil fractional maps is performed with respect to the model grid in ArcMap to obtain fraction of clay, sand and silt for each grid. USDA soil classification is then used to generate mean soil texture for each VIC model grid. As per the global soil map, clay loam and clay are the dominant soil types in the river basin.

We observe differences in the soil textures, and also fractional area covered by each soil type, while comparing both soil maps. Local soil map indicates loam (54%) and clay (42%) are the dominant soil textures within the basin whereas clay (29) and clay loam (69) are found to be dominant in the global soil map.

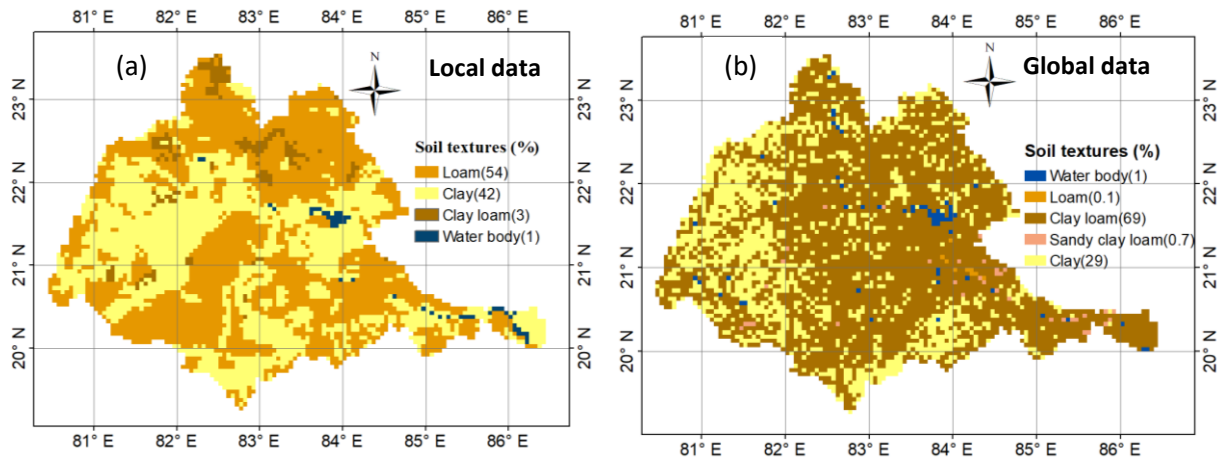


Figure 2.6 (a) National soil map derived from National Bureau of Soil Survey and Land Use Planning (NBBSSLUP) with a spatial resolution of 500 metres and (b) Global soil map derived from SoilGrids with a spatial resolution 250 metres for the Mahanadi river basin. The spatial resolution of the maps shown here is 5km which is used by the VIC model to perform the simulations.

2.2.2.2. LULC dataset

Local LULC dataset

National level or local LULC map is derived from National Remote Sensing Centre (NRSC) of year 2005 and 2014 (scale 1:250000) of resolution 56 meters. Figure 2.7 a shows LULC map of year 2014 to enable comparison with the global LULC map.

Global LULC dataset

Global LULC map (Figure 2.7 b) for the year 2015 is obtained from the recently released, European Space Agency Climate Change Initiative (ESA CCI) (version 2.0.7) (Jiang and Yu, 2019). ESA CCI is a consistent series of annually generated land cover products for the period 1992-2015 at a complete range of 38 land cover types.

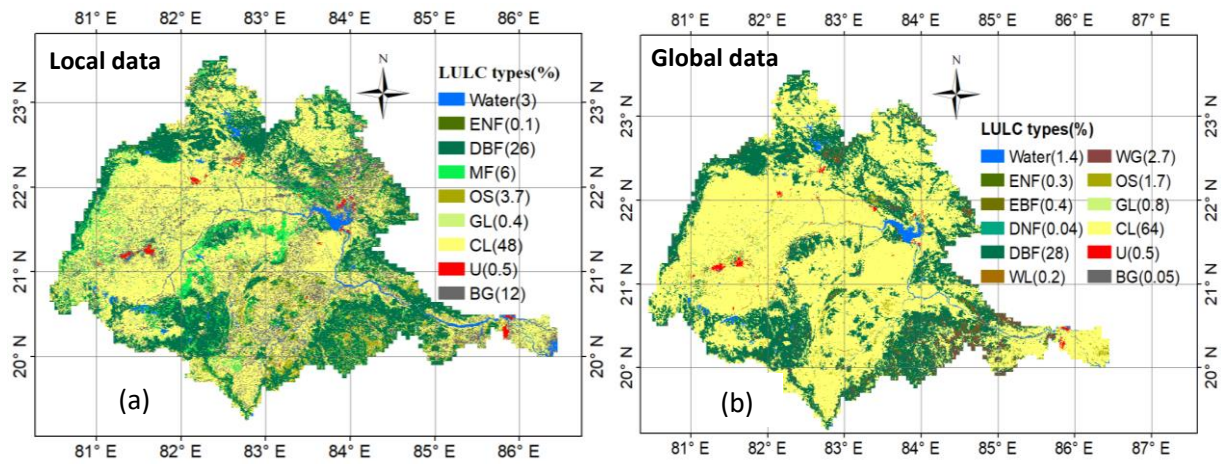


Figure 2.7 (a) National LULC map derived from National Remote Sensing centre (NRSC), India of year 2013-2014 of resolution 56 meters and (b) Global LULC map derived from ESA CCI of year 2014 of resolution 250 metres

Both the local and global LULC maps are resampled to the model grid size of $0.05^\circ \times 0.05^\circ$. Both the local and global LULC maps are reformatted and reclassified into USGC LULC types as required by the VIC model. Both LULC maps show that Deciduous Broadleaf Forest (DBF) and cropland (CL) are the major land cover types in the basin. However, we observe that percentage of area covered by both land cover types varies, especially in cropland, which covers 64% in global map whereas 48% in the local map.

2.2.2.3. Historical and Future land cover scenarios

We used a set of land use scenarios based on Socio-economic Pathways (SSPs) and Representative Concentration Pathways (RCPs), from the recently released , Land Use Harmonization Project (LUH2) data set (release “LUH2v2h” and LUH2v2f) for the time period of (850–2005) and (2015-2100) respectively (Hurtt et al., 2018) (Table 2.3). These scenarios are the combination of RCP’s projecting the magnitude and extent of climate change (Taylor et al., 2012; van Vuuren et al., 2011) and SSP’S (Hausfather, 2018) based on worlds of various levels of challenges to adaptation and mitigation (van Vuuren et al., 2014).

Table 2.3 LUH2 future scenarios and models used in the thesis. Description of the Scenarios can be found in Table 2.2.

Scenarios	Models
RCP2.6 SSP1	IMAGE
RCP3.4 SSP4	GCAM
RCP4.5 SSP2	MESSAGE-GLOBIOM
RCP6.0 SSP4	GCAM
RCP7.0 SSP3	AIM
RCP8.5 SSP5	REMIND-MAGPIE

The LUH2 approach estimates the gridded land use fractions, annually at a resolution of 0.25°. The land use fraction maps are therefore available for each land use type at a resolution of 0.25°. So, we have first obtained LUH2 fraction maps of different LULC types for Mahanadi basin extent at a resolution of 0.25° and further re-gridded to the model grid size of 0.05°. Land cover changes and fractional area covered in each of these scenarios are shown in Figure 2.8.

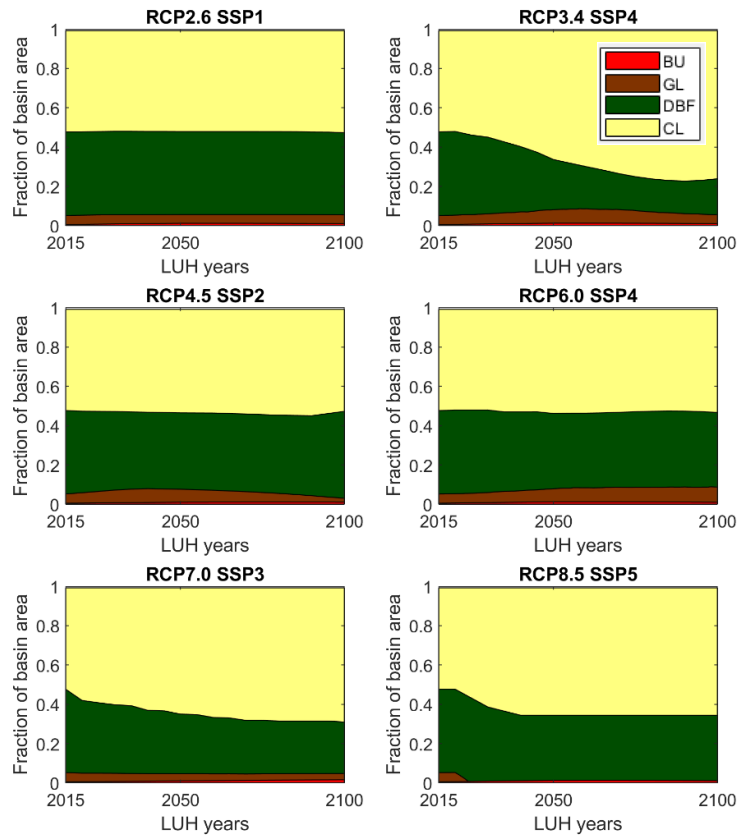


Figure 2.8 Land cover changes and fractional area covered in all LUH2 scenarios mentioned in Table 2.3.

2.2.3. Validation data

Observed streamflow data for five subbasins Basantpur, Kantamal, Kesinga, Sundergarh and Salebhata (shown in Figure 2.1), are obtained at a daily scale, for the time period 1989 – 2016 from Central Water Commission (CWC), India. Observed streamflow data obtained are used for model set up, calibration and validation. Information about the gauging locations is given in Table 2.4.

Table 2.4 Gauging stations and their descriptions

Gauging station	Catchment area (km ²)	Period	Mean discharge (m ³ s ⁻¹)	Maximum discharge (m ³ s ⁻¹)
Basantpur	57780	1989-2016	665	33088
Kantamal	19,600	1989-2016	375	20000
Kesinga	11,960	1989-2016	246	21192
Sundergarh	5870	1989-2016	102	10404
Salebhata	4650	1989-2016	63	7916

2.2.4. Summary of datasets used in each chapter

All result chapters i.e., chapter 3 to 6 have used the meteorological datasets (precipitation, maximum and minimum temperature) from Indian Meteorological Department (IMD), and soil and LULC datasets from NBBSS&LUP and IGBP respectively. However, the time period of the meteorological forcings used in each chapter are different. Land cover scenarios from LUH2 and climate scenarios from CMIP6 are used in chapter 4 and 5 respectively. Global soil and LULC datasets from SoilGrids and ESA CCI respectively, and meteorological datasets from satellite (IMERG) and reanalysis products (ERA5-Land) are used in Chapter 6. The detailed information of all input datasets used in the chapters is summarized in Table 2.5.

Table 2.5: Data information used in this thesis.

Chapter	Input data	Data type	Data Source	Resolution	Period/Year
Chapters 3,4,5,6	Precipitation			0.25° X 0.25°	
	Max. Temp.	Local gridded	IMD	1° X 1°	1989-2010
	Min. Temp.				
	Wind Speed	Reanalysis	NCEP	1° X 1°	
	Soil	Local	NBSS&LUP	500 m	2005/2006
	Land cover	Local	IGBP	56 m	
Chapter 4,5	Land cover scenarios	Global	LUH2	0.25° X 0.25°	2005-2100
Chapter 5	Climate scenarios	Global	CMIP6	0.25° X 0.25°	1990-2100
Chapter 6	Precipitation	Satellite	GPM IMERG		
	Precipitation			0.01° X 0.01°	2014-2016
	Max. Temp.	Reanalysis	ERA5-Land		
	Min. Temp.				
	Precipitation	Local gridded	IMD	0.25° X 0.25°	
	Soil	global	SoilGrids	250m	-
Land cover	global	ESA CCI	300m	2015	

2.2.5. Comparisons between local, satellite and reanalysis meteorological observations

Quality comparisons of the precipitation and temperature products for the analysis period (2014-2016) are performed prior to using these datasets as the model inputs to capture the hydrological responses in Chapter 6. Note that year 2014-2016 is the common period of data for both precipitation and temperature, available from all three different sources mentioned in the previous section.

To enable comparisons, precipitation datasets from IMERG and ERA5-Land are re-gridded to the spatial resolution of the reference precipitation dataset, IMD (0.25° X 0.25°). To achieve

this, IMERG and ERA5-Land gridded precipitation values (0.1°) are first resampled to 0.05° and then spatially averaged to 0.25° to match each target grid of IMD. Similar approach has also been applied in other studies (Essou et al., 2016; Mahto and Mishra, 2019; Prakash et al., 2018). Figure 2.9 shows spatial distributions of mean annual rainfall over Mahanadi river basin for all three datasets averaged for the time period 2014-2016 at a common resolution of 0.25°.

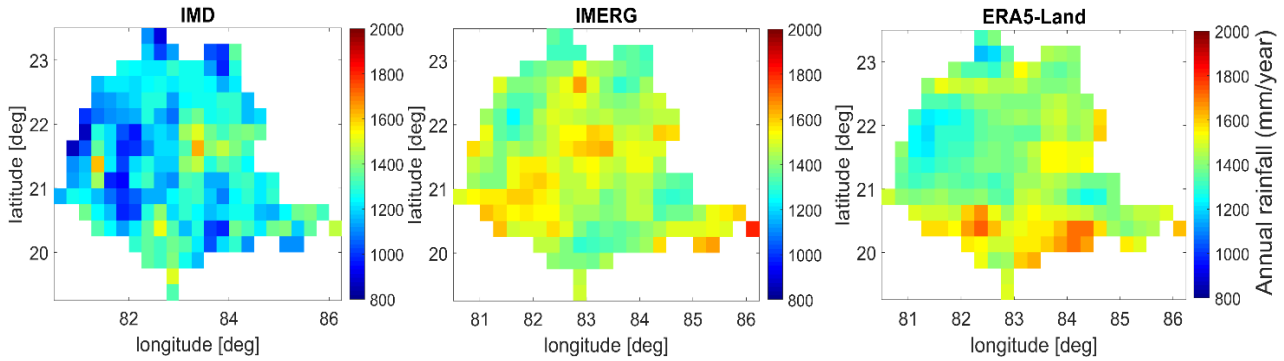


Figure 2.9: Spatial distributions of mean annual rainfall over Mahanadi river basin averaged for the time period 2014-2016, derived from IMD gauge-based, IMERG, and ERA5-LAND precipitation datasets

Two skill measures are used to statistically evaluate the different precipitation and temperature datasets (Pearson correlation coefficient (r) (Eq. 2.1), and percentage bias (PBIAS) (Eq. 2.2). The comparison between the rainfall and temperature products from different sources are beneficial to understand their error characteristics and how it propagates to the estimated hydrological components.

$$r = \left(\frac{\sum_{i=1}^n (O - \bar{O})(P - \bar{P})}{\sqrt{\sum_{i=1}^n (O - \bar{O})^2 \sum_{i=1}^n (P - \bar{P})^2}} \right)^2 \quad \text{Eq. 2.1}$$

$$PBIAS = \frac{\sum_{i=1}^n (O - P) \cdot 100}{\sum_{i=1}^n O} \quad \text{Eq. 2.2}$$

Where O and P are the observed (IMD) and predicted (IMERG and ERA5-Land) rainfall and temperature values respectively and \bar{O} and \bar{P} are the observed mean and predicted mean. n is the number of data points. The skill measures for the global rainfall and temperature products against locally available data from IMD are computed and represented spatially for the entire Mahanadi river basin averaged for the time 2014-2016, shown in Figure 2.10 and 2.12.

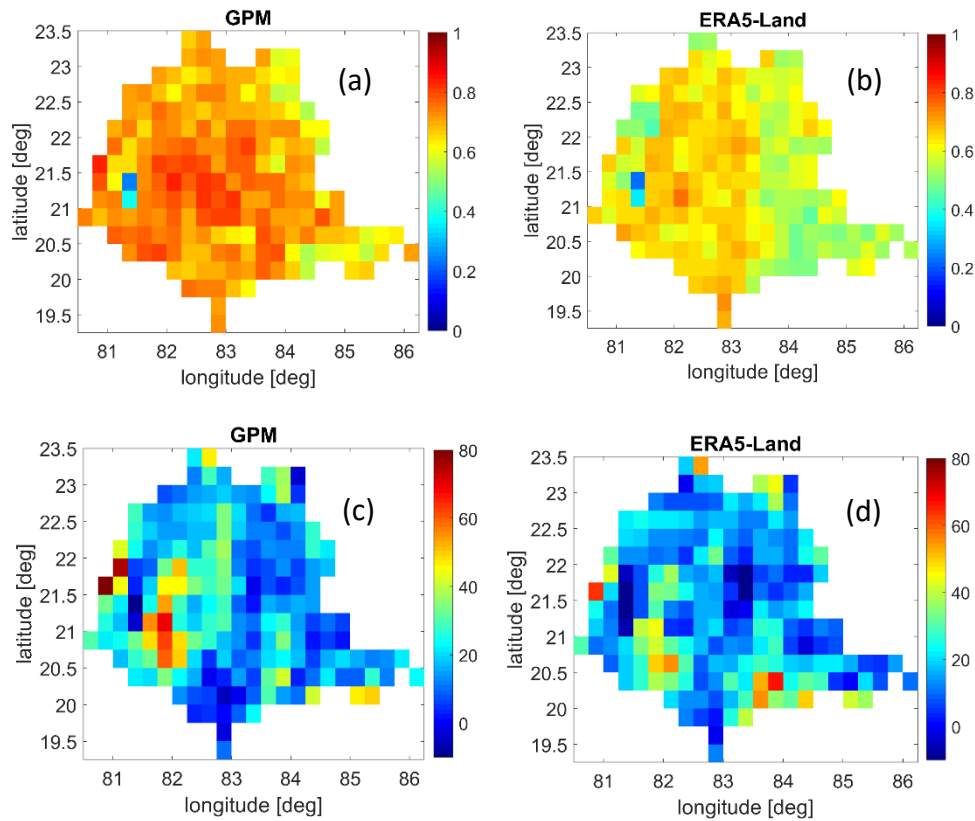


Figure 2.10: Spatial distributions of (a) Correlation between GPM and IMD (b) Correlation between ERA5-Land and IMD (c) PBIAS of GPM against IMD (d) PBIAS of ERA5-Land and IMD daily rainfall over Mahanadi river for 2014-2016.

Correlation pattern suggests IMERG precipitation is more correlated to the reference precipitation, IMD in the basin with an average correlation of 0.7 compared to ERA5-Land of average correlation 0.6. Spatial bias maps suggest similar bias pattern in both IMERG and ERA5-Land precipitation in almost entire basin and both rainfall products are found to be positively biased indicating overestimation of rainfall values. But the overestimation is higher in IMERG with an average (spatially) positive bias of 21% than ERA5-Land of 17%. Temporal correlation between IMD and IMERG is in the range of 0.72-0.86 across the subbasins which is higher than ERA5-Land (0.59-0.79) (Not shown here). Minimum correlation in Figure 2.10, a & b and maximum negative bias in Figure 2.10, c & d is observed in 2 grids (See the grids with latitude-21-21.5 and longitude 81.25-81.5). This is because annual precipitation in IMD gridded data (in the range of 1434-1619 mm) at these grids are higher than the annual precipitation in GPM (1387-1393 mm) and ERA5-Land (1278-1337 mm). We have analyzed IMD precipitation of individual years 2014, 2015 and 2016, and found that the higher annual

precipitation values in IMD is mainly due to the very high daily precipitation values (such as 397mm and 673mm) recorded in year 2016.

Daily maximum and minimum temperatures from ERA5-Land of spatial resolution 0.1° are re-gridded to 1° , spatial resolution of IMD maximum and minimum temperatures. Owing to the coarse resolution of IMD temperatures, there are only few grids in the entire basin. So, we compared max. and min. temperatures from ERA5-Land and IMD (See Figure 2.11) for the entire river basin. Both maximum and minimum temperatures from ERA5-Land showed high spatial correlation with an average of 0.93 and 0.96 (Figure 2.12). The temporal correlation coefficient between the daily time series of IMD max. temp. and ERA5-Land max. temp. is 0.94 and IMD min. temp. and ERA5-Land min. temp. is 0.95. Spatial RMSE shows that in overall, error in the maximum temperature (2.39) is more than the minimum temperature (1.6). Spatial bias maps indicate that the maximum temperature in ERA5-Land is mostly negatively biased i.e., has the tendency to underestimate whereas minimum temperature is mostly positively biased i.e., has the tendency to overestimate. Average bias in the maximum temperature and minimum temperature across the basin is (-5%) and (4%) respectively.

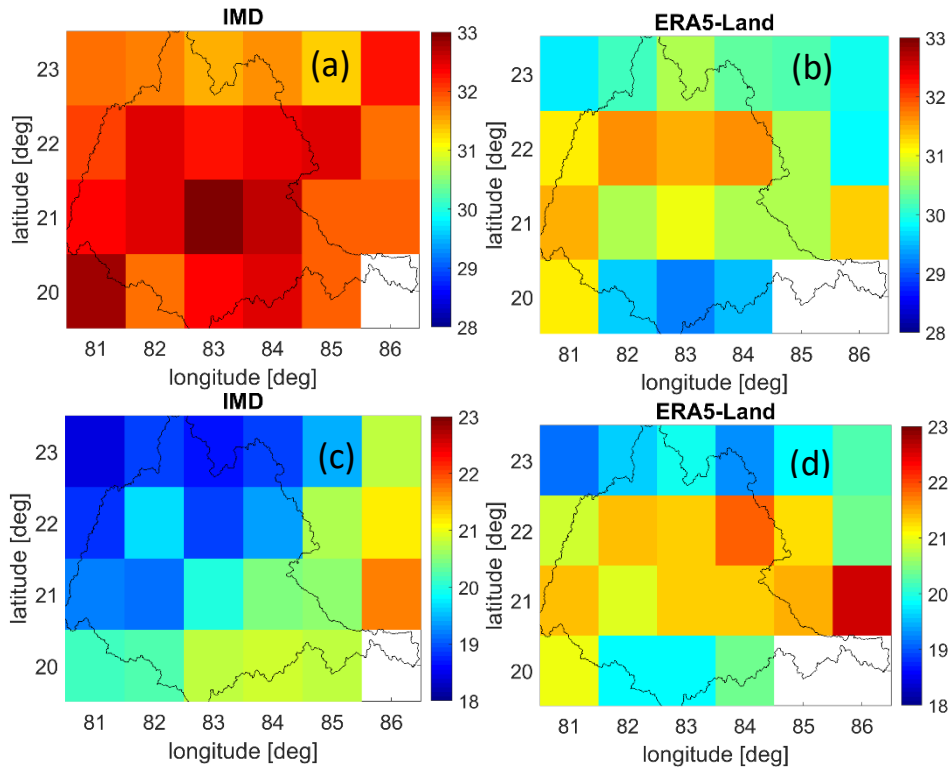


Figure 2.11: Spatial distributions of mean daily maximum temperature derived from (a) IMD and (b) ERA5-LAND. Spatial distributions of mean daily minimum temperature derived from (c) IMD and (d) ERA5-Land. averaged for the time 2014-2016

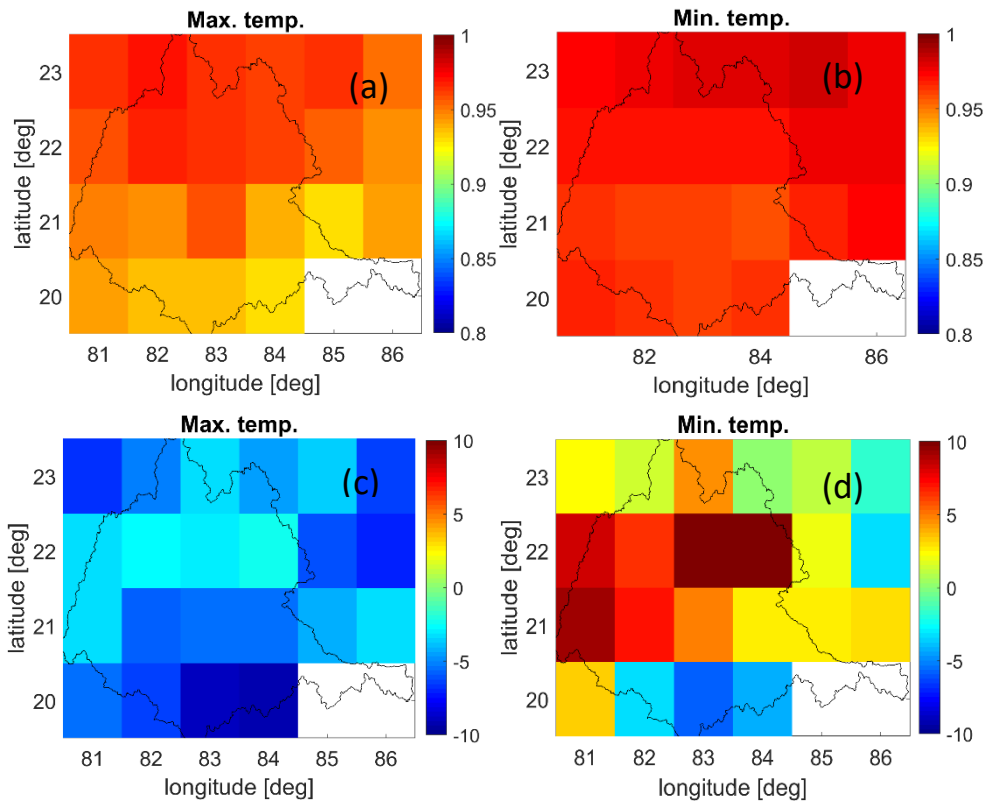


Figure 2.12: Spatial distributions of (a) Correlation between maximum temperature from ERA5-Land and IMD (b) Correlation between minimum temperature from ERA5-Land and IMD (c) P-Bias between maximum temperature from ERA5-Land and IMD (d) P-Bias between minimum temperature from ERA5-Land and IMD, over Mahanadi river averaged for 2014-2016.

2.3. Variable Infiltration Capacity (VIC) model

The VIC model (Figure 2.13 a) is a semi-distributed, land surface hydrologic model which solves both water and energy balance within the grid cells (Cherkauer and Lettenmaier, 1999). VIC was originally developed as a land surface model, however, the model has been predominantly employed in uncoupled modelling studies, where there is no feedback from the land surface to the atmosphere (Hamman et al., 2018). VIC model was first described as a single soil layer model and employed the runoff and infiltration scheme from Xianjiang model (Zhao et al., 1980). Next, (Liang et al., 1994) introduced the two soil layer VIC model (VIC-2L) which included multiple soil layers and spatially varying vegetation types within the grid cells. (Liang et al., 1996) found, VIC-2L had a tendency to underestimate the ET due to the lack of soil moisture movement from the bottom soil layer to the topsoil layer. The diffusion of moisture between the layers is then enabled and an additional 10cm soil layer is

added on top to generate VIC-3L model. To obtain the discharge at the basin outlet, the VIC-3L model is coupled to a stand-alone routing model (Lohmann et al., 1996).

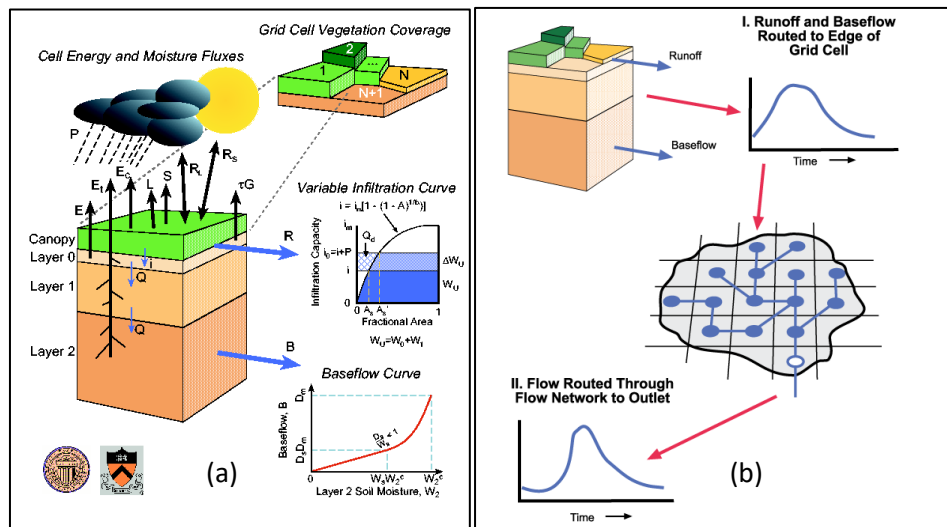


Figure 2.13: (a) Schematic diagram for Variable Infiltration Capacity (VIC) macroscale hydrological model (b) Schematic diagram of VIC river network routing model (Gao et al., 2010)

2.3.1. Water balance processes

Equation 2.3 (Gao et al., 2010) below shows the water balance in the VIC model, computed at every time step.

$$\partial s / \partial t = P - E - R \quad \text{Eq. 2.3}$$

$$\frac{\partial w_i}{\partial t} = P - E_C - P_t \quad \text{Eq. 2.4}$$

where $\partial s / \partial t$, P , E , and R are the change of soil moisture storage, precipitation, evapotranspiration, and runoff, respectively. Within the time step, all variables are in mm. Precipitation when falls over vegetated areas is termed as throughfall (P_t). Eq. 2.4 (Liang et al., 1994) shows the water balance equation in the canopy layer (interception), where w_i is canopy intercepted water (mm), E_C is evaporation from canopy layer (mm), and P_t is throughfall (mm) (Gao et al., 2010).

Evapotranspiration

The model considers three kinds of evaporation to compute the total evapotranspiration: evaporation from canopies from each vegetation tile, transpiration from each vegetation tile and evaporation from bare soil. Total evaporation is computed by using Eq. 2.5 shown below.

$$E = \sum_{n=1}^N C_n (E_{c,n} + E_{t,n}) + C_{N+1} \cdot E_1 \quad \text{Eq. 2.5}$$

Where C_n is the fractional area of n^{th} vegetation tile, $E_{c,n}$ and $E_{t,n}$ is the canopy evaporation and transpiration for n^{th} vegetation tile respectively, E_1 is the bare soil evaporation, N is the total number of vegetation types, C_{N+1} is the fraction of bare soil and $\sum_{n=1}^{N+1} C_n = 1$ (Gao et al., 2010).

Another important vegetation parameter in VIC is Leaf Area Index (LAI) which governs the amount of water intercepted by the canopy. The relationship between vegetation transpiration (E_t) and LAI is shown in Eq. 2.6 and Eq. 2.7.

$$E_t = \left(1 - \left(\frac{W_i}{W_{im}}\right)^{2/3}\right) E_p \frac{r_w}{r_w + r_0 + r_c} \quad \text{Eq. 2.6}$$

$$r_c = \frac{r_0 g_t g_{vpd} g_{PAR} g_{sm}}{LAI} \quad \text{Eq. 2.7}$$

W_{im} (mm) is the maximum amount of rain that canopy can intercept. E_p is the potential evaporation, computed using the Penman-Monteith equation. Aerodynamic resistance r_w ($s\ m^{-1}$) is the transfer of heat and water vapor from the canopy surface to the air. r_0 ($s\ m^{-1}$) is the architectural resistance, which is caused by the variation of the humidity gradient between the canopy and the air above canopy. r_c is the canopy resistance ($s\ m^{-1}$), is a function of LAI, minimum canopy resistance ($s\ m^{-1}$) and four environmental factors, temperature factor g_t , vapor pressure deficit factor g_{vpd} , photosynthetically active radiation flux g_{PAR} , and soil moisture factor g_{sm} respectively (Gao et al., 2010).

Bare soil evaporates only from the top thin soil layer. When the surface soil is saturated, bare soil evapotranspiration occurs at a same rate of potential ET. When top thin soil layer is not saturated, bare soil ET in VIC is a function of infiltration capacity of the surface soil, estimated using the ARNO formulations by (Franchini and Pacciani, 1991). The infiltration capacity is expressed as

$$i = i_m (1 - (1 - A)^{1/b_i}) \quad \text{Eq. 2.8}$$

$$i_m = (1 + b_i) \cdot \theta_s \cdot |Z| \quad \text{Eq. 2.9}$$

Where i_m is the maximum infiltration capacity (mm), A is the fraction of area for which the infiltration capacity is less than i , b_i is the infiltration shape parameter, θ_s is the soil porosity, and z is the soil depth (m).

Soil Moisture and Runoff

A Variable Infiltration Curve (Zhao et al., 1980) is used to generate the grid based runoff within the model. Surface runoff or the direct runoff occurs from the top thin layer and middle soil layer in the model. Sub surface runoff or baseflow is estimated by Arno model conceptualization. Q (Eq. 2.10) is the total runoff comprising of surface runoff and baseflow.

$$Q = \sum_{n=1}^{N+1} C_n \cdot (Q_{d,n} + Q_{b,n}) \quad \text{Eq. 2.10}$$

Where Q_d is the direct or surface runoff and Q_b is the sub-surface runoff or baseflow.

VIC model assumes there is no lateral flow in the top two soil layers and movement of soil moisture only occurs vertically. The movement of soil moisture i.e., the drainage from one layer to another is designed using one dimensional Richard's equation, which is a function of saturated hydraulic conductivity (Wang et al., 2008). Drainage and sub-surface drainage occurring from the third soil layer combine to form baseflow. The parameters used by the Arno formulation to compute baseflow are maximum sub surface flow ($dsmax$), fraction of $dsmax$ (ds), fraction of maximum soil moisture in the third soil moisture layer (ws). Maximum soil moisture is the porosity of the soil layer θ_s multiplied by the soil depth. Baseflow is assumed to be linear below threshold ($ws\theta_s$) and non-linear above the threshold. More details on soil moisture and runoff generation processes can be found in Liang et al., (1996).

2.3.2. Routing model

VIC has a stand-alone routing model (Figure 2.13b) that mainly calculates the concentration time of the runoff flowing to the outlet of the grid cell as well as channel flow in the river network. Most horizontal flows at each grid joins the channel network within the grid cell before it passes on to the adjacent grid cell. Daily surface and subsurface flows from the channel network are first routed to the outlet of the grid using a triangular shaped unit hydrograph and then routed to the basin outlet through the river network using the linearized Saint-Venant equation (Lohmann et al., 1996). Wave velocity (v) and Diffusivity ($diff$) are the two effective river routing parameters, used in Saint-Venant equation.

The model version used in this study is VIC 4.2.d. We implemented VIC-3L model in the water balance mode at a daily time step and at a grid resolution of 0.05° over the 5 subcatchments of the Mahanadi river basin. Flows are routed to the subcatchments of Basantpur (Ba), Kantamal (Ka), Kesinga (Ke), Sundergarh (Su) and Salebhata (Sa) (Figure 2.1). We abstained from routing the flow for the entire Mahanadi river basin due to the presence of a major water management structure, Hirakud dam at the middle reach of the basin.

2.3.3. Model parameterization

2.3.3.1. Soil parameters

VIC requires a soil parameter file as an input, where the unique soil properties are described for each grid cells in the model domain. This file also indicates which grids are to be simulated and their latitude and longitudes to find the forcing files (having meteorological input values) for the grid cells. The VIC model developers categorizes the soil parameters into two types: parameters that can be derived from the existing global databases and literatures (Cosby et al., 1984; FAO 1998; Rawls et al., 1998; Reynolds et al., 2000), hence need not to be adjusted. These parameters are soil porosity (θ_s), field capacity (fc), wilting point (Wp), saturated hydraulic conductivity ($Ksat$), and the exponent for the unsaturated flow (Exp). Next are those which are most sensitive for most climatic, edaphic and physiographic watershed settings and cannot be obtained by field measurements and therefore are subjected to calibration. These include infiltration related parameter ($binf$), depths of each soil layer ($d1$, $d2$ and $d3$) and baseflow related parameters, $dsmax$, ds and ws . However, we also test the sensitivity of some rarely implemented soil properties, that are selected based on our preliminary experiments, known sensitive model properties and previous studies. These parameters are Bulk density (BD), Fractional water content at wilting point (Wcr_f) and at critical point (Wcr_f), $ksat$ and Exp . The dominant soil textures within the basin derived from national level soil map, are loam, clay loam and clay. The specific soil characteristics for each dominant soil texture obtained from (Cosby et al., 1984; Rawls et al., 1998; Reynolds et al., 2000) are given below in table 2.6 and the equations for estimating these soil parameters are given in Table 2.7.

Table 2.6 Hydraulic properties of the dominant soil textures in Mahanadi river basin

Texture	Bulk Density (kg/m ³)	Field Capacity (FC)	Saturated Hydraulic Conductivity (<i>K_{sat}</i>) (cm/hr)	Slope of Retention Curve (in log space) <i>b</i> **
Loam	1490	0.29	1.97	5.3
Clay loam	1430	0.34	1.77	8.02
Clay	1390	0.36	3.18	12.28

Table 2.7 Soil parameters and equations used for estimation of these soil parameters

Parameters	Equations
Porosity	$\theta_s = 1 - \frac{BD}{PD}$
Soil moisture at critical point	$W_{cr} = 0.7 * FC$
Initial soil content	$Ini.SM = 0.7 * Max.SM$
Maximum soil moisture	$Max.SM = P * d_n$
Fractional Soil moisture content at critical point	$W_{cr_f} = \frac{W_{cr}}{P}$
'n' is the exponent used in Campbell's equation for hydraulic conductivity	$n = 3 + 2 * b$

where BD is bulk density, and PD is particle density. A standard value of 2.65 g/cm³ was used for PD, as spatial measurements were not available.

2.3.3.2. Vegetation parameters

We first prepare a vegetation parameter file that states the vegetation composition of each grid cell within the basin. Vegetation in VIC is represented by a mosaic scheme where a single grid cell can have multiple vegetation types i.e., VIC maintains vegetation heterogeneity within a grid cell. We then set up a vegetation library file for the selected land cover classes for the study area which consists of the vegetation properties of all vegetation types. Each vegetation type in the parameter file is then cross-indexed to the vegetation library file. Land cover classes from different input data sources are converted into representative land use types for the VIC model based on the classes in its standard vegetation library. Land cover

classes are described using the vegetation parameters such as LAI, albedo, roughness length, rooting depths and fractions, and other related biophysical parameters. Monthly LAIs were obtained from the moderate resolution imaging spectroradiometer (MODIS)/terra+Acqua, 8-day product (MCD15A2H) of 500 m resolution (Myneni et al., 2015). Parameters such as albedo, roughness length and displacement height are assembled based on Land Data Assimilation System (LDAS) (<http://ldas.gsfc.nasa.gov/>) and Hansen et al., (2000). Details of the vegetation parameters including LAI, albedo, displacement height and roughness, for the dominant vegetation types in the study area are shown in Table 2.8. Vegetation parameters are kept same for all the simulations conducted in this study. Therefore, hydrological impacts of land cover change are limited to the changes in the distribution of different land cover types and not in the parameter values of the land cover types themselves (Mishra et al., 2010). Minimum stomatal resistance and architectural resistance are subjected to sensitivity analysis (see Table 3.1, Chapter 3). Most vegetation parameters in VIC are static, only LAI changes monthly to capture the seasonal variability. However, these monthly values remain constant throughout the simulation period. The root allocation approach employed in this study is described in section 2.3.5.

Table 2.8 Details of the vegetation parameters for the dominant vegetation types in Mahanadi river basin

Description	Albedo	LAI _{min}	LAI _{max}	Roughness length (m)	Displacement height (m)
Deciduous broadleaf forest	0.08	0.91	2.75	0.83	15.36
Cropland	0.09	1.72	0.27	0.08	0.26
Grassland	0.11	0.68	2.39	0.08	0.26
Open shrubland	0.17	0.70	2.03	0.04	0.27

LAI_{min} : minimum LAI ; LAI_{max}: maximum LAI

2.3.3.3. Meteorological forcing

VIC model is forced with observed surface meteorological variables such as precipitation, maximum temperature, minimum temperature, and wind speed at a daily scale. VIC requires meteorological forcing file for each grid cells containing all four meteorological variables.

2.3.4. Model calibration and validation

Description of model calibration and validation can be found in Chapter 3 of this thesis.

2.3.5. Root depth and fraction estimation approach in VIC model

Typical implementation of VIC-3L model includes three soil layers and three root zones to represent soil moisture uptake through the plant roots. Depths and fractions of the root zones are user-defined for each land use types so that shorter vegetation draw soil moisture from the upper soil layer and deep-rooted plants from the deeper soil layers. VIC assumes that the roots are linearly distributed within the root zones and computes the root fractions for each soil layer by linear interpolation (Figure 2.14 left). Soil moisture depths are generally calibrated which requires the model to redistribute the user-defined root fractions specified for each root zone, in the soil layer by linear interpolation. Most of the studies related to VIC model have adopted this approach where the soil depths are calibrated and allocation of roots are kept constant (Demaria et al., 2007; Lilhare et al., 2020; Mishra et al., 2010; Park and Markus, 2014; Parr et al., 2015; Yeste et al., 2020). Demaria et al., (2007) tested the sensitivity of root distribution on the second soil layer in VIC-3L and found that different root allocations have impacted the ET and baseflow in the basin.

In this study we replace typical system of using fixed root depths and root fractions for varying soil depths in VIC model by determining the root allocations for the changed soil depths considering Zeng (2002) root distribution approach. We first obtained the effective rooting depth of each vegetation types from Zeng (2002). The three root zone depths add up to the effective rooting depth. We assumed that the depth of the root zones is same as the depth of the soil layer i.e., if the effective rooting depth is exactly equal to the total soil depth, then each soil layer corresponds to each root zone. However, there may be cases where the effective rooting depth are less than the total soil depths, for example as in Figure 2.14 (right). In this case, third root zone depth (z_3) is obtained after subtracting root depths of first two root zones (z_1, z_2) from the total root depth (z_t). Therefore, the root depths of each vegetation

type in our approach are a function of effective rooting depth, that is kept fixed for each vegetation types, and the soil depths are subjected to change during calibration. Although the root depths are not subjected to SA in this study, causing change in root depths by this approach will have implications on the sensitivity of soil depths. Next, the root fractions for each land cover type is determined using Zeng's (2002) vegetation root distribution approach.

$$f = 1 - \frac{1}{2}(e^{-az_r} + b^{-bz_r}) \quad \text{Eq (2.9)}$$

Where f is the cumulative root fraction from the surface to the effective root depth z_r . a and b are the vegetation coefficients that depends on the vegetation types. We used this equation directly to derive root fractions for each layer. Vegetation coefficients and the effective root depths used for the vegetation types are given in Table 2.9.

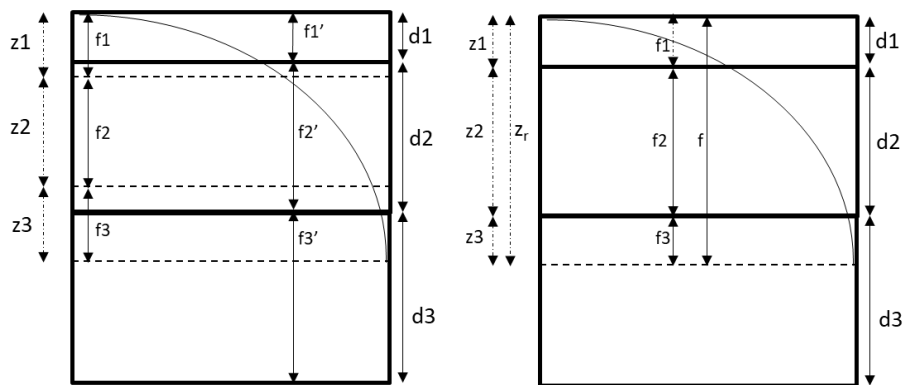


Figure 2.14: (left) Representation of rooting distributions in VIC-3L model. z_1 , z_2 and z_3 are the user-defined depths of three root zones, respectively. d_1 , d_2 , d_3 are the depths of three soil layers. f_1 , f_2 and f_3 are user-defined fractions of root in each zone, respectively. f_1' , f_2' and f_3' are fractions of root in each soil layer computed by VIC. (right) Our approach of representation of rooting distributions in VIC-3L model. z_t is the total root depth.

Table 2.9: Coefficients a and b in vegetation root distribution for Eq 2.9 for the land cover types used in this study. The depth of the rooting zone z_t is also given (Zeng, 2002)

Land cover type	a (m^{-1})	b (m^{-1})	z_t (m)
Deciduous broadleaf Forest	5.99	1.95	2
Cropland	5.56	2.61	1.5
Grassland	10.74	2.61	1.5
Open shrubland	7.72	1.26	3.1
Barren	4.37	0.98	4

3. Sensitivity analysis and model calibration

This chapter is adapted from paper and its supplementary section, published in the Hydrology and Earth System Sciences journal (HESS). This paper has been modified to enhance consistency all through this dissertation.

Citation: Naha, S., Rico-Ramirez, M. A., & Rosolem, R. (2021). Quantifying the impacts of land cover change on hydrological responses in the Mahanadi river basin in India. *Hydrology and Earth System Sciences*, 25(12), 6339-6357.

3.1. Introduction

Streamflow modelling of a river basin plays a crucial role in many practical hydrological problems such as flood or drought forecasting, water resources management and management of ecological services (Gou et al., 2020a). The ongoing changes in climate and land cover because of global warming has been impacting the hydrological behaviour of river basins significantly across the world. This necessitates use of regional hydrological or land surface models to represent the fundamental runoff mechanisms controlling the streamflow generation (Yeste et al., 2020) and to identify the changes in magnitudes and timings of associated hydrological processes (Wang et al., 2018). However, with the increasing complexity of these new generation models (e.g., in terms of parameters to be prescribed a priori), modelling such hydrological changes is an extremely challenging task, especially in data sparse regions in developing countries (Sheffield et al., 2014). In this respect, model calibration helps in adjusting parameters that conceptually represents the physical characteristics of a river basin, so that the modelled streamflow matches the observations more accurately (Eum et al., 2014). Therefore, emphasis should be laid on strengthening model parameter calibration approaches when solving aforementioned practical water-related issues.

The increase in computing power, more complete data sets and growing demand for better representation of physical processes within the river basins have led to the development of more complex hydrological models (Beven and Cloke, 2012; Chaney et al., 2015; Demaria et al., 2007). The complexity within these models is accompanied by a large number of tuneable

parameters which further increases the calibration burden (Muleta and Nicklow, 2005). Some parameters can be estimated from field or remote sensing observations such as vegetation types, albedo and LAI whereas some can be obtained from small scale in-situ or laboratory experiments. However, parameters values estimated based on laboratory experiments such as saturated hydraulic conductivity, may lose their physical meaning when applied over large scales, therefore are often subjected to model calibration (Demaria et al., 2007). Nonetheless, calibrating unnecessary parameters can lead to overparameterization (Her et al., 2019). For instance, there are studies where calibration is performed for the parameters based on expert judgement from other studies or as recommended by the model developers without the understanding of how sensitive the parameter to the model output is. Also, the sensitivity of model parameters varies from watershed to watershed based on the climate and other characteristics of river basin (Demaria et al., 2007). Therefore, Sensitivity Analysis is required to screen out the most important parameters and to reduce the number of parameters prior to calibration process. Parameters having little effects on model outputs can either be eliminated or can be assigned constants during calibration.

The parameter estimation methods for hydrological model calibration are also sometimes questionable. For instance, manual calibration using trial and error method is still frequently performed (Rodriguez and Tomasella, 2016), which is not only a tedious and time-consuming process, but also can be quite subjective and highly depends on the modeler's experience level (Muleta and Nicklow, 2005). Since 1960's, the research community has been devoted towards developing automatic model calibration methods or optimization programs such as Genetic Algorithms (GA) and Shuffled Complex Evaluation Algorithms (SCEA) with the aim of producing a very high speed and an objective calibration process (Beven and Binley, 1992; Gou et al., 2020a). However, researchers till date mostly tends to identify the best or an 'optimal' parameter set, using these automatic optimization techniques (Eum et al., 2014) to predict the hydrological changes. Using a single calibrated model for hydrological predictions ignores the concept of 'equifinality' i.e., there may exist several models that can produce equally good model simulations, often known as 'behavioural models' (Beven and Binley, 1992; Mantovan and Todini, 2006; Yeste et al., 2020). The existence of many sets of parameters that could result in equally good simulations is thus unavoidable and hence recognising the equifinality concept is necessary (Beven and Freer, 2001). Major focus has been given to structural uncertainties while performing hydrological modelling, whereas

studies relating to uncertainties resulting from different parameterisation is relatively less (Blöschl et al., 2019). Therefore, the correct identification of modelling uncertainties remains an important question for hydrologic models after even several decades of continuous progress in the field of model calibration and parameter identification.

In this thesis, the Variable Infiltration Capacity (VIC) model (For, more details, please refer to Chapter 2). is a physically semi-distributed macroscale hydrologic model (Liang et al., 1994) which has also played the role of land surface models in many previous studies (Yeste et al., 2020). This model has been widely used for streamflow simulations for various hydrological applications such as climate and land cover impacts in hydrology across the world (Eum et al., 2016a; Liu et al., 2011; Mao and Cherkauer, 2009; Mishra et al., 2010) including India (Chawla and Mujumdar, 2015; Dadhwal et al., 2010; Garg et al., 2019; Hengade et al., 2018; Joseph et al., 2018). Within the context of model calibration, VIC has more than 40 tuneable parameters (Bennett et al., 2018). There exist about 190 peer-reviewed studies where VIC model is calibrated and validated for various river basins, wherein majority of researchers have either straightaway calibrated the seven default or recommended parameters (Hengade et al., 2018; Linde et al., 2007; Niraula et al., 2017; Park and Markus, 2014; Xie et al., 2007) or have used manual calibration methods (Xie et al., 2007). Very few studies exist that have tested the sensitivity of VIC parameters (Demaria et al., 2007; Gou et al., 2020a; Joseph et al., 2018; Yeste et al., 2020) and findings of these studies indicates that sensitivity of parameters is dynamic in nature i.e., varies with respect to the climate conditions and basin characteristics. Therefore, using the default parameters for regional VIC calibration might preclude our ability to understand the hydrologic behaviour of a particular basin. Also, the common practise of using the 'best fit' model for hydrological applications hides the potential uncertainties associated with model performances that may arise from different model parameterisation (Chen et al., 2019b).

Our study region, the Mahanadi river basin, is mainly characterised by south-west monsoon rainfall and has been facing seasonal fluctuations in water availability (Asokan and Dutta, 2008). Moreover, the spatial variability of rainfall within the basin which makes it vulnerable to floods and cyclones at some parts while droughts at other parts of the basin. Some studies anticipated that these catastrophic hazards in the basin could be due to the isolated or combined impacts of increase in extreme precipitation and changes in land use land cover (Das et al., 2018; Gosain et al., 2006). Several studies investigated the hydrological impacts

owing to climate and land cover changes using hydrological modelling tools including VIC. However, the existing modelling studies for this basin and the nearby basins using VIC are mostly confined to using single deterministic calibrated model and not testing the sensitivity of the parameters prior to the calibration (Dadhwal et al., 2010; Das et al., 2018; Garg et al., 2019; Raje et al., 2014). Therefore, the results obtained from these studies are less reliable as it does not consider the uncertainties due to model parameterisation, hence not effective for decision making towards the water resources management of the basin.

In this study, we provide a large-scale comprehensive simulation of discharge and other water balance components in the Mahanadi river basin for 1990 to 2010. In support of this goal, we perform a detailed sensitivity analysis and calibrate catchment-specific parameters for streamflow simulations in the VIC model over 5 subcatchments of Mahanadi basin. We attempt to address the following two questions:

1. What are the sensitive VIC model parameters across Mahanadi River basin?
2. How does our calibration framework perform over the basin?

3.2. Model input datasets and uncertain parameters

The key input data required by the VIC model are meteorological forcings (precipitation, maximum temperature, minimum temperature, and wind speed), soil type, land cover information and topographic features. Topographical features are determined using the 30-meter CARTO-DEM (Cartosat-1 Digital Elevation Model), a national DEM developed by ISRO (Indian Space Research Organization) (Sivasena Reddy and Janga Reddy, 2015). Daily gridded precipitation (resolution, 0.25°) and maximum and minimum temperature (resolution, 1°) for the time period (1988-2010) are obtained from India Meteorological Department (IMD) (Pai et al., 2014). All climate variables are resampled to the model grid resolution of 0.05° . Soil textures are derived from the digitized soil map as provided by National Bureau of Soil Survey and Land Use Planning (NBSSLUP) (Scale 1:250000) (Figure 2.6a, Chapter 2). The local LULC map (Figure 4.1a) is derived from National Remote Sensing Centre (NRSC), India of year 2005 (scale 1:250000; resolution 56 meters)

VIC has more than 40 tuneable parameters, however we have selected 16 VIC model parameters (Table 3.1) for the Sensitivity Analysis (SA), as these parameters cannot be (or are difficult to be) measured directly and are typically subjected to calibration. The choice of these parameters are also based on our preliminary experiments (considering more than 16

parameters) and expected sensitive properties from previous studies (Demaria et al., 2007; Gou et al., 2020a; Joseph et al., 2018; Yanto et al., 2017) (See Table 3.1).

Typical calibration in VIC involves only streamflow related parameters as also recommended by VIC model developers (Gao et al., 2010; Gou et al., 2020b; Xie et al., 2007). However a few studies have reported that runoff simulated by VIC are sensitive to the vegetation parameters (Demaria et al., 2007; Joseph et al., 2018). Parameters subjected to SA in this study include, among others, rarely tested soil properties: Bulk Density (BD), Fractional water content at wilting point (Wp_f) and at critical point (Wcr_f); vegetation properties: architectural resistance (r_{arc}) Stomatal Resistance (r_{min}); and routing parameters: velocity (v) and diffusion ($diff$). Note that a multiplier of Wcr_f is used to compute Wp_f , to meet the criteria that soil moisture at wilting point should always be less than soil moisture at critical point and the multiplier is tested for sensitivity rather than the actual parameter. Similar approach is followed by Rosolem et al., (2012) while testing sensitivity of parameters in a land surface model. Feasible ranges (minimum and maximum values) of soil parameters (BD , Wcr_f , $Ksat$, Exp) are obtained based on average hydraulic properties of USDA soil textural classes (Cosby et al., 1984; Rawls et al., 1998; Reynolds et al., 2000) considering only the dominant soil textures within the basin. Ranges for the rest of the soil parameters are based on suggestions from the VIC model developers and published studies. Feasible ranges of the vegetation parameters are obtained based on the recommended ranges provided in the Land Data Assimilation System values (LDAS) for the dominant vegetation types in the basin (Hansen et al., 2000). Our preliminary experiments suggest Canopy height is not sensitive hence, Roughness length (RL) and Displacement Heights ($Disp$), which are computed from canopy height are not accounted for SA. Sensitivity analysis for all five subcatchments of Mahanadi river basin are performed using the ranges shown in Table 3.1.

In addition, Leaf Area Index (LAI) is an important vegetation factor, having substantial control over the water balance by directly influencing the evapotranspiration (ET) rates (Gao et al., 2010; Matheussen et al., 2002). LAI is specified at a mean monthly basis in VIC. We compared the monthly mean LAI averaged over the time period 2000-2015 from MODIS AQUA/TERRA with the LAI values from Global Land Data Assimilation (GLDAS) database for the river basin (Figure 4.1, Chapter 4). The plots show that MODIS LAI has a seasonal pattern with lower values of LAI during June/July and increases with the progress of a monsoon, whereas LAI values in GLDAS is maximum in June and reduces thereafter. Also, an overestimation in LAI

values is observed for all LULC types in GLDAS compared to MODIS. We find that both seasonal pattern and values of LAI obtained for each LULC type from MODIS are well in agreement with LAI studies carried out in India (Patidar and Behera, 2019; Paul et al., 2016). Thus, the monthly mean LAI from MODIS captures the phenological characteristics more realistically than the GLDAS LAI which shall have further implications on water balance. Several VIC related studies exist which have used LAI from MODIS products (Bennett et al., 2018; Patidar and Behera, 2019; Tesemma et al., 2015).

Table 3.1: VIC and routing model parameters tested for sensitivity analysis and feasible ranges.

Parameters	Description	Units	Minimum	Maximum
Soil parameters				
Wcr_f	Fraction of water content at critical point ^b	-	0.40	0.60
Wp_f * ($Wp_f = M * Wcr_f$)	Fraction of water content at wilting point ^b	-	0.50	0.99
BD	Bulk density of soil (used in VIC estimation of porosity) ^b	Kg/m ³	1350	1550
Ksat	Saturated hydraulic conductivity ^b	mm/day	240	840
Exp	Parameter characterizing the variation of saturated hydraulic conductivity with soil moisture ^b	-	10	30
d1	Thickness of first soil layer ^a	m	0.01	0.3
d2	Thickness of second soil layer ^a	m	0.31	3.5
d3	Thickness of third soil layer ^a	m	0.31	3.5
dsmax	Max. velocity of baseflow^a	mm/day	10⁻⁴	10^{1.48}
ds	Fraction of max. velocity of baseflow^a	-	10⁻⁴	10⁰
binf	Parameter to describe the Variable Infiltration Curve^a	-	10⁻⁴	10^{0.6}
ws	Fraction of maximum soil moisture of the third layer^a	-	10⁻⁴	10⁰
Vegetation parameters				
r_{arc}	Architectural Resistance ^b	(sm ⁻¹)	20	70
r_{min}	Minimum stomatal resistance ^b	(sm ⁻¹)	100	170
routing				
v	Flow velocity ^b	m/s	0.1	3
diff	Flow diffusivity ^b	m ² /s	500	5000

* Wp_f is analyzed based on its multiplier (i.e., the M term in Wp_f parameter's equation). Although description and units refer to actual parameter in VIC, parameter range represent the multiplier values (instead of actual parameter).

Parameter names in bold are sampled on log domain. "a" indicates parameters that are suggested by VIC model developers as the most sensitive parameters (Gao et al., 2010). "b" indicates parameters suggested in the literatures to be tested for sensitivity (Demaria et al., 2007; Gou et al., 2020b; Joseph et al., 2018; Yanto et al., 2017). A complete list of VIC model parameters can be found in <https://vic.readthedocs.io/en/vic.5.0.0/Documentation/Drivers/Image/Params/>.

Another important factor linking vegetation characteristics to hydrological processes in VIC is the root zone distribution. Typically, root zone allocation in VIC requires parameters such as user-defined root-zone depths and fractions for each land cover types that are kept fixed during the calibration process. We derived root zone depths and estimated the fractions of roots in each zone following (Zeng, 2002) for each vegetation type, and used a simplified approach to vary the root zone distributions with respect to the soil depths during calibration. This ensures root zone properties vary for different model calibration with a reduced number of parameters, hence providing a more manageable calibration strategy. For details on our root allocation approach, please refer to Chapter 2.

3.3. Methods

3.3.1. Morris Sensitivity Analysis Method

Morris (1991) is a well-established and widely used global sensitivity analysis (GSA) methods. There are many studies that have conducted parameter sensitivity analysis for hydrological models based on Morris screening method (Herman et al., 2013; Huang et al., 2020; Pappenberger et al., 2008; Pianosi et al., 2015; Sarrazin et al., 2016, 2018; Wang and Solomatine, 2019). It is a global extension of One-factor-At-the-Time local SA method (Morris, 1991). It is based on estimation of several elementary effects. The *EE* of the i^{th} input factor, x_{i-1} , at a single baseline point and for a known perturbation Δ can be calculated as given below (Campolongo et al., 2011).

$$EE = \frac{y(x_1, x_2, \dots, x_{i-1}, x_i + \Delta, \dots, x_m) - y(x_1, x_2, \dots, x_{i-1}, x_i, \dots, x_m)}{\Delta} \quad \text{Eq. (3.1)}$$

' m ' is the total number of parameters subjected to sensitivity analysis and ' y ' is EEs for each input parameter, which is estimated at ' r ' (See Eq. 3.2) random baseline points across the input parameter space. The estimated mean (μ_i) of the EEs is a measure of total-order effects of the i^{th} input parameter and standard deviation (σ_i) indicates the interaction effects of i^{th} input factor with another.

Morris method in this study is implemented as follows:

1. We performed the computational experiments using the SAFE (SA For Everybody) Toolbox (Pianosi et al., 2015)
2. ' m ' denotes the number of factors (model input parameters) subjected to sensitivity analysis, which is 16 in our case.

3. We used the radial design strategy proposed by Campolongo et al., (2011) to define the baseline points and the perturbation Δ .
4. ' r ' baseline points sampled across the input parameter space are generated by the Maximin Latin Hypercube Sampling.
5. In this method, total number of model simulations (N) required depends on the base sample size or the number of EEs (r) and number of parameters (m). It is worth mentioning that EET can be used for three purposes: parameter screening, parameter ranking and parameter mapping. And the choice of r depends on the purpose of EET. In this study, we are more interested in screening out the non-influential parameters. We choose r as 70, and the choice is made based on the recommendations in the existing literatures, where EET is used for screening purposes (Saltelli et al., 2008; Sarrazin et al., 2016; Vanuytrecht et al., 2014, Ruano et al., 2012).
6. Base sample size of $r = 70$ have resulted in over 1000 model evaluations (N):

$$N = r(m + 1) \quad \text{Eq. (3.2)}$$

Next, we compute the sensitivity measures for each input factor (Eq. 3.3). To avoid the problems due to effects of opposite signs, we estimate the mean of the absolute values of elementary effects ($|EE_i|$) as proposed by Campolongo et al., (2011)

$$\mu_i^* = \frac{1}{r} \sum_1^r |EE_i| \quad \text{Eq. (3.3)}$$

3.3.2. Screening of input parameters

The screening objective consists of separating the model input parameters into two distinct groups, parameters that are: influential (sensitive) and non-influential (insensitive) for streamflow simulation. There may be parameters with sensitivity index value, zero, which is completely insensitive. However, our goal is not only to screen out a completely insensitive parameters but also the parameters having small or negligible impact. We therefore assumed a threshold value for the sensitivity index, below which the parameters can be regarded as either completely insensitive or less influential (Eq. 3.4). This is a common practice followed in several studies while dealing with parameter screening using different SA methods (Gou et al., 2020b; Sarrazin et al., 2016; Tang et al., 2007; Vanrolleghem et al., 2015).

$$X_0 = \{X_i \text{ when } S_i < \text{threshold}\} \quad \text{Eq. (3.4)}$$

Where X_0 is the non-influential parameter, X_i is the i^{th} input parameter and S_i is the sensitivity index (mean of EE, μ_i^*) of the i^{th} input parameter. The choice of screening threshold can be subjective depending on the screening objective and case-specific threshold value are usually used (Sarrazin et al., 2016; Vanuytrecht et al., 2014), however very little information exists on this topic in the literature (Vanrolleghem et al., 2015). In this study, we set a screening threshold of 0.05 based on the visual analysis of the sensitivity index values of all factors at all subcatchments. We choose this threshold with the intention of screening out also the less sensitive parameters, apart from completely insensitive parameters with an aim of reducing the over-parameterization effects in the model. One should evaluate the SA results by assessing the screening convergence which can be assessed by quantifying the stability in the partitioning of sensitive and insensitive parameter as derived from Eq. 6. However, the results would then depend on the choice of threshold value which is not predefined. Therefore, to achieve a more objective screening convergence result, we compute the width of the 95% confidence interval of the sensitivity indices, estimated by the bootstrap method (Archer et al., 1997; Efron and Tibshirani, 1993), also followed in studies (Herman et al., 2013; Wang and Solomatine, 2019). We then use maximum width of the 95% confidence interval, as a statistic, across the lower influential input parameters, X_0 suggested by (Sarrazin et al., 2016) shown in Eq. 3.5.

$$Stat_{Screen} = \max_{x_i \in X_0} S_i^{ub} - S_i^{lb} \quad \text{Eq. (3.5)}$$

where S_i^{ub} and S_i^{lb} are the upper and lower bounds of the sensitivity index of the i^{th} input factor while m is the number of input factors. We consider screening convergence is reached, when $Stat_{Screen}$ value for the non-influential parameters (found in Eq. 3.5) is below 10% of the sensitivity index value of the most influential parameter. This is also followed in Herman et al., (2013) whereas Sarrazin et al., (2016), assessed convergence by directly using a threshold value. If the convergence is not reached for the lower influential parameters, it would require adding more samples to our previously chosen base sample size and run the model again and repeat this process again.

3.3.3. Calibration strategy

Next, we calibrate sensitive parameters separately on a subbasin level for the time (1990-2000) with a 2-year warm up period (defined as 1988-1999). We use a sequence of Monte-Carlo simulation, by generating 5000 near-random parameter sets from within the specified

range using Latin Hypercube Sampling Method (LHSM) with uniform distribution. LHS is one of the most effective and economical sampling methods that reduces the computational time and cost significantly (Wang and Solomatine, 2019). This method has been used in several studies relating to sensitivity and calibration problems in hydrology (Abe et al., 2018b; Bennett et al., 2018; Chaney et al., 2015; Muleta and Nicklow, 2005; Yeste et al., 2020). Different number of Latin hypercube samples were generated in these studies, for instance, Muleta and Nicklow, (2005) generated 5000 SWAT model parameter sets to calibrate daily streamflow; Yeste et al., (2020) calibrated VIC model using 10000 parameter samples. The choice of 5000 simulations in our study is based on the findings of some preliminary calibration experiments wherein we have tested 2000 to 10000 parameter sets for calibration. Calibration success is highly dependent on the choice of objective function or known as 'performance metric' that measures the goodness of fit between the model simulations and observations. An objective function can have significant impact on the calibration performance. The most commonly used performance metrics are based on comparisons of simulated and observed response time series (e.g. Streamflow), such as the mean squared error (MSE), Nash–Sutcliffe efficiency (NSE), and root mean squared error (RMSE) (Mizukami et al., 2018). The objective function should be aligned with the modelling applications (Gupta et al., 1998). Our overall objective in this study is to achieve a reasonable simulation of streamflow. In most of the studies, also including this study, models are calibrated using observed river discharge due to its better availability than other variables such as soil moisture and ET. We use Kling-Gupta Efficiency KGE (Eq. 3.6-3.8) as the objective function to assess the model performance in the calibration period. The KGE metric balances the contribution to the error coming from all three main components, namely correlation (e.g., timing/dynamics), variability (e.g., seasonality), and systematic bias, and is now a widely used metric in hydrometeorological studies (Gupta et al., 2009; Knoben et al., 2019; Lilhare et al., 2020; Mishra et al., 2020b; Rodriguez and Tomasella, 2016). For instance, (Mizukami et al., 2018) compared VIC simulations calibrated with NSE and KGE and found the later results in overall better performance than NSE by improving mean and variability of the flow. KGE ranges in $[-\infty, 1]$ with larger values indicating better performance. Additionally, we use the Percent-Bias (PBIAS) (Eq. 3.9) to evaluate our model performance specially to account for the high flow conditions. We adopt a common practice of selecting the best model simulations by using a top certain percentage of the total simulations (Chaney et al., 2015; Mockler et al.,

2016). This is relevant in our study as choosing model simulations based on a particular KGE score is subjective given that the behavioral performance, as well as the behavioral parameters, vary across the subcatchments. Therefore, we first assess the performance of top 10%, 5% and 2% of model simulations at every subbasin and choose the top 2% and top 5% based on overall model performance across the subcatchments, hence not compromising with the performance quality and also accounting for equifinality. These behavioral models are further used to simulate streamflow in the validation period (2001-2010) for all the subcatchments. Top2% simulations are used for simulating the land cover and climate change impacts on hydrology (Chapter 4 and 5) and top5% simulations are used for evaluating the impacts of using local and global datasets in VIC (Chapter 6). Please note that choosing 2% models for chapter 4 and 5 is a compromise made, to have an ensemble of (best) calibrated models which are to be run in conjunction with different land cover and climate scenarios, and also to be able to perform the model runs within a reasonable time.

$$KGE = 1 - \sqrt{(r - 1)^2 + (\alpha - 1)^2 + (\beta - 1)^2}, \quad \text{Eq. (3.6)}$$

$$\alpha = \frac{\sigma_{sim}}{\sigma_{obs}} \quad \text{Eq. (3.7)}$$

$$\beta = \frac{\mu_{sim}}{\mu_{obs}} \quad \text{Eq. (3.8)}$$

Where r is the linear correlation between observed and simulated discharge, α is an estimate of flow variability error and β is a bias term. σ_{sim} and σ_{obs} are standard deviations in simulated and observed discharge, respectively. μ_{sim} and μ_{obs} are mean of simulated and observed discharge, respectively.

$$PBIAS = \frac{\sum_{i=1}^n (O-P) \cdot 100}{\sum_{i=1}^n O} \quad \text{Eq. (3.9)}$$

Where O and P are the observed and predicted discharge values respectively and \bar{O} and \bar{P} are the mean of observed and predicted discharge. n is the number of data points.

3.4. Results

3.4.1. Morris screening

We first obtain the sensitivity indices for all the subcatchments shown in Figure 2.1 (Chapter 2). We apply Eq. 3.4 on all the subcatchments to obtain five different sets of X_0 i.e., five sets of non-influential parameters. We notice that there is a common set of parameters ($binf$, ds , $dsmax$, ws) which is more influential across all five subbasins. Also, there is a common set of

non-influential parameters (K_{sat} , $diff$, $d1$, $d3$, bd , r_{arc}). Although the resulting influential and non-influential parameters at the subcatchments are comparable, we see few parameters which might be slightly influential for one subbasin whereas non-influential for the others. For instance, parameters exp and Wp_f are slightly above the threshold for Salebhata, whereas for other subbasins they are non-influential. Note that we cannot compare the value of the sensitivity indices of the parameters among the subcatchments, as μ_i depends on scale of measurements of the model output, we can only compare the rank of the parameters.

We realize there are no major differences in the sensitivity results of these subcatchments (Figure 3.1), hence we choose to obtain a single set of influential parameters for the whole basin and discard the rest (Figure 3.1, weighted average). We compute the weighted average of the sensitivity indices of each subcatchment, and the weights are assigned based on the catchment area (Eq. 3.10).

$$\mu_{i(wa)} = (A_{Ba} \cdot \mu_i + A_{ka} \cdot \mu_i + \dots + A_{Sa} \cdot \mu_i) / (A_{Ba} + A_{ka} + \dots + A_{Sa}) \quad \text{Eq. (3.10)}$$

Where $\mu_{i(wa)}$ is the weighted average of the i^{th} input parameter; A_{Ba} , A_{ka} and A_{Sa} are the catchment areas of Basantpur, Kantamal and Salebhata, respectively. We observe that the influential parameters obtained for the whole subbasin is ds_{max} , $d2$, $binf$, v , ws and ds , which is same as the common set of influential parameters obtained earlier for all the subbasins, with only one additional parameter, v . Convergence analysis of the Morris screening results suggest that the convergence for the non-influential parameters (Figure 3.2) has reached before reaching the total number of simulations (1190 simulations) and that the total number of model simulations run for Morris screening method was sufficient. Figure 3.3 shows maximum width of the 95% confidence interval of all the parameters below 0.08 (10% of the sensitivity index value of the most influential input factors) are indicated by a red dotted line. It satisfies the criteria that we set in Eq 3.5: all the parameters that are considered non-influential in Figure 3.3, $Stat_{screen}$ values of those parameters (marked in red) are below 0.08. The influential parameters identified by the Morris Method for the entire Mahanadi river basin are 4 soil parameters ($binf$, ds , ds_{max} , ws) and one routing parameter (v). ds_{max} is the most sensitive parameter found in 4 out of 5 subbasins and having the largest interaction and direct effects on KGE. In the largest catchment, Basantpur, $d2$ is having the largest direct effect on KGE, however, ds_{max} is having the largest interaction effect. There is a clear separation in the sensitivity indices of ds_{max} from the sensitivity indices of the other

influential parameters. *d2* and *binf* are the second most influential parameters followed by *ws* and *v*. *d2* is the most important soil layer probably because it is the thickest soil layer and majority of the roots are placed in this layer which controls ET. *Dsmax*, *ds* and *ws* are the baseflow related parameters, interlinked with each other, associated with the third layer of soil moisture *d3*.

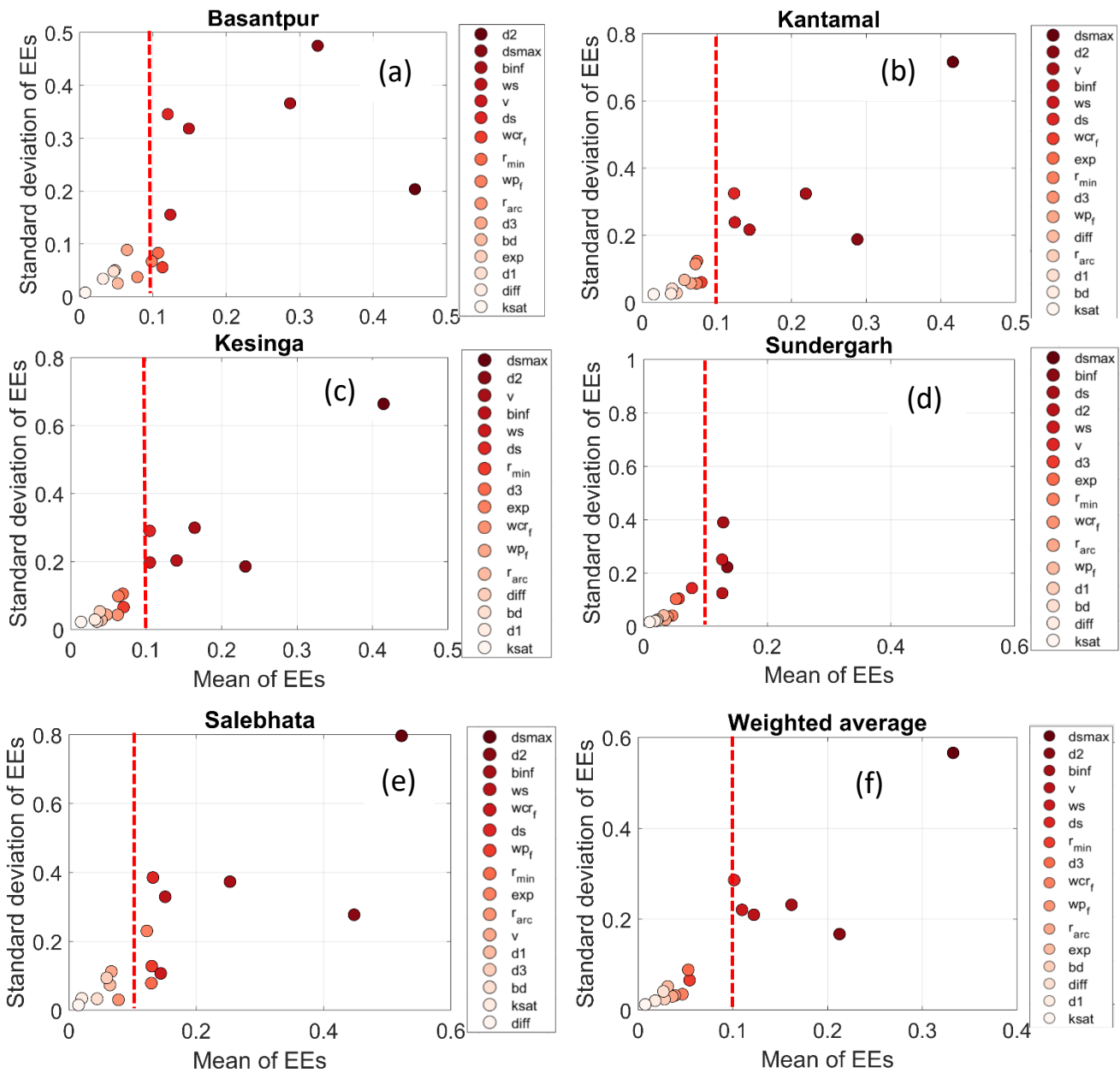


Figure 3.1: Sensitivity indices (Mean and Standard deviation) of Morris Method for VIC-3L parameters for (a-e) individual subbasins of Mahanadi river basin respectively (f) weighted average of all subcatchments. Parameters, top to bottom, listed on the right side are in ranking order, highest to lowest respectively, based on Mean of EEs. Red dashed vertical line is the screening threshold. Parameters that are Influential i.e., above the screening threshold are within the black dashed box. Rest of the parameters are non-influential.

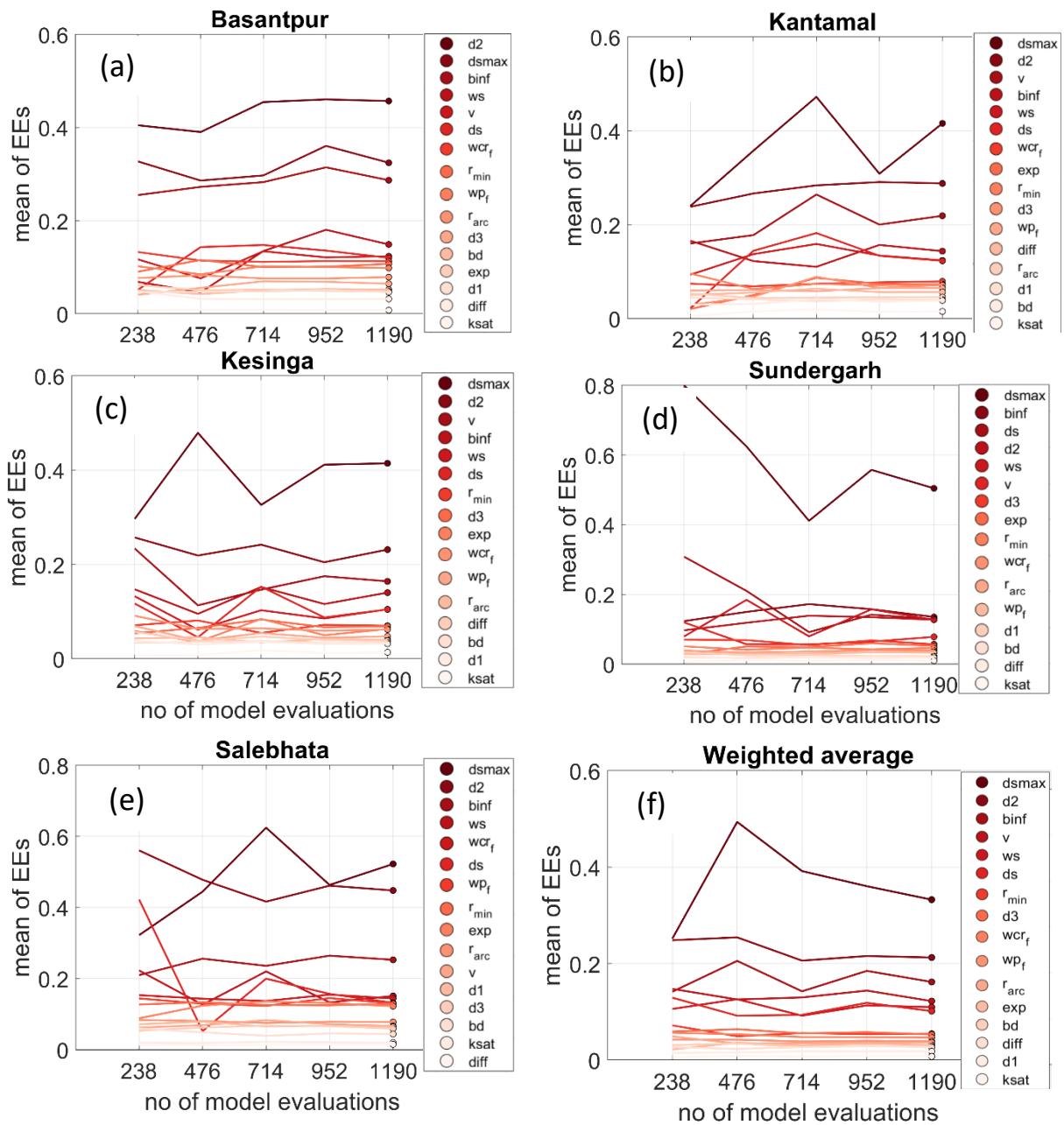


Figure 3.2: Convergence analysis with increasing sample size (expressed as number of simulations) for (a-e) all individual subcatchments respectively (f) weighted average of all subcatchments.

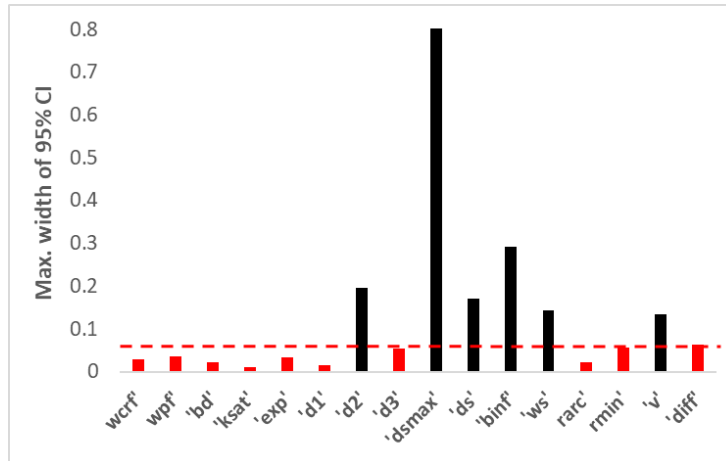


Figure 3.3: Maximum width of the 95% bootstrap confidence interval of all parameters for all subbasins. Dotted red line is the $Stat_{Screen}$ threshold, below which are the non-influential parameters that have converged.

3.4.2. Calibration and validation

Figure 3.4 shows the performance of VIC with respect to KGE and PBIAS in the calibration and validation period for all the subcatchments in the highest order of their catchment size. In overall, evaluation result suggests the model reproduced the observed flows remarkably well with the median KGE values of 0.85, 0.86, 0.82, 0.75, 0.63 in calibration and 0.77, 0.82, 0.72, 0.60, 0.59 in validation at Basantpur, Kantamal, Kesinga, Salebhata and Sundergarh, respectively for top 2% model simulations. This is a considerable improvement, when compared to the total number (5000) of simulations with median KGE values of 0.46, 0.60, 0.55, 0.51 and 0.02 at Basantpur, Kantamal, Kesinga, Salebhata and Sundergarh, respectively, and with lowest KGE values ranging from -0.08 to -0.91 across subcatchments. However, we observe a relative reduction in the daily KGE values at the smaller subcatchments (Sundergarh and Salebhata) in both calibration and validation period. The PBIAS values obtained in the calibration period (Figure 3.4 b) indicate that the model tends to be more biased (positively) as the catchment size decreases and that the largest catchment, Basantpur is least biased. The median PBIAS values at Sundergarh and Salebhata are +9% and +23% respectively in the calibration period and +19% and +55% in the validation period. It is to be noted that subbasins analyzed are human intervened and observed streamflow are controlled by minor reservoirs and dams which will affect the VIC simulations especially in the smaller subcatchments. Moreover, non-consideration of groundwater recharge and irrigation in VIC can also possibly

affect performance at smaller subcatchments (Chawla and Mujumdar, 2015). We observe a systematic reduction of performance (as measured by KGE and PBIAS) when moving from calibration to validation dataset. In overall, models reproduced the daily flows consistently when compared to the observed flows, during both calibration and validation period. Figure 3.5 shows simulated and observed discharge in a calibration and validation year (zoomed to the monsoon period) for all subcatchments. Similar performance is observed throughout the simulation period. The overestimation in discharge (or the peak flows) in the smaller subcatchments as observed in Figure 3.4b is also reflected in the hydrographs of Figure 3.5. Overall, calibration and validation performances indicate that the model parameters were robust enough across both periods with comparable skills. Figure 3.7 shows plots of the water balance components (runoff and ET) resulting from the Monte Carlo simulation for all subcatchments.

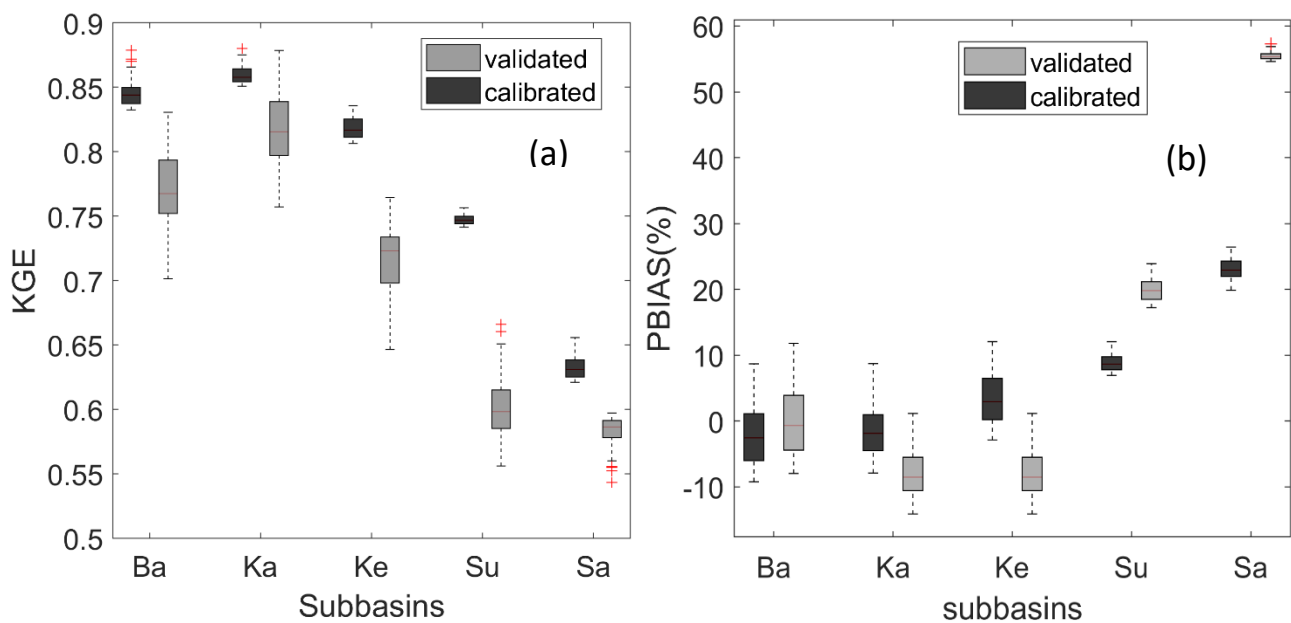


Figure 3.4: Boxplots showing (a) KGE and (b) PBIAS range for calibrated (black) and validated (grey) simulations, respectively.

Figure 3.6 shows that the distribution of behavioral parameters/ best parameter sets within their respective variability ranges differs from one parameter to another as well as across subcatchments. The values of ds and ws are more broadly distributed in entire range of parameter space, reflecting high effect of these parameters on modelled streamflow through their interaction with other parameters. Contrarily, calibrated values of $binf$, $dsmax$, $d2$ and v

are relatively constrained in smaller ranges across subcatchments, towards either higher, mid, or lower values indicating direct influence of these parameters on the behavioral simulations. For instance, higher values of $d2$ and v , lower values of $dsmax$ and mid values of $binf$ resulted in the behavioral model simulations at the smaller subcatchment, Salebhata. Thickness of second soil layer, $d2$ is the most identifiable parameter across all subcatchments.

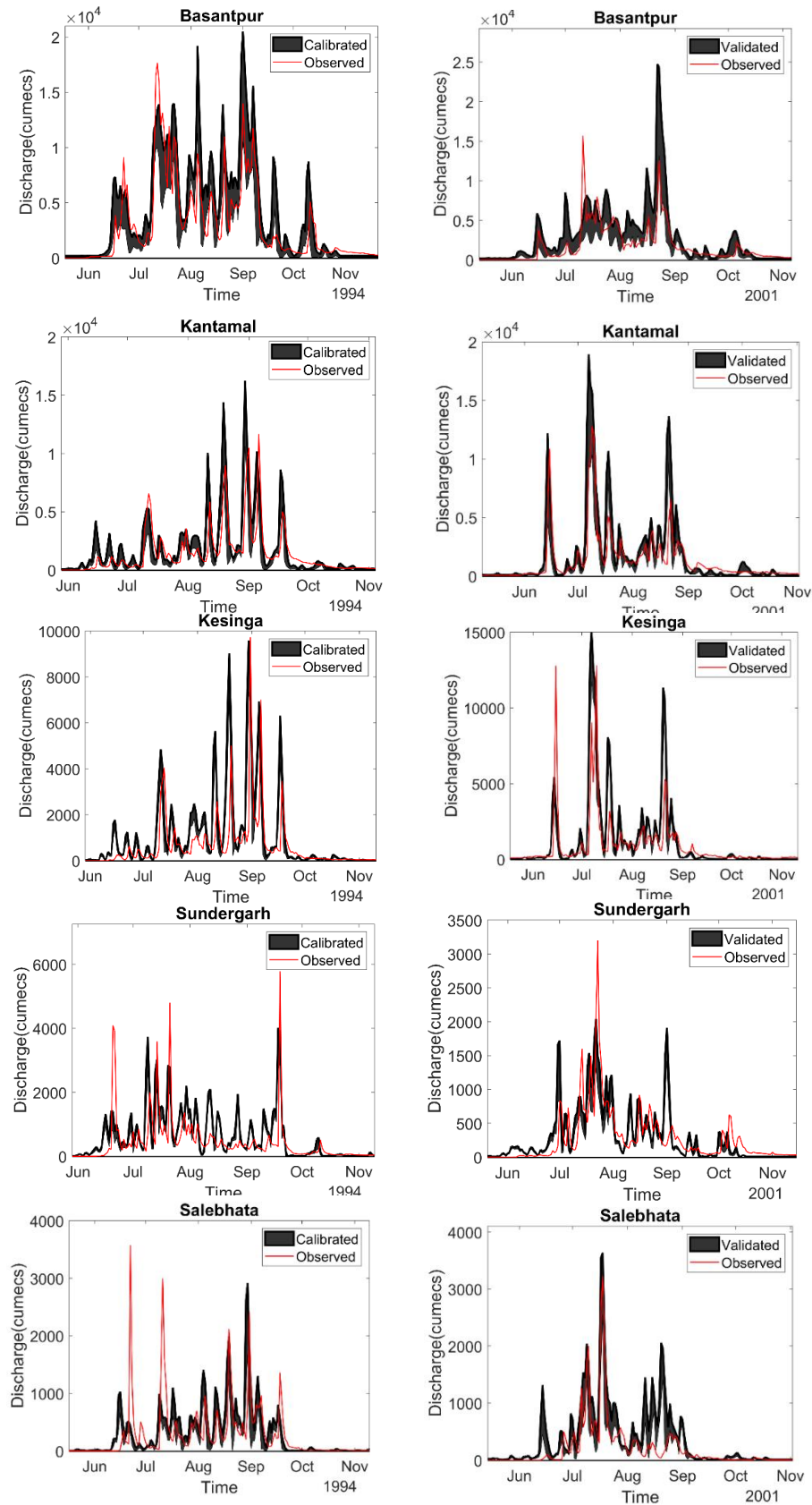


Figure 3.5: Simulated and observed discharge in the calibration and validation period for all subcatchments. Hydrographs are zoomed in to the monsoon season of the most wet year during the calibration and validation period; model performance is similar in other years.

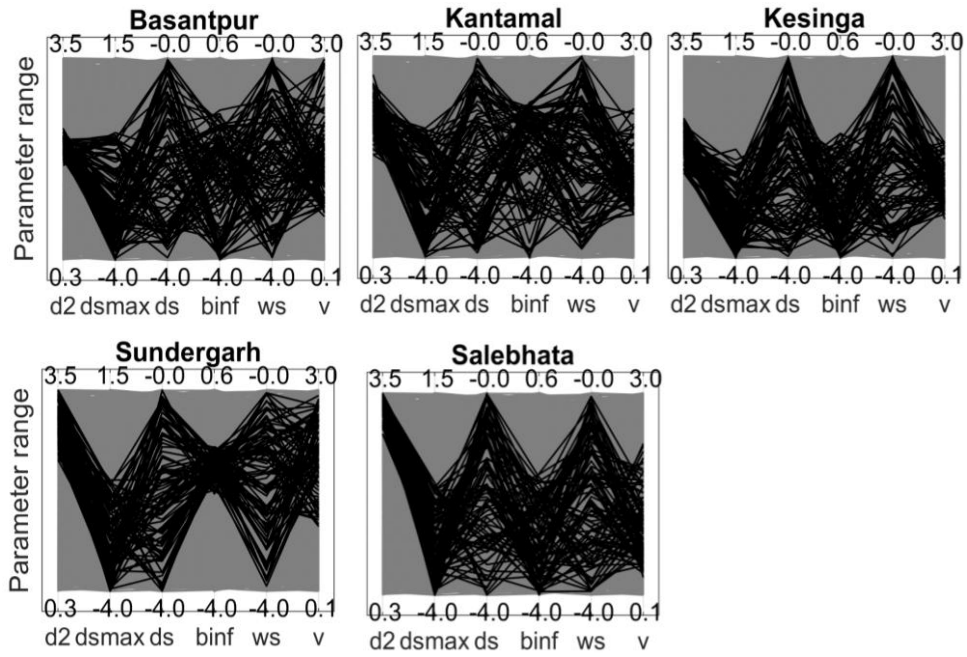


Figure 3.6: Parallel coordinate plot representing VIC-3L behavioural parameterization for all subcatchments obtained during model calibration. Lines in black are simulations where KGE lies within top 2% i.e., behavioural simulations and lines in grey are non-behavioural simulations. Behavioural KGE at Ba, Ka, Ke, Su and Sa ranges from 0.83 to 0.88, 0.85-0.88; 0.81-0.84; 0.74-0.76 and 0.62 to 0.66 respectively. Parameters are defined in Tables 1.

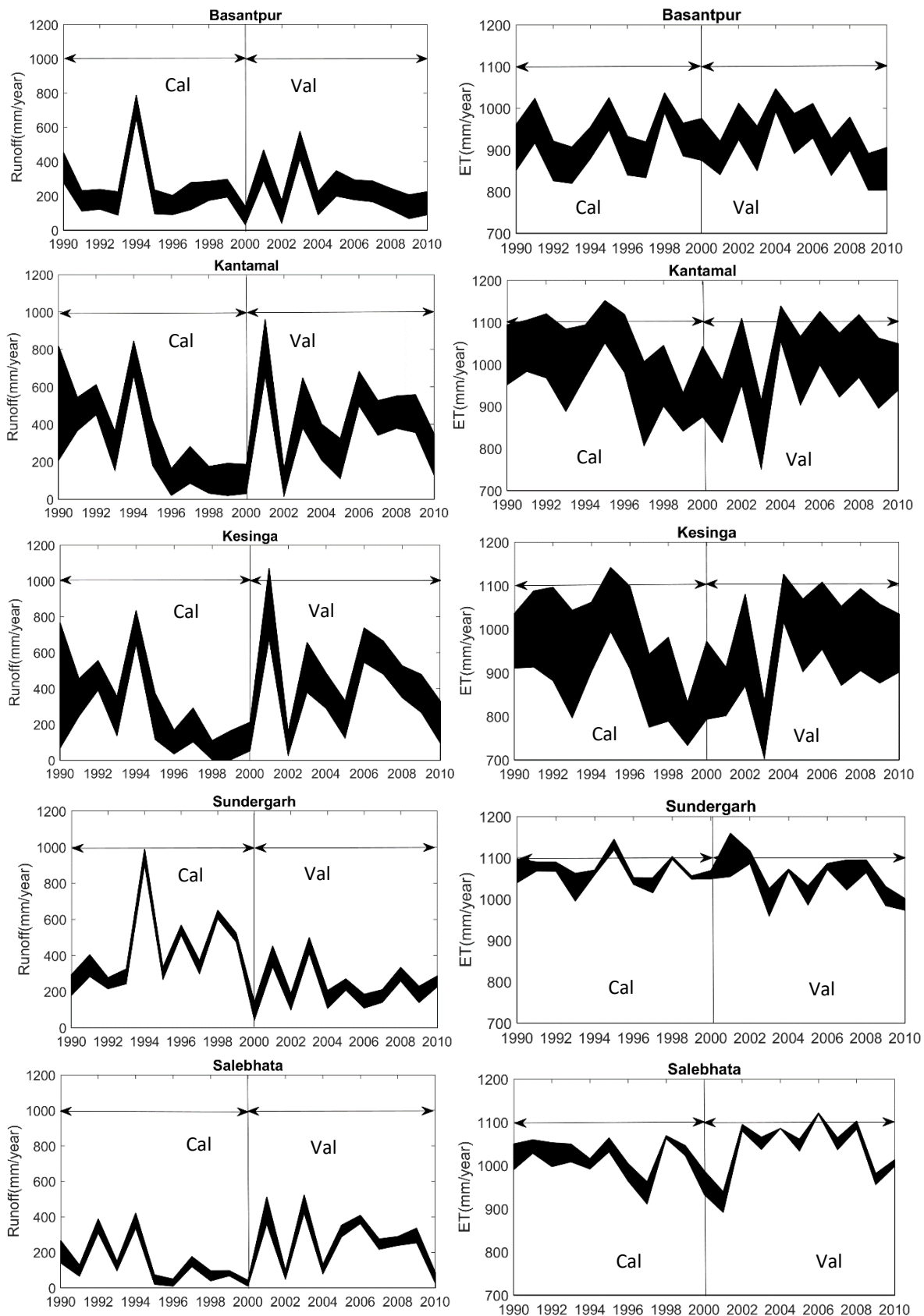


Figure 3.7: Plots of the water balance components (runoff and ET) resulting from the Monte Carlo simulation for all subcatchments in the calibration and validation period. 'Cal' indicates calibration and 'val' indicates validation.

3.5. Discussions

Our results are in agreement with previous VIC related studies conducted on several basins which show *binf* and *d2* are the most sensitive parameters (Demaria et al., 2007; Gou et al., 2020b; Lilhare et al., 2020; Yanto et al., 2017; Yeste et al., 2020). The most sensitive VIC model parameters as recommended by the model developers for most climatic, edaphic, and physiographic water settings are *binf*, *d1*, *d2*, *d3*, *ds*, *dsmax* and *ws* (Gou et al., 2020b). However, first- and third-layer soil depth (*d1* and *d3*) are not found sensitive in this study. *d1* is the thinner topmost soil layer having no control on ET and subsurface processes. *d3* although have been tested within same (thick) range as *d2*, our root allocation approach in VIC probably would have affected the sensitivity of *d3*. Therefore, in line with (Gou et al., 2020b), calibrating all seven soil parameters without SA screening would result in including unnecessary parameters. This result also agrees with the findings of (Bao et al., 2011; Demaria et al., 2007), that not all the default recommended parameters are sensitive, and also parameters not within the recommended list can be sensitive. For instance (Gou et al., 2020b) found only three parameters are sensitive for simulated streamflow across China among the default or recommended parameters whereas drainage parameter, *exp* (not recommended for calibration) is found sensitive in (Demaria et al., 2007). Also, the sensitivity is largely dependent on the objective function used, for instance most of these studies tested the sensitivity on NSE that focusses on peak flows. *binf* partitions the rainfall into surface runoff and soil moisture storage thus influencing the peak flows in the basin. On the contrary, baseflow parameters like *Ds* and *Dsmax* are found unimportant when tested against PBIAS, relative to NSE and KGE in (Lilhare et al., 2020).

Typically, only the soil parameters are calibrated in VIC and vegetation parameters are kept constant. Varying soil depths (during calibration) pose indirect influences on both timing and magnitude of the soil water available for ET, thereby influencing the ET rates. However, our approach of varying root zone depths and fractions during each model run provides substantial control over the water balance by directly influencing the ET rates. Also, in many LSM's (Ex: Noah) in contrast to the practice surrounding VIC, soil depths are kept constant whereas vegetation parameters which influences ET are varied. However, soil depths affects many characteristics of the rainfall runoff response, thus having greater control on overall model performance than the vegetation parameters (Newman et al., 2017).

Our calibration results suggests that parameter ds and ws requires more intensive calibration to constrain their ranges whereas $d2$ and $binf$, although being more important, but are easier to calibrate as the values are more concentrated in smaller ranges. This contradicts the findings of (Zhao et al., 2012) that parameters $d2$ and $binf$ require intensive calibration, but other parameters only need minor adjustments. Interaction between VIC parameters related to subsurface flows, $dsmax$, ds and ws appears to play an important role in the calibration process which is also outlined in (Huang and Liang, 2006). We observe that the calibrated parameter ranges are quite different for individual subbasins i.e., different parameterization favors different subbasins, which have implications on the simulated hydrological components for each subbasin. Therefore, selecting a common set of parameter for simulating the hydrological processes in entire basin, as done in previous studies in this region (Dadhwal et al., 2010; Das et al., 2018) would introduce errors in the hydrological response in some subbasins. For instance, higher values of $binf$ in Sundergarh and lower values of $binf$ at kesinga may lead to large differences in their corresponding hydrological processes which shall have a consequence on partition of water in soil layer. We observe even after the rigorous sensitivity analysis and model calibration process, top 2% of the model simulations have resulted in KGE uncertainties that ranges from 0.63 to 0.88 across subcatchments. This suggests that calibrating all parameters without reduction of parameters through SA would have resulted in more equifinality i.e., resulting in a greater number of comparable simulations. Therefore, careful screening of the model parameters is required to reduce the impacts of uncertainties due to model parameters on model simulations.

Despite the available automatic calibration techniques, it is difficult to find a unique set of optimal parameters in the calibration period (Huang and Liang, 2006). Moreover, the optimal or the best parameter set during calibration are not necessarily the best parameter sets for the validation period as also observed in our case (not shown here). Therefore, it is important that we identify and represent the model simulation uncertainties that are associated with model parameter uncertainties in our studies, especially for basins having limited data available for streamflow, for instance, only streamflow in our case. Also, the uncertainty bound of the simulations are likely to be compensating for errors due to other model prediction uncertainty sources, such as input data and structural uncertainties associated with the underlying model (Gou et al., 2020b).

3.6. Conclusions

A sensitivity analysis is carried out prior to the calibration process to identify the important parameters that would have a major control in simulating discharge and other water balance components of Mahanadi river basin and also reduce the number of parameters for calibration. We found that not all the recommended parameters (by VIC model developers) are sensitive, for instance, first and third depth of soil layer ($d1$ and $d3$) is not found sensitive, instead routing parameter, flow velocity (v) is found sensitive. However, in line with other studies, soil parameters ($binf$, $d2$, ds , $dsmax$ and ws) are found more sensitive than the vegetation parameters.

The sensitivity guided VIC calibration technique was efficient and yielded very good to good simulations for all subbasins with median KGE ranging between (0.63-0.86) in calibration and (0.59-0.82) in validation across subcatchments. Calibration using Monte Carlo simulations showed that there are many parameters sets that can be regarded as 'equally good simulations' based on their KGE values, which is known as equifinality and hence should be taken into consideration in hydrological modelling. This technique is also in agreement with other possible practical applications of the VIC model for studying the hydrological impacts of environmental changes, where a parameter set forming an uncertainty bound, must be chosen prior to the simulations using land cover and climate scenarios (Yeste et al., 2020).

4. Quantifying the impact of land cover changes on hydrological responses

This chapter is published in the Hydrology and Earth System Sciences journal (HESS). This paper has been modified to enhance consistency all through this dissertation.

Citation: Naha, S., Rico-Ramirez, M. A., & Rosolem, R. (2021). Quantifying the impacts of land cover change on hydrological responses in the Mahanadi river basin in India. *Hydrology and Earth System Sciences*, 25(12), 6339-6357.

4.1. Context and Background

Land use and land cover change (LULC) induced by the rapid anthropogenic activities, is one of the major causes of change in hydrological and watershed processes (Rogger et al., 2016). Alterations of existing land cover types and land management practices in a catchment can thereby, significantly modify the rainfall path into runoff by changing the hydrological dynamics such as surface runoff, baseflow, Evapotranspiration (ET), water holding capacity of the soil, interception and groundwater recharge, thus reflecting a change in the water demand (Berihun et al., 2019; Bosch and Hewlett, 1982; Costa et al., 2003; Foley et al., 2005; Garg et al., 2017; Hamman et al., 2018; Mao and Cherkauer, 2009; Rogger et al., 2016; Zhang et al., 2014). For instance, developing countries like India are facing rapid growth in population which has prominent effects on LULC dynamics through deforestation, rapid urbanization, and agricultural intensification, subsequently modifying the hydrological cycle in many river basins of India. A recent analysis on global land cover change have shown a significant increase of 82% in the croplands in India (Chen et al., 2019a; IPCC, 2019). Therefore, a comprehensive understanding and evaluation of land cover change impacts on hydrological processes are essential for decision makers to plan environmental policies which focuses on water resource allocations, riparian ecosystem protection and river restoration (Chen et al., 2019b; Chu et al., 2013).

Many studies have attempted to evaluate the hydrological responses to different LULC patterns on specific geographic locations (Abe et al., 2018a; Chu et al., 2013; Eum et al., 2016b; Li et al., 2015; Ma et al., 2010; Rodriguez and Tomasella, 2016; Viola et al., 2014; Woldesenbet et al., 2017) including Indian river basins (Babar and Ramesh, 2015; Dadhwal et al., 2010; Das et al., 2018; Gebremicael et al., 2019; Wilk and Hughes, 2002). Most of these studies used physically distributed hydrological models (e.g., SWAT, VIC, MIKE-SHE) to simulate the complex hydrological processes and to examine the impact of LULC changes on those processes. Conventionally, this is done by calibrating and validating the hydrological model against the observed data and then setting up that single calibrated model for a baseline land cover scenario. The calibrated model is then run for different land use scenarios and subsequently the differences in simulations are compared. However, it is widely recognised that hydrological predictions obtained from single calibrated model can be biased and therefore the measure of their reliability is always questionable (Beven and Binley, 1992; Huang and Liang, 2006). There may exist 'equally probable parameter set' or 'behavioural set' that can yield equally good or acceptable model predictions, due to the complex interactions among the model parameters to represent the complex hydrological processes (Beven and Binley, 1992). This is known as equifinality and is considered as one of the main sources of uncertainty in hydrological modelling (Her et al., 2019). Recent climate change studies have acknowledged the uncertainties stemming from model parameters, and therefore they take into account these uncertainties while predicting the hydrological responses due to climate change (Chaney et al., 2015; Feng and Beighley, 2020; Her et al., 2019; Huang and Liang, 2006; Joseph et al., 2018; Mockler et al., 2016; Singh et al., 2014). However, little is known about the contributions of model parameter uncertainties to the land use change impacts and thus, very few studies exist (Breuer et al., 2006; Chen et al., 2019b) which reported that uncertainties associated with the model parameters could significantly influence land cover change impacts and hence should not be overlooked while modelling hydrologic responses to LULC change.

This paper specifically focusses on the Mahanadi river basin, an easterly flowing river basin in India. Eastern part of India is amongst the most rapidly changing landscape over the country, specifically, Mahanadi river basin has undergone drastic land cover changes in the last

decades (Behera et al., 2018; Dadhwal et al., 2010). In this study, we address the science questions:

1. What are the expected impacts of LULC changes on the water balance of the Mahanadi river basin?
2. How these predicted impacts vary as a result of model parameter uncertainties?

The major objectives of this study are:

1. To predict the changes in hydrological processes owing to historical and future changes in LULC
2. To understand the contribution of uncertainty from hydrologic parameterization to the hydrologic projections due to LULC change.

To this end, a large scale physically semi-distributed hydrological model, the Variable Infiltration Capacity (VIC) (Liang et al., 1994) and historical and future land cover scenarios from the Land Use Harmonisation 2 (LUH2) database (Hurtt et al., 2011) are used to simulate the discharge and other hydrological components at daily time scales in the Mahanadi river basin.

We first perform sensitivity analysis of the model parameters and calibrate the hydrological model using Monte Carlo simulations to identify behavioural model simulations that implicitly account for the uncertainties from model parameterisation. Behavioural models are then used to predict the hydrological impacts due to different LULC scenarios. The land cover scenarios used in this study are most up-to-date scenarios, available from version 2 of the Land Use Harmonization (LUH2) dataset, which represents future changes in the LULC based on Shared Socioeconomic Pathways (SSPs) (O'Neill et al., 2016). Previous studies (Breuer et al., 2006; Chen et al., 2019b) have focussed only on the historical land use scenarios to evaluate the hydrological impacts, however and to our knowledge , this is the first study that uses applications of the VIC model in conjunction with future land cover datasets produced under combined SSP and RCP scenarios (descriptions in Chapter 2) . While most past studies in other catchments used aggregated (monthly) time steps to model the change, we use daily time steps to capture the dynamics of daily flow variability. Moreover, analysis in most land use impact studies is limited just with the streamflow, missing an overall picture of the hydrological processes.

4.2. Materials and Methods

4.2.1. Model input datasets and parameters

We implement VIC model, version 4.2.d in the water balance mode at a daily time step and at a grid resolution of 0.05° over the 5 subcatchments of the Mahanadi river basin. Flows are routed to the subcatchments of Basantpur (Ba), Kantamal (Ka), Kesinga (Ke), Sundergarh (Su) and Salebhata (Sa) (See Figure 2.1, Chapter 2). The ability of VIC model to simulate the impacts of LULC changes on hydrology are well documented in various research articles (Garg et al., 2017, 2019; Hurkmans et al., 2009; Mao and Cherkauer, 2009; Patidar and Behera, 2019; Zhang et al., 2014). For, descriptions about the structure and formulations of the model please refer to Chapter 2 of this thesis.

The key input data required by the VIC model are meteorological forcings (precipitation, maximum temperature, minimum temperature, and wind speed), soil type, land cover information and topographic features. Topographical features are determined using the 30-meter CARTO-DEM (Cartosat-1 Digital Elevation Model), a national DEM developed by ISRO (Indian Space Research Organization) (Sivasena Reddy and Janga Reddy, 2015). Daily gridded precipitation (resolution, 0.25°) and maximum and minimum temperature (resolution, 1°) for the time period (1988-2010) are obtained from India Meteorological Department (IMD) (Pai et al., 2014). All climate variables are resampled to the model grid resolution of 0.05° .

Soil textures are derived from the digitized soil map as provided by National Bureau of Soil Survey and Land Use Planning (NBSSLUP) (Scale 1:250000) (Figure 2.6a, Chapter 2). Land cover maps from two different sources i.e., local and global, are used in this study. The local LULC map (Figure 4.1a) is derived from National Remote Sensing Centre (NRSC), India of year 2005 (scale 1:250000; resolution 56 meters) and is used in the model runs while performing sensitivity analysis, model calibration and validation. Global land cover scenarios are obtained from LUH2 (Section 2.2.2.3, Chapter 2) which are used in model simulations for predicting impacts of land cover changes on hydrological components. All LULC maps used in this study are reformatted and reclassified into USGC LULC types as required by the VIC model (Figure 2.7 a, Chapter 2). Leaf Area Index (LAI) is an important vegetation parameter which is specified at a mean monthly basis in VIC. We obtained monthly mean LAI averaged over the time period (2000-2015) from MODIS AQUA/TERRA, shown in Figure 4.1b. Wind speed for the period 1988-2010 is obtained from NCEP/NCAR reanalysis of resolution 1° . The observed discharge

at daily scales at multiple gauges (Figure 2.1) for the simulated time (1988-2010) are obtained from the Central Water Commission (CWC), India, for validating the simulated discharge.

To analyse the parameter space uncertainty, we calibrated the influential parameters which we obtained from sensitivity analysis (performed over 16 VIC model parameters) at all subcatchments of Mahanadi river basin using Monte Carlo simulations, to obtain the best or ‘behavioural’ set of VIC models. Ten years (1990–2000) of daily discharge was used for model calibration with a warmup period of two years 1988-1989, and 14 years of data (2001–2014) was used for validation. These behavioural parameter set was selected, based on Kling-Gupta Efficiency (KGE). More details regarding sensitivity analysis, model calibration and validation can be found in Chapter 3 of this thesis.

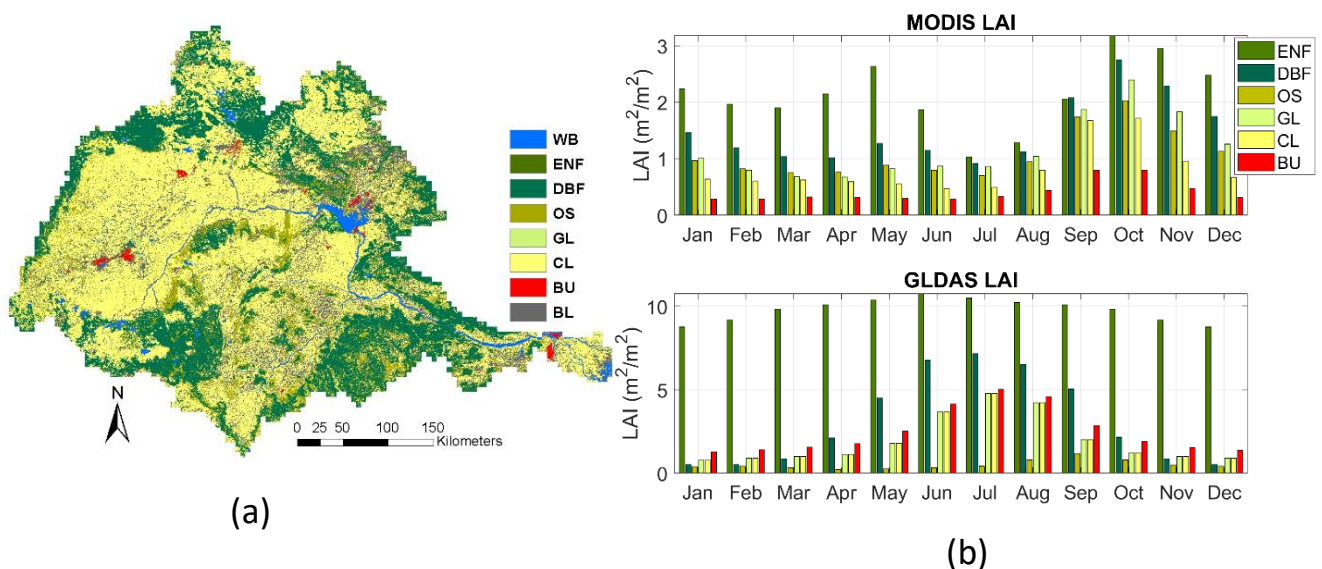


Figure 4.1 (a) LULC map of Mahanadi river basin from NRSC of year 2005 (b) Comparison of LAI values from MODIS, averaged over the time period, 2000-2015 and GLDAS for the land cover classes shown in LULC map on (a).

Another important factor linking vegetation characteristics to hydrological processes in VIC is the root zone distribution. We derived root zone depths and estimated the fractions of roots in each zone following Zeng, (2002) for each vegetation type, and used a simplified approach to vary the root zone distributions with respect to the soil depths during calibration. For details on our root allocation approach, please refer to Chapter 2 of this thesis.

4.2.2. LULC scenarios

All the simulations in the calibration and validation period are performed using a static local LULC map of year 2005 derived from NRSC (Figure 4.1a). Simulations using this land use map shall be termed as NRSC2005 henceforth. Next, we used a set of land use scenarios based on Socio-economic Pathways (SSPs) and Representative Concentration Pathways (RCPs), from the recently released , Land Use Harmonization Project (LUH2) data set (release “LUH2v2h” and LUH2v2f) for the time period of (850–2005) and (2015-2100) respectively (Hurtt et al., 2018) (Table 2.3, Chapter 2). The LUH2 approach estimates the gridded land use fractions, annually at a resolution of 0.25°.

Table 4.1 LUH2 LULC classes remapped to VIC LULC cover classes.

LUH	VIC
Forested primary land	Deciduous Broadleaf Forest (DBF)
Non forested primary land	Deciduous Broadleaf Forest (DBF)
Potentially forested secondary land	Deciduous Broadleaf Forest (DBF)
Potentially non-forested secondary land	Deciduous Broadleaf Forest (DBF)
Managed pasture	Grassland (GL)
Rangeland	Grassland (GL)
Urban land	Urban/built up (UB)
C3 annual crops	Cropland (CL)
C3 perennial crops	Cropland (CL)
C4 nitrogen-fixing crops	Cropland (CL)

The land use fraction maps are available for each land use type at a resolution of 0.25°. So, we have first obtained LUH2 fraction maps of different LULC types for Mahanadi basin extent at a resolution of 0.25° and further re-gridded to VIC grid size of 0.05°. Next, to run the VIC model, we have prepared a vegetation parameter file where we included the fractional coverage of all LULC types for each grid cell ensuring that each grid will contain more than one vegetation type. The land use classes are reduced to simplify our model application, and consequently remapped to the VIC land use classes by assuming all primary (Forested or Non-

forested) and secondary (Forested and Non-forested) land to Deciduous Broadleaf Forest (DBF), Managed pasture and Rangeland are considered as Grassland and all crops are merged into a single Cropland class. Urban land and water bodies are retained (See Table 4.1). It is worth mentioning that the 'potentially non-forested secondary land' class in the LUH2 datasets matched to the forested areas in NRSC2005 and hence both mapped into DBF which is the dominant forest type in the basin (Figure 4.2).

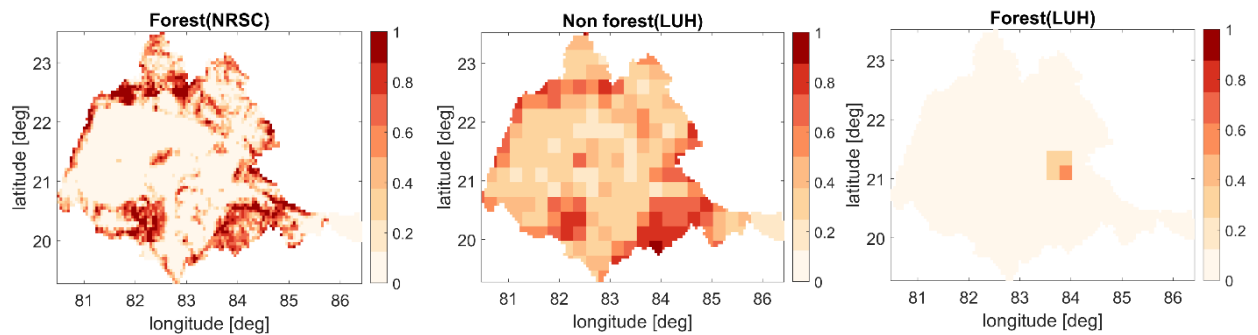


Figure 4.2 Forested areas in NRSC, 'Potential Non-Forested areas' in LUH2 and 'potentially forested areas' in LUH2. 'Potential Non-Forested areas' in LUH2 is comparable with the Forested areas in NRSC, through visual inspection. Therefore, both the 'potentially forested area' and 'potentially non-forested area' are combined and mapped as forest.

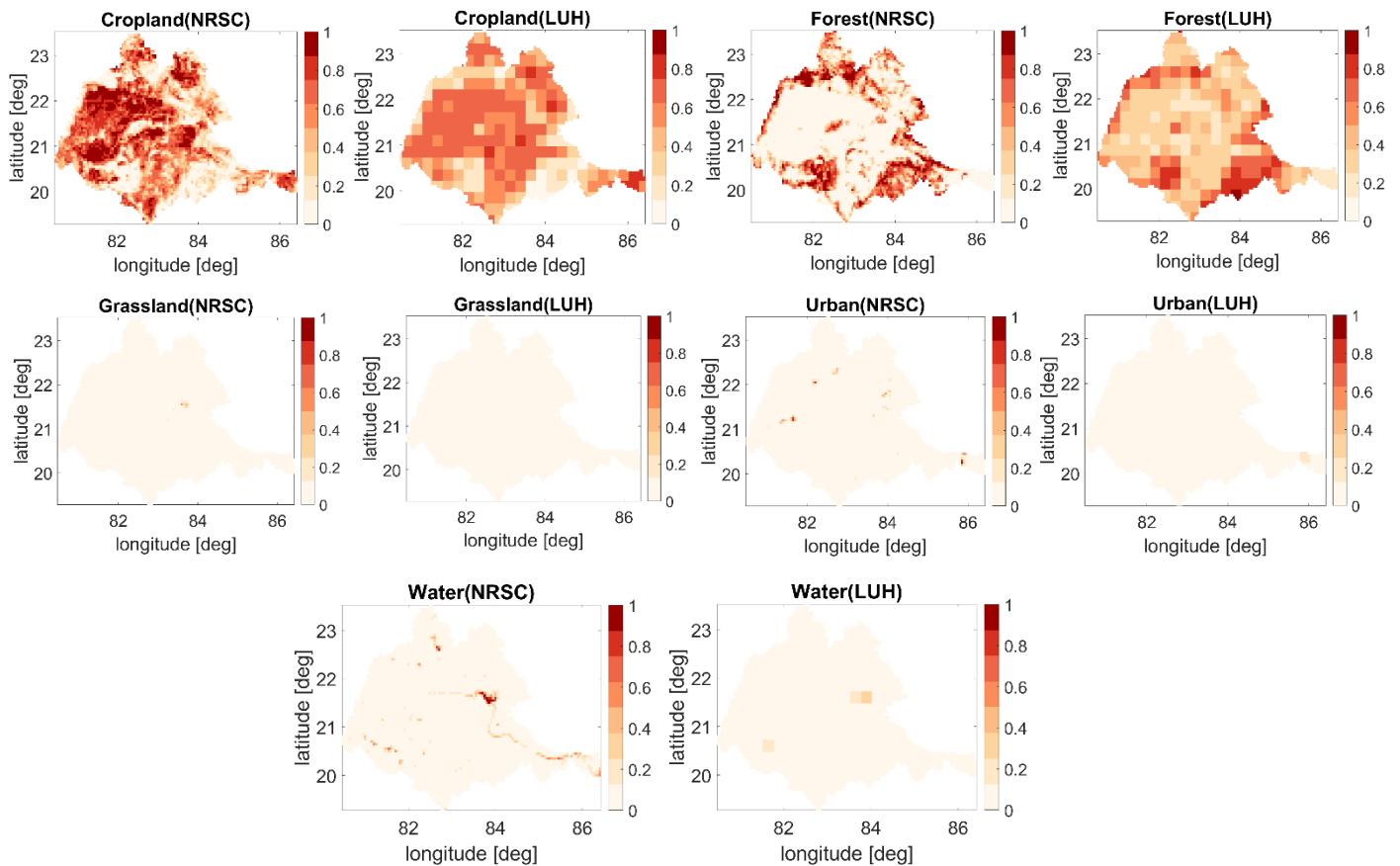


Figure 4.3 Comparison of spatial patterns of land cover types from NRSC and LUH for the baseline year, 2005. All land cover classes shown here are resampled to the model grid resolution of 5km. The color bar represents the fraction of area covered by each land cover type.

We used the behavioural models to simulate discharge for the baseline scenario using land cover map from LUH2 of year 2005 so as to attain more confidence in the future scenarios. We compare LULC maps, NRSC2005 and LUH2005 (Figure 4.3) and observe spatial patterns of the most dominant land-use classes, Cropland (CL) and Forest (F), shows a similar spatial distribution and having comparable aerial coverage. The only notable difference in both maps is that the Barren ground (BG) class is missing in LUH2005. Table 4.2 shows the percentage of area covered by each land use classes in the basin. Note that we will refer to DBF as Forest (F) henceforth.

Table 4.2 Percent of each Land use type in NRSC2005 and LUH2005 in the entire Mahanadi river basin (WB – Water Body; ENF – Evergreen Needleleaf Forest; DBF – deciduous Broadleaf Forest; GL- Grassland; CL- Cropland; U – Urban)

LULC classes (%)	NRSC2005	LUH2005
W	2.6	0.76
ENF	0.08	0
DBF	35.98	41
GL	0.13	4.7
CL	49	53
U	0.52	0.4
BG	12.3	0

Among the future scenarios, owing to the large computational demand of our simulations, we only considered the ‘worst’ case scenario, RCP3.4 SSP4, which resulted in maximum change in the land cover fractional area (Figure 4.4). For our study, we have not taken into account the actual uncertainty due to the land cover scenarios. However, the percentage of land cover change relative to the baseline from other LUH2 scenarios is either negligible or are comparable to our chosen scenario. Therefore, our chosen scenario which shows the maximum changes in land cover will likely produce the largest impact.

Land cover changes and fractional area covered in other future scenarios are shown in Figure 2.7 in Chapter 2. Four distinct years have been chosen for this study: 2005 (Baseline), 2015 (Present), 2050 (Near Future) and 2100 (Far Future) to study the impacts of LULC change in the Mahanadi river basin. A sharp decrease in the forest cover is observed at the expense of agriculture in the years 2050 and 2100 (Figure 4.4). We run the behavioural models three times using the individual LUH datasets: (1) with land use map ‘LUH2015’, termed as the ‘present’ (P) scenario (2) with land use map ‘LUH2050’, termed as the ‘Near Future’ (NF) scenario (3) and with land use map ‘LUH2100’ which is termed as the ‘Far Future’ (FF) scenario. To account for the extreme hydrological effects that these changes could cause, two hypothetical scenarios are framed (1) ‘All Cropland’ (CL) scenario where all the grassland and

forest areas are transformed into cropland (2) 'All Forest' (F) scenario where all the cropland and grassland areas are transformed into forest. The urban and water bodies in these hypothetical scenarios are retained as per the baseline scenario. Notice that the daily meteorological forcing used in all the model simulations is the same and obtained from the current climatology (i.e., 1990-2010). Here, we focus on identifying the impacts on hydrological responses mainly by applying individual land cover scenarios. Therefore, any changes observed in the predicted hydrological components will be only attributed to changes in LULC. It is also worth mentioning that running model simulations with different land cover scenarios would not directly impact the soil parameters identified in our chosen behavioural models. That is because all soil related parameter values in VIC are assigned solely based on soil textures.

In all the five cases of model simulations, meteorological forcing for the time (2001-2010) is held constant i.e., the daily precipitation, maximum and minimum temperatures and wind speed are same across all the scenarios. Therefore, any changes observed in the hydrological components in these scenarios will be only due to the change in land use. The percent areas covered by each land use classes at all subcatchments across the scenarios are shown in Table 4.3.

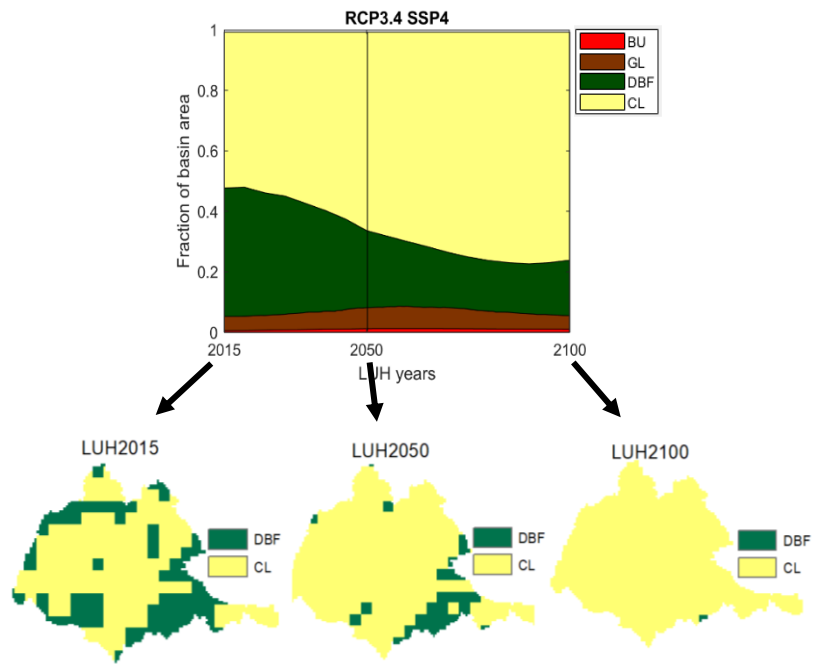


Figure 4.4: Top: Fraction of catchment area occupied by Land use classes for scenario RCP3.4 SSP4 Bottom: land cover scenarios from LUH (resolution- 25 km) for years 2015, 2050 and 2100 used in this study. LUH land cover classes shown here are resampled to the model grid resolution and only the predominant class is shown here for clarity. For actual model simulations VIC accounts for the individual proportion for each land cover type at each grid point.

Table 4.3 Land cover area change across all subcatchments of Mahanadi river basin

LULC classes (%)	Baseline 2005	Present 2015	Near Future 2050	Far Future 2100	All Cropland	All Forest
Basantpur						
CL	40	54	69	78	94	0
F	54	41	23	16	0	94
GL	1	4	6	4	0	0
w	5	1	1	1	5	5
U	1	1	1	1	1	1
Kantamal						
CL	51	44	58	70	95	0
F	44	51	33	25	0	95
GL	0	5	8	5	0	0
w	5	0	0	0	5	5
U	0	0	1	1	0	0
Kesinga						
CL	44	50	62	73	95	0
F	51	45	30	22	0	95
GL	0	5	7	5	0	0
w	5	0	0	0	5	5
U	0	0	1	1	0	0
Sundergarh						
CL	29	67	77	83	96	0
F	67	29	17	15	0	96
GL	0	3	4	2	0	0
w	4	0	0	0	4	4
U	0	0	1	1	0	0
Salebhata						
CL	34	61	73	83	95	0
F	61	34	19	11	0	95
GL	0	0	7	6	0	0
w	5	0	0	0	5	5
U	0	0	1	0	0	0

4.3. Results

4.3.1. Sensitivity Analysis, Model Calibration and Validation

It is to be noted that SA is conducted for all subbasins individually, hence the Morris screening results obtained for each subbasin are independent of each other. However, we observe that the non-influential parameters match closely with each other across subbasins (Figure 3.1, Chapter 3). Based on the Morris sensitivity measures, there are six sensitive (or influential) parameters namely *dsm_{ax}*, *d₂*, *bin_f*, *v*, *ws* and *ds*.

Figure 3.4a (Chapter 3) shows the performance of VIC with respect to KGE in the calibration and validation period for all the subcatchments in the highest order of their catchment size. In overall, evaluation result suggests the model reproduced the observed flows remarkably well with the median KGE values of 0.85, 0.86, 0.82, 0.75, 0.63 in calibration and 0.77, 0.82, 0.72, 0.60, 0.59 in validation at Basantpur, Kantamal, Kesinga, Salebhata and Sundergarh, respectively. Figure 3.6 shows that the distribution of behavioral parameters within their respective variability ranges differs from one parameter to another as well as across subcatchments. Thickness of second soil layer, *d₂* is the most identifiable parameter across all subcatchments. More details on the results of sensitivity analysis and model calibration can be found in Chapter 3.

4.3.2. Baseline scenario performance

We compare the performance of calibrated VIC models in the baseline scenario (using LUH2005) against the validation performance (using the NRSC2005) for the period 2001-2010. The boxplots in Figure 4.5(a) shows daily KGE values for the baseline and validation simulations for all subcatchments studied here. The KGE range for the calibration, validation and baseline simulations of daily streamflow for all subcatchments are listed in Table 4.4. The median KGE values for the baseline at Ba, Ka, Ke, Su and Sa are 0.62, 0.64, 0.58, 0.62 and 0.72 respectively. The model performed relatively better (to the calibration) at the smaller subcatchments, Sa and Su in the baseline whereas decline in the performance is observed at subcatchments, Ba, Ka and Ke. PBIAS values (Figure 4.5(b)) indicates that baseline simulations are more biased (negatively) than validation simulations at bigger catchments. The median PBIAS values at Ba, Ka and Ke are -28%, -29% and -33% respectively. This underestimation can be attributed to the absence of 12% Barren Ground in the baseline land cover, which is replaced by croplands (4%), forests (5.02%), grasslands (4.57). The increase in flows due to

the increase in cropland is compensated by the decrease in flows due to the increase in forest. Therefore, the underestimation in the simulated flows using LUH2005 may result from the increasing grasslands which increased LAI, thus resulting in an increase in ET and decrease in surface runoff, respectively. Contrarily, a slight positive bias of 3% is observed at the smallest subcatchment (Sa) in the baseline simulation, compared to +55% in the validation simulation. KGE values obtained across calibration, validation and baseline period indicates an overall good performance of the basin as per the existing studies that have used KGE as a performance metric (Knoben et al., 2019). In overall, baseline land cover map, LUH show comparable model performance against local land cover map, NRSC, in the historical period with the model being able to capture the seasonality and LULC dynamics while simulating the daily flows.

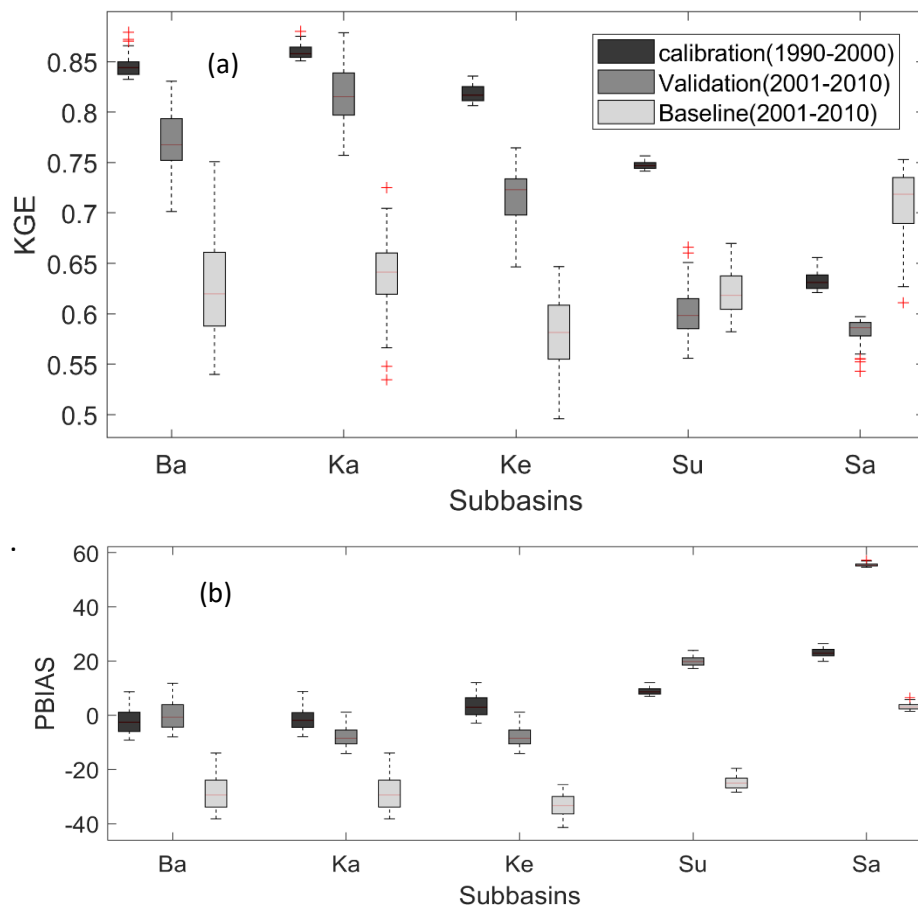


Figure 4.5 Box plot showing (a) KGE range and (b) PBIAS for calibrated, validated and baseline scenario simulations

Table 4.4 Range of KGE'S for the daily calibration and validation at all subcatchments.

Subcatchments	Calibration (1990-2000)	Validation (2001-2010)	Baseline (2001-2010)
Ba	0.83-0.88	0.70-0.83	0.54-0.75
Ka	0.85-0.88	0.76-0.88	0.54-0.73
Ke	0.81-0.84	0.65-0.76	0.50-0.65
Sa	0.74-0.76	0.55-0.67	0.58-0.67
Su	0.62-0.66	0.54-0.60	0.61-0.75

4.3.3. LULC impacts and uncertainties

Mahanadi river basin receives approximately 85% of the total annual rainfall during the monsoon months (June-Sept) which also results in 85% of the annual river discharge during the monsoon months. Moreover peak discharge also mostly occurs during the monsoon (Jin et al., 2018). Therefore, we first compute the percent change in annual average of extreme flows, i.e., flows of 95th percentile or higher (to represent the peak flows). Figure 4.6a shows percent change in annual average of extreme flows (i.e., 95th percentile or higher) for the time 2001-2010 in scenarios NF, FF, All Cropland (CL) and All Forest (F) with respect to baseline scenario for the behavioural models. The range of percent change represents the related uncertainty in model predictions arising from the behavioural model parameters. We observe an insignificant positive change in projected extreme flows in the Present (P) scenario despite a major increase 6% to 36% in croplands replacing forests across four out of five subcatchments (not shown Figure 4.6a). We observe a prominent increase in the extreme flows at all subcatchments in both future scenarios (NF and FF). The projected change in extreme flows in NF ranges between 1.3% and 10.7% across the subcatchments. The median percent change in the NF scenarios at subcatchments Ba, Ka, Ke, Su and Sa are 3.6%, 2.6%, 1.8%, 8.1% and 3.8%, respectively. This increase in extreme flows in NF can be attributed to the reduction in forest cover (-20% to -42%) at the expense of cropland (+7% to +48%) across the subcatchments. Percent increase of slightly higher magnitudes are observed in FF scenario in response to further increase in croplands. The projected changes in extreme flows in FF ranges between 1.4% and 15.4% across the subcatchments. The median percent change

in FF scenario at subcatchments Ba, Ka, Ke, Su and Sa are 4%, 2.8%, 2.3%, 11.3% and 4.1% respectively in response to reduction in forest cover (-19 to -50%) at the expense of cropland (+19 to +54%) across the subcatchments. As anticipated, maximum percent increase in the extreme flows (1.2 to 20.5%) are observed in hypothetical 'All Cropland' scenario where all forests and grasslands are replaced by cropland and maximum reduction (-2 to -41%) observed in 'All forest' scenario where all the croplands and grasslands are converted to forests. The projected percent changes in mean annual flows (Figure 4.6c) are slightly higher than the extreme flows across all scenarios and subcatchments. The median values in both future and CL scenario shows slightly higher positive percent change in the range of 3 to 11% and higher negative percent change -5 to -25% in F scenario.

Maximum increment in extreme flows and annual flows across all scenarios, is recorded at the largest subcatchment Basantpur which is in the range of 194 to 496 m^3s^{-1} and 31 to 35 m^3s^{-1} respectively. The maximum reduction of 712 m^3s^{-1} and 59 m^3s^{-1} is observed in 'All Forest' scenario at Basantpur. Much lesser change in terms of magnitudes is observed in the annual flows (Figure 4.6b) compared to the extreme flows (Figure 4.6d). This can be explained by the fact that the basin receives approximately 85% of the total annual rainfall during the monsoon months (June-Sept). Therefore, with negligible changes occurring during rest of the year, changes in extreme flows occurring only during the monsoon months are masked out when computed for the entire year. We further computed the difference between maximum and minimum values (ranges) of projected extreme flows as a measure of the amount of uncertainty contained in ensemble predictions made using land cover scenarios and multiple (behavioural) parameter sets (Table 4.5). Among all the scenarios, maximum uncertainty is observed in the hypothetical 'AllForest' scenario followed by 'All Cropland' scenario. In overall the uncertainty of hydrological model parameterization is observed at the largest subcatchment Basantpur and decrease with respect to the decrease in the catchment size.

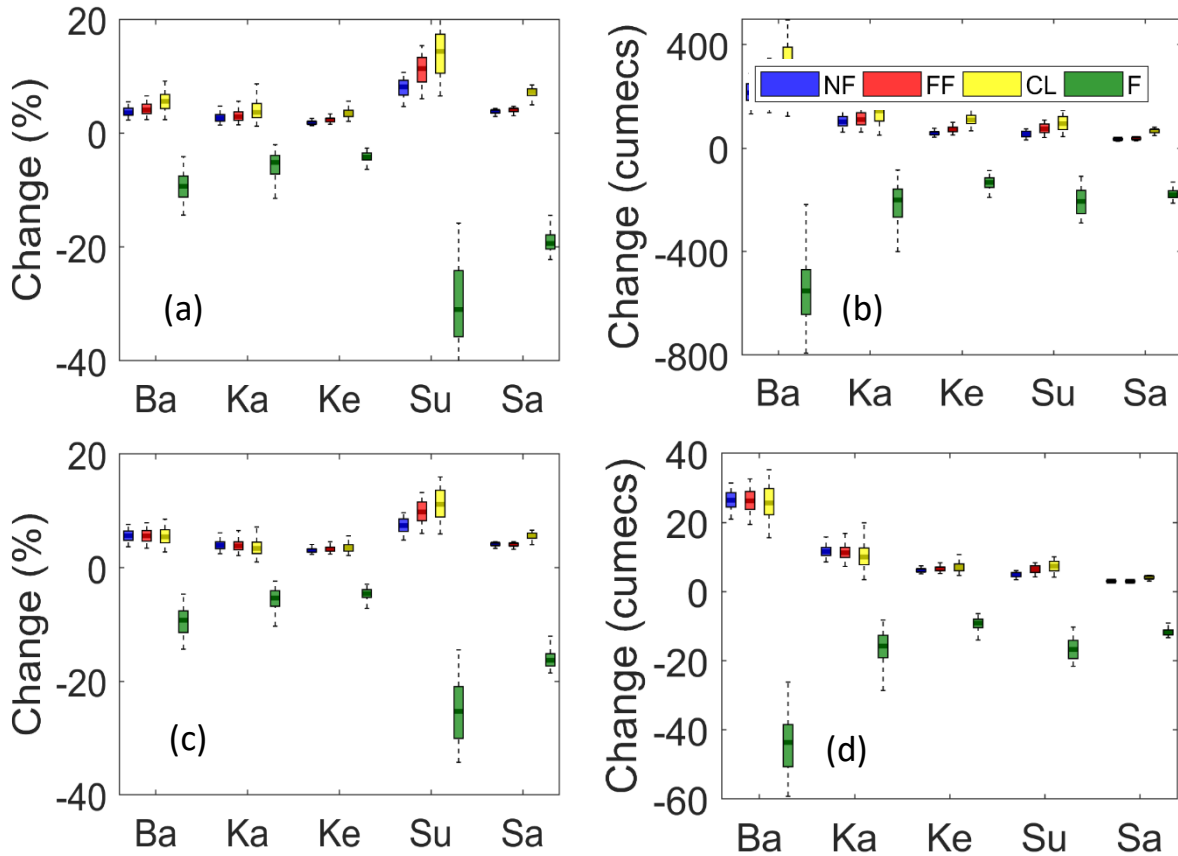


Figure 4.6: (a) Percent change in extreme flows (i.e., 95th percentile or higher) (b) Change in extreme flows in m^3s^{-1} (c) Percent change in mean flows (d) Change in mean flows in m^3s^{-1} , averaged annually over the time 2001-2010 in the Near future (NF), Far future (FF), Cropland (CL) and Forest (F) scenarios with respect to baseline scenario for all the subcatchments. Please note that the climate forcing is kept fixed for the period corresponding to year (2001-2010) The results are shown for the behavioural model simulations obtained through calibration.

We analysed the water balance components to understand the factors causing changes in the streamflow. We notice that the model is able to estimate all the water budget components and maintain proper closure of the water balance in all the scenarios across the subcatchments. In overall, we found that the increase in the mean annual flows is caused due to the increment in runoff and reduction in ET across all subcatchments.

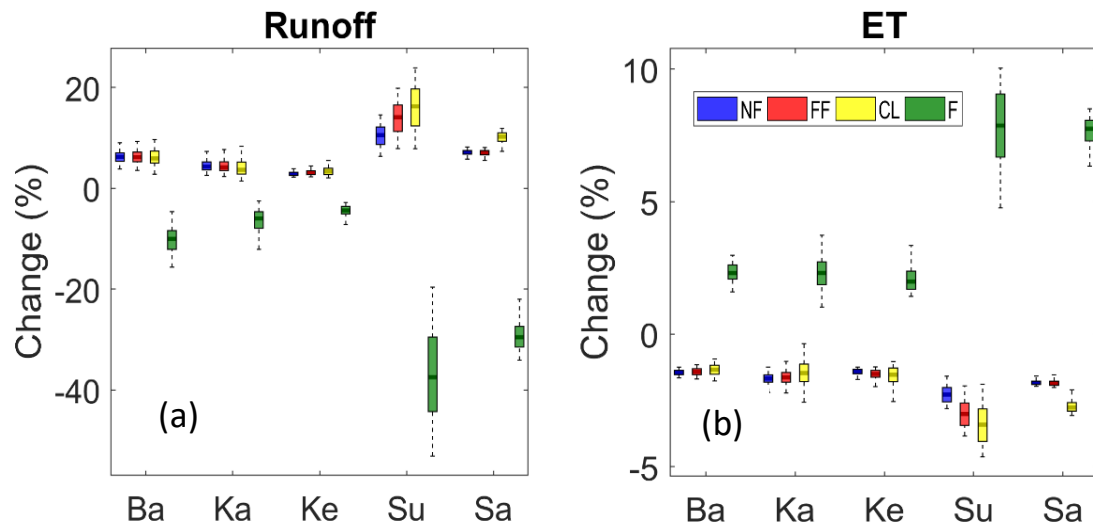


Figure 4.7: Percent change in (a) mean runoff (b) mean ET averaged annually over the time (2001-2010) in the Near future (NF), Far future (FF), Cropland (CL), Forest (F) scenarios with respect to baseline scenario for all the subcatchments. Please note that the climate forcing is kept fixed for the period corresponding to year (2001-2010). The results are shown for the behavioural model simulations obtained through calibration.

Figure 4.7 shows the percent change in mean runoff mean ET averaged annually over the time (2001-2010) in the future scenarios with respect to baseline scenario for all the subcatchments. Positive median changes are observed in runoff in scenarios (NF, FF and CL) ranging between 2.8 to 14 % and negative changes of -4 to -37 % in F scenario. Negative median changes are observed in ET in scenarios (NF, FF and CL) ranging between -1.4 to -3.4 % and positive changes of 1.9 to 7.8 % in F scenario. Removal of forests at the expense of cropland decreases the LAI of the natural vegetation and hence decreases ET. Moreover, the removal of forest cover reduces the root water uptake by plants which increases the water content of the second and third layer of the soil. The top thin soil layer in VIC model helps in partitioning the rainfall amount into direct runoff and the amount entering the soil. Therefore, the increase in the cropland results in more direct runoff thus reducing the soil moisture content in the first soil layer. The increase in runoff is not significant, despite the occurrence of major deforestation in the future scenarios. This is because the decrease in ET due to forests removal is compensated as increment in croplands also leads to a major

Table 4.5 Ranges of percent change, change in flows, and uncertainty (i.e., difference between max. and min. predicted flow) in extreme and mean annual flows in all the scenarios with respect to the baseline scenario.

Mean annual extreme	Ba	Ka	Ke	Su	Sa
		Near future			
Change (%)	2.3 to 5.5	1.4 to 4.7	1.3 to 2.7	4.7 to 10.7	2.7 to 4.3
change (m ³ s ⁻¹)	132 to 289	62 to 166	42 to 77	32 to 75	27 to 41
Uncertainty (m ³ s ⁻¹)	157	104	36	41	14
		Far future			
Change (%)	2.4 to 6.5	1.4 to 5.6	1.6 to 3.5	6 to 15.4	3 to 4.7
change (m ³ s ⁻¹)	137 to 347	63 to 195	51 to 100	42 to 109	28 to 45
Uncertainty (m ³ s ⁻¹)	210	132	49	67	17
		All Cropland			
Change (%)	2.4 to 1.2	1.2 to 8.6	2.1 to 5.7	6.5 to 20.5	5 to 8.5
change (m ³ s ⁻¹)	124 to 496	51 to 301	67 to 164	45 to 147	49 to 81
Uncertainty (m ³ s ⁻¹)	372	250	97	102	32
		All Forest			
Change (%)	-4 to -14.4	-2 to -11.4	-2.6 to -6.6	-15.8 to -41	-13.5 to -22
change (m ³ s ⁻¹)	-218 to -712	-85 to -400	-86 to -190	-109 to -289	-131 to -213
Uncertainty (m ³ s ⁻¹)	494	315	104	180	82
		Mean annual flows			
		Near future			
Change (%)	3.7 to 7.6	2.5 to 6.13	2.4 to 4.2	4.9 to 9.7	3.4 to 4.6
change (m ³ s ⁻¹)	21 to 31	8.6 to 16	5.2 to 7.5	34 to 61	2.6 to 3.3
Uncertainty (m ³ s ⁻¹)	10	7.4	2.3	27	0.7
		Far future			
Change (%)	3.4 to 7.9	2.12 to 6.5	3.4 to 4.6	6 to 13.2	3.24 to 4.6
change (m ³ s ⁻¹)	19 to 32.6	7.3 to 16.8	5 to 8.8	4 to 8.3	2.4 to 3.3
Uncertainty (m ³ s ⁻¹)	13.6	9.5	3.8	4.3	0.9
		All Cropland			
Change (%)	2.8 to 8.5	1 to 7.7	2.1 to 5.6	6 to 16	4.1 to 6.6
change (m ³ s ⁻¹)	15.6 to 35	3.4 to 20	4.7 to 12	4.2 to 10	3.1 to 5
Uncertainty (m ³ s ⁻¹)	19.4	16.6	7.3	5.8	2
		All Forest			
Change (%)	-4.6 to -14.34	-2.4 to -11.1	-2.9 to -7.2	-14.5 to -34.2	-12 to -18.6
change (m ³ s ⁻¹)	-26.2 to -59	-8.2 to -29	-6.4 to -15.8	-10.2 to -21.3	-9.1 to -13.3
Uncertainty (m ³ s ⁻¹)	33	20.8	9.4	11	4.2

increase in ET rates, which is why we do not see a sharp reduction in the ET rates. Negligible changes are observed in baseflow while slight increase in total soil moisture is noticed across the subcatchments (Not shown). The water balance indicates that 15 to 21% of precipitation is direct runoff and 64 to 80% is ET across all subbasins and all land cover scenarios whereas negligible baseflow and soil moisture change are observed. This is probably because the third soil moisture layer in the model does not reach saturation to cause the non-linear baseflow, as precipitation in the basin is highly concentrated in only three to four months in monsoon and rest of the year remains dry.

4.4. Discussions

Performing a comprehensive sensitivity analysis and model calibration enhances the accuracy for predicting hydrological responses, which subsequently improves the representations of changes in the hydrological regime due to land cover changes. Our SA results are in agreement with existing studies conducted on several basins using VIC which show *binf* and *d2* are the most sensitive parameters (Demaria et al., 2007; Gou et al., 2020b; Lilhare et al., 2020; Yeste et al., 2020). Moreover, not all the parameters recommended for calibration by VIC model developers (*binf*, *d1*, *d2*, *d3*, *ds*, *dsmax* and *ws*) are sensitive to this basin which is also in line with findings of Bao et al., (2011), Demaria et al., (2013) and Gou et al., (2020) for other basins. For, instance, first- and third-layer soil depth (*d1* and *d3*) are not found sensitive in this study. *d1* is the thinner topmost soil layer having not much control on ET and subsurface processes. *d3* is probably not sensitive as most of the roots are present in the second soil layer, hence not contributing to the soil moisture uptake through the roots. We found that soil properties impose greater control on model performance than the vegetation parameters. However, while varying soil depths influences the ET rates by posing indirect influences on both timing and magnitude of the soil water available for ET, varying root depths and fractions (using our root zone allocation approach) has provided substantial control over the water balance by directly influencing the ET rates, thereby improving KGE (not shown). The weakness in reproducing flows at smaller subcatchments in Mahanadi basin are also reported previously in some studies (Kneis et al., 2014; Mishra et al., 2008; Nayak, Venkatesh, Thomas, & Rao, 2010).

LUH2 is a new dataset, not yet extensively used in basin-scale hydrology. A recent study by Krause et al., (2019) predicted worldwide increment in runoff (67%) and a variable response

of ET across different land use scenarios using LUH2 dataset. The major changes occurring in Mahanadi in the future scenarios as predicted by LUH2 agrees with a recent study by Behera et al., (2018) in the same basin, wherein they found a prominent conversion of DBF to croplands in year 2025 relative to year 2005.

Our findings indicate increase of $27\text{--}496\text{ m}^3\text{s}^{-1}$ in extreme flows and $2.6\text{--}35\text{ m}^3\text{s}^{-1}$ in annual mean flows due to deforestation, across the subbasins and scenarios (including the hypothetical cropland scenario). These increasing trends are consistent with other studies in the Mahanadi river basin in India (Dadhwal et al., 2010), neighbouring basins (Das et al., 2018; Kundu et al., 2017) and elsewhere (Abe et al., 2018a; Berihun et al., 2019; Cornelissen et al., 2013; Costa et al., 2003). Kundu et al., (2017) found an increase in runoff and decrease in ET due to the expansion in projected agricultural land in Narmada river basin in India. Das et al., (2018) predicted that deforestation, urbanization and cropland expansion in eastern river basins of India, in the future would increase runoff and baseflow and decrease ET%. It should be noted that 15% of the agricultural land in the basin is under the irrigation effects; however, this version of VIC (version 4.2.d) does not represent irrigation. Therefore, reduction in ET rates due to conversion of forest to cropland could be compensated by the moisture available due to the irrigation during the non-monsoon season. However, this may not have a significant effect on the assessments of impacts on runoff, especially on extreme flows, because those events are likely to be related to the monsoon season, where the effect of irrigation is minimum.

We found a small change in mean annual discharge as well as in water balance components despite a major change in land cover. This correlates with research (Ashagrie et al., 2006; Fohrer et al., 2001; Hurkmans et al., 2009; Kumar et al., 2018; Patidar and Behera, 2019; Rogger et al., 2016; Viglione et al., 2016; Wagner et al., 2013; Wilk and Hughes, 2002) wherein they have reported that the impacts of land cover change on water balance components in a large-scale river basin are too small to be detected due to the compensation effects. Wilk and Hughes, (2002) showed that removal of large forests led to little or no changes in annual runoff in large heterogeneous catchments in South India. Patidar and Behera, (2019) in a recent study in a large river basin in India, reported that the conversion of forest to agriculture may not alter the water balance significantly as the impacts on ET and runoff cancels out at the basin scale.

The range of these hydrological estimates (Figures 4.6, 4.7 and Table 4.5) provides more straightforward and explicit quantification of uncertainty than other statistical measures such as variance, interquartile ranges (Her et al., 2019). Our results suggest that even a small set of calibrated models can predict a wide range of flows through different hydrological processes occurring within the basin and therefore the impacts of uncertainty derived from model parameters on the relative changes cannot be neglected. The uncertainty due to model parameters did not alter the trend of changes in extreme flow, mean annual flow and hydrological components due to land use change in comparison to the baseline simulations. However, a considerable variation is observed especially in the magnitudes of extreme flows simulated for the different land cover scenarios. For instance, the competing interactions among *Ds* and *Ws*, lead to the varying hydrological processes occurring within the basin, thereby affecting the partition of water in the soil column. Similar conclusions are outlined in Chen et al., (2019b) that the projected monthly and annual flows simulated for different land use scenarios were having significant uncertainty due to model parameterization. In addition, we found that the trends within the scenarios especially in the mean annual flows, runoff and ET are not consistent. For instance, we expect the increase in flows to be more in Far Future scenarios than Near Future, given that the increase in agricultural land in the Far Future is relatively more. However due to different parametrization, some models predicted decrease in Far Future flows relative to Near Future (Figure 7). This clearly indicates that the impact of land use could be biased when a single model prediction is used, as the impacts could be potentially hidden within simulation uncertainty derived from model parameters (Chen et al., 2019b). Only a small percentage of model simulations (2%; 100 model simulations) with relatively high daily KGE scores ($KGE > 0.8$ at 3 out of 5 subcatchments) were used for assessing the impacts, yet significant variations in extreme flow magnitudes and trends (in some cases) are observed. Therefore, selecting models with relatively lower KGE values might have led to larger uncertainty bound and inconsistent trends in the relative change. Equifinality in hydrological modelling and its influence on hydrological analysis of climate change has been discussed in several studies. However, its influence on hydrological analysis of land cover change has not been studied enough to provide a clear idea about the contributions of model parameter uncertainty to hydrological projections. Our results thus underline the importance of considering model uncertainty and consequently equifinality while modelling the landcover change impacts.

4.5. Conclusions

In this study an attempt is made to quantify the hydrologic response of the subcatchments of Mahanadi river basin owing to different land cover scenarios obtained from LUH, through the implementation of a sensitivity based calibrated semi-distributed hydrological model. Our findings are insights to the plausible hydrological scenarios in future at a river basin level. These findings are particularly important for developing countries, at the backdrop of today's growing focus on integrated water resources management (IWRM) in river basins (Behera et al., 2018). In overall, VIC captured the observed daily flows well in calibration, validation and baseline period across subcatchments. Deforestation at the expense of cropland dominated the land cover change processes across all scenarios and subcatchments, which has led to an increase in the extreme flows and mean annual flows. Analysis of other hydrological components have shown that the increase in flows is caused by the increase in runoff and decrease in ET. The uncertainties due to model parameterization in land use change impacts, varies from one subcatchment to another. The uncertainties did not alter the trend of changes when compared to the baseline; however, a considerable variation is observed especially in the magnitudes of extreme flows simulated for the different land cover scenarios. This result suggests a significant constraint on the usage of hydrological models for the variations of extreme flows due to land use change, even with high KGEs at daily time step as the impacts could be potentially hidden within simulation uncertainty derived from the model parameters. Therefore, uncertainties associated with model parameterization needs to be considered in land cover change impact assessment for more robust and reliable analysis (Chen et al., 2019b). This shall make the land cover change mitigation strategies and water resources management plans more effective.

This study indicates that the recurrent flood events occurring in the Mahanadi river basin might be influenced by the changes in LULC at the catchment scale. However, projected increase in precipitation due to climate change might have more pronounced effect on the streamflow on this basin, especially extreme flows (Asokan and Dutta, 2008; Ghosh et al., 2010; Jin et al., 2018), thereby hiding the hydrological impacts of LULC changes. Therefore, future studies shall focus on modelling the combined impacts of climate and land cover changes on hydrology of Mahanadi river basin, considering the uncertainties from model parameterization, which is currently lacking in many studies.

5. Assessing the impact of future climate changes on hydrological responses

5.1. Context and background

The impacts of climate change on the hydrological cycle and water resource systems have been an important concern worldwide in recent years (Hengade et al., 2018). Especially, developing countries like India is facing some of the serious consequences through changes in magnitude and intensity of rainfall, changes in hydrological extremes related to floods and droughts and changes in water availability (Singh and Saravanan, 2020; Thokchom, 2020). However, these hydrological responses to climate change have regional variations because of the local climate, geographical characteristics, and regional physical processes (Hengade et al., 2018; Mondal and Mujumdar, 2015).

The Mahanadi river basin in India is one of the recognized climatic vulnerable regions (Panda et al., 2013). Few studies exist that assess future climate change induced impacts on regional scale hydrology in context of Mahanadi river basin. Panda et al., (2013) found increasing and decreasing trends in streamflow in different months during monsoon and also reported an overall decline in discharge in the basin. Studies such as Asokan and Dutta, (2008), Ghosh et al., (2010) and Jin et al., (2018) predicted an increase either in the high (peak) flows or monsoon flows in the future, that would potentially enhance the flood potential, whereas, insignificant to significant decline in low flows and water availability is reported. Jena et al., (2014) reported that the recent floods in the basin is caused by the increased extreme rainfall events, contradicted by Ghosh et al., (2010) observing a significant decreasing trend in streamflow. Gosain et al., (2006) found an increase in evapotranspiration under future climate change. Understanding these regional hydrologic implications of changing climate has crucial role in the management of water resources (Joseph et al., 2018).

Global climate Models (GCM's) simulates time series of climate variables and provide the possible future climate projections. However, GCM's are at very coarse resolution, and downscaling is required to reproject it to the finer scale, to get reliable projections at the

regional scales (Christensen et al., 2008). A variety of statistical and dynamic approaches are developed for downscaling and bias correction of GCM climate projections (Janes et al., 2019; Mishra et al., 2020a; Raje et al., 2014; Singh and Saravanan, 2020; Wood et al., 2004). The downscaled projections from different GCM products are directly used in hydrological impact assessment studies (Chawla and Mujumdar, 2015; Jin et al., 2018; Joseph et al., 2018; Mishra et al., 2010, 2020b; Rickards et al., 2020; Wang et al., 2018). For instance, Janes et al., (2019) dynamically downscaled GCMs from the recent generation of Climate Model Intercomparison Project 5 (CMIP5) GCM, to a high resolution of 25 kms for South Asia. Recently, these downscaled climate projections are used by Jin et al., (2018) for hydrological impact assessment in Mahanadi river basin in India, which predicted an increase in the peak flows in future. Several studies pointed out the drawbacks of CMIP5 models such as under/overestimating the monsoon characteristics over Indian subcontinent (Saha et al., 2014; Sharmila et al., 2015) and to overcome these challenges, most recent generation of climate models i.e., the sixth phase, CMIP6 was released. These are now the most improved version of climate models available. CMIP6 models shows significant improvement in reproducing the characteristics of Indian monsoon such as mean and extreme precipitation, intra-seasonal variability and seasonal climatology, which is comparable to that of observations (IMD), when compared to its predecessor, CMIP5. However, the spatial improvement is inconsistent among the models, especially in capturing the seasonal climatology i.e., active and break spell variations in observations. However, averaging across the models has shown better representation of the intra-seasonal variations. These improvements in CMIP6 simulations can be attributed to the Modified deep convective schemes, advanced microphysics parameterization options, improved spatial and vertical resolution, incorporating indirect effects of aerosols in cloud formation, and improved ocean-ice models (Gusain et al., 2020; Rajendran et al., 2021). CMIP6 has produced new scenarios called Shared Socioeconomic Pathway (SSP) 1–2.6, SSP 2–4.5, SSP 3–7.0, and SSP 5–8.5 (described in Chapter 2 of this thesis) (O’Neill et al., 2016). Gusain et al., (2020) reported a significant improvement in CMIP6 models in reproducing the monsoon characteristics over India. Recently, Mishra et al., (2020a) used climate models from CMIP6 to develop high resolution bias corrected climate projections over Indian subcontinent. It is essential to derive the hydrological change projections for the Indian river basins under these new scenarios for the ongoing climate change mitigation and adaptation activities.

Climate impact assessment studies suffer from several uncertainties associated with the choice of climate models, greenhouse gas emissions scenario, downscaling techniques, hydrological models and parameterisation (Chen et al., 2011; Eum et al., 2014; Hagemann et al., 2013; Jiang et al., 2007; Xu et al., 2005). Uncertainties associated with climate models are considered to be the largest and are represented using information from multiple GCMs (Her et al., 2019), and some other approaches are also employed such as probabilistic approaches (Mujumdar and Ghosh, 2008) and non-parametric approach (Ghosh and Mujumdar, 2007b). The choice of downscaling techniques also adds to the uncertainty and has been addressed in many studies (Chen et al., 2011; Joseph et al., 2018). Given the availability of a wide range of climate models, emission scenarios and downscaling techniques, it is becoming a difficult task to assess the uncertainties resulting from these sources and their combination (Wilby and Harris, 2006). Further difficulties arise when we consider the choice of a hydrological model and its parameterization, which contribute to the total uncertainty.

Distributed hydrological models are highly parameterised and are commonly used in climate impact studies. Hydrological processes are non-linear in nature and different combinations of model parameters can produce similar model performance, known as equifinality (Beven and Freer, 2001). Therefore, simulated hydrological impacts based on single set of model parameters can be difficult to interpret. Despite this, most of the hydrological studies in the context of climate change, especially in India are carried out using a single calibrated hydrological model (Chawla and Mujumdar, 2015; Gosain et al., 2006; Hengade et al., 2018; Jin et al., 2018; Raje et al., 2014; Singh and Saravanan, 2020) and therefore, this approach underestimates or ignores the uncertainties associated with the model parameters. Jin et al., (2018) emphasized on proper model calibration and consideration of uncertainties associated with inputs and parameters while simulating future hydrologic projections. Since previous studies showed that the calibration of hydrological models contributes little to overall uncertainty (Chen et al., 2011), there are only few known studies about the influence of model parameter uncertainties on climate change impact assessment (Eum et al., 2014; Feng and Beighley, 2020; Her et al., 2019; Joseph et al., 2018). Feng and Beighley, (2020) found that the contributions from model parameters to the total uncertainty is relatively less whereas Eum et al., (2014) reported that the annual peak flows in a river basin in Canada is significantly impacted by the choice of parameter set. These studies underlined the need of climate

change impact assessment based on multiple hydrological models and parameterisation. In this chapter, we address the following science questions: - 1. How does future climate projections impact the hydrological responses of Mahanadi River basin in India? 2. How are those projected hydrological responses impacted by different hydrological model parameterisation?

To respond to these questions, we used a behavioural set of Variable Infiltration Capacity (VIC) models in conjunction with climate projections from most recently available GCMs from CMIP6, to predict the hydrological responses in Mahanadi river basin. Ensemble VIC models for the individual subcatchments of the basin are obtained after performing rigorous sensitivity analysis and calibration experiments under the Monte Carlo framework (described in Chapter 3 of this thesis). Changes in hydrological responses under future climate conditions and its associated uncertainties are essential to assess the vulnerability of Mahanadi river basin and make adaptation strategies to evaluate the impacts of climate change.

5.2. Materials and methods

5.2.2. Model Input datasets and parameters

VIC model has been used in several regional-scale climate impact assessment studies (Eum et al., 2014; Feng and Beighley, 2020) including river basins in India (Chawla and Mujumdar, 2015; Hengade et al., 2018). Model descriptions can be found in Chapter 2 of this thesis.

The key input data required by the VIC model are meteorological forcings (precipitation, maximum temperature, minimum temperature, and wind speed), soil type, land cover information and topographic features. Topographical features are determined using the 30-meter CARTO-DEM (Cartosat-1 Digital Elevation Model), a national DEM developed by ISRO (Indian Space Research Organization) (Sivasena Reddy and Janga Reddy, 2015). Soil textures are derived from the digitized soil map as provided by National Bureau of Soil Survey and Land Use Planning (NBSSLUP) (Scale 1:250000) (Figure 2.6a, Chapter 2).

Daily gridded precipitation (resolution, 0.25°) and maximum and minimum temperature (resolution, 1°) for the historical time period 1990-2014 are obtained from India Meteorological Department (IMD) (Pai et al., 2014). Global climate projections for precipitation, maximum temperature, and minimum temperatures for the time 2015-2100 are obtained from Coupled Model Intercomparison Project-6 (CMIP6) which are used in model simulations for predicting hydrological impacts of future climate changes. All climate

variables (precipitation, maximum temperature, and minimum temperature) from both sources, IMD and CMIP6 are resampled to the model grid resolution of 0.05° . LULC map for the historic period is derived from National Remote Sensing Centre (NRSC), India of year 2005 (scale 1:250000; resolution 56 meters) (see Figure 4.1a, chapter 4). This LULC map is used in all the model runs during historic period, i.e., while performing sensitivity analysis, model calibration and validation. Future land cover maps are obtained from Land Use Harmonisation 2 (LUH2) database which are used in model simulations for predicting impacts of future climate changes. All LULC maps used in this study are reformatted and reclassified into USGC LULC types as required by the VIC model. Wind speed for the historical period is obtained from NCEP/NCAR reanalysis of resolution 1° .

We have used daily climate data from 13 GCMs under four combined scenarios of the SSPs and the Representative Concentration Pathways (RCPs), viz, SSP1–2.6, SSP2–4.5, SSP3–7.0, and SSP5–8.5 scenarios (O’Neill et al., 2016). These models are selected based on the availability of daily precipitation, maximum and minimum temperatures for the historical and future time period and four scenarios (Mishra et al., 2020a). Please note that time series of wind speed for the future i.e., 2015-2100 was not available from all the climate models and scenarios used in this study. Therefore, we computed the mean monthly wind speed and averaged over the historical time 1990-2014 to obtain the long-term seasonal variation of wind speed. We used these values for wind speed and kept it constant throughout the future period 2015-2100. Prior to the model runs for the future period, we performed an experiment where we compared the hydrological components simulated using wind speed from NCEP/NCAR to that of using constant mean monthly wind speed, during the historical period. We observed insignificant changes between these two simulations.

The observed discharge at daily scales at multiple locations of Mahanadi river basin (Figure 1, Chapter 2) for the simulated time (1988-2015) are obtained from the Central Water Commission (CWC), India, for validating the simulated discharge.

To analyse the parameter space uncertainty, we calibrated the influential parameters (obtained from sensitivity analysis) at all subcatchments of Mahanadi river basin using Monte Carlo simulations and obtained the best or behavioural set of VIC models. Ten years (1990–2000) of daily discharge was used for model calibration with a warmup period of two years 1988-1989, and 14 years of data (2001–2014) was used for validation. These behavioural

parameter set was selected, based on Kling-Gupta Efficiency (KGE). More details regarding sensitivity analysis, model calibration and validation can be found in Chapter 3 of this thesis.

5.2.3. Setting up climate scenarios impact study

5.2.3.1. Bias-corrected climate projections from Coupled Model Intercomparison Project-6 (CMIP6)

Climate projections used in this study for Mahanadi river basin are derived from the recently released, bias corrected climate projections for South Asia from Coupled-Model intercomparison project-6 (Mishra et al., 2020a). These bias corrected data of precipitation, maximum temperatures and minimum temperatures are available at daily temporal and 0.25° spatial resolution for South Asian countries including 18 river basins in India. A total of thirteen GCMs are considered for bias correction based on the availability of all three variables and four scenarios (SSP126, SSP245, SSP370, SSP585).

Mishra et al., (2020a) employed Empirical Quantile Mapping (EQM) for the bias corrections of the historic (1951–2014) and projected (2015–2100) climate data. EQM is a statistical approach, based on the distribution and relationship between the observed and projected data for the historical period (Pierce et al., 2015). EQM based statistical bias correction method has been extensively used, and its performance was found to be satisfactory when compared to the other methods (Mishra et al., 2020a). Observed daily gridded climate variables (gridded precipitation, maximum and minimum temperatures) from IMD (spatial resolution of 0.25°) is considered as a reference for the bias correction in Mishra et al., (2020a), i.e. bias in mean annual precipitation, maximum and minimum temperatures from 13 CMIP6 models in the historical period were estimated against IMD observations. IMD gridded observations are used for bias corrections as station data are not available and also IMD gridded datasets are widely used for hydroclimatic studies in India. The CMIP6 models showed a negative (dry) bias (15-20%) in mean annual precipitation and also in extreme precipitation in the majority of South Asia. CMIP6 models also showed warm bias in mean annual minimum temperature and also 90th percentile of maximum and minimum temperatures in the majority of South Asia. However, Mishra et al., (2020a) reported that EQM based bias correction has resulted in substantial reduction in the bias of both mean and extreme annual precipitation in the historical period and also has successfully removed the bias in maximum and minimum temperatures across South Asia. The seasonal cycle of the

CMIP6 bias-corrected precipitation, maximum, and minimum temperatures also compare well against the observations. Moreover, the bias-corrected dataset is also able to capture the covariability of the monsoon season precipitation and air temperature. Since the bias-corrected dataset is consistent with observation for a climatological mean period, it would be easier to infer the predicted changes and its implications that it might have for our results. We would assume that a slight dry bias in the bias corrected precipitation dataset along with the warm bias in the mean annual temperatures might lead to slight underestimation of projected flows (both mean annual and extreme flows).

Figure 5.1 shows the comparison of total monthly precipitation produced by IMD against thirteen CMIP6 models used in this study, spatially averaged for the entire Mahanadi river basin in the historical period. We observe that IMD precipitation is lying within the upper and lower ranges of precipitation from CMIP6 ensembles, which indicates IMD precipitation could represent one of the CMIP6 ensembles. The majority of CMIP6 models tend to overestimate precipitation, especially during the monsoon months, compared to IMD, and few models are underestimating precipitation. We computed the percent bias (PBIAS) of monthly precipitation from CMIP6 models against IMD, which ranges from -8.67 to 8.2 across CMIP6 ensembles. The mean annual precipitation for the historical time period, from IMD is 1329 mm year⁻¹, whereas from CMIP6 models ranges between 1210 and 1438 mm year⁻¹.

Figure 5.2 shows the comparison of monthly mean maximum and minimum temperatures produced by IMD against thirteen CMIP6 models, spatially averaged for the entire Mahanadi river basin in the historical period. We observe an overestimation in both maximum and minimum temperatures from CMIP6 during the monsoon months whereas slight underestimation is observed during January to May. Annual average maximum temperature derived from IMD is 32.44°C and from CMIP6 ranges from 32.57 to 32.97°C. Annual average minimum temperature from IMD is 20°C and from CMIP6 ranges from 20.52 to 20.98°C.

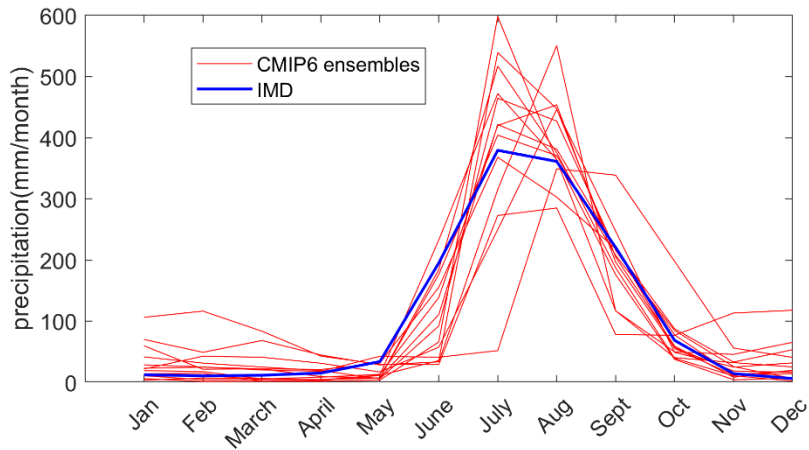


Figure 5.1. Comparison of monthly mean precipitation produced by IMD (blue) against thirteen CMIP6 models (red), spatially averaged for the entire Mahanadi river basin for the historical time 1990-2014 considered in this study.

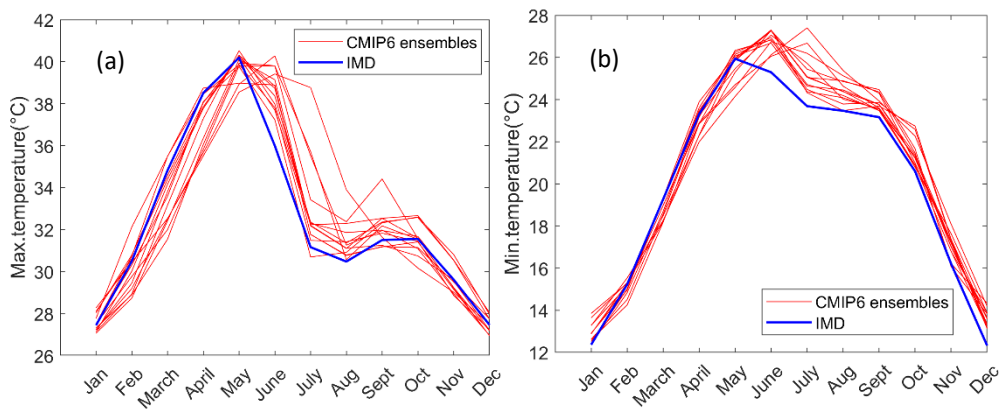


Figure 5.2. Comparison of monthly mean (a) maximum temperature and (b) minimum temperature produced by IMD (blue) against thirteen CMIP6 models (red), spatially averaged for the entire Mahanadi river basin for the historical time 1990-2014 considered in this study.

Figure 2.4 (a-c) (Chapter 2) shows the total annual precipitation, mean annual maximum and minimum temperatures, for the fifty-two ensembles (i.e., 13 CMIP6 models * 4 SSPs) (red colour) and the mean of the ensemble (blue colour) for the future period 2015-2100. The increase of both mean annual minimum and maximum temperature, based on the mean of the ensemble, is 0.3 °C per decade and mean annual rainfall shall increase with a rate about 42 mm per decade. We want to understand how strongly these future climate change might impact the hydrological responses of the Mahanadi river basin. Within the hydrological responses, we specifically focus on the impacts on mean annual flows and peak flows (and monsoon flows) in the future. We specifically focus on peak flows because Mahanadi river

basin receives approximately 85% of the total annual rainfall during the monsoon months (June-Sept) which also results in 85% of the annual river discharge during the monsoon months. Moreover peak discharge also mostly occurs during the monsoon (Jin et al., 2018).

5.2.3.2. Sampling of CMIP-6 Projections

This subsection describes the methodology we follow to select samples of the climate projections for our model runs. There are 13 climate models, 4 scenarios and 101 behavioral VIC models i.e., in total 5200 ensembles ($13 \times 4 \times 101$) are formed, and each ensemble is to be run for a long-term period of 86 years i.e., 2015-2100. Running all these ensemble members would probably result in more robust impact modelling activities. However, this is not always feasible due to the computational restrictions and modelling capabilities (Janes et al., 2019). For this reason, many researchers have been limited either in their selection of GCMs to only few models (Janes et al., 2019; Singh and Saravanan, 2020) or choosing specific time periods, such as in (Chen et al., 2020).

Despite recent advancements in GCMs, large uncertainties still exist in GCM predictions, downscaling and bias correction techniques (Jiang et al., 2007). Hence, choosing a few decades to represent a short-term and a long-term future is considered subjective and not well informative, as we cannot project the exact climate conditions of the future decades due to the inherent uncertainty from GCMs (Wootten et al., 2017). For instance, given the deficiencies in GCM predictions, Jiang et al., (2007) adopted hypothetical future climate change scenarios based on IPCC report, which includes a combinations of few temperature and precipitation increases. For example, the combinations of changes in mean annual temperature of 1°C, 2°C, 3°C, 4°C and annual precipitation of 5%, 10%, 15%, 20%, 25%, relative to the baseline climate. Moreover, VIC simulations are computationally very expensive and time consuming and therefore, we have adopted a relatively new methodology to choose the sample simulations from all the ensembles following the approach by Batelis, (2021). We refrain from using a selective approach, rather we use a new more objective approach that could give a better insight on the impact of climate change. We try to identify the hydrological impacts of a specific change in mean annual temperature and precipitation (e.g., +3 °C of mean annual temperature and +30% of mean annual precipitation) on the hydrological responses, instead of simulating the climate change impacts for a specific decade or specific scenarios in the future (e.g., 2080s or scenario SSP585).

The 25-year period [1990-2014] from IMD is used as the reference period in this study. First, we estimated the 25-year moving average for precipitation and temperature for the 52 (13 models * 4 scenarios) ensembles. For each ensemble, the 86-year time series (2015-2100) gives 62 values of 25-year average precipitation and temperature. Therefore, in total, 3224 (62*52) sets of 25-year periods for 52 ensembles are formed.

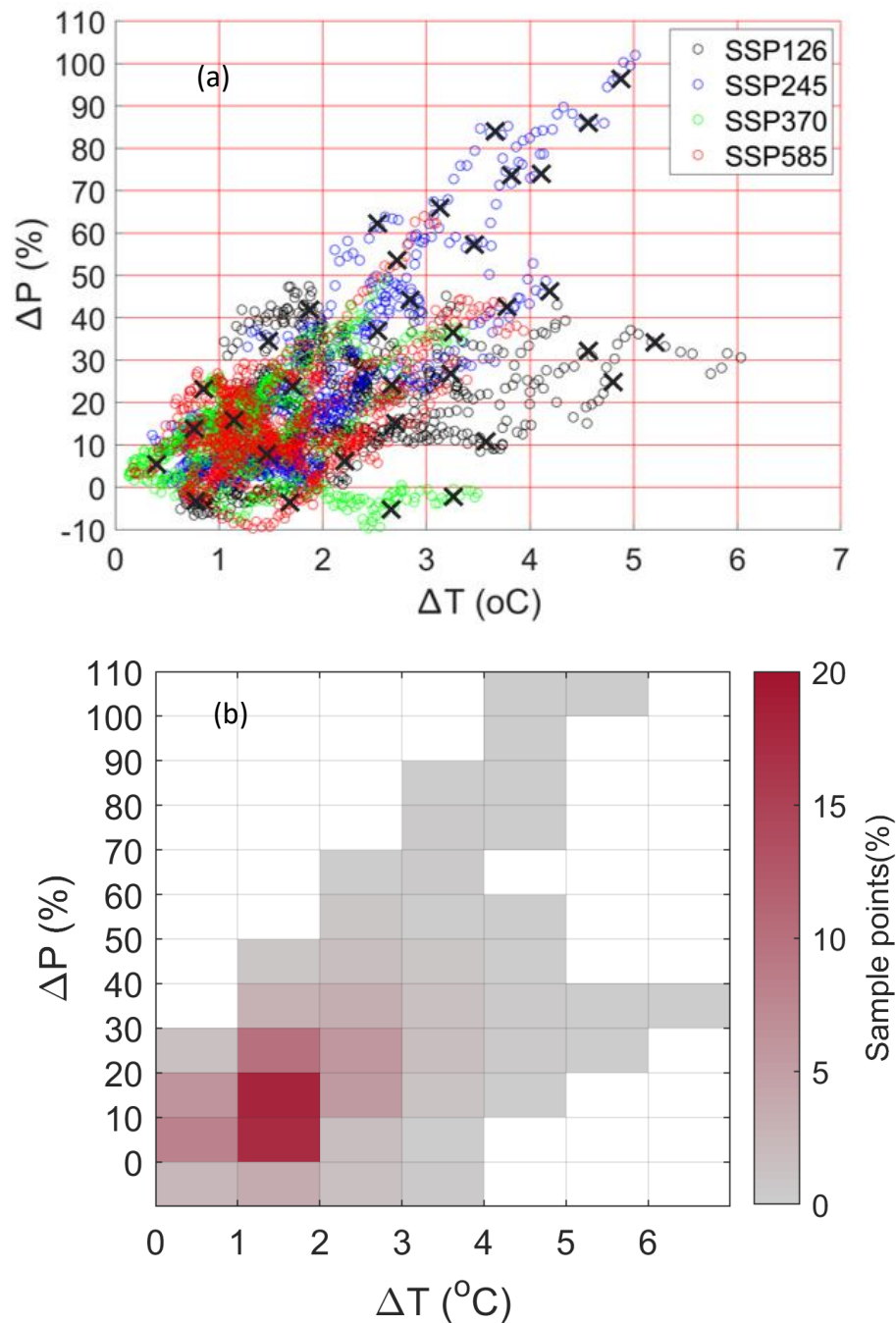


Figure 5.3 (a) Different possible combinations of normalized differences for temperature ΔT (°C) and precipitation ΔP (%) between the 3224 sets of 25-year periods from the 52 (13

models*4 scenarios) ensembles of CMIP6 against the 25-year Control Period from IMD, averaged over the entire Mahanadi river basin. Black cross denotes that one sample point is chosen from each bin for model simulation (b) Heat map showing the density of sample points lying within each bin of Figure 5.3 (a).

Next, we compute the deviations of these values against the control 25-year representative values for precipitation (P_{ctrl}) and temperature (T_{ctrl}) from IMD. In case of precipitation (P), we compute the percentage deviation (ΔP) (Equation 5.1); whereas, for the temperature (T), we estimate difference of the two values (ΔT) (Equation 5.2).

$$\Delta P = [(\bar{P}(mn) - \bar{P}_{ctrl}) / \bar{P}_{ctrl}] 100 \quad \text{Eq. 5.1}$$

$$\Delta T = (\bar{T}(mn) - \bar{T}_{ctrl}) \quad \text{Eq. 5.2}$$

Where P and T are the 25-year mean annual precipitation and temperature respectively, for every one of the 62 values ($m = 62$) from each model/scenario ($n = 52$).

Figure 5.3 a shows the difference (ΔT) of each 25-year mean temperature $T(m,n)$ with the control 25-year representative mean (\bar{T}_{ctrl}) against the percentage deviation (ΔP) of each 25-year mean precipitation $P(m,n)$ with the control precipitation (\bar{P}_{ctrl}). The range of x and y axis are divided into 12 and 7 bins, respectively. The range of bins in x axis is 1°C and in y axis is 10%. Figure 5.3b shows percentage of sample points located in each grid, from which we can find the scenarios that are most likely to occur in the future. We observe that maximum number of sample points are in the grids where precipitation increases from 0 to 30% and temperature rises from 0 to 3°C . Note that we are not predicting hydrological impacts of any specific scenarios (shown in Figure 5.3b), rather we are predicting the impacts with respect to the increase in precipitation and temperature.

We observe there are 40 bins (Figure 5.3a) in total, having at least one climate sample point. We then choose a climate sample point from each bin as a representative of that bin; therefore, we choose a total of 40 sample points from 40 bins. These points (i.e., each point from each grid) are chosen based on an approach given below.

1. First, we choose a scenario (ex: SSP126 or SSP245) which occurs maximum times in a bin. To find this, we have computed the mode of the scenarios in every bin (See Figure 5.4a).

2. Next, we choose a 25-year time period (ex: 2037-2062) from within the time periods, linked to our chosen scenario (in step 1). To find this, we have computed the median of the time periods. Remember that each point in a bin could represent a different 25-year time period from within 2015-2100.
3. Next, we choose a climate model that is occurring maximum times in a bin. To find this, we have computed the mode of the models in the bin. If the model that occurs maximum times in a bin, is not linked to the scenario (step1) and time period (step2) we have already chosen, we then choose any other model linked to our chosen scenario and time period. This is because we are giving maximum priority to the scenario followed by the time period.
4. Finally, we choose a future land cover map from LUH2 land cover scenarios, based on the chosen scenario and chosen time period (year). For example, if the median time period is 2037-2062, then we choose a land cover map of year 2050 (i.e., middle of the median time period). Notice that same scenarios that we use for climate projections are also available from LUH2 database.

Figure 5.4 a-d further explains choosing a sample point from a particular grid, where temperature (ΔT) varying from 1°C to 2°C and precipitation (ΔP) varying from 10% to 20%.

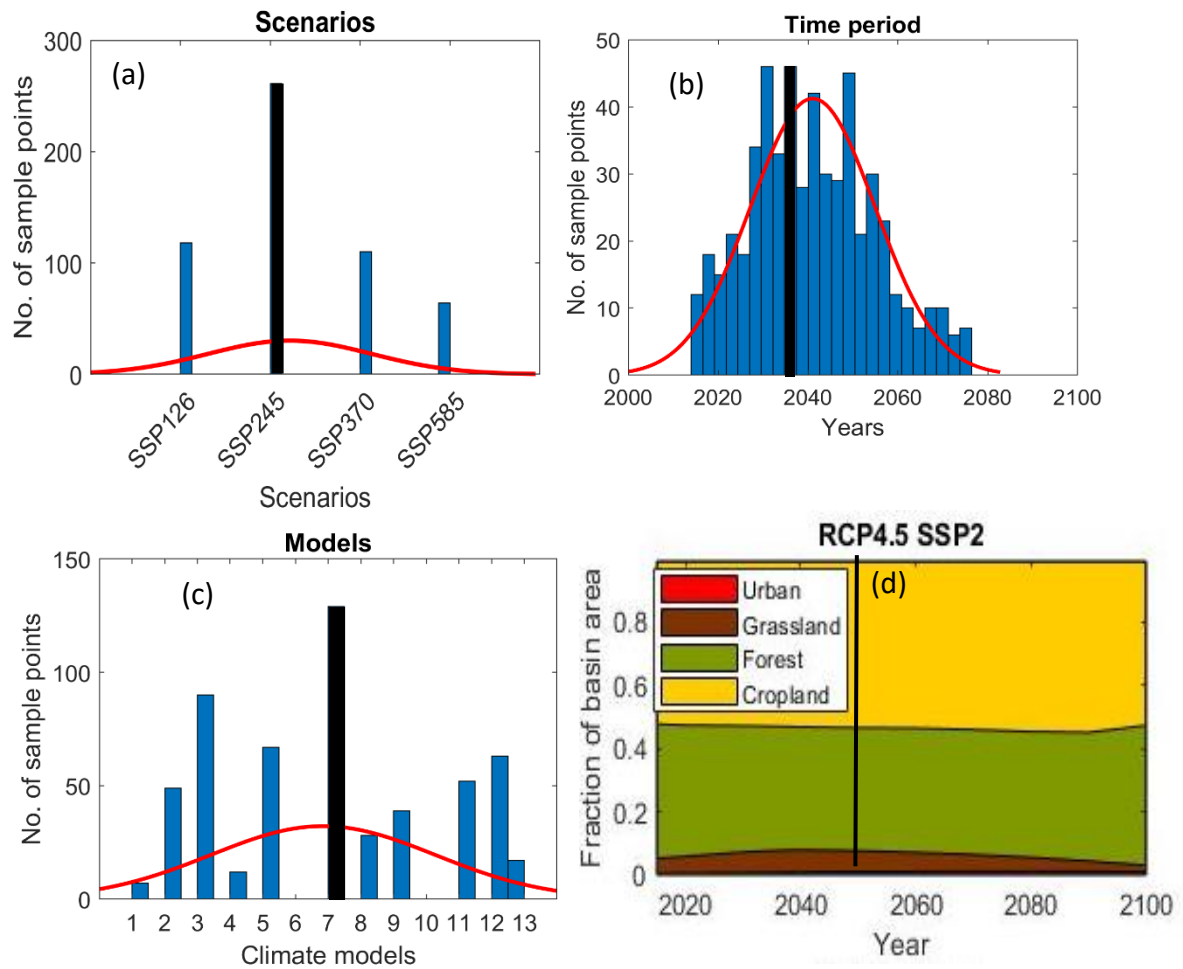


Figure 5.4 Procedure to choose a climate sample point from a particular grid, for instance for a grid where temperature (ΔT) varying from 1°C to 2°C and precipitation (ΔP) varying from 10% to 20%. (a) choosing a scenario based on the maximum occurrences (i.e., computed from mode of the scenarios), SSP245 (marked in black) is the chosen scenario for this particular grid (b) choosing a time period from within the time periods linked to our chosen scenario (SSP245) based on the median of time periods. 2037-2062 (marked in black) is the chosen time period for this particular grid (c) choosing a model based on maximum occurrences (i.e., computed from mode of the models) Model 7 (marked in black) is the chosen model for this particular grid (d) Choosing a future land cover map from LUH2 land cover scenarios, based on our chosen scenario and time period. Land cover map for year (2050) (marked in black) is chosen for this particular grid.

5.3. Results

5.3.1. Model performance in historical period

The VIC model is calibrated for the period 1990-2000. In overall, evaluation result suggests the model reproduced the observed flows remarkably well with the median KGE values of 0.85, 0.86, 0.82, 0.75, 0.63 in calibration period. More details about the model performance in calibration period is described in Chapter 3. Next, we consider the historical time 1990-2014 as the reference period to assess the climate change impacts in future, therefore, we assess the model performance of the entire time 1990-2014. Figure 5.5 presents the KGE and PBIAS values over the whole record 1990-2014, obtained with the behavioral parameter sets, i.e., each boxplot represents 101 values for the subcatchments of Mahanadi river basin. In overall, the model reproduced the observed flows well in the reference period with the daily median KGE values of 0.68, 0.59, 0.50, 0.59, 0.54 at Basantpur, Kantamal, Kesinga, Salebhata and Sundergarh, respectively. However, we observe best performance at the largest subcatchment, Basantpur and relative reduction in the daily KGE values at the smaller subcatchments. The PBIAS values obtained indicate that the model tends to be negatively biased i.e., tending to underestimate the daily discharge values, with the maximum reduction observed at Kesinga. The median PBIAS values are -22%, -32%, -37%, -25%, -18% at Basantpur, Kantamal, Kesinga, Salebhata and Sundergarh, respectively.

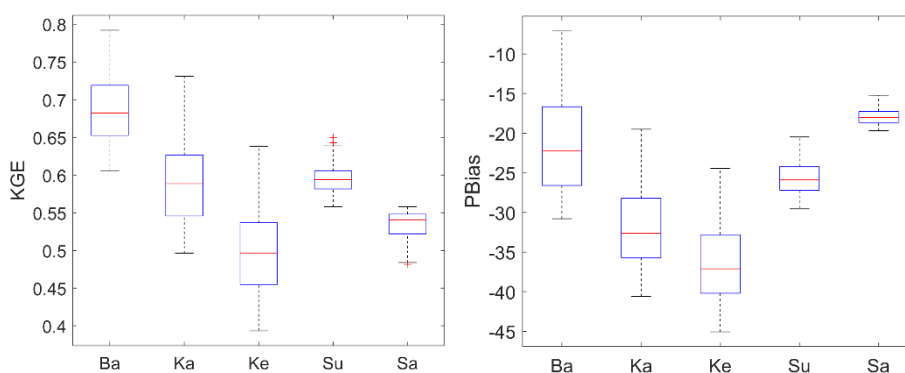


Figure 5.5: Boxplots showing KGE and PBIAS range for 101 VIC model simulations for the subcatchments of Mahanadi river basin (Ba- Basantpur; Ka- Kantamal; Ke- Kesinga; Su- Sundergarh; Sa- Salebhata).

Note that the bias in terms of flow volume in the non-monsoon or the dry season is negligible (not shown) compared to the wet or monsoon season, therefore percentage of bias computed for the entire time period (shown above) mainly represents bias in the monsoon flows, where the effect of irrigation is supposed to be minimum.

2.1.1. Impacts on mean annual flows and model parameter uncertainties

The percentage change in mean annual flow is computed for future climate projections based on the combination of change in precipitation and temperature as shown in Figure 5.3 (a). Figure 5.6 (A) shows the percentage change in the mean annual discharge in the future period relative to the control case simulation in the historical period 1990-2015. Note that the percentage change is computed for each sample point shown in Figure 5.3, that represents a different 25-year time period in the future. Percent changes in mean annual flows in Figure 5.6 (A) are the average of percent changes resulting from behavioral set of VIC models i.e., we do not consider the parameter uncertainty in this figure. The results are analyzed for individual subcatchments of Mahanadi river basin. In overall, we observe that the change in precipitation from -5 to +105% and change in temperature from 0-7°C has resulted in change in mean annual flows ranging from -95 to +645% across subcatchments. The change in mean annual flows in terms of flow magnitudes varies from +728 to +2849 m^3s^{-1} across subcatchments.

We observe that percent increase in mean annual discharge across subcatchments is more prominent with the percent increase in rainfall above 20%, irrespective of the rise in temperature. Negative or small percentage change in annual rainfall (in the range of -10 to 10%) combined with increase in temperature ranging from 0 to 4°C in most subcatchments, has resulted in decrease in the mean annual flows. In these cases, the increase in temperature might have resulted in the increase of ET thereby reducing the runoff. In relatively bigger catchments like Basantpur and Kantamal, almost all grids show an increase in the mean annual flows with the increase in annual rainfall, with an average percentage change of +80% ($614 \text{ m}^3\text{s}^{-1}$) and +24% ($100 \text{ m}^3\text{s}^{-1}$) respectively. At Kesinga, we observe reduction in mean annual flows even with an increase of precipitation upto 50%, with an average percentage change of -20% ($-44 \text{ m}^3\text{s}^{-1}$). In smaller subcatchments like Salebhata and Sundergarh, all precipitation and temperature combinations, even including those with slight precipitation increase, has resulted in positive percent change with an average change of +206% ($+98 \text{ m}^3\text{s}^{-1}$).

¹) and +215% (+116 m³s⁻¹) respectively. This indicates a strong positive correlation between precipitation and streamflows in the smaller subcatchments. Maximum increase in the percent change of mean annual flow (+645%, +296 m³s⁻¹) is observed at the smaller subcatchment, Salebhata with about +100% percent increase in precipitation and +7% increase in temperature respectively. Likewise, maximum decline in flows of (-78%, -170 m³s⁻¹) is also observed at Basantpur when the percent change in rainfall and temperature lies between 20 to 30% and 2-3°C respectively.

From Figure 5.3 (b), we observe that the changes in precipitation and temperature that are most likely to occur in the future lies within the temperature range of 1 to 2 °C and precipitation ranging from 0 to 30%. Particularly, within these ranges of precipitation and temperature change, change in mean annual flows ranges from -77 to +174% across subcatchments and in terms of flow volume is -169 to 300 m³s⁻¹. Maximum percent increase in discharge within the ranges most likely to occur, is observed at Sundergarh (+174%), however, maximum increase in flow volume (300 m³s⁻¹) is observed at Basantpur.

Next, we want to understand the uncertainties associated with the predicted mean annual flows, from model parameterization. Figure 5.6 (C) shows standard deviation in the percent changes of mean annual flows resulting from 100 behavioral models, representing the hydrological model parameter uncertainty. The uncertainties vary from about being negligible to 50% across subcatchments, with the maximum uncertainty of 50 m³s⁻¹ at Basantpur. On an average, we observe that 3 to 17% uncertainties across subcatchments exists in the predicted mean annual flows for the future. We observe that with the increase in both precipitation and catchment size, uncertainties in the predicted mean annual flows increase which attributes to the increase in flow magnitudes (Figure 5.6 B).

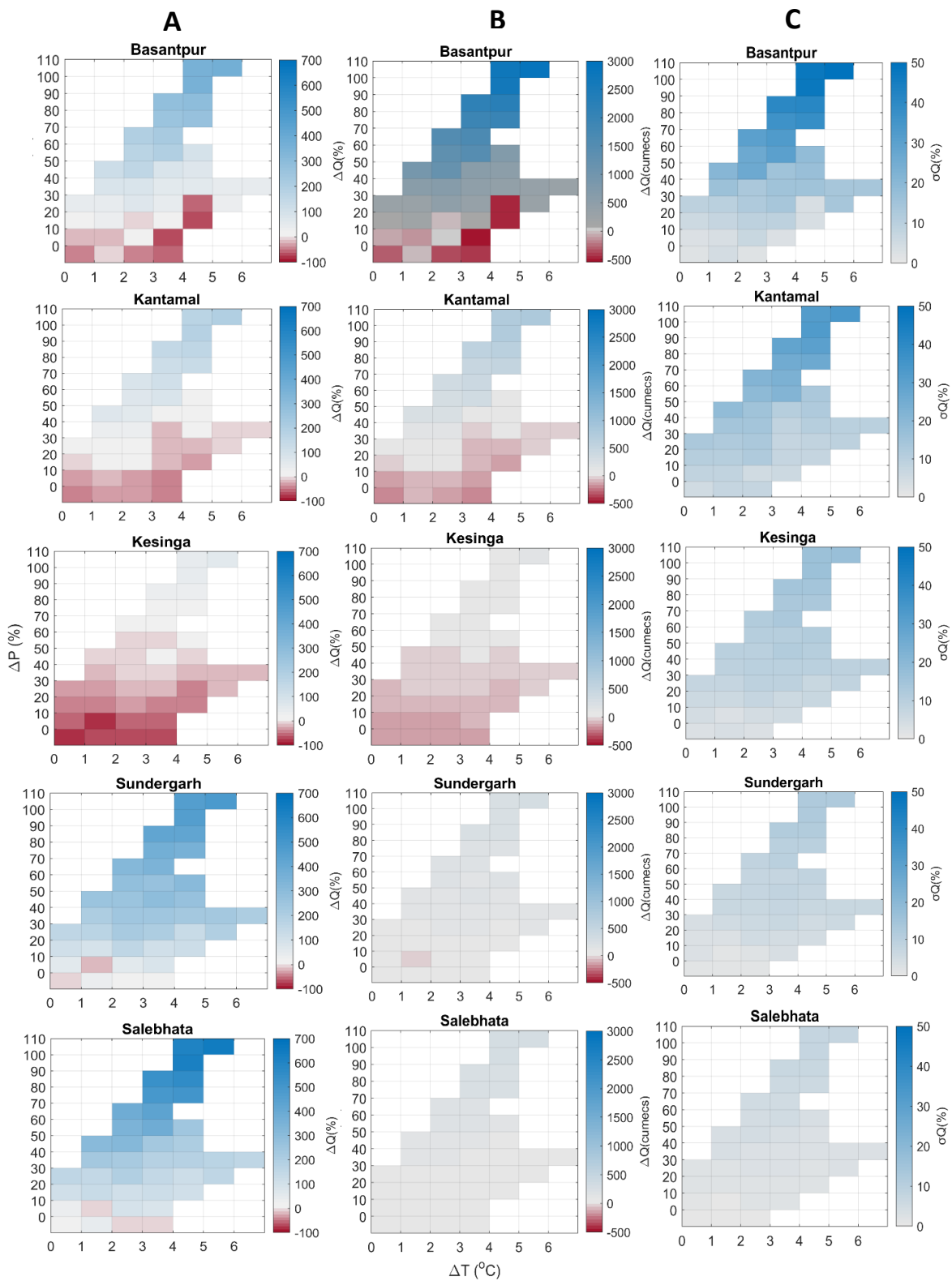


Figure 5.6 (A) Percentage change in mean annual flows (B) change in mean annual flows in m^3s^{-1} (C) Standard deviation in the percent change of mean annual flows resulted from 100 behavioral VIC models, representing the VIC model parameter uncertainty, at all subcatchments in the future period against the control case simulation in the historical period 1990-2015.

5.3.2. Impacts on peak flows and model parameter uncertainties

Figure 5.7A shows percentage change of peak flows (flows above 95 percentile) at all subcatchments in the future period against the peak flows in control case simulation in the historical period 1990-2015. We have also considered predicting the hydrological responses during the monsoon season, as maximum flows in Indian river basins occurs during the monsoon. However, we found that both the magnitudes and direction of change are identical to that of peak flows, so we restrict our results and discussions to only peak flows.

We observe that the patterns in the change in peak flows with respect to the change in precipitation and temperature (Figure 5.7A) are similar to that of change in mean annual flows (Figure 5.6A). Overall change in precipitation and temperature from -5 to +105% and 0 to 7°C respectively, has caused -93 to 485% change in peak flows across subcatchments. The percent changes are lesser compared to the annual flows, however, much higher in terms of flow magnitudes. Change in peak flows ranges from -5723 to 29,776 m^3s^{-1} across subcatchments. Likewise, average change in peak flows across subcatchments (-3.4% to +173%) is lesser in terms of percentage, compared to mean annual flows (-20 to -240%). However, average change in terms of flow magnitudes is much higher in peak flows (-1058 to +10181 m^3s^{-1}) compared to annual flows (-56 to +586 m^3s^{-1}).

Increase in precipitation (even those with slightest increase in precipitation, unlike in case of mean annual flows) has resulted in positive percent change in peak flows across most subcatchments. The average percentage change at Basantpur and Kantamal in peak flows in the future is +93% (11,144 m^3s^{-1}) and +58% (3445 m^3s^{-1}) respectively. At Kesinga, the average percent change in the peak flows is negligible. Relatively, higher number of precipitation/temperature combinations has indicated reduction in peak flows at this subcatchment. A non-identical behavior of the hydrological responses at Kesinga can be attributed to the fact that this subcatchment is negatively biased relative to other subcatchments in the historical period (See Figure 5.5 PBIAS). In smaller subcatchments like Salebhata and Sundergarh, an average change of +70% (+1227 m^3s^{-1}) and +85% (+1164 m^3s^{-1}) respectively, is observed. Like the mean annual flows, maximum increase in peak flows (+29776 m^3s^{-1}) is also observed at the largest subcatchment, Basantpur with an increase in precipitation above 100% and rise in temperature by 5°C respectively. Maximum decline in flows (-2443 m^3s^{-1}) is also observed at Basantpur with an increase in precipitation between 20 to 30% and increment in temperature between 3 to 4°C respectively.

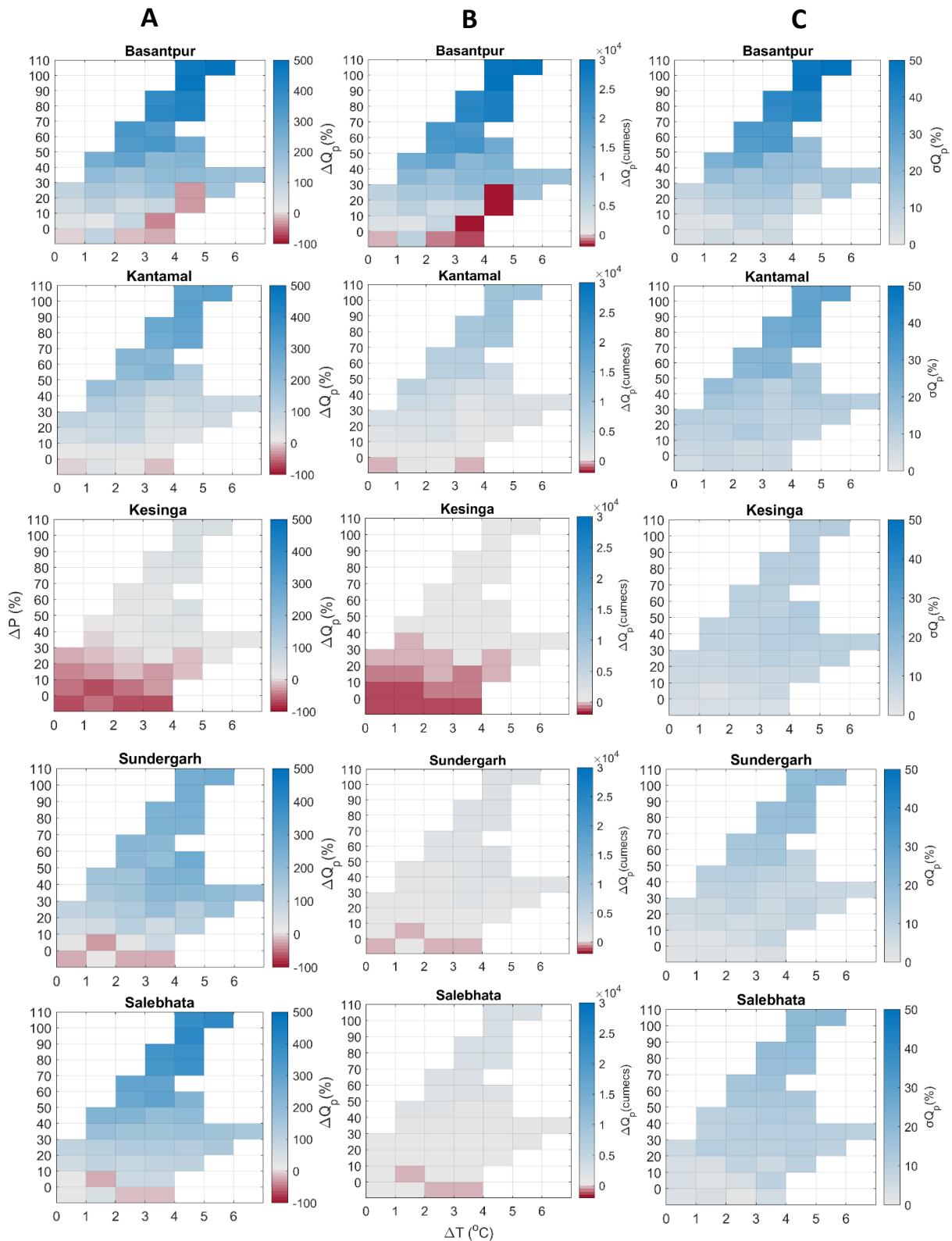


Figure 5.7 (A) Percentage change in peak flows (flows above 95 percentile) (B) change in peak flows in m^3s^{-1} (C) Standard deviation in the percent change of peak flows resulted from 100 behavioral VIC models, representing the VIC model parameter uncertainty, at all subcatchments in the future period against the control case simulation in the historical period 1990-2015.

For the climate changes that are most likely to happen (See Figure 5.3b), change in peak flows are predicted to be varying between -1494 and +8318 m^3s^{-1} (-70 to +136%) with the negative percent change is mostly observed at Kesinga.

In overall, uncertainties in the predicted peak flow magnitudes varies from 13 to 1211 m^3s^{-1} (1.5 to 50%) across subcatchments, which is considerably higher than the uncertainties in the predicted annual flow magnitudes. On an average, we observe (7 to 17%) uncertainties across subcatchments in the predicted peak flows for the future. The uncertainties associated with the model parameters are however only observed in the magnitudes of the predicted change, and not in direction of change. Prediction uncertainties are found more prominent in the bigger subcatchments with higher flow rates, such as maximum uncertainty is observed at Basantpur and minimum uncertainty at Salebhata.

5.4. Discussions

Mahanadi river basin is a peninsular river, where precipitation mainly controls the entire water flows, since 85% of the annual river discharge occurs during the monsoon months (Jin et al., 2018). This holds true also in case of future predicted flows in the basin, especially peak or monsoon flows, as indicated by the findings in this study. Bias corrected climate projections from CMIP6 showed a considerably large increase in both precipitation and temperature under the highest emission scenario of SSP585 for the entire South Asian region (Mishra et al., 2020a). CMIP6 datasets indicates a rise in the temperatures upto 7°C in the future for Mahanadi river basin, which also agrees with few studies (Jin et al., 2018; Singh and Saravanan, 2020) where a rise in average temperature ranging from 2 to 6°C is found using CMIP5 models. Maximum increment in both annual precipitation and mean annual temperature for the basin are found under the highest emission scenario of SSP585, which agrees with several studies (Jin et al., 2018; Mishra et al., 2020a; Singh and Saravanan, 2020). Jin et al., (2018) also reported a maximum of 50-70% increase of precipitation during monsoon in 2090's. On contrary, Singh and Saravanan, (2020) found only a small increase in monthly rainfall (2%) and a decline in rainfall during the monsoon months for Mahanadi basin. These differences can be attributed to the use of different climate models for predictions.

In our study, both reduction and increment in the mean annual flows are observed in the future, depending upon the changes in the precipitation and temperature. While in most cases, we found an increment, there are some instances where despite the increase in rainfall

(upto 20%), we observe either reduction in mean annual discharge or negligible change. This is consistent with other studies where either increase in rainfall under future climate conditions have a neutral impact on Indian river basins including Mahanadi river basin (Gosain and Rao, 2004) or indicating a declining trend of surface runoff in the future (Singh and Saravanan, 2020). We expect that the decline in runoff is probably due to the overall increase in ET as found in other studies (Gosain et al., 2006; Gosain and Rao, 2004; and Kundu et al., 2017).

Future scenarios consistently indicate an increase (of same flow rates) in both peak flows and the monsoon flows (not shown here) which is much higher than the mean annual flows. This indicates the potential for increased flooding. Peak discharge mostly occurs during the monsoon months and as 85% of total annual water discharge occurs during the monsoon (Jin et al., 2018), flow dynamics in the Mahanadi river basin are largely controlled by monsoon. Results related to the change in peak flows also agrees with previous studies in Mahanadi river basin (Asokan and Dutta, 2008; Ghosh et al., 2010; Jin et al., 2018). However, some studies exist (Ghosh and Mujumdar, 2007b, 2007a; Jin et al., 2018; Mujumdar and Ghosh, 2008) which predicted reduction in the occurrence of extreme high flow events thereby resulting in increasing trend of extreme meteorological drought and claimed that this reduction flows are due to the significant increase in temperature due to surface warming. For instance, despite an increase in the precipitation in monsoon, minor reduction of 5 to 7% in peak flows are observed in Jin et al., (2018).

Findings of previous studies on Mahanadi river basin indicates that dissimilarity exists between bias corrected GCM simulations under different scenarios, even in two scenarios of a single GCM, despite both scenarios project similar changes in rainfall. These dissimilarities are often attributed to the wide range of uncertainties associated with future projections of flow including GCM and emission scenario selection, downscaling techniques and hydrological model structures and parameterization. In this study, we refrain from using a particular GCM or a particular scenario to assess the hydrological impacts. Instead, we take into consideration all possible combinations of precipitation and temperature changes in the future, and also attempted to investigate the uncertainties in the hydrological predictions associated with the hydrological model parameterization. Majority of the impact assessments, however, only use a single hydrological impact model (Hagemann et al., 2013). Streamflow

calibration is performed carefully at every subcatchment to represent the main processes that controls the flow dynamics in the Mahanadi river basin. We observe that the equifinality has provided significant amount of uncertainty in the prediction of flows in the future, especially peak flows or flows during the monsoon season. These uncertainties indicate the importance of considering multiple calibrated models which shall give more confidence to a hydrologist to further use the projections for water management. Hagemann et al., (2013), while predicting future global water resources, reported that different hydrological models with different model parameterization results in considerably different results and the spread of the hydrological models in some regions is even larger than that of the climate models. Our results are contradictory with findings of many studies (Chen et al., 2011; Joseph et al., 2018) where the impact of hydrological model parameterization on future hydrological predictions is found to be negligible. However, some of these studies have not considered enough number of behavioral models, for instance, Chen et al., (2011) used only ten different parameter sets to represent uncertainties associated with model parameterization. Also, most of these studies compared the hydrological model parameter uncertainties with other uncertainties such as associated with choice of GCMs or downscaling techniques. GCMs are commonly recognized as the largest contributor to uncertainty (Chen et al., 2011), however comparisons among the sources of uncertainties is beyond the scope of this study.

Note, that we are linking the changes in mean annual flows (and peak flows) at every subcatchment with the changes in both precipitation and temperature (i.e., the different possible combinations) predicted for the entire Mahanadi river basin. Therefore, investigating the link between the changes in climate of individual subcatchments and their projected streamflow would help to better understand or differentiate among the hydrological responses of each subcatchments.

In this study, the percent change in the hydrologic predictions using GCM models in the future are computed with respect to the simulations in reference period (1990–2014) using IMD climate variables. Despite the availability of CMIP6 climate variables during the historical period from all GCM models, we use IMD as a common reference point to compute the percent changes which shall enable comparisons among future hydrological predictions from different climate models. However, although CMIP6 ensembles fairly captures the seasonal variations of precipitation and temperature of IMD in the historical period, a control scenario

experiment comparing simulations using IMD and CMIP6 models in the historical period would have provided more confidence into the future hydrologic projections. Further, it is also essential to understand the role of hydrological components such as Runoff, ET and soil moisture storage to have a proper idea about the potential factors causing the increase or decrease in the basin discharge in future.

It is noteworthy, since we are analyzing the climate change impacts on the mean state of annual flow and the peak flows (or by aggregating flows over the monsoon season), the information on the contrasting characteristics of flows in different monsoon months (sub-seasonal variability) or different years (inter annual variability) is probably lost. For instance, in the context of Mahanadi river basin, Panda et al., (2013) found a significant difference in the sub seasonal rainfall patterns and streamflow during the monsoon, with a predominance of the increasing trends in June and decreasing trends in August. This contradictory rainfall patterns in different monsoon months would necessitate the reservoir managers to store water based on the flow curve to meet the requirements of the existing hydropower plant, irrigation and industrial facilities. Moreover, huge inflow into the dam resulting from heavy rainfall at some months would compel the dam authorities to open gates abruptly, causing flash floods in the coastal areas of the basin within a few hours of release (Panda et al., 2013). Also, Indian monsoon rainfall exhibits interannual variation with a standard deviation of 9.7% of its climatological mean of ~837 mm during 1951–2010 (Rajendran et al., 2021).

Climate change analyses are usually performed by driving hydrological models using future climate scenarios, assuming that the model parameters calibrated to historical flows are representative of the future. However, Interannual and interdecadal variations in climate conditions, such as mainly for precipitation (mainly controls streamflow), can also cause parameter estimates to vary. For instance, calibrating a hydrological model for a certain period of time (say 1990-2010), may result in different parameter values when compared to calibrating a model for another period of time (say 2000-2010), depending on drier or wetter catchment conditions. This temporal changes in the calibrated parameters can be related to the climate conditions of that particular time period when the hydrological model is calibrated for. This might have important implications for hydrologic prediction, such as might increase model uncertainty, especially for climate impact analysis. However, certain rainfall features such as the variability of rainfall on a sub seasonal scale or intra annual scale and its impacts

on model calibration and flows are beyond the scope of this study and further studies are required to analyze these features due to their high relevance, e.g., for high-risk flooding events.

5.5. Conclusions

This research assessed the impact of climate change on the hydrology of Mahanadi river basin and outlined the contribution of uncertainty associated with model parameters in quantifying the impact of climate change. Hydrological impacts due to climate change in this basin are assessed in several studies, however either using the previous climate projections (E.g., CMIP3, CMIP5), or not accounting for the uncertainties associated with hydrological model parameters. This is the first study in Mahanadi river basin, where we assess the hydrological impacts using the recently released climate projection from CMIP6, moreover also considering the importance of model calibration in climate impact studies. We here try to identify the impacts all possible combinations of changes in mean annual temperature and precipitation, irrespective of any GCM or scenarios, on the mean annual flow and peak flows over the subcatchments of Mahanadi river basin. To analyze the parameter uncertainty space of VIC model, 101 best calibrated models are used to assess the climate change impacts.

From the analysis of outcomes, following key conclusions can be drawn:

1. VIC model reproduced the observed flows well in the historical or reference period (1990-2014) with the daily median KGE values of 0.54 to 0.68 across subcatchments.
2. All climate variables (precipitation, maximum and minimum temperature) from bias corrected CMIP6 models in the historical period well captured the seasonal pattern of the reference dataset, IMD. However, majority of CMIP6 models tend to overestimate these variables, during the monsoon.
3. Future projections for the time 2015-2100 indicate increase in total annual precipitation by 42 mm/year, maximum and minimum temperatures by 0.3°C respectively.
4. Overall change in mean annual precipitation in the entire basin ranges from -5 to +105% across all models and scenarios and in mean annual average temperature from 0-7°C. This has resulted in change in mean annual flows ranging from -95 to +645% (-

728 to +2849 m^3s^{-1}) and -93 to +485% (-5723 to +29,776 m^3s^{-1}) change in peak flows across subcatchments.

5. Uncertainties associated with the VIC model parameters, while predicting percent change of mean annual flows varies from about being negligible to 50% (+ 50cumces), and in peak flows 1.5 to 50% (+13 to +1211 m^3s^{-1}) across subcatchments.
6. Increase in precipitation, in majority cases has resulted in increase in discharge at most of subcatchments, especially in peak flows. However, in some cases, despite a small increment in precipitation, decrease in temperature has led to reduction in streamflow, probably caused by the increase in ET.

This study has provided a set of results on the likely future behavior of the subcatchments of Mahanadi river system for mean annual and peak flows under the CMIP6 biased corrected projections. Future projections of hydrologic variables, along with the associated model parameter uncertainties shall help in better hydrologic impact assessment and developing adaptation strategies for Mahanadi river basin in India.

6. Assessing the impact of local versus global datasets on hydrological responses

6.1. Introduction

Land Surface Models (LSMs) have evolved considerably in the past decades to incorporate the sophisticated representation of biochemical, biophysical and detailed surface and subsurface hydrological processes (Fisher and Koven, 2020; Van Den Hurk et al., 2011). This accelerating advances in land surface models also led to the increase in resolution for large-scale modelling (Beven and Cloke, 2012) and resulted in the need for novel global high resolution data (Wood et al., 2011). While current land surface models with their increased spatial resolutions entails an unprecedented demand for high resolution data sets which should allow in principle, for improved simulations, the problem lies with the availability of local/in-situ observations (Lorenz and Kunstmann, 2012; Rodríguez et al., 2020). Many developed countries have models devoted in modelling the hydrological changes under environmental impacts to support water resources management and planning. However, in many developing countries, high resolution LSM's are poorly constrained because of acute shortages of in-situ hydro-meteorological data (Bierkens et al., 2015, Hannah et al., 2011, Essou et al., 2016). This is either due to the decline in the in-situ monitoring gauges (Connor, 2015) or the data not being openly accessible for research (Beria et al., 2017). For example, Mujumdar, (2015) has recently highlighted about the difficulties faced by the Indian hydrologic community, owing to the lack of keenness of the relevant governmental organisations, to openly share required hydro-meteorological data and its metadata to the research bodies. This limits the ongoing research of analysing real-time hydro-meteorological processes, amidst the continuously changing climate and its impact on water resources. This urges the need for integrating high-quality global datasets into the LSM's (Beria et al., 2017; Liu et al., 2011; Mujumdar, 2015; Strömquist et al., 2009; Zubieta et al., 2016).

In recent years, there have been enormous advances in the global data availability of the geophysical attributes, such as soil, vegetation and fine-scale meteorological data (Bierkens et al., 2015; Clark et al., 2015) from the ever-expanding remote sensing activities, reanalysis

products and other large data sets. A major focus is required to utilize these datasets in parameterizing high resolution global LSM's to improve representations of hydrological processes by capturing the sub grid heterogeneity more explicitly. As such, Clark et al., (2015) stated that understanding the information content in these available data and also how the land models use this information, is crucial for advancing the hydrologic benchmarking activities for improving process representations in land surface models.

Both satellite and global reanalysis data sets are widely used for hydrological applications especially in data sparse regions (Collischonn et al., 2007; Essou et al., 2016; Mahto and Mishra, 2019; Shah and Mishra, 2014a; Voisin et al., 2008). The launching of new earth observatory missions and better sensors has led to improvements in the quality of precipitation estimates worldwide (Huffman et al., 2007, 2015, 2018). For instance, emergence of The Integrated Multi-satellite Retrievals for GPM (IMERG) in 2014 have improved the hydrologic applications of satellite-based precipitation (Gilewski and Nawalany, 2018). Recent studies have noted improvement in precipitation quality of different version of GPM IMERG over other satellite rainfall products such as TRMM Multi-satellite , TRMM Multi-satellite Precipitation Analysis (TMPA-3B42), TMPA V7, and others; particularly in India and elsewhere (Beria et al., 2017; Gilewski and Nawalany, 2018; Prakash et al., 2018; Sharifi et al., 2016; Sungmin et al., 2017; Tang et al., 2020; Zubieta et al., 2016). Simultaneously, the numerical weather prediction systems are also continuously improving (Mahto and Mishra, 2019). For instance, Mahto and Mishra, (2019) evaluated five new reanalysis products against local observations for hydrological applications in India. Analysis showed ERA5 captured best monsoon season rainfall and maximum temperature over other reanalysis products such as MERRA-2, ERA-Interim, CFSR, and JRA55. A recent development in ECMWF is the release of a global dataset for land component of ERA5, hereafter named as ERA5-Land (Muñoz-Sabater et al., 2021). In a recent study by Gao et al., (2020) ERA5-Land performed better than other reanalysis products while outperformed by GPM IMERG for hydrological applications in China. Ability of reanalysis datasets for hydrological predictions are less explored compared to the satellite datasets (Essou et al., 2016)

Global soil and land cover information are also available on a much finer spatial scale. Among the current global soil maps, the latest version of SoilGrids at a resolution 250 metres (Hengl et al., 2017) involves most detailed estimation of soil distribution having highest accuracy and resolution (Dai et al., 2019). Very few studies exist that tested the impact of using global soil

in a hydrological model (Dembélé et al., 2020; Krpec et al., 2020), for instance Krpec et al., (2020), tested the impacts of using global soil from SoilGrids on hydrological responses. Recently released time series of global land cover product from European Space Agency Climate Change Initiative (ESA CCI) of relatively finer resolution is an advancement over other available global land cover products such as IGBP, Global Land Cover 2009, Glob cover 2009 and global land cover from GLC (Jiang and Yu, 2019). Therefore, it is essential to evaluate the advancements and updates of these datasets for their suitability for hydroclimatic applications in regional scale studies. With the above motivation, we intend to answer the following research questions:

1. How does the inclusion of global datasets in a regional scale hydrological model impact model predictions in a subtropical climate? or, how reliable are global datasets in producing a comparable hydrological model performance when compared against local observations?
2. How does the impacts of those different inputs can propagate to different hydrological components simulated by the model?

This study is driven by the hypothesis that using all local datasets will result in better model performance compared to when introducing global datasets in the model. We seek to understand the usefulness and applicability of recently released global datasets within a land surface model for hydrological simulations in a data scarce region in India. To this end, we employed a Variable Infiltration Capacity (VIC) hydrological or land surface model over the Mahanadi river basin located on the eastern part of India which drains an area of 141,589 km².

The objectives of this study are to 1) perform various model experiments combining forcings, soil, and land use datasets from local and global products for hydrological predictions 2) to comprehensively analyse the model performance of each experiment and identify critical input datasets or combinations of input dataset which may have significant impacts on model performance. Overall, this analysis aims to discern the hydrological impacts caused due to the changes in a model input (local or global) or a combination of model inputs (local and global) to provide a basis for relying on the global data in a hydrological or land surface model for future use. Very few studies exist that explore various combinations of input in LSM to achieve maximum gain in model performance. Later groups focussed on selecting a proper combination of model inputs prior to model calibration (Famarzi et al., 2015; Tarawneh et

al., 2016). Our study is also an advancement from few published studies (Ghodichore et al., 2018; Kneis et al., 2014; Mahto and Mishra, 2019; Prakash et al., 2018; Shah and Mishra, 2014b) on this domain as we evaluate the recently released and finer resolution global datasets which to our knowledge have not been tested yet in India river basins for hydrological applications.

6.2. Data and Methods

6.2.1. Model input datasets and parameters

We applied the VIC model version VIC 4.2.d using the water balance mode at a daily time step and 0.05° spatial resolution over the 5 subcatchments of the Mahanadi river basin. The inputs required by VIC model are meteorological forcing (precipitation, maximum and minimum temperature, and wind speed), soil properties, land use and vegetation properties, and topographical details. DEM CARTO 30, a national DEM developed by ISRO (Indian Space Research Organization) is used for extracting all topographical features and for delineating the Mahanadi river basin. Sivasena Reddy and Janga Reddy, (2015) evaluated 6 DEM's of different resolutions including SRTM 90, CARTO 30 and ASTER 30 in an Indian river basin and found that CARTO 30 provided accurate estimates of runoff and watershed areas than other DEMs. Therefore, we refrained from testing any global DEM in this study. Table 6.1 provides a summary of the input data used in this study and a detailed description of the inputs are given below.

Table 6.1: Summary of model input datasets used in this study

Inputs	Resolution	Data type
Land Use		
NRSC	50 metres	Local
ESA CCI	300 metres	Global
Soils		
NBSSLUP	500 metres	Local
SOILGRIDS	250 metres	Global
Precipitation		
IMD	0.25 ° X 0.25 °	Local
GPM IMERG	0.1 ° X 0.1 °	Global
ERA5-Land	0.1 ° X 0.1 °	Global
Temperature		
IMD	1 ° X 1 °	Local
ERA5-Land	0.1 ° X 0.1 °	Global

6.2.1.1. Soil type and land cover maps

National level soil map is derived from the digitized soil map as provided by National Bureau of Soil Survey and Land Use Planning (NBSSLUP) with a spatial resolution of 500 metres (Figure 2.6a) (Scale 1:250000). Global gridded soil textures are derived from SoilGrids (Figure 2.6b). For the sake of clarity, global soil map for the basin is shown at a model grid resolution of 5 kms (instead of showing 3 different soil texture maps of clay, sand and silt at 250 m resolution).

National level LULC map is derived from National Remote Sensing centre (NRSC) of year 2013-2014 (scale 1:250000) of resolution 56 meters (Figure 2.7a). Global LULC map for the year 2014 (Figure 2.7b) is obtained from the consistent series of annually generated land cover products from ESA CCI (version 2.0.7) (Jiang and Yu, 2019) for the period 1992-2015 at a resolution of 300 meters. Both LULC maps show that Deciduous Broadleaf Forest (DBF) and cropland (CL) are the major land cover types in the basin.

6.2.1.2. Meteorological forcings

Precipitation datasets in this study are obtained from 3 different sources (i) Daily gridded precipitation data from IMD at a grid resolution, 0.25° X 0.25°. (ii) Half-hourly precipitation

data from The Integrated Multi-Satellite Retrievals for GPM IMERG, early run (Near real-time product- VO6) with a spatial resolution $0.1^\circ \times 0.1^\circ$ (iii) Hourly precipitation data from ERA5-Land, recently released new-era reanalysis product of ECMWF and replay of the land component of ERA5 climate reanalysis with much finer spatial resolution of $\sim 9\text{km}$ compared to ERA5 (31 km) and ERA-Interim (80 km).

IMERG algorithm uses all available sensors of TRMM and GPM eras to provide global precipitation estimates at a spatial resolution of 0.1° and a temporal resolution of 30 min. The latest version of this product, V06 is a retrospective processing of IMERG to TRMM era and uses new algorithm with several major improvements, which could enhance the quality of the precipitation estimates (Tang et al., 2020). As ERA5-Land is based on several improvements, which is most importantly, the enhanced horizontal resolution (9km vs 31km) than ERA5, it is crucial to assess its suitability in hydrometeorological applications. Temperature data in this study is obtained from 2 different sources (i) Daily gridded maximum and minimum temperature data from IMD at a resolution, $1^\circ \times 1^\circ$. developed using 395 stations and having 20 grids within Mahanadi river basin. (ii) hourly temperature from ERA-Land with a horizontal resolution of $\sim 9\text{km}$. The daily maximum and minimum temperature are derived from hourly temperature. Wind speed is obtained from NCEP/NCAR reanalysis of resolution 1° . Please note that both rainfall datasets from GPM and ERA5-Land and temperature from ERA5-Land were accumulated to daily time scale and the spatial resolutions of all datasets including IMD are kept at VIC model resolution of 0.05° . Figure 6.1 shows cumulative daily precipitation and temperature at Basantpur from IMD, GPM IMERG and ERA5-Land, for the period 2014–2016. A dense network of rain gauges consisting of 7000 stations is well-spread across India (Beria et al., 2017), among which 201 rain gauges exists within this basin. We choose a basin in India which contains relatively sufficient local data to enable comparisons among the model performances using local and global datasets. This will be useful in validating the use of these global datasets and understanding the value in case these local datasets are not available or utilizing these datasets in data sparse regions of tropical climate zone. Similar concept is also followed in (Essou et al., 2016).

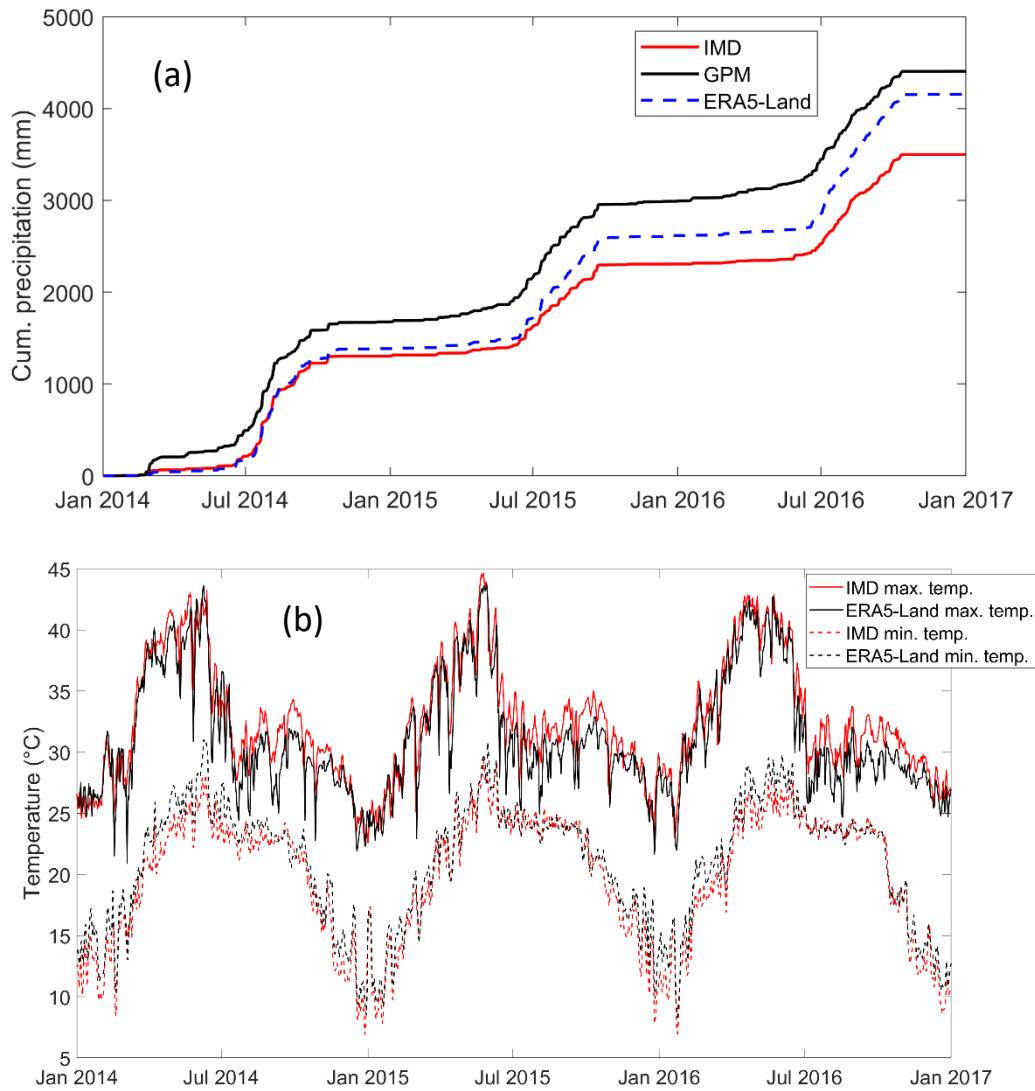


Figure 6.1 (a) Cumulative daily precipitation of Subbasin Basantpur from IMD, GPM IMERG and ERA5-Land, for the time 2014–2016. (b) Daily minimum and maximum temperatures from IMD and ERA5-Land, for the time 2014–2016 of Subbasin Basantpur

6.2.1.3. Model parameters

The VIC model has 46 tuneable parameters (Bennett et al., 2018). We had performed a Global Sensitivity Analysis (GSA) on some soil, vegetation and routing parameters based on the suggestions by VIC model developers (Gao et al., 2010) and existing literatures (Demaria et al., 2007; Gou et al., 2020b; Joseph et al., 2018; Yanto et al., 2017). Among those parameters, soil parameters, infiltration capacity (*binf*), fraction of maximum velocity of baseflow (*ds*), velocity of baseflow (*dsmax*), soil moisture in third soil layer (*ws*), second and third soil layer depth (*d2*) and (*d3*) respectively and routing parameters, (*vel*) are found sensitive hence are subjected to calibration. The rest of the soil properties such as soil porosity (θ_s), field capacity

(*FC*), Wilting point (*Wp*), Saturated Hydraulic Conductivity (*Ksat*), and Initial soil moisture etc. are obtained based on average hydraulic properties of USDA soil textural classes (Cosby et al., 1984; Rawls et al., 1998; Reynolds et al., 2000). Among the vegetation parameters, monthly mean LAI values are derived from the daily LAI product for the time 2000-2015 from MODIS AQUA/TERRA. We derived root zone depths and estimated the fractions of roots in each zone following Zeng, (2002). Other related biophysical parameters required by VIC such as roughness length, albedo and displacement height etc., are assembled based on Land Data Assimilation System (LDAS).

6.2.2. Experimental design and model evaluation

Precipitation, temperature, soil, and land use datasets from local and global products are combined to yield 11 different model experiments (Table 6.2). These experiments are designed with an objective of testing the impacts on model performance of using (i) all local datasets (Experiment 1) (ii) combinations of local and global datasets (Experiments 2 to 9) and (3) all global datasets in a hydrological model (Experiments 10 and 11). Exp3 and exp4 uses global precipitation datasets from GPM and ERA5-Land respectively, while the rest of the inputs are local. Exp7 and exp8 is designed to test global soil and land cover respectively. Exp9 is a follow up Experiment to exp7 and exp8 where we test the hydrological response of using both soil and land cover from global sources. In exp 2 we are replacing coarse resolution local temperature from IMD with fine resolution temperature from ERA5-Land. Both exp5 and exp6 is framed to understand the impact of using both rainfall and temperature datasets from global products. Exp 10 and exp 11 is to test the impact of using all global datasets as model inputs. The difference between exp 10 and exp 11 is the source of global rainfall product i.e., GPM and ERA5-Land, respectively.

A set of behavioural models (250 models) are first obtained by calibrating the model using all local datasets, using a sequence of 5000 Monte Carlo simulations, for the time 1990-2010 including 2-year warm up period (1988-1999). These behavioural models were derived based on Kling-Gupta Efficiency (KGE) (Gupta et al., 2009) (More details can be found in Chapter 3). We calibrated the model using the measured local data, which is believed to be the most accurate data available. Satellite data produce indirect measurements, as it provides 'estimates' of precipitation as the satellite do not measure rainfall directly.

Next, all experiments, including exp1 (experiment using all local dataset) are run using these behavioural models for an entirely different time period (2014-2016), owing to the availability of all datasets. These behavioural models shall consider uncertainties in the model outcome stemming from model parameterization or any biases in the input datasets. The VIC model in this study is set up to produce daily streamflow at all subcatchments shown in Figure 2.1 (Chapter 2). To ensure accurate initialization of the VIC soil moisture for the rest of the experiments (exp2-11), the behavioural models are spun up by forcing data of time 2014-2016 repeatedly for 21 years (7 loop cycles through a 3-year period) following similar recommendation by Rodell et al., (2005). Since we calibrated the models using local datasets, exp 1 is considered as the reference or a benchmark simulation. It is worth mentioning that we restrict to a shorter analysis period, i.e., only 3 years, due to the lack of availability of the local daily estimates of maximum and minimum IMD temperature beyond year 2016. The observed discharge data at multiple gauges for the time 1988-2010 are available from the Central Water Commission (CWC), India.

The model performance was evaluated by quantitative comparison with the observed discharge using performance metric KGE (Eq. 6.1-6.3). KGE metric balances the contribution to the error coming from all three main components, namely correlation (e.g., timing/dynamics), variability (e.g., seasonality), and systematic bias, and is now a widely used metric in hydrometeorological studies (Gupta et al., 2009; Knoben et al., 2019; Mishra et al., 2020b; Rodriguez and Tomasella, 2016; Tang et al., 2020). KGE ranges in $[-\infty, 1]$ with values closer to one indicating better performance.

Table 6.2: Describing the experiments performed in this study

Experiments	Local	Global
1	IMD rainfall, IMD temperature, soil, LULC types	-
2	IMD rainfall, soil textures, LULC types	ERA5-Land temperature
3	IMD temperature, soil textures, LULC types	GPM rainfall
4	IMD temperature, soil textures, LULC types	ERA5-Land rainfall
5	soil textures, LULC types	GPM rainfall, Reanalysis ERA5-Land temperature
6	soil textures, LULC types	ERA5-Land rainfall, ERA5-Land temperature
7	IMD rainfall, IMD temperature, LULC types	Soil textures
8	IMD rainfall, IMD temperature, soil textures	LULC types
9	IMD rainfall, IMD temperature	Soil textures, LULC types
10	-	GPM rainfall, ERA5-Land temperature, soil, LULC
11	-	ERA5-Land rainfall, ERA5-Land temperature, soil, LULC

Where r is the linear correlation between simulated and observed discharge, α is an estimate of flow variability error and β is a bias term. σ_{sim} and σ_{obs} are standard deviations in simulated and observed discharge, respectively. μ_{sim} and μ_{obs} are mean of simulated and observed discharge, respectively.

6.3. Results

6.3.1. Model performance of all experiments

Calibration of VIC model is performed against local dataset on a daily time scale with respect to KGE for the time 1990-2000 for all the subcatchments. Overall, the model reproduced the observed flows remarkably well with the median KGE values of 0.85, 0.86, 0.82, 0.75, 0.63 at Basantpur, Kantamal, Kesinga, Salebhata and Sundergarh, respectively (see Figure 4.5a in Chapter 4). These calibrated models are then used, however, in a completely different period 2014-2016 to evaluate the simulated daily discharge from eleven VIC model experiments (table 2) for the subcatchments of the Mahanadi river basin. Figure 6.2 (top panel) shows the model performance (KGE) for the simulated discharge obtained from 11 model experiments against the observed discharge for all subcatchments. The boxplots represent uncertainties in the KGE values due to different model parameterizations (or 250 behavioural models). We averaged the ranks achieved by each experiment at all subbasins to have an overview of the model performances. Reference experiment (exp1) shows the best performance. Similar performance to the reference experiment is observed for the simulation using global soil (exp7) thereby having negligible difference in the KGE values. Simulation using precipitation from GPM (exp3) has shown a comparable performance to the reference experiment. Among all experiments, lowest performances are obtained by the experiments driven by precipitation from ERA5-Land (exp4,6,11). Experiments using global temperatures, land cover, combination of global soil and land cover, and combination of global precipitation (both sources) and temperature, have shown a moderate performance in overall.

KGE exhibit significant variability in model response among 11 experiments across subcatchments. The median of KGE suggests reference (exp1) produced the best performance at Basantpur, Kantamal and Sundergarh, while performed moderately for the rest subcatchments. The median KGE values for the reference (exp1) simulation across subcatchments Ba, Ka, Ke, Sa and Su are 0.80, 0.74, 0.46, 0.66 and 0.25 respectively. Simulation driven by GPM rainfall (exp3) outperformed reference simulation and simultaneously have produced the best performance at 2 subcatchments (Kantamal and Kesinga), while slight to significant deterioration in KGE is observed for the rest subcatchments. Conversely, the other global source of precipitation, ERA5-Land (exp4) have shown relatively much poorer performance, with respect to both reference and exp3, with

decline in KGE at every subcatchment. Simulations using ERA5-Land temperatures (exp2) have performed well across all subcatchments with a slight decline in KGE as compared to the reference simulation. Simulations using both precipitation and temperature from global sources (exp5,6) caused more decline in KGE than using either of them as a sole input from global sources. Especially, combination of ERA5-Land precipitation and temperature (exp6) have shown significant deterioration at all subcatchments. Global soil map from SoilGrids (exp7) yielded KGE values identical to (lying almost in the same interquartile range) benchmark (exp1) at four subcatchments, suggesting an insignificant change in overall model performance. On the contrary, the use of the global land cover map from ESA CCI (exp8) has shown deterioration in model performance at four subcatchments while producing best performance at one subcatchment, Salebhata. The impacts of replacing all local datasets by global datasets in the VIC model (exp10,11) varies across subcatchments. However, at most of the instances, experiments using all global datasets (exp10,11) showed better performances than experiments using only precipitation and temperature from global sources (exp4,10), implying that global soil and LULC in exp10 and 11 compensates for the poor performances in exp4 and 10.

On some occasions, we observe that KGE enable a finer distinction among experiments, exhibiting clear trends stemming from the influence of the various input datasets, however varying across subcatchments (see Figure A.1 in Appendix A). For instance, at Basantpur, we observe a finer distinction between experiments driven by IMD precipitation (exp 1,2,7,8,9) and global precipitation (exp 3,4,5,6,10,11). The later yielded much lesser KGE values than the experiments using IMD precipitation, emphasizing on the importance of local precipitation estimates at this subcatchment. At Kesinga, simulations involving GPM precipitation (exp3,5,10) produced best results whereas simulations using reanalysis forcings (exp4,6,11) have shown maximum deterioration in KGE. Simulations using local forcings performs moderately at this subcatchment. At Salebhata, we observe that all experiments involving global land cover (8,9,10,11) outperformed the experiments involving local land cover (1,2,3,4,5,6,7).

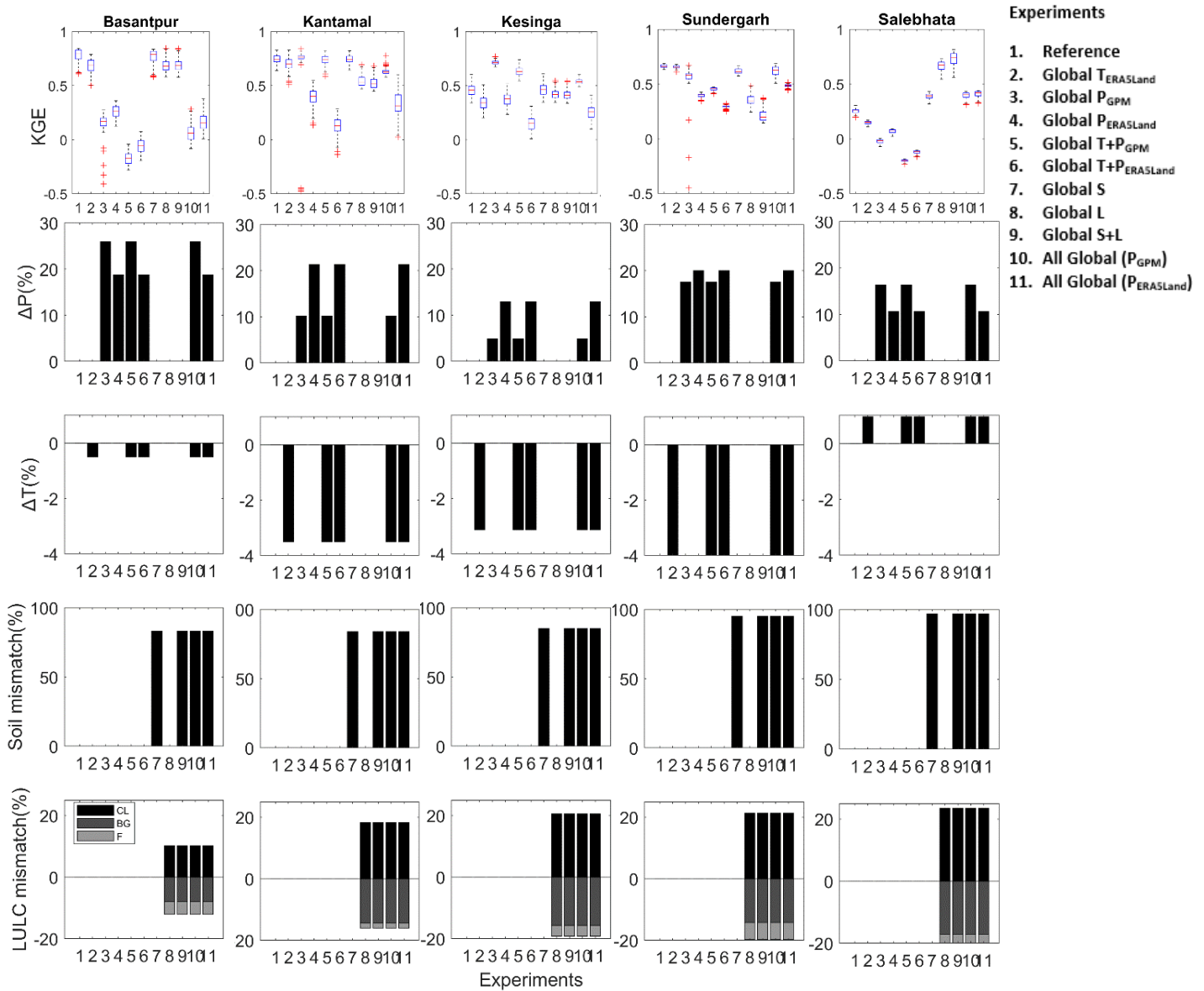


Figure 6.2: (top) Values of KGE calculated for prediction of discharge of all experiments at all subbasins. Boxplot of KGE values represents 250 behavioural models, meaning the uncertainties stemming from 250 model parameters sets (b) Bar charts representing the percent changes in datasets (precipitation, temperature, soil and land cover) obtained from global sources with respect to that of datasets from local source. In the legend, T, P, S and L are temperature, precipitation, soil and LULC respectively.

6.3.2. Factors causing changes in model performance due to different data sources

6.3.2.1. Weather datasets

Figure 6.2 (bottom panels) shows the percent change in the input factors (precipitation, temperature, soil and land cover) obtained from global sources relative to the datasets from local sources. Each of the experiments (shown in the horizontal axis) in bottom panel

represented by the bar plots for different factors corresponds to the same experiment numbers in the top panel showing boxplot of KGE values. The performance produced by each experiment (shown by KGE boxplot in top panel) can be related to all four factors of the corresponding experiment to understand which factor is responsible for the change in the KGE values.

Both global rainfall datasets, GPM and ERA5-Land have overestimated the daily rainfall values when compared to IMD rainfall across subcatchments. However, the decline in KGE is mainly caused while using ERA5-Land rainfall datasets. Moderate to large overestimation (11-20%) in ERA5-Land rainfall have produced consistently poor performance (See exp4 in Figure 6.2). 5% increase in GPM annual rainfall at Kesinga outperformed benchmark simulation by improving slight positive biases and variability (not shown here) in streamflow implying that, precipitation estimates of IMD resulted in slight overestimation in discharge at this subcatchment. However, to understand the factor causing reduction in discharge despite 5% increase in GPM precipitation, we assessed the water balance components (Figure 6.3). We observe that replacing IMD precipitation with GPM, had induced more evapotranspiration thereby reducing total runoff. Annual average of runoff and ET for rest of the subcatchments are shown in appendix (Figure A.2, Appendix A). Further increase (16-26%) in GPM annual rainfall have largely overestimated the streamflow at Basantpur, Sundergarh and Salebhata.

The decline in KGE while using ERA5-Land temperatures is attributed to the decrease in average temperature by 0.5-4.8% that tends to overestimate the discharge. Decrease in maximum temperature have reduced the evapotranspiration thereby increasing runoff (see Figure A.2, Appendix A). Please note that both maximum and minimum temperatures are used as inputs in the model, however for sake of simplicity, only the change in the average temperatures is shown in Figure 6.2. The overestimating tendency of both precipitation and temperatures from ERA5-Land, caused further deterioration in exp 6.

Figure 6.4 shows a visual comparison between observed and simulated discharges of the experiments at Basantpur to understand how prediction of discharge differs between experiments and to visually assess the model performance. Visual comparison of observed and simulated discharge for the rest of the subcatchments is in Figure A.3, Appendix A. Figure 6.4a clearly illustrates that at Basantpur, benchmark simulation using IMD rainfall closely matches the observed flow whereas some overestimation is observed in simulations driven

by GPM (exp3) and ERA5-Land (exp4) rainfall. At this subcatchment, simulations driven by reanalysis precipitation, ERA5-Land (exp4,6,11) have performed better than GPM precipitation (exp 3,5 and 10). This is because ΔP for GPM (303 mm) is higher than ERA5-Land (219 mm) therefore relative overestimation is higher in GPM.

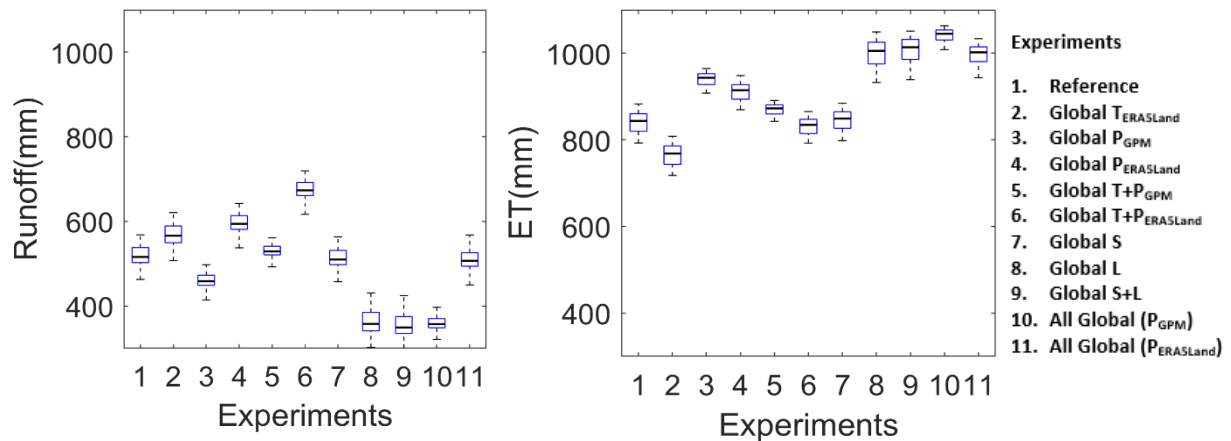
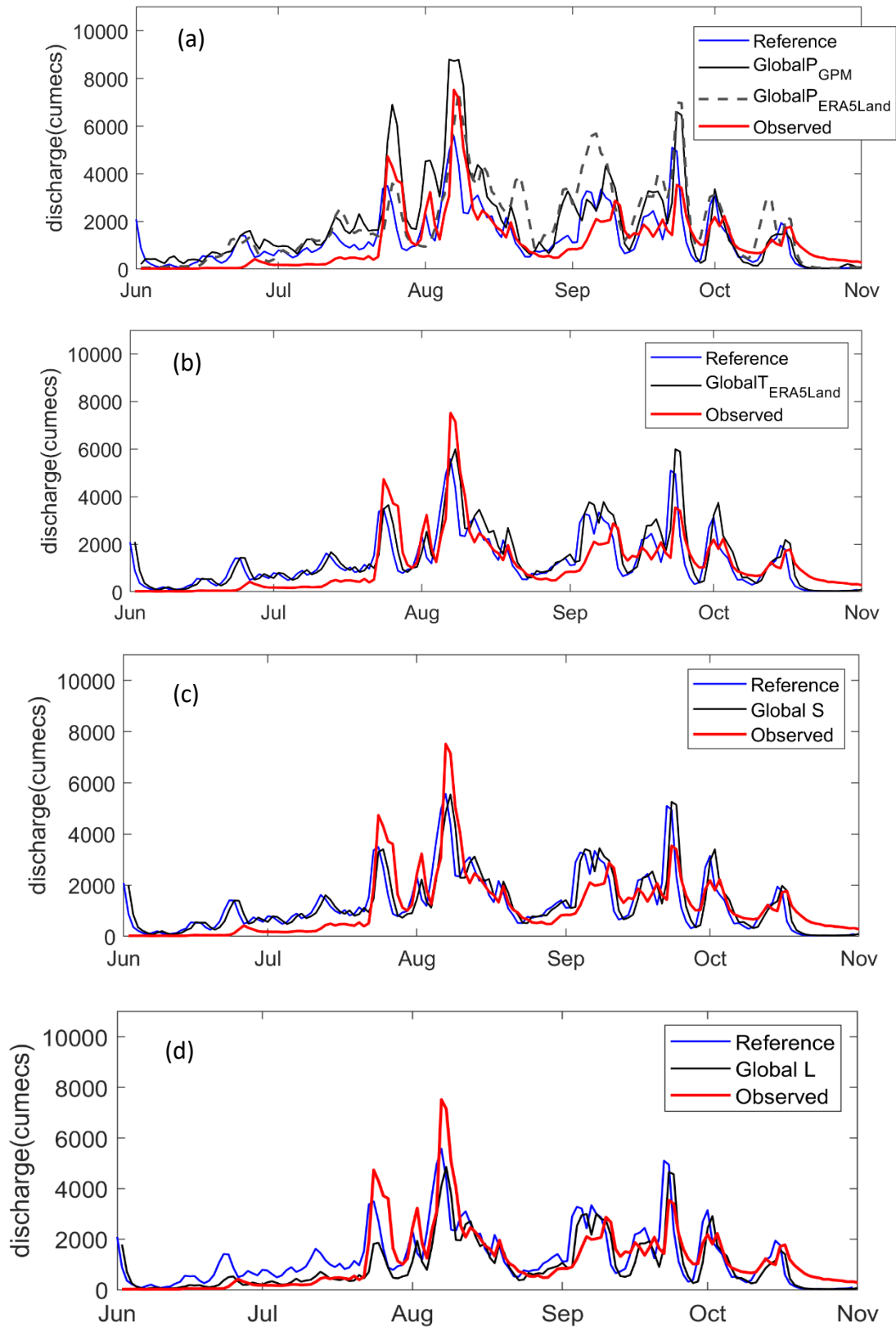


Figure 6.3: Annual average of runoff and evapotranspiration at Basantpur for all experiments. In the legend, T, P, S and L are temperature, precipitation, soil and LULC respectively. Please note that the precipitation varies across experiments.

6.3.2.2. Soil and land cover datasets

The significant difference in the granularity of data is clearly visible in the soil maps which ranges from 83-97% across subcatchments (Figure 2.6, Chapter 2). Loam and some percentage of clay in the local soil map is mapped as clay loam in SoilGrids. Despite a significant variation in the percentage of soil textures and spatial distribution in both soil maps, we observe insignificant changes in model performance i.e., closely represents the benchmark flows which is simulated using local soil. This is because the mismatch in soil classification is among the soil types of comparable hydraulic properties thereby having least influence on the predicted discharge. Figure 6.4c clearly illustrates that discharge patterns using global soil closely represents the benchmark flows and observed flows.



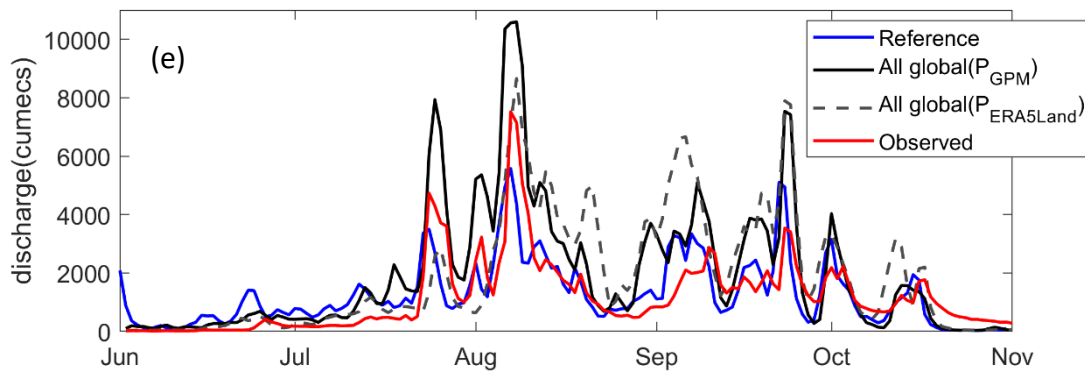


Figure 6.4: Comparison of daily observed discharge and ensemble mean of simulated discharge of experiments at Basantpur using (a) precipitation from GPM, ERA5-land and IMD (reference) (b) temperature from ERA5-Land and IMD (reference) (c) soil from SoilGrids and local soil (reference) (d) LULC from ESA CCI and local LULC (reference) (e) all global datasets and all local datasets (reference), averaged for the years (2014-2016). In order to show the details of the hydrographs, they are zoomed in to the monsoon (wet) months; Results for other subcatchments are similar and can be found in the Appendix (Figure A.3).

Global land cover map has an underestimating tendency primarily due to reduced barren grounds in ESA CCI, thereby deteriorating the model performance across the subcatchments except for Salebhata. Underprediction in discharge might also be caused due to agricultural expansion (10-21) % through increased ET (See Figure A.2 and Figure A.3). However, global map captured the low flows better than the local land cover across the subcatchment, as can be observed from Figure 6.4d. This indicates ESA CCI mainly under-predicted the peak flows. At Salebhata, reduction in barren ground by 17% and expansion in cropland by 24% in the global land cover (exp8,9) had outperformed all other experiments related to local land cover. The local land cover seems to have overpredicted the flows at this subcatchment. Interestingly, using all model inputs from global sources did not yield the worst KGE values as we hypothesized. This is because simulation using all global inputs includes global land cover that compensates for the poor performance due to the overestimating tendency of global weather inputs, specifically precipitation.

6.4. Discussion

Precipitation estimates from both GPM IMERG, and ERA5-Land have overestimated the discharge. Overestimation using IMERG rainfall estimates is in line with the findings of Beria et al., (2017); Zubieta et al., (2016). For instance, Beria et al., (2017) found overestimation in low runoff at Hirakud subcatchment of Mahanadi river basin during 2014 monsoon. Peak discharge simulated by GPM IMERG, although are well captured, showed an overestimation which contradicts the findings of Beria et al., (2017), that the runoff peaks are underreported. Gilewski and Nawalany, (2018) also reported overestimation of extreme rainfall events by GPM in monsoon dominated regions. ERA5-Land is a recent advancement among the ECMWF reanalysis products, therefore very limited studies exist worldwide. A recent study by Gao et al., (2020) evaluated the state-of-the-art gridded rainfall products, wherein IMERG outperforms all reanalysis datasets including ERA5-Land at both hourly and daily scales. As reported in literatures (Dhanya and Villarini, 2017; Mahto and Mishra, 2019; Shah and Mishra, 2014a) the majority of the reanalysis products including ERA5 show consistent increasing trend during Indian monsoons and largely fail to reproduce observed flows in the monsoon season in most parts of India. This finding correlates with our analysis as ERA5-Land overestimated the discharge at all subbasins and 90% of rainfall is received during the monsoon. This overestimation in discharge while using both IMERG and ERA5-Land can directly be linked to the overestimation of rainfall estimates at these subcatchments as also reported by Mahto and Mishra, (2019) and Zubieta et al., (2016). For instance, in Zubieta et al., (2016) both over/underprediction in runoff occurs when the rainfall estimates are over/underestimated respectively. However, much larger overestimation is observed in reanalysis products than satellite products as reanalysis models generate too much light rainfall. IMD gridded rainfall products are acquired from reasonably good network of rain gauge observations spread across the country, hence might be expected to capture average daily events more accurately. To the best of our knowledge, Indian Meteorological Department (IMD) (Pai et al., 2014) never reported of any errors in this gridded precipitation dataset across the Indian region, except for the observations in the mountainous areas due to the orographic precipitation effects. However, errors might result from the interpolation effects (while interpolating the rain gauge observations to obtain the gridded observation)

and the fact that how well maintained and calibrated the rain gauge measurement instrumentations are.

Moreover, very high resolution IMERG rainfall products might be a reason to produce better simulations than IMD rainfall which is relatively coarse. Maximum and minimum temperatures from ERA5-Land had overestimated discharge, however lesser than caused by precipitation from ERA5-Land. Generally, temperature exhibits smaller biases compared to precipitation as also found in Essou et al., (2016). Overestimation of monsoon runoff caused by an increase in maximum temperature, is also reported by Mahto and Mishra, (2019) and Ghodichore et al., (2018) for ERA5 and other reanalysis product over India.

Global soil texture information from SoilGrids of resolution 1km has resulted in a comparable performance to the reference experiment at all subbasins. In line with our findings, Yeste et al., (2020) obtained good hydrological responses using textural information from SoilGrids1km in the north of the Iberian Peninsula. In contrary, Tarawneh et al., (2016) found that the local detailed soil map produced much better simulations than the global soil map. However, the difference between the impact of using global or local soil map on the simulated discharge depends on the difference between the soil textures present in both the sources. For instance, replacing local soil with global did not have much impact on simulations in Faramarzi et al., (2015) and Strömqvist et al., (2009). In Strömqvist et al., (2009) change of soil type from clay to loam (both having similar hydraulic properties) have little effect on streamflow. The global LULC in overall, tends to underpredict the discharge. However, global LULC map, when used across rest of scenarios, with other inputs showing overestimating tendency (such as global rainfall and global temperature), it compensates for the positive bias and improves the model performance. As also found in our study, global LULC map from USGS improved the biases however significantly did not improve the streamflow in Tarawneh et al., (2016), and global LULC map had least influence on model performance.

Although we conducted the analysis for selected subbasins to avoid the effects of a major dam/reservoir in the middle reach, subbasins analyzed are also human intervened and observed streamflow are still controlled by minor reservoirs and dams. This will affect the VIC model simulations especially in the smaller subcatchments which is possibly the reason behind poor benchmark performance at Kesinga and Salebhata, despite being calibrated using local datasets. Moreover, non-consideration of groundwater recharge and irrigation in

the model could also affect the performance. This is in line with some literatures (Kneis et al., 2014; Mishra et al., 2008; Nayak et al., 2010) wherein the calibrated hydrological models yielded poor performance at smaller subbasins of Mahanadi.

VIC (and other land surface models) has a large number of parameters which often contribute to uncertainties in the simulated discharge and there may exist multiple model parameter sets that can yield equally good or behavioral model output which can lead to widely divergent results under novel conditions (Her et al., 2019). Therefore, using 250 behavioral VIC models while capturing the hydrological responses, driven by datasets of multiple sources, makes our analysis more robust and reliable. Instead, employing only one parameter set could have led to improper representation of hydrological processes thus making it difficult to disentangle the impacts of using these datasets on discharge predictions.

Model performances using all these global datasets varies from one subcatchment to another which might be due to the regional differences in quality of these datasets particularly, satellite datasets. But to clearly understand, whether the poor performance at some stations is due to limitations in input datasets, or due to the process representations in the VIC model, other land surface models or hydrological models should be used.

6.5. Conclusions

Lack of availability of local/in-situ observations in developing countries like India limit the ongoing research of analyzing real-time hydrological processes. This urges the need for integrating high-quality global datasets into a regional scale hydrological model. In this study, we seek to understand the impacts of using new high resolution global datasets as inputs in a macroscale hydrological or a land surface model, VIC, on hydrological responses of Mahanadi river basin. To elucidate those impacts, we frame different model experiments using precipitation, temperature, soil, and land use datasets from both local and global products and perform comprehensive evaluation of the model performance. Global precipitation datasets are acquired from GPM IMERG and ERA5-Land and global temperature dataset from ERA5-Land. Global soil and land cover data are obtained from SoilGrids and ESA CCI respectively.

From the analysis of outcomes, following key conclusions can be drawn:

1. Reference produced best simulation results at three out of five subcatchments in the evaluation period with median KGE ranging from 0.66-0.80. Note that the calibration using all local datasets are performed in a completely different period (1990-2000). Replacing local precipitation with IMERG improved model performance at 2 subcatchments, specifically at Kesinga with median KGE value 0.7 compared to 0.5 for reference simulation. Replacing local land cover map with ESA CCI map produced best result at one subcatchment with median KGE 0.67.
2. Both satellite and reanalysis product, GPM and ERA5-Land respectively overestimated daily rainfall estimates (5-26%), which has caused overprediction in discharge compared to the reference experiment, however, decline in performance is significantly more, using ERA5-Land, at all subcatchments. Performance of GPM at three out of five subcatchment (KGE 0.58-0.76) is better than ERA5-Land (KGE 0.37-0.40) and could be used as an alternative to local precipitation estimates from IMD.
3. Maximum and minimum temperatures from ERA5-Land slightly overestimated discharge, however in overall showed a moderate performance with KGE values slightly lower than the reference experiment.
4. Not many changes are observed in the hydraulic properties of the soil textures in both (global and local) maps, hence global soil from SoilGrids produced a performance comparable to the reference experiment.
5. Global land cover map from ESA CCI tends to underestimate the discharge at all subcatchments primarily due to reduced barren grounds. However, the low flows are better captured compared to the local map.
6. Experiments using all input datasets from global sources (exp8 and 11) outperformed some experiments involving local land cover. This is because underestimating tendency of global land cover and overestimating tendency of global forcings ultimately improves the biases in streamflows.
7. The ranking of the global products (used in this study) most suitable for this region are SoilGrids, GPM rainfall, ERA5-Land temperatures, ESA CCI land cover and ERA5-Land rainfall. However, effects of inclusion of different combination of these datasets may vary the model predictions.

These results are based on 3 years (2014-2016) analysis, primarily due to the unavailability of local maximum and minimum temperature records from IMD. Moreover, retrospectively processed fully GPM-based IMERG data starting from 1998 became available during the later stage of our study. The future work should involve a long-term hydrological analysis using these datasets and it is also essential to test the global products, esp. rainfall and temperature at their native resolution against IMD observations, which would provide an in-depth aspect of these new datasets.

7. Conclusions and future outlook

7.1. Summary

Variability in land cover and climate are the important factors determining changes in hydrological processes in a river basin. These factors are expected to pose serious impacts in countries like India due to their agricultural-based rural economy. The Mahanadi river basin, located under a sub-tropical climate zone in India, is vulnerable to the hydrological extremes including floods and droughts (Jin et al., 2018). The hydrological cycle in the basin is expected to be altered further because of human induced land use activities, such as deforestation and agricultural activities (Behera et al., 2018), as well increase in precipitation and temperature (Jin et al., 2018). Therefore, evaluation and prediction of likely future behaviour of the basin flows are necessary for judicious planning and management of water resources. Distributed hydrological models like the Variable Infiltration Capacity (VIC) are typically employed to better understand the complex hydrological processes and their interactions under land cover and climate changes. However, there is still limitation in its accuracy of the outputs because of the uncertainties associated with the modelling predictions. These uncertainties can arise from model structures, model parameterisation and calibration procedures, and can also be associated with data availability such as availability of meteorological forcing and other input data.

This thesis presents an approach to predict hydrological responses under changing environment and model input datasets for Mahanadi river basin in India, using a regional-scale hydrological model and analysing the model performance under these changed conditions while properly reporting model uncertainties due to parameter estimation. The key findings of each chapter are summarised below:

Identifying behavioural parameter sets for regional scale hydrological modelling resulted in very good model performance

Physically distributed hydrological models are commonly employed to model the hydrological responses under the impacts of environmental changes. However, with the growing complexity of these new generation models (e.g., in terms of parameters to be prescribed a

priory), modelling hydrological changes is an extremely challenging task, especially in data sparse regions in developing countries. Using uncalibrated or poorly calibrated hydrological models can induce model parameter uncertainties on model simulations. To minimize these uncertainties, these models should pass through a careful calibration procedure, aiming to reduce the number of model parameters, prior to applying the model to address practical problems. Most regional based hydrological studies have applied the VIC model using a single model realization while predicting the hydrological impacts. This hides the potential uncertainties associated with model performances that may arise from different model parameterisation. Further, in those studies, calibration is mostly performed considering parameters that are either recommended by the model developers or has been considered as sensitive parameters in other river basins with different basin characteristics. This can lead to involving unnecessary parameters or excluding the important parameters which will ultimately reduce the model calibration accuracy and efficiency. For my research, I use a methodological approach where I first perform a detailed sensitivity analysis of the VIC model parameters to screen out the non-influential parameters at each subcatchment, followed by the calibration of only the influential parameters across those subcatchments to generate streamflow. This sensitivity-guided model calibration is performed within a Monte Carlo framework to generate behavioural models for subcatchments of the Mahanadi river basin. We found that the soil related parameters such as the infiltration parameter and second soil layer depth are the most influential parameters affecting the modelled streamflow while vegetation parameters have a very little impact on discharge. We also found that the routing parameter, flow velocity, is also a sensitive parameter which is however not often recommended for model calibration. The behavioural models that we obtained showed a substantial improvement compared to the non-behavioural models with median KGE ranging between 0.63 to 0.86 in calibration and 0.59 to 0.82 in validation across subcatchments. This KGE range suggests equifinality (equally good models resulting from different parameter combinations), however representing the uncertainties associated with the model parameterisation can help with a more robust quantification of hydrological impacts.

Future land cover changes are likely to result in an increase by up to 347 m³s⁻¹ in Mahanadi river basin discharge

Commonly, hydrological impact assessments are accomplished by using distributed hydrological models in conjunction with different land use scenarios. However, these models, through their complex interactions among parameters, can introduce significant uncertainties to the hydrological projections. Therefore, we seek to understand the change in hydrological responses due to different land cover scenarios while also including the uncertainties associated with model parameterization in those simulated hydrological responses. The behavioural models which we obtained are used in conjunction with historical and future land cover scenarios from the recently released, Land use Harmonisation (LUH2) to generate hydrological predictions and related uncertainties from behavioural model parameterisation. The LUH2 dataset indicates a noticeable increase in the cropland (23.3% cover) at the expense of forest (22.65% cover) by the end of year 2100 compared to the baseline year, 2005. As a result, my simulations indicate percent increase in the peak flows and mean annual flows upto 347 m³s⁻¹ and 33 m³s⁻¹ respectively in the basin. The direct conversion of forested areas to agriculture (on the order of 30,000 km²) reduces the Leaf Area Index and which subsequently reduces the Evapotranspiration (ET) and increases surface runoff. Further, the range of behavioural hydrological predictions indicated variation in the magnitudes of extreme flows simulated for the different land cover scenarios, for instance uncertainty in peak river discharge of upto 210 m³s⁻¹ is found in far future scenario. These findings indicate that the recurrent flood events occurring in the Mahanadi river basin might be influenced by the changes in LULC at the catchment scale and suggests that model parameterisation represents an important source of uncertainty in the hydrological predictions, and this should be accounted for in any land-use change impact assessment study.

Climate change impacts in the future would have a more pronounced effect (relative to LULC impacts) and would increase the river flows by up to 29,776 m³s⁻¹ in the Mahanadi river basin

Some of the serious hydrological consequences of climate change faced by developing countries like in India show regional variability, caused sometimes due to local climate, geographical characteristics, and regional physical processes. Understanding these regional hydrologic impacts has crucial role in the management of water resources. Several studies

dealing with hydrological impacts due to climate change in the Mahanadi basin (and other basins) are often contradictory depending on factors, for example which climate models are used, or scenarios used, as well as the hydrological model and calibration approaches employed. We employed a new, and arguably more objective, approach that could give a better insight on the impact of climate change. We try to identify the impacts of all possible combinations of specific change within the possible mean annual temperature and precipitation 2-dimensional scenario space (derived from thirteen CMIP6 models) on the hydrological responses. This is done instead of simulating the climate change impacts for a specific decade, specific scenarios, or specific models in the future (e.g., 2080s or scenario SSP585), which are more commonly done. Our methodological approach also involves using an ensemble of VIC models, representing the overall model uncertainty due to parameter choices, in conjunction with these climate projections, instead of using a single calibrated model to predict the hydrological responses. The climate projections show an overall change in mean annual precipitation and mean annual average temperature that ranges from -5 to +105% and 0-7°C respectively. This has resulted in significant changes in both mean annual flows and peak flows of upto 2849 and 29,776 m³s⁻¹ respectively. Uncertainties associated with the model parameters, of upto 1211 m³s⁻¹ is observed in the predicted peak flow magnitudes, which is considerably higher than in predicted annual flow magnitudes. Our findings indicate that precipitation mainly controls the future predicted flows in the basin, especially peak or monsoon flows. In some cases, small percentage change in annual rainfall combined with rise in temperature has resulted in decrease in the mean annual flows possibly due to the increase in ET. This study has provided a set of results on the likely future behavior of the subcatchments of Mahanadi river system mean annual and peak flows under the CMIP6 biased corrected projection. Future projections of hydrologic variables, along with the associated model parameter uncertainties can help with better hydrologic impact assessment and developing adaptation strategies for Mahanadi river basin in India.

Global input datasets (meteorological, soil and land cover) might can be a viable alternative to the local datasets for regional scale modelling in data scarce region in India

Land Surface Models (LSMs) used for large scale applications are getting finer in terms of their spatial resolution which should allow in principle for improved simulations. However, the problem lies with the availability of local/in-situ observations and therefore, high resolution

LSMs are still poorly constrained in many developing countries. On the other hand, there are enormous advances in global data availability. With this motivation, we seek to understand how reliable these global datasets are in producing a comparable hydrological model performance when replacing local observations. To this end, we designed VIC model experiments to explicitly examine the impacts of specific local and global datasets (global meteorological inputs from IMERG GPM and ERA5-Land; global soil and land cover from SoilGrids and ESA CCI, respectively) on model performance. Our results showed that model performances varied substantially across subcatchments depending on the input combinations. Experiment using 'all local datasets' is considered as the reference (or benchmark) simulation, which have most closely represented the observed discharge across subcatchments, as suggested by the performance metric. Both global rainfall datasets (IMERG GPM and ERA5-Land) have overestimated the rainfall values however, simulations, particularly using ERA5-Land rainfall (due to relatively more overestimation) underperformed at all subcatchments. Performance using global temperature and global soil has shown comparable model performance to the reference scenario performance. We have found mismatch in soil classification of local and global data, however, which is among the soil types of comparable hydraulic properties, thereby having least influence on the predicted discharge. Global land cover map has an underestimating tendency primarily due to reduced barren grounds in ESA CCI, thereby deteriorating the model performance across the subcatchments, however, captured the low flows better than the local land cover. Our findings indicate that some of these global datasets could be used as a viable alternative to local observations in this river basin and potentially in nearby basins where there is a lack of in-situ observations.

7.2. Overarching remarks

This thesis provided a set of results on the likely future behavior of the subcatchments of Mahanadi river discharge (mean annual and peak flows) under the future climate and land cover projections. We have used recently released meteorological forcing data, soil and land cover datasets from satellite and reanalysis products, and climate and land cover scenarios. In addition, this thesis also presents results on the differences in hydrological responses with respect to using different combinations of local and global input datasets in a regional scale hydrological model. All the hydrological predictions presented here are presented with

proper uncertainty estimates, resulting from varying model parameters within realistic uncertainty bounds using a Monte Carlo framework. While the modelled hydrological impacts are helpful for catchment management and planning, the uncertainty associated with these models should be considered carefully. For instance, sensitivity analysis techniques may help modellers in selecting influential and non-influential parameters as well as identifying interactions among parameters prior performing model calibration to reduce uncertainties in model simulations. The results and analysis in the thesis have implications to the manner in which we calibrate and evaluate models, and the calibration framework can be considered for relevant simulation studies in other parts of India. Some key findings are that the increase in temperature and precipitation in the Mahanadi river basin can result in a significant increase in river discharge in the future. The recurrent flood events occurring in the Mahanadi river basin might also be influenced by the changes in LULC at the catchment scale, however relatively much lesser than the change in climate. Uncertainties associated with these predicted river discharge (mean annual or peak flows) indicates that the uncertainties in hydrological projections are higher in case of climate change than the land cover change. These findings are based on land cover scenarios from recently released LUH2 dataset and climate scenarios from latest climate model generation, CMIP6. The latest update of the climate models in CMIP6 are expected to produce more accurate projections, as also the ability to simulate climate variables, especially Indian monsoon have improved over time (Katzenberger et al., 2020). It is therefore essential to evaluate these updates and advancements in these datasets and scenarios for their suitability for hydroclimatic applications.

The predicted high volume flood discharges of a certain magnitude along with the uncertainty bound in future will enable modification of the rule curve of the major dam (Hirakud dam, see Figure 2.1) in the basin, and also would be useful in designing the proposed second reservoir in the middle reaches of the basin (Jena et al., 2014). This will have a positive impact on resilience, lives and livelihoods of over 10 million people living in the deltaic region of the basin. Moreover, a study on hydrological impacts of future LULC change at basin scale can also offer much needed inputs for policy decision making and adequate water resource management. With a widespread consensus that the Indian monsoon rainfall will increase due to climate change in the 21st century, and a notable increase in the agricultural

production over the last decade, the findings of this research are expected to help the water managers for decision making and policy makers to develop the adaptation and mitigation strategies in the vulnerable regions within the basin.

7.3. Recommendations for future work

Availability of wider range of modern hydrologic modelling applications

Several macroscale hydrological models like VIC have been used in addressing issues related to historical and future water resources over the last few decades. However, most studies focussed on climate and land cover change impacts on only natural water resources and water availability. The version of the model used in this thesis, VIC 4.2.d although incorporates many upgrades compared to the older versions, however, further model developments are needed for comprehensively assessing the anthropogenic impacts on water resources.

- **Incorporating anthropogenic impact modules into water resource assessments in future studies**

Recently, efforts have been put on incorporating anthropogenic impacts into water resource assessments, including dam operations and water withdrawals (Droppers et al., 2019; Haddeland et al., 2006; Hanasaki et al., 2017). Dams and reservoirs are built to make water available for different sectors including hydropower, irrigation and domestic uses, which will strongly affect river discharge. Haddeland et al., (2006) had developed a reservoir model to implement in VIC model, which included important modules such as dam operation and irrigation, which is also used by few other studies. Future river flows, especially water availability under the low flows is predicted to be affected by the increase in irrigation water demand from the changing land uses (agricultural expansion) in the Mahanadi river basin (Jin et al., 2018). Specifically in Mahanadi river basin in India, where agriculture is mainly supported by large scale irrigation infrastructure, consideration of these anthropogenic impact modules would be helpful in implementing agricultural policies. In our thesis, VIC model has been set up for five major subcatchments, located upstream of Hirakud dam, which is a major dam (See Figure 3.1, Chapter3) within the Mahanadi river basin. However, during the high rainfall events, very high flows released from Hirakud dam and other minor irrigation dams in upstream, floods the downstream of the basin (Jena et al., 2014). Therefore, future studies dealing with hydrological impacts of climate or land cover changes shall also focus on

the effects of reservoir operations and irrigation water withdrawals on hydrological components.

- **Utilizing the Improved model infrastructure**

The anthropogenic modules (Haddeland et al., 2006) (dam operation, water withdrawals for several purposes) were however not fully integrated, requiring several successive model runs which was computationally expensive. Hamman et al., (2018), recently have attempted to improve the model infrastructure and released a recent version of the model, VIC-5. Not many improvements have been noticed in the model infrastructure since the VIC's initial release in 1990's until the release of version 5 (VIC-5). Major improvements in VIC-5 includes supporting a wide range of modelling applications, parallel computing strategy to enable efficient large-scale simulations and improvements on input/output formats required by the model. Previous versions including VIC 4.2.d (used in this thesis) involved extensive pre/post processing and reformatting of model input and output files, however, representation of hydrological processes in VIC-5 is same as VIC 4.2.d. Since previous versions did not allow for parallelising model runs (i.e., running VIC simulations for different grid cells on separate cores or computers), this had direct implications on the number of model simulations performed in some chapters of this thesis. A more recent work by Droppers et al., (2019) have utilized this improved model infrastructure (Hamman et al., 2018) and fully integrated the anthropogenic impacts into the VIC model framework while also reducing computation times.

- **Representation of groundwater processes**

Moreover, large-scale hydrological models also require better representations of groundwater processes to improve simulations of regional scale hydrology and climate, as in most models, groundwater is either ignored or crudely represented (Scheidegger et al., 2021). The standard version of VIC used in our study does not have the groundwater storage component, thus results in a poor representation of baseflow. In Indian scenario, groundwater gets recharged during the monsoon season, which contributes to the surface flows during the dry season. Our PBIAS indicates negative bias in the non-monsoon season i.e., underestimation in low flow conditions in most of the subcatchments which attributes to the non-consideration of groundwater in VIC. This is also reported by Chawla and Mujumdar, (2015) and Joseph et al., (2018) in other river basins in India. For instance, lack of baseflow contributions from groundwater had resulted in decrease of simulated flows after the end of monsoons, in the river Ganga in India. This limitation is partially addressed in some studies (Rosenberg et al., 2013; Sridhar et al., 2018). This is an important issue as VIC is applied widely in Indian river basins across scales and range of hydrologic applications. To address these issue, Scheidegger et al., (2021), recently incorporated a 2D lateral groundwater flow model into the VIC model, which will simulate baseflow contributions from diffusive groundwater flow to the rivers and will enable considering more realistic groundwater irrigation schemes especially within India.

Considering uncertainty sources while modelling hydrological changes

Modelling hydrological changes and the associated uncertainties are vital for water management including planning of water resources, assessments of floods and droughts etc. Decision makers are increasingly interested in the uncertainty bound of the streamflow predictions therefore modellers are required to quantify the uncertainties and communicate them for policy development (Mockler et al., 2016). Climate and land cover change assessments are generally accomplished using a hydrological model. From hydrological modelling perspective, dominant sources of uncertainties are three different sources i.e., model structure, model parameterisation and forcing data (Mockler et al., 2016). In this thesis, we have accounted for the uncertainties in hydrologic predictions resulting from model parameterisation in both Chapter 4 and Chapter 5, also accounted for uncertainties in streamflow predictions due to different model input datasets including forcing data in

Chapter 6. There are also studies which showed that choice of model, i.e., model structure has significant effect on predicted river discharge (Karlsson et al., 2016). Apart from these three dominant sources, uncertainties may also arise due to using the observed discharge, for performing the hydrological model calibration, which thereafter is used to understand the model parameter uncertainty issues. Most models do not account for water regulation (due to non-availability of data), while considering the observed flows for model calibration. For instance, in this study, although we have calibrated flows upstream to the major reservoir present in the basin, there are also minor water related structures present in the analysed subbasins that we have not considered. This can make the calibration process erroneous and difficult, particularly for Indian case studies, as flows are mostly regulated. It is therefore further recommended to consider other hydrological variables such as ET, soil moisture etc., for hydrological model calibration.

Considering all these uncertainty sources while modelling hydrological changes, would result in total predictive uncertainty. Most studies have focussed on addressing one or two uncertainty sources (Bennett et al., 2018; Karlsson et al., 2016) and very few studies have addressed all (or most of) the aspects of these uncertainty sources, while simulating hydrological responses under changing climate and land cover (Chen et al., 2019b; Feng and Beighley, 2020; Mockler et al., 2016). In this context, Blöschl et al., (2019) raised an important research question “How can we disentangle and reduce model structural/parameter/input uncertainty in hydrological prediction?”. Future land cover and climate change studies shall therefore focus on assessing the relative importance of these uncertainties and their interactions in model simulations and reducing the total predictive uncertainty while assessing hydrological impacts, which is important for the decision makers.

We understand that the exact nature of impacts on the water sector at regional, river basin scales are associated with a notable uncertainty and methodologies are framed to quantify and constrain that uncertainty. However, in the context of water management, scientific community are responsible for communicating the results along with these uncertainties in such a manner that policy makers and stakeholders find it useful and easy to understand, while planning for future. For example, there may be many sources of uncertainty that a modeller may consider, but details of these sources are not necessarily required by end users.

The modellers will have to be responsible for understanding the sources of uncertainty and minimizing it, before communicating the results to the decision makers. Modellers while explaining the results should emphasize on the consequences of ignoring or underestimating the uncertainty range or ignoring the extreme events (outliers), which often tend to be rejected by the operational hydrologists. For instance, while communicating the probable changes in peak flows at the Mahanadi river basin outlet, rather than offering a range of increase in flow magnitudes, it is better to convey the loss of lives, property and costs associated with these uncertain impacts. Moreover, the choice of appropriate terminology is particularly important such as “probabilities”, “frequencies” in conveying these uncertainties, as well as the choice of exact information, modellers would like to convey based on users’ goal.

Enormous advances in global data availability

The advent of global hyper resolution hydrological modelling and its needs has led to enormous advances in global data availability from both satellite and reanalysis products (Beven and Cloke, 2012). The quality and number of these high-resolution datasets are expected to increase even more with the launch of new missions with better sensors hence can be used for parameterizing regional scale hydrological model, especially in developing countries where there is a shortage of in-situ data. It is worth mentioning that our judgement of the performances of eleven VIC model experiments (using eleven combinations of local and global datasets) was based on a benchmark model, which is the model calibrated against local datasets i.e., deterioration or improvement of the models are measured with respect to the benchmark model. It would be interesting to further understand whether all models (11 models experiments) if calibrated against their respective combination of input datasets, would produce similar model performance as presented in Chapter 6. To address this, notwithstanding all the calibration efforts presented in Chapter 3, the performances of 11 VIC model experiments can be treated as a pre-calibration approach to help in selection of the most robust suite of input datasets for this region, also allowing rapid estimation of quality of input datasets. Calibration of the model using the right combination of input datasets would also minimize the systematic bias and predictive uncertainty introduced during model calibration.

Looking at other important aspects of hydrological analysis

Mahanadi river basin receives approximately 85% of the total annual rainfall during the monsoon months (June-Sept) which also results in 85% of the annual river discharge during these months. The discharge hydrograph at all subbasins (Figure B.1 in appendix) for the time period 2014-2016, shows negligible flows occurring during the rest of the year. Moreover peak discharge in the basin mostly occurs during the monsoon (Jin et al., 2018). Various studies in the past such as Asokan and Dutta, (2008), Ghosh et al., (2010) and Jin et al., (2018) predicted an increase either in the high (peak) flows or monsoon flows in the future, that would potentially enhance the flood risk, whereas, insignificant to significant decline in low flows and water availability is reported. Therefore, in this study, we choose to restrict our analysis to the high flows, (in Chapter 4, land cover change impacts), and peak flows or monsoon flows (in Chapter 5, Climate change impacts) instead of analysing all percentiles of flows. We have also considered analysing the mean state i.e., the mean annual flows in all chapters. However, full comprehensive analysis of all percentiles of flow along with the evaluation of the changes in flow regime based on the flow duration curve analysis is recommended for future studies to discuss modelling efforts. We observed that the relative changes in land cover change impacts on river discharge were insignificant, further analysis can be carried out to understand if the impacts are more embodied in the timing change rather than magnitudes or variability of streamflow. Besides, changes in annual peak flow estimates in future can also be used in the flood frequency analysis i.e., to estimate the frequency of high-flow events (number of days exceeding high flow threshold) under the projected future land cover and climate scenarios.

Data availability

Dem is freely available from <https://bhuvan-app3.nrsc.gov.in/data/download/index.php>.

Unit Hydrograph is adopted from

<https://vic.readthedocs.io/en/vic.4.2.d/Documentation/Routing/UH/>.

Daily gridded rainfall, maximum and minimum temperature are freely available from

http://www.imdpune.gov.in/Clim_Pred_LRF_New/Grided_Data_Download.html.

Observed discharge data are available from <http://cwc.gov.in/>.

The source code for VIC-3L version 4.2.d is available from

<https://github.com/UW-Hydro/VIC/releases/tag/VIC.4.2.d>.

Wind speed data is freely available from

https://psl.noaa.gov/cgi-bin/db_search/DBSearch.pl?Dataset=NCEP+Reanalysis+Daily+Averages

LUH2 datasets are downloaded from <https://luh.umd.edu/data.shtml>.

Soil textural information to prepare soil map of soilGrids is derived from

[\(https://soilgrids.org/\)](https://soilgrids.org/)

Land cover map from ESA CCI is downloaded from www.esa-landcover-cci.org/.

ERA5-Land precipitation and temperature products are obtained from

<https://cds.climate.copernicus.eu/cdsapp#!/dataset/reanalysis-era5-land?tab=form>

BIBLIOGRAPHY

A. K. Srivastava, M. R. and S. R. K.: Development of a high resolution daily gridded temperature data set (1969 – 2005) for the Indian region, *Atmos. Sci. Lett.*, 10(October), 249–254, doi:10.1002/asl, 2009.

Abe, C. A., Lobo, F. de L., Dibike, Y. B., Costa, M. P. de F., Dos Santos, V. and Novo, E. M. L. M.: Modelling the effects of historical and future land cover changes on the hydrology of an Amazonian basin, *Water (Switzerland)*, 10(7), doi:10.3390/w10070932, 2018a.

Abe, C. A., Lobo, F. de L., Dibike, Y. B., Costa, M. P. de F., Dos Santos, V. and Novo, E. M. L. M.: Modelling the effects of historical and future land cover changes on the hydrology of an Amazonian basin, *Water (Switzerland)*, 10(7), doi:10.3390/w10070932, 2018b.

Archer, G. E. B., Saltelli, A. and Sobol, I. M.: Sensitivity measures, anova-like techniques and the use of bootstrap, *J. Stat. Comput. Simul.*, 58(2), 99–120, doi:10.1080/00949659708811825, 1997.

Ashagrie, A. G., De Laat, P. J. M., De Wit, M. J. M., Tu, M. and Uhlenbrook, S.: Detecting the influence of land use changes on discharges and floods in the Meuse River Basin - The predictive power of a ninety-year rainfall-runoff relation?, *Hydrol. Earth Syst. Sci.*, 10(5), 691–701, doi:10.5194/hess-10-691-2006, 2006.

Asokan, S. M. and Dutta, D.: Analysis of water resources in the Mahanadi River Basin, India under projected climate conditions, *Hydrol. Process. An Int. J.*, 22(18), 3589–3603, 2008.

Babar, S. and Ramesh, H.: Streamflow response to land use-land cover change over the Nethravathi River Basin, India, *J. Hydrol. Eng.*, 20(10), doi:10.1061/(ASCE)HE.1943-5584.0001177, 2015.

Bao, Z., Liu, J., Zhang, J., Fu, G., Wang, G., Yan, X., Zhang, A., Xu, Q. and Shang, M.: Estimation of baseflow parameters of variable infiltration capacity model with soil and topography properties for predictions in ungauged basins, *Hydrol. Earth Syst. Sci. Discuss.*, 8(4), 7017–7053, doi:10.5194/hessd-8-7017-2011, 2011.

Batellis, S.: *The Impact of Groundwater Representation in Land Surface Models Under Current and Future Climate Scenarios in Great Britain*, University of Bristol., 2021.

Behera, M. D., Patidar, N., Chitale, V. S., Behera, N., Gupta, D., Matin, S., Tare, V., Panda, S. N. and Sen, D. J.: Increase in agricultural patch contiguity over the past three decades in Ganga River Basin, India, *Curr. Sci.*, 502–511, 2014.

Behera, M. D., Tripathi, P., Das, P., Srivastava, S. K., Roy, P. S., Joshi, C., Behera, P. R., Deka, J., Kumar, P., Khan, M. L., Tripathi, O. P., Dash, T. and Krishnamurthy, Y. V. N.: Remote sensing based deforestation analysis in Mahanadi and Brahmaputra river basin in India since 1985, *J. Environ. Manage.*, 206, 1192–1203, doi:10.1016/j.jenvman.2017.10.015, 2018.

Bennett, K. E., Urrego Blanco, J. R., Jonko, A., Bohn, T. J., Atchley, A. L., Urban, N. M. and Middleton, R. S.: Global Sensitivity of Simulated Water Balance Indicators Under Future Climate Change in the Colorado Basin, *Water Resour. Res.*, 54(1), 132–149, doi:10.1002/2017WR020471, 2018.

Bergström, S. and Graham, L. P.: On the scale problem in hydrological modelling, *J. Hydrol.*,

211(1–4), 253–265, doi:10.1016/S0022-1694(98)00248-0, 1998.

Beria, H., Nanda, T., Bisht, D. S. and Chatterjee, C.: Does the GPM mission improve the systematic error component in satellite rainfall estimates over TRMM? An evaluation at a pan-India scale, *Hydrol. Earth Syst. Sci.*, 21(12), 6117–6134, doi:10.5194/hess-21-6117-2017, 2017.

Berihun, M. L., Tsunekawa, A., Haregeweyn, N., Meshesha, D. T., Adgo, E., Tsubo, M., Masunaga, T., Fenta, A. A., Sultan, D., Yibeltal, M. and Ebabu, K.: Hydrological responses to land use/land cover change and climate variability in contrasting agro-ecological environments of the Upper Blue Nile basin, Ethiopia, *Sci. Total Environ.*, 689, 347–365, doi:10.1016/j.scitotenv.2019.06.338, 2019.

Betts, R. A., Jones, C. D., Knight, J. R., Keeling, R. F. and Kennedy, J. J.: El Niño and a record CO₂ rise, *Nat. Clim. Chang.*, 6(9), 806–810, doi:10.1038/nclimate3063, 2016.

Beven, K. and Binley, A.: The future of distributed models: Model calibration and uncertainty prediction, *Hydrol. Process.*, 6(3), 279–298, doi:10.1002/hyp.3360060305, 1992.

Beven, K. and Freer, J.: Equifinality, data assimilation, and uncertainty estimation in mechanistic modelling of complex environmental systems using the GLUE methodology, *J. Hydrol.*, 249(1–4), 11–29, 2001.

Beven, K. J.: *Rainfall-runoff modelling: the primer*, John Wiley & Sons., 2011.

Beven, K. J. and Cloke, H. L.: Comment on “hyperresolution global land surface modeling: Meeting a grand challenge for monitoring Earth’s terrestrial water” by Eric F. Wood et al., *Water Resour. Res.*, 48(1), 1–10, doi:10.1029/2010WR010090, 2012.

Bierkens, M. F. P., Bell, V. A., Burek, P., Chaney, N., Condon, L. E., David, C. H., de Roo, A., Döll, P., Drost, N., Famiglietti, J. S., Flörke, M., Gochis, D. J., Houser, P., Hut, R., Keune, J., Kollet, S., Maxwell, R. M., Reager, J. T., Samaniego, L., Sudicky, E., Sutanudjaja, E. H., van de Giesen, N., Winsemius, H. and Wood, E. F.: Hyper-resolution global hydrological modelling: What is next?: “Everywhere and locally relevant” M. F. P. Bierkens et al. Invited Commentary, *Hydrol. Process.*, 29(2), 310–320, doi:10.1002/hyp.10391, 2015.

Blöschl, G., Bierkens, M. F. P., Chambel, A., Cudennec, C., Destouni, G., Fiori, A., Kirchner, J. W., McDonnell, J. J., Savenije, H. H. G., Sivapalan, M., Stump, C., Toth, E., Volpi, E., Carr, G., Lupton, C., Salinas, J., Széles, B., Viglione, A., Aksoy, H., Allen, S. T., Amin, A., Andréassian, V., Arheimer, B., Aryal, S. K., Baker, V., Bardsley, E., Barendrecht, M. H., Bartosova, A., Batelaan, O., Berghuijs, W. R., Beven, K., Blume, T., Bogaard, T., Borges de Amorim, P., Böttcher, M. E., Boulet, G., Breinl, K., Brilly, M., Brocca, L., Buytaert, W., Castellarin, A., Castelletti, A., Chen, X., Chen, Y., Chen, Y., Chiffard, P., Claps, P., Clark, M. P., Collins, A. L., Croke, B., Dathe, A., David, P. C., de Barros, F. P. J., de Rooij, G., Di Baldassarre, G., Driscoll, J. M., Duethmann, D., Dwivedi, R., Eris, E., Farmer, W. H., Feiccabrino, J., Ferguson, G., Ferrari, E., Ferraris, S., Fersch, B., Finger, D., Foglia, L., Fowler, K., Gartsman, B., Gascoin, S., Gaume, E., Gelfan, A., Geris, J., Gharari, S., Gleeson, T., Glendell, M., Gonzalez Bevacqua, A., González-Dugo, M. P., Grimaldi, S., Gupta, A. B., Guse, B., Han, D., Hannah, D., Harpold, A., Haun, S., Heal, K., Helfricht, K., Herrnegger, M., Hipsey, M., Hlaváčiková, H., Hohmann, C., Holko, L., Hopkinson, C., Hrachowitz, M., Illangasekare, T. H., Inam, A., Innocente, C., Istanbuluoglu, E., Jarihani, B., et al.: Twenty-three unsolved problems in hydrology (UPH)—a community perspective, *Hydrol. Sci. J.*, 64(10), 1141–1158, doi:10.1080/02626667.2019.1620507, 2019.

Bosch, J. M. and Hewlett, J. D.: A review of catchment experiments to determine the effect of

vegetation changes on water yield and evapotranspiration, *J. Hydrol.*, 55(1–4), 3–23, doi:10.1016/0022-1694(82)90117-2, 1982.

Bosmans, J. H. C., Van Beek, L. P. H., Sutanudjaja, E. H. and Bierkens, M. F. P.: Hydrological impacts of global land cover change and human water use, *Hydrol. Earth Syst. Sci.*, 21(11), 5603–5626, doi:10.5194/hess-21-5603-2017, 2017.

Breuer, L., Huisman, J. A. and Frede, H. G.: Monte Carlo assessment of uncertainty in the simulated hydrological response to land use change, *Environ. Model. Assess.*, 11(3), 209–218, doi:10.1007/s10666-006-9051-9, 2006.

Campolongo, F., Saltelli, A. and Cariboni, J.: From screening to quantitative sensitivity analysis. A unified approach, *Comput. Phys. Commun.*, 182(4), 978–988, doi:10.1016/j.cpc.2010.12.039, 2011.

Chaney, N. W., Herman, J. D., Reed, P. M. and Wood, E. F.: Flood and drought hydrologic monitoring: The role of model parameter uncertainty, *Hydrol. Earth Syst. Sci.*, 19(7), 3239–3251, doi:10.5194/hess-19-3239-2015, 2015.

Chawla, I. and Mujumdar, P. P.: Isolating the impacts of land use and climate change on streamflow, *Hydrol. Earth Syst. Sci.*, 19(8), 3633–3651, doi:10.5194/hess-19-3633-2015, 2015.

Chen, C., Park, T., Wang, X., Piao, S., Xu, B., Chaturvedi, R. K., Fuchs, R., Brovkin, V., Ciais, P., Fensholt, R., Tømmervik, H., Bala, G., Zhu, Z., Nemani, R. R. and Myneni, R. B.: China and India lead in greening of the world through land-use management, *Nat. Sustain.*, 2(2), 122–129, doi:10.1038/s41893-019-0220-7, 2019a.

Chen, J., Brissette, F. P., Poulin, A. and Leconte, R.: Overall uncertainty study of the hydrological impacts of climate change for a Canadian watershed, *Water Resour. Res.*, 47(12), 1–16, doi:10.1029/2011WR010602, 2011.

Chen, Y., Xu, C. Y., Chen, X., Xu, Y., Yin, Y., Gao, L. and Liu, M.: Uncertainty in simulation of land-use change impacts on catchment runoff with multi-timescales based on the comparison of the HSPF and SWAT models, *J. Hydrol.*, 573(December 2018), 486–500, doi:10.1016/j.jhydrol.2019.03.091, 2019b.

Chen, Z., Zhou, T., Zhang, L., Chen, X., Zhang, W. and Jiang, J.: Global Land Monsoon Precipitation Changes in CMIP6 Projections, *Geophys. Res. Lett.*, 47(14), doi:10.1029/2019GL086902, 2020.

Cherkauer, K. A. and Lettenmaier, D. P.: Hydrologic effects of frozen soils in the upper Mississippi River basin, *J. Geophys. Res. Atmos.*, 104(D16), 19599–19610, doi:10.1029/1999JD900337, 1999.

Christensen, J. H., Boberg, F., Christensen, O. B. and Lucas-Picher, P.: On the need for bias correction of regional climate change projections of temperature and precipitation, *Geophys. Res. Lett.*, 35(20), doi:10.1029/2008GL035694, 2008.

Chu, M. L., Knouft, J. H., Ghulam, A., Guzman, J. A. and Pan, Z.: Impacts of urbanization on river flow frequency: A controlled experimental modeling-based evaluation approach, *J. Hydrol.*, 495, 1–12, doi:10.1016/j.jhydrol.2013.04.051, 2013.

Clark, M. P., Fan, Y., Lawrence, D. M., Adam, J. C., Bolster, D., Gochis, D. J., Hooper, R. P., Kumar, M., Leung, L. R., Mackay, D. S. and Maxwell, R. M.: Hydrological partitioning in the critical zone: Recent advances and opportunities for developing transferable understanding

of water cycle dynamics, *Water Resour. Res.*, 1–28, doi:10.1002/2015WR017096. Received, 2015.

Collischonn, W., Allasia, D., da Silva, B. C. and Tucci, C. E. M.: The MGB-IPH model for large-scale rainfall-runoff modelling, *Hydrol. Sci. J.*, 52(5), 878–895, doi:10.1623/hysj.52.5.878, 2007.

Connor, R.: The United Nations world water development report 2015: water for a sustainable world, UNESCO publishing., 2015.

Cornelissen, T., Diekkrüger, B. and Giertz, S.: A comparison of hydrological models for assessing the impact of land use and climate change on discharge in a tropical catchment, *J. Hydrol.*, 498, 221–236, doi:10.1016/j.jhydrol.2013.06.016, 2013.

Cosby, B. J., Hornberger, G. M., Clapp, R. B. and Ginn, T. R.: A Statistical Exploration of the Relationships of Soil Moisture Characteristics to the Physical Properties of Soils, *Water Resour. Res.*, 20(6), 682–690, doi:10.1029/WR020i006p00682, 1984.

Costa, M. H., Botta, A. and Cardille, J. A.: Effects of large-scale changes in land cover on the discharge of the Tocantins River, Southeastern Amazonia, *J. Hydrol.*, 283(1–4), 206–217, doi:10.1016/S0022-1694(03)00267-1, 2003.

Dadhwal, V. K., Mishra, N. and Aggarwal, S. P.: Hydrological Simulation of Mahanadi River Basin and Impact of Land Use / Land Cover Change on Surface Runoff Using a Macro Scale Hydrological Model, *ISPRS TC VII Symp. – 100 Years ISPRS, Vienna, Austria, XXXVIII*, 165–170, 2010.

Dai, Y., Shangguan, W., Wei, N., Xin, Q., Yuan, H., Zhang, S., Liu, S., Lu, X., Wang, D. and Yan, F.: A review of the global soil property maps for Earth system models, *Soil*, 5(2), 137–158, doi:10.5194/soil-5-137-2019, 2019.

Das, P., Behera, M. D., Patidar, N., Sahoo, B., Tripathi, P., Behera, P. R., Srivastava, S. K., Roy, P. S., Thakur, P., Agrawal, S. P. and Krishnamurthy, Y. V. N.: Impact of LULC change on the runoff, base flow and evapotranspiration dynamics in eastern Indian river basins during 1985–2005 using variable infiltration capacity approach, *J. Earth Syst. Sci.*, 127(2), 1–19, doi:10.1007/s12040-018-0921-8, 2018.

DeFries, R. and Eshleman, K. N.: Land-use change and hydrologic processes: a major focus for the future, *Hydrol. Process.*, 18(11), 2183–2186, doi:10.1002/hyp.5584, 2004.

Demaria, E. M., Nijssen, B. and Wagener, T.: Monte Carlo sensitivity analysis of land surface parameters using the Variable Infiltration Capacity model, *J. Geophys. Res. Atmos.*, 112(11), 1–15, doi:10.1029/2006JD007534, 2007.

Demaria, E. M. C., Maurer, E. P., Sheffield, J., Bustos, E., Poblete, D., Vicuña, S. and Meza, F.: Using a gridded global dataset to characterize regional hydroclimate in central Chile, *J. Hydrometeorol.*, 14(1), 251–265, doi:10.1175/JHM-D-12-047.1, 2013.

Dembélé, M., Schaeffli, B., van de Giesen, N. and Mariéthoz, G.: Suitability of 17 rainfall and temperature gridded datasets for largescale hydrological modelling in West Africa, *Hydrol. Earth Syst. Sci. Discuss.*, 1–39, doi:10.5194/hess-2020-68, 2020.

Dhanya, C. T. and Villarini, G.: An investigation of predictability dynamics of temperature and precipitation in reanalysis datasets over the continental United States, *Atmos. Res.*, 183, 341–350, doi:10.1016/j.atmosres.2016.09.017, 2017.

- Dilley, M.: Natural disaster hotspots: a global risk analysis, World Bank Publications., 2005.
- Droppers, B., Franssen, W., van Vliet, M., Nijssen, B. and Ludwig, F.: Simulating human impacts on global water resources using VIC-5, *Geosci. Model Dev. Discuss.*, 1–40, doi:10.5194/gmd-2019-251, 2019.
- Dwarakish, G. S. and Ganasri, B. P.: Impact of land use change on hydrological systems: A review of current modeling approaches, *Cogent Geosci.*, 1(1), 1–18, doi:10.1080/23312041.2015.1115691, 2015.
- Eccles, R., Zhang, H. and Hamilton, D.: A review of the effects of climate change on riverine flooding in subtropical and tropical regions, *J. Water Clim. Chang.*, 10(4), 687–707, doi:10.2166/wcc.2019.175, 2019.
- Efron, B. and Tibshirani, R. J.: Chapter 17: Cross-Validation, *An Introd. to Bootstrap*, 1993.
- Essou, G. R. C., Sabarly, F., Lucas-Picher, P., Brissette, F. and Poulin, A.: Can precipitation and temperature from meteorological reanalyses be used for hydrological modeling?, *J. Hydrometeorol.*, 17(7), 1929–1950, doi:10.1175/JHM-D-15-0138.1, 2016.
- Eum, H. Il, Yonas, D. and Prowse, T.: Uncertainty in modelling the hydrologic responses of a large watershed: A case study of the Athabasca River basin, Canada, *Hydrol. Process.*, 28(14), 4272–4293, doi:10.1002/hyp.10230, 2014.
- Eum, H. Il, Dibike, Y. and Prowse, T.: Comparative evaluation of the effects of climate and land-cover changes on hydrologic responses of the Muskeg River, Alberta, Canada, *J. Hydrol. Reg. Stud.*, 8, 198–221, doi:10.1016/j.ejrh.2016.10.003, 2016a.
- Eum, H. Il, Dibike, Y. and Prowse, T.: Comparative evaluation of the effects of climate and land-cover changes on hydrologic responses of the Muskeg River, Alberta, Canada, *J. Hydrol. Reg. Stud.*, 8, 198–221, doi:10.1016/j.ejrh.2016.10.003, 2016b.
- Faostat, F. A. O.: Available online: <http://www.fao.org/faostat/en/#data>, QC (accessed January 2018), 2017.
- Faramarzi, M., Srinivasan, R., Iravani, M., Bladon, K. D., Abbaspour, K. C., Zehnder, A. J. B. and Goss, G. G.: Setting up a hydrological model of Alberta: Data discrimination analyses prior to calibration, *Environ. Model. Softw.*, 74, 48–65, doi:10.1016/j.envsoft.2015.09.006, 2015.
- Feng, D. and Beighley, E.: Identifying uncertainties in hydrologic fluxes and seasonality from hydrologic model components for climate change impact assessments, *Hydrol. Earth Syst. Sci.*, 24(5), 2253–2267, doi:10.5194/hess-24-2253-2020, 2020.
- Fisher, R. A. and Koven, C. D.: Perspectives on the Future of Land Surface Models and the Challenges of Representing Complex Terrestrial Systems, *J. Adv. Model. Earth Syst.*, 12(4), doi:10.1029/2018MS001453, 2020.
- Fohrer, N., Haverkamp, S., Eckhardt, K. and Frede, H. G.: Hydrologic response to land use changes on the catchment scale, *Phys. Chem. Earth, Part B Hydrol. Ocean. Atmos.*, 26(7–8), 577–582, doi:10.1016/S1464-1909(01)00052-1, 2001.
- Foley, J. A., DeFries, R., Asner, G. P., Barford, C., Bonan, G., Carpenter, S. R., Chapin, F. S., Coe, M. T., Daily, G. C., Gibbs, H. K., Helkowski, J. H., Holloway, T., Howard, E. A., Kucharik, C. J., Monfreda, C., Patz, J. A., Prentice, I. C., Ramankutty, N. and Snyder, P. K.: Global consequences

- of land use, *Science* (80-.), 309(5734), 570–574, doi:10.1126/science.1111772, 2005.
- Franchini, M. and Pacciani, M.: Comparative analysis of several conceptual rainfall-runoff models, *J. Hydrol.*, 122(1–4), 161–219, doi:10.1016/0022-1694(91)90178-K, 1991.
- Gao, H., Tang, Q., Shi, X., Zhu, C. and Bohn, T.: Water budget record from Variable Infiltration Capacity (VIC) model, *Algorithm Theor. Basis Doc. Terr. Water Cycle Data Rec.*, (Vic), 120–173 [online] Available from: [http://scholar.google.com/scholar?hl=en&btnG=Search&q=intitle:Water+Budget+Record+from+Variable+Infiltration+Capacity+\(+VIC+\)+Model#2](http://scholar.google.com/scholar?hl=en&btnG=Search&q=intitle:Water+Budget+Record+from+Variable+Infiltration+Capacity+(+VIC+)+Model#2), 2010.
- Gao, Z., Huang, B., Ma, Z., Chen, X., Liu, D. and Qiu, J.: Comprehensive comparisons of state-of-the-art gridded precipitation estimates for hydrological applications over southern China, *Remote Sens.*, 12(23), 1–20, doi:10.3390/rs12233997, 2020.
- Gardelin, M. and Lindström, G.: Priestley-Taylor evapotranspiration in HBV-simulations, *Nord. Hydrol.*, 28(4–5), 233–246, doi:10.2166/nh.1998.13, 1997.
- Garg, V., Aggarwal, S. P., Gupta, P. K., Nikam, B. R., Thakur, P. K., Srivastav, S. K. and Senthil Kumar, A.: Assessment of land use land cover change impact on hydrological regime of a basin, *Environ. Earth Sci.*, 76(18), 1–17, doi:10.1007/s12665-017-6976-z, 2017.
- Garg, V., Nikam, B. R., Thakur, P. K., Aggarwal, S. P., Gupta, P. K. and Srivastav, S. K.: Human-induced land use land cover change and its impact on hydrology, *HydroResearch*, 1, 48–56, doi:10.1016/j.hydres.2019.06.001, 2019.
- Gebremicael, T. G., Mohamed, Y. A. and Van der Zaag, P.: Attributing the hydrological impact of different land use types and their long-term dynamics through combining parsimonious hydrological modelling, alteration analysis and PLSR analysis, *Sci. Total Environ.*, 660, 1155–1167, doi:10.1016/j.scitotenv.2019.01.085, 2019.
- George, J. H., Bolvin, D. T., Braithwaite, D., Hsu, K., Joyce, R., Kidd, C., Nelkin, E. J., Sorooshian, S., Tan, J. and Xie, P.: Algorithm Theoretical Basis Document (Atbd) Version 06 Nasa Global Precipitation Measurement (Gpm) Integrated Multi-Satellite Retrievals for Gpm (Imerg), *Natl. Aeronaut. Sp. Adm. Washington, DC, USA*, 2019.
- Ghodichore, N., Vinnarasi, R., Dhanya, C. T. and Roy, S. B.: Reliability of reanalyses products in simulating precipitation and temperature characteristics over India, *J. Earth Syst. Sci.*, 127(8), 1–21, doi:10.1007/s12040-018-1024-2, 2018.
- Ghosh, S. and Mujumdar, P. P.: Modeling GCM and Scenario Uncertainty: An Imprecise Probability Approach., in *IICA*, pp. 836–846., 2007a.
- Ghosh, S. and Mujumdar, P. P.: Nonparametric methods for modeling GCM and scenario uncertainty in drought assessment, *Water Resour. Res.*, 43(7), 1–19, doi:10.1029/2006WR005351, 2007b.
- Ghosh, S., Raje, D. and Mujumdar, P. P.: Mahanadi streamflow: climate change impact assessment and adaptive strategies, *Curr. Sci.*, 98(8), 1084–1091, 2010.
- Gidden, M. J., Riahi, K., Smith, S. J., Fujimori, S., Luderer, G., Kriegler, E., Van Vuuren, D. P., Van Den Berg, M., Feng, L., Klein, D., Calvin, K., Doelman, J. C., Frank, S., Fricko, O., Harmsen, M., Hasegawa, T., Havlik, P., Hilaire, J., Hoesly, R., Horing, J., Popp, A., Stehfest, E. and Takahashi, K.: Global emissions pathways under different socioeconomic scenarios for use in CMIP6: A dataset of harmonized emissions trajectories through the end of the century, *Geosci.*

Model Dev., 12(4), 1443–1475, doi:10.5194/gmd-12-1443-2019, 2019.

Gilewski, P. and Nawalany, M.: Inter-comparison of Rain-Gauge, Radar, and Satellite (IMERG GPM) precipitation estimates performance for rainfall-runoff modeling in a mountainous catchment in Poland, *Water (Switzerland)*, 10(11), 1–23, doi:10.3390/w10111665, 2018.

Gordon, L. J., Steffen, W., Jönsson, B. F., Folke, C., Falkenmark, M. and Johannessen, Å.: Human modification of global water vapor flows from the land surface, *Proc. Natl. Acad. Sci. U. S. A.*, 102(21), 7612–7617, doi:10.1073/pnas.0500208102, 2005.

Gosain, A. K. and Rao, S.: Impact of Climate Change on Water Sector. *Climate Change and India--Vulnerability Assessment and Adaptation*, 2004.

Gosain, A. K., Rao, S. and Basuray, D.: Climate change impact assessment on hydrology of Indian river basins, *Curr. Sci.*, 90(3), 346–353, 2006.

Gou, J., Miao, C., Duan, Q., Tang, Q., Di, Z., Liao, W., Wu, J. and Zhou, R.: Sensitivity Analysis-Based Automatic Parameter Calibration of the VIC Model for Streamflow Simulations Over China, *Water Resour. Res.*, 56(1), 1–19, doi:10.1029/2019WR025968, 2020a.

Gou, J., Miao, C., Duan, Q., Tang, Q., Di, Z., Liao, W., Wu, J. and Zhou, R.: Sensitivity Analysis-Based Automatic Parameter Calibration of the VIC Model for Streamflow Simulations Over China, *Water Resour. Res.*, 56(1), 1–19, doi:10.1029/2019WR025968, 2020b.

van Griensven, A., Meixner, T., Grunwald, S., Bishop, T., Diluzio, M. and Srinivasan, R.: A global sensitivity analysis tool for the parameters of multi-variable catchment models, *J. Hydrol.*, 324(1–4), 10–23, doi:10.1016/j.jhydrol.2005.09.008, 2006.

Groisman, P. Y., Knight, R. W., Easterling, D. R., Karl, T. R., Hegerl, G. C. and Razuvaev, V. N.: Trends in intense precipitation in the climate record, *J. Clim.*, 18(9), 1326–1350, doi:10.1175/JCLI3339.1, 2005.

Gupta, H. V., Kling, H., Yilmaz, K. K. and Martinez, G. F.: Decomposition of the mean squared error and NSE performance criteria: Implications for improving hydrological modelling, *J. Hydrol.*, 377(1–2), 80–91, doi:10.1016/j.jhydrol.2009.08.003, 2009.

Gusain, A., Ghosh, S. and Karmakar, S.: Added value of CMIP6 over CMIP5 models in simulating Indian summer monsoon rainfall, *Atmos. Res.*, 232(June 2019), 104680, doi:10.1016/j.atmosres.2019.104680, 2020.

Haddeland, I., Skaugen, T. and Lettenmaier, D. P.: Anthropogenic impacts on continental surface water fluxes, *Geophys. Res. Lett.*, 33(8), 2–5, doi:10.1029/2006GL026047, 2006.

Hagemann, S., Chen, C., Clark, D. B., Folwell, S., Gosling, S. N., Haddeland, I., Hanasaki, N., Heinke, J., Ludwig, F., Voss, F. and Wiltshire, A. J.: Climate change impact on available water resources obtained using multiple global climate and hydrology models, *Earth Syst. Dyn.*, 4(1), 129–144, doi:10.5194/esd-4-129-2013, 2013.

Hamman, J. J., Nijssen, B., Bohn, T. J., Gergel, D. R. and Mao, Y.: The variable infiltration capacity model version 5 (VIC-5): Infrastructure improvements for new applications and reproducibility, *Geosci. Model Dev.*, 11(8), 3481–3496, doi:10.5194/gmd-11-3481-2018, 2018.

Hanasaki, N., Yoshikawa, S., Pokhrel, Y. and Kanae, S.: A global hydrological simulation to specify the sources of water used by humans, *Hydrol. Earth Syst. Sci. Discuss.*, 08, 1–53, doi:10.5194/hess-2017-280, 2017.

Hansen, M. C., Sohlberg, R., Defries, R. S. and Townshend, J. R. G.: Global land cover classification at 1 km spatial resolution using a classification tree approach., 2000.

Hausfather, Z.: Analysis: How much 'carbon budget' is left to limit global warming to 1.5 C, Carbon Br., 9, 2018.

He, M. and Hogue, T. S.: Integrating hydrologic modeling and land use projections for evaluation of hydrologic response and regional water supply impacts in semi-arid environments, Environ. Earth Sci., 65(6), 1671–1685, doi:10.1007/s12665-011-1144-3, 2012.

Hengade, N., Eldho, T. I. and Ghosh, S.: Climate change impact assessment of a river basin using CMIP5 climate models and the VIC hydrological model, Hydrol. Sci. J., 63(4), 596–614, doi:10.1080/02626667.2018.1441531, 2018.

Hengl, T., de Jesus, J., Heuvelink, G. B. M., Ruiperez Gonzalez, M., Kilibarda, M., Blagotić, A., Shangquan, W., Wright, M. N., Geng, X., Bauer-Marschallinger, B. and others: SoilGrids250m: Global gridded soil information based on machine learning, PLoS One, 12(2), e0169748, 2017.

Her, Y., Yoo, S. H., Cho, J., Hwang, S., Jeong, J. and Seong, C.: Uncertainty in hydrological analysis of climate change: multi-parameter vs. multi-GCM ensemble predictions, Sci. Rep., 9(1), 1–22, doi:10.1038/s41598-019-41334-7, 2019.

Herman, J. D., Kollat, J. B., Reed, P. M. and Wagener, T.: Technical Note: Method of Morris effectively reduces the computational demands of global sensitivity analysis for distributed watershed models, Hydrol. Earth Syst. Sci., 17(7), 2893–2903, doi:10.5194/hess-17-2893-2013, 2013.

Hinz, R., Sulser, T. B., Huefner, R., Mason-D’Croz, D., Dunston, S., Nautiyal, S., Ringler, C., Schuengel, J., Tikhile, P., Wimmer, F. and Schaldach, R.: Agricultural Development and Land Use Change in India: A Scenario Analysis of Trade-Offs Between UN Sustainable Development Goals (SDGs), Earth’s Futur., 8(2), 1–19, doi:10.1029/2019EF001287, 2020.

Hirabayashi, Y., Tanoue, M., Sasaki, O., Zhou, X. and Yamazaki, D.: Global exposure to flooding from the new CMIP6 climate model projections, Sci. Rep., 11(1), 1–7, doi:10.1038/s41598-021-83279-w, 2021.

Huang, J. B., Wen, J. wei, Wang, B. and Hinokidani, O.: Parameter sensitivity analysis for a physically based distributed hydrological model based on Morris’ screening method, J. Flood Risk Manag., 13(1), 1–13, doi:10.1111/jfr3.12589, 2020.

Huang, M. and Liang, X.: On the assessment of the impact of reducing parameters and identification of parameter uncertainties for a hydrologic model with applications to ungauged basins, J. Hydrol., 320(1–2), 37–61, doi:10.1016/j.jhydrol.2005.07.010, 2006.

Huffman, G. J., Adler, R. F., Bolvin, D. T., Gu, G., Nelkin, E. J., Bowman, K. P., Hong, Y., Stocker, E. F. and Wolff, D. B.: The TRMM Multisatellite Precipitation Analysis (TMPA): Quasi-global, multiyear, combined-sensor precipitation estimates at fine scales, J. Hydrometeorol., 8(1), 38–55, doi:10.1175/JHM560.1, 2007.

Huffman, G. J., Bolvin, D. T. and Nelkin, E. J.: Day 1 IMERG Final Run Release Notes, , (January), 1–9 [online] Available from: https://pmm.nasa.gov/sites/default/files/document_files/IMERG_FinalRun_Day1_release_notes.pdf, 2015.

Huffman, G. J., Bolvin, D. T., Nelkin, E. J., Stocker, E. F. and Tan, J.:

https://pmm.nasa.gov/sites/default/files/document_files/IMERG_QI.pdf), , (November 2017), 1–8, 2018.

Hundecha, Y. and Bárdossy, A.: Modeling of the effect of land use changes on the runoff generation of a river basin through parameter regionalization of a watershed model, *J. Hydrol.*, 292(1–4), 281–295, doi:10.1016/j.jhydrol.2004.01.002, 2004.

Van Den Hurk, B., Best, M., Dirmeyer, P., Pitman, A., Polcher, J. and Santanello, J.: Acceleration of land surface model development over a decade of glass, *Bull. Am. Meteorol. Soc.*, 92(12), 1593–1600, doi:10.1175/BAMS-D-11-00007.1, 2011.

Hurkmans, R. T. W. L., Terink, W., Uijlenhoet, R., Moors, E. J., Troch, P. A. and Verburg, P. H.: Effects of land use changes on streamflow generation in the Rhine basin, *Water Resour. Res.*, 45(6), 1–15, doi:10.1029/2008WR007574, 2009.

Hurttt, G. C., Chini, L. P., Frohking, S., Betts, R. A., Feddema, J., Fischer, G., Fisk, J. P., Hibbard, K., Houghton, R. A., Janetos, A., Jones, C. D., Kindermann, G., Kinoshita, T., Klein Goldewijk, K., Riahi, K., Shevliakova, E., Smith, S., Stehfest, E., Thomson, A., Thornton, P., van Vuuren, D. P. and Wang, Y. P.: Harmonization of land-use scenarios for the period 1500-2100: 600 years of global gridded annual land-use transitions, wood harvest, and resulting secondary lands, *Clim. Change*, 109(1), 117–161, doi:10.1007/s10584-011-0153-2, 2011.

Hurttt, G. C., Chini, L. P., Sahajpal, R., Frohking, S. E., Bodirsky, B., Calvin, K. V., Doelman, J. C., Fisk, J., Fujimori, S., Goldewijk, K. and others: LUH2: Harmonization of global land-use scenarios for the period 850-2100, *AGUFM*, 2018, GC13A--01, 2018.

IPCC, I. P. O. C. C.: Special report on global warming of 1.5 C (SR15), 2019.

Jain, S. K., Agarwal, P. K. and Singh, V. P.: *Hydrology and water resources of India*, Springer Science & Business Media., 2007.

Janes, T., McGrath, F., Macadam, I. and Jones, R.: High-resolution climate projections for South Asia to inform climate impacts and adaptation studies in the Ganges-Brahmaputra-Meghna and Mahanadi deltas, *Sci. Total Environ.*, 650, 1499–1520, doi:10.1016/j.scitotenv.2018.08.376, 2019.

Jena, P. P., Chatterjee, C., Pradhan, G. and Mishra, A.: Are recent frequent high floods in Mahanadi basin in eastern India due to increase in extreme rainfalls?, *J. Hydrol.*, 517, 847–862, doi:10.1016/j.jhydrol.2014.06.021, 2014.

Jiang, L. and Yu, L.: Analyzing land use intensity changes within and outside protected areas using ESA CCI-LC datasets, *Glob. Ecol. Conserv.*, 20(July 2018), doi:10.1016/j.gecco.2019.e00789, 2019.

Jiang, T., Chen, Y. D., Xu, C. yu, Chen, X., Chen, X. and Singh, V. P.: Comparison of hydrological impacts of climate change simulated by six hydrological models in the Dongjiang Basin, South China, *J. Hydrol.*, 336(3–4), 316–333, doi:10.1016/j.jhydrol.2007.01.010, 2007.

Jin, L., Whitehead, P. G., Rodda, H., Macadam, I. and Sarkar, S.: Simulating climate change and socio-economic change impacts on flows and water quality in the Mahanadi River system, India, *Sci. Total Environ.*, 637–638, 907–917, doi:10.1016/j.scitotenv.2018.04.349, 2018.

Jin, Q. and Wang, C.: A revival of Indian summer monsoon rainfall since 2002, *Nat. Clim. Chang.*, 7(8), 587–594, doi:10.1038/NCLIMATE3348, 2017.

- Joseph, J., Ghosh, S., Pathak, A. and Sahai, A. K.: Hydrologic impacts of climate change: Comparisons between hydrological parameter uncertainty and climate model uncertainty, *J. Hydrol.*, 566(September), 1–22, doi:10.1016/j.jhydrol.2018.08.080, 2018.
- Kalnay, E., Kanamitsu, M., Kistler, R., Collins, W., Deaven, D., Gandin, L., Iredell, M., Saha, S., White, G., Woollen, J. and others: The NCEP/NCAR reanalysis 40-year project, *Bull. Am. Meteorol. Soc.*, 77(3), 437–471, 1996.
- Kapuria, P. and Modak, S.: An eco-hydrological perspective to monsoon high flows in the Ganga-Padma system: Imperatives for flood management . [online] Available from: <https://www.orfonline.org/research/eco-hydrological-perspective-monsoon-high-flows-ganga-padma-system-imperatives-flood-management-55944/>, 2019.
- Karlsson, I. B., Sonnenborg, T. O., Refsgaard, J. C., Trolle, D., Børgesen, C. D., Olesen, J. E., Jeppesen, E. and Jensen, K. H.: Combined effects of climate models, hydrological model structures and land use scenarios on hydrological impacts of climate change, *J. Hydrol.*, 535, 301–317, doi:10.1016/j.jhydrol.2016.01.069, 2016.
- Katzenberger, A., Schewe, J., Pongratz, J. and Levermann, A.: Robust increase of Indian monsoon rainfall and its variability under future warming in CMIP-6 models, *Earth Syst. Dyn. Discuss.*, (October), 1–30, doi:10.5194/esd-2020-80, 2020.
- Kneis, D., Chatterjee, C. and Singh, R.: Evaluation of TRMM rainfall estimates over a large Indian river basin (Mahanadi), *Hydrol. Earth Syst. Sci.*, 18(7), 2493–2502, doi:10.5194/hess-18-2493-2014, 2014.
- Knoben, W. J. M., Freer, J. E. and Woods, R. A.: Technical note: Inherent benchmark or not? Comparing Nash-Sutcliffe and Kling-Gupta efficiency scores, *Hydrol. Earth Syst. Sci.*, 23(10), 4323–4331, doi:10.5194/hess-23-4323-2019, 2019.
- Krpec, P., Horáček, M. and Šarapatka, B.: A comparison of the use of local legacy soil data and global datasets for hydrological modelling a small-scale watersheds: Implications for nitrate loading estimation, *Geoderma*, 377(February), doi:10.1016/j.geoderma.2020.114575, 2020.
- Kumar, N., Tischbein, B., Kusche, J., Beg, M. K. and Bogardi, J. J.: Impact of land-use change on the water resources of the Upper Kharun Catchment, Chhattisgarh, India, *Reg. Environ. Chang.*, 17(8), 2373–2385, doi:10.1007/s10113-017-1165-x, 2017.
- Kumar, N., Singh, S. K., Singh, V. G. and Dzwairo, B.: Investigation of impacts of land use/land cover change on water availability of Tons River Basin, Madhya Pradesh, India, *Model. Earth Syst. Environ.*, 4(1), 295–310, doi:10.1007/s40808-018-0425-1, 2018.
- Kundu, S., Khare, D. and Mondal, A.: Individual and combined impacts of future climate and land use changes on the water balance, *Ecol. Eng.*, 105, 42–57, doi:10.1016/j.ecoleng.2017.04.061, 2017.
- Legesse, D., Vallet-Coulomb, C. and Gasse, F.: Hydrological response of a catchment to climate and land use changes in Tropical Africa: Case study south central Ethiopia, *J. Hydrol.*, 275(1–2), 67–85, doi:10.1016/S0022-1694(03)00019-2, 2003.
- Li, Z., Liu, W. zhao, Zhang, X. chang and Zheng, F. li: Impacts of land use change and climate variability on hydrology in an agricultural catchment on the Loess Plateau of China, *J. Hydrol.*, 377(1–2), 35–42, doi:10.1016/j.jhydrol.2009.08.007, 2009.
- Li, Z., Deng, X., Wu, F. and Hasan, S. S.: Scenario analysis for water resources in response to

land use change in the middle and upper reaches of the heihe river Basin, *Sustain.*, 7(3), 3086–3108, doi:10.3390/su7033086, 2015.

Liang, X., Lettenmaier, D. P., Wood, E. F. and Burges, S. J.: A Simple hydrologically Based Model of Land Surface Water and Energy Fluxes for GSMs, *J. Geophys. Res.*, 99(D7), 14415–14428, 1994.

Liang, X., Wood, E. F. and Lettenmaier, D. P.: Surface soil moisture parameterization of the VIC-2L model: Evaluation and modification, *Glob. Planet. Change*, 13(1–4), 195–206, doi:10.1016/0921-8181(95)00046-1, 1996.

Lilhare, R., Pokorny, S., Déry, S. J., Stadnyk, T. A. and Koenig, K. A.: Sensitivity analysis and uncertainty assessment in water budgets simulated by the variable infiltration capacity model for Canadian subarctic watersheds, *Hydrol. Process.*, 34(9), 2057–2075, doi:10.1002/hyp.13711, 2020.

Linde, A. te, Hurkans, R., Aerts, J. and Dolman, H.: Comparing model performance of the HBV and VIC models in the Rhine basin, *Symp. HS2004 IUGG2007*, (July), 278–285, 2007.

Liu, Y., Zhang, X., Xia, D., You, J., Rong, Y. and Bakir, M.: Impacts of Land-Use and Climate Changes on Hydrologic Processes in the Qingyi River Watershed, China, *J. Hydrol. Eng.*, 18(11), 1495–1512, doi:10.1061/(asce)he.1943-5584.0000485, 2011.

Lohmann, D. A. G., NOLTE-HOLUBE, R. and Raschke, E.: A large-scale horizontal routing model to be coupled to land surface parametrization schemes, *Tellus A*, 48(5), 708–721, 1996.

Lorenz, C. and Kunstmann, H.: The hydrological cycle in three state-of-the-art reanalyses: Intercomparison and performance analysis, *J. Hydrometeorol.*, 13(5), 1397–1420, doi:10.1175/JHM-D-11-088.1, 2012.

Ma, X., Xu, J. and van Noordwijk, M.: Sensitivity of streamflow from a Himalayan catchment to plausible changes in land cover and climate, *Hydrol. Process.*, 24(11), 1379–1390, doi:10.1002/hyp.7602, 2010.

Mahto, S. S. and Mishra, V.: Does ERA-5 Outperform Other Reanalysis Products for Hydrologic Applications in India?, *J. Geophys. Res. Atmos.*, 124(16), 9423–9441, doi:10.1029/2019JD031155, 2019.

Maity, R. and Nagesh Kumar, D.: Hydroclimatic influence of large-scale circulation on the variability of reservoir inflow, *Hydrol. Process. An Int. J.*, 23(6), 934–942, 2009.

Mall, R. K., Gupta, A., Singh, R., Singh, R. S. and Rathore, L. S.: Water resources and climate change: An Indian perspective, *Curr. Sci.*, 90(12), 1610–1626, 2006.

Mantovan, P. and Todini, E.: Hydrological forecasting uncertainty assessment: Incoherence of the GLUE methodology, *J. Hydrol.*, 330(1–2), 368–381, doi:10.1016/j.jhydrol.2006.04.046, 2006.

Mao, D. and Cherkauer, K. A.: Impacts of land-use change on hydrologic responses in the Great Lakes region, *J. Hydrol.*, 374(1–2), 71–82, doi:10.1016/j.jhydrol.2009.06.016, 2009.

Matheussen, B., Goodman, I. A., Lettenmaier, D. P., Kirschbaum, R. L. and O'Donnell, G. M.: Effects of land cover change on streamflow in the interior Columbia River Basin (USA and Canada), *Hydrol. Process.*, 14(5), 867–885, doi:10.1002/(sici)1099-1085(20000415)14:5<867::aid-hyp975>3.0.co;2-5, 2002.

May, W.: Simulation of the variability and extremes of daily rainfall during the Indian summer monsoon for present and future times in a global time-slice experiment, *Clim. Dyn.*, 22(2–3), 183–204, doi:10.1007/s00382-003-0373-x, 2004.

Mishra, N., Aggarwal, S. P. and Dadhwal, V. K.: Macroscale Hydrological Modelling and Impact of land cover change on stream flows of the Mahanadi River Basin, A Master thesis Submitt. to Andhra Univ. Indian Inst. Remote Sens. (National Remote Sens. Agency) Dept. Space, Govt. India, 2008.

Mishra, V., Cherkauer, K. A., Niyogi, D., Lei, M., Pijanowski, B. C., Ray, D. K., Bowling, L. C. and Yang, G.: A regional scale assessment of land use/land cover and climatic changes on water and energy cycle in the upper Midwest United States, *Int. J. Climatol.*, 30(13), 2025–2044, doi:10.1002/joc.2095, 2010.

Mishra, V., Bhatia, U. and Tiwari, A. D.: Bias-corrected climate projections for South Asia from Coupled Model Intercomparison Project-6, *Sci. Data*, 7(1), 1–13, doi:10.1038/s41597-020-00681-1, 2020a.

Mishra, V., Shah, H., López, M. R. R., Lobanova, A. and Krysanova, V.: Does comprehensive evaluation of hydrological models influence projected changes of mean and high flows in the Godavari River basin?, *Clim. Change*, doi:10.1007/s10584-020-02847-7, 2020b.

Mizukami, N., Rakovec, O., Newman, A., Clark, M., Wood, A., Gupta, H. and Kumar, R.: On the choice of calibration metrics for high flow estimation using hydrologic models, *Hydrol. Earth Syst. Sci. Discuss.*, 1–16, doi:10.5194/hess-2018-391, 2018.

Mockler, E. M., Chun, K. P., Sapriza-Azuri, G., Bruen, M. and Wheeler, H. S.: Assessing the relative importance of parameter and forcing uncertainty and their interactions in conceptual hydrological model simulations, *Adv. Water Resour.*, 97, 299–313, doi:10.1016/j.advwatres.2016.10.008, 2016.

Mohammed, K., Islam, A. S., Islam, G. tarekul, Alfieri, L., Bala, S. K. and Khan, M. J. U.: Extreme flows and water availability of the Brahmaputra River under 1.5 and 2 °C global warming scenarios, *Clim. Change*, 145(1–2), 159–175, doi:10.1007/s10584-017-2073-2, 2017.

Mondal, A. and Mujumdar, P. P.: Regional hydrological impacts of climate change: Implications for water management in India, *IAHS-AISH Proc. Reports*, 366(March), 34–43, doi:10.5194/piahs-366-34-2015, 2015.

Morris, M. D.: Factorial sampling plans for preliminary computational experiments, *Technometrics*, 33(2), 161–174, 1991.

Mujumdar, P. P.: Share data on water resources, *Nature*, 521(7551), 151–152, 2015.

Mujumdar, P. P. and Ghosh, S.: Modeling GCM and scenario uncertainty using a possibilistic approach: Application to the Mahanadi River, India, *Water Resour. Res.*, 44(6), 1–15, doi:10.1029/2007WR006137, 2008.

Muleta, M. K. and Nicklow, J. W.: Sensitivity and uncertainty analysis coupled with automatic calibration for a distributed watershed model, *J. Hydrol.*, 306(1–4), 127–145, doi:10.1016/j.jhydrol.2004.09.005, 2005.

Muñoz-Sabater, J., Dutra, E., Agustí-Panareda, A., Albergel, C., Arduini, G., Balsamo, G., Boussetta, S., Choulga, M., Harrigan, S., Hersbach, H. and others: ERA5-Land: A state-of-the-art global reanalysis dataset for land applications, *Earth Syst. Sci. Data Discuss.*, 1–50, 2021.

Myneni, R., Knyazikhin, Y. and Park, T.: MCD15A2H MODIS/Terra+ Aqua Leaf Area Index/FPAR 8-day L4 Global 500m SIN Grid V006. NASA EOSDIS L. Process. DAAC 2015, n.d.

Nayak, P. C., Venkatesh, B., Thomas, T. and Rao, Y. R. S.: Assessing the impact of climate change for Mahanadi basin using SWAT model, 2010.

Newman, A. J., Mizukami, N., Clark, M. P., Wood, A. W., Nijssen, B. and Nearing, G.: Benchmarking of a Physically Based Hydrologic Model, *J. Hydrometeorol.*, 18(8), 2215–2225, doi:10.1175/jhm-d-16-0284.1, 2017.

Nijssen, B., Lettenmaier, D. P., Liang, X., Wetzel, S. W. and Wood, E. F.: Streamflow simulation for continental-scale river basins and radiative forcings) applications of the model to the Columbia and annual flow volumes to within a few percent . Difficulties in reproducing the Sacramento Model [Burnash is dominated using an, *Water Resour. Res.*, 33(4), 711–724, 1997.

Niraula, R., Meixner, T., Dominguez, F., Bhattarai, N., Rodell, M., Ajami, H., Gochis, D. and Castro, C.: How Might Recharge Change Under Projected Climate Change in the Western U.S.?, *Geophys. Res. Lett.*, 44(20), 10,407–10,418, doi:10.1002/2017GL075421, 2017.

O'Neill, B. C., Tebaldi, C., Van Vuuren, D. P., Eyring, V., Friedlingstein, P., Hurtt, G., Knutti, R., Kriegler, E., Lamarque, J. F., Lowe, J., Meehl, G. A., Moss, R., Riahi, K. and Sanderson, B. M.: The Scenario Model Intercomparison Project (ScenarioMIP) for CMIP6, *Geosci. Model Dev.*, 9(9), 3461–3482, doi:10.5194/gmd-9-3461-2016, 2016.

Pai, D. S., Sridhar, L., Rajeevan, M., Sreejith, O. P., Satbhai, N. S. and Mukhopadhyay, B.: Development of a new high spatial resolution (0.25° × 0.25°) long period (1901–2010) daily gridded rainfall data set over India and its comparison with existing data sets over the region, *Mausam*, 65(1), 1–18, 2014.

Panda, D. K., Kumar, A., Ghosh, S. and Mohanty, R. K.: Streamflow trends in the mahanadi river basin (India): Linkages to tropical climate variability, *J. Hydrol.*, 495, 135–149, doi:10.1016/j.jhydrol.2013.04.054, 2013.

Pappenberger, F., Beven, K. J., Ratto, M. and Matgen, P.: Multi-method global sensitivity analysis of flood inundation models, *Adv. Water Resour.*, 31(1), 1–14, doi:10.1016/j.advwatres.2007.04.009, 2008.

Park, D. and Markus, M.: Analysis of a changing hydrologic flood regime using the Variable Infiltration Capacity model, *J. Hydrol.*, 515, 267–280, doi:10.1016/j.jhydrol.2014.05.004, 2014.

Parr, D., Wang, G. and Bjerklie, D.: Integrating Remote Sensing Data on Evapotranspiration and Leaf Area Index with Hydrological Modeling: Impacts on Model Performance and Future Predictions, *J. Hydrometeorol.*, 16(5), 2086–2100, doi:10.1175/jhm-d-15-0009.1, 2015.

Patidar, N. and Behera, M. D.: How Significantly do Land Use and Land Cover (LULC) Changes Influence the Water Balance of a River Basin? A Study in Ganga River Basin, India, *Proc. Natl. Acad. Sci. India Sect. A - Phys. Sci.*, 89(2), 353–365, doi:10.1007/s40010-017-0426-x, 2019.

Paul, S., Ghosh, S., Oglesby, R., Pathak, A., Chandrasekharan, A. and Ramsankaran, R.: Weakening of Indian Summer Monsoon Rainfall due to Changes in Land Use Land Cover, *Sci. Rep.*, 6(December 2015), 1–10, doi:10.1038/srep32177, 2016.

Philip, S., Sparrow, S., Kew, S., van der Wiel, K., Wanders, N., Singh, R., Hassan, A., Mohammed, K., Javid, H., Haustein, K., Otto, F., Hirpa, F., Rimi, R., Islam, A. S., Wallom, D. and van

- Oldenborgh, G. J.: Attributing the 2017 Bangladesh floods from meteorological and hydrological perspectives, *Hydrol. Earth Syst. Sci. Discuss.*, 1–32, doi:10.5194/hess-2018-379, 2018.
- Pianosi, F., Sarrazin, F. and Wagener, T.: A Matlab toolbox for Global Sensitivity Analysis, *Environ. Model. Softw.*, 70, 80–85, doi:10.1016/j.envsoft.2015.04.009, 2015.
- Piao, S., Friedlingstein, P., Ciais, P., De Noblet-Ducoudré, N., Labat, D. and Zaehle, S.: Changes in climate and land use have a larger direct impact than rising CO₂ on global river runoff trends, *Proc. Natl. Acad. Sci. U. S. A.*, 104(39), 15242–15247, doi:10.1073/pnas.0707213104, 2007.
- Pierce, D. W., Cayan, D. R., Maurer, E. P., Abatzoglou, J. T. and Hegewisch, K. C.: Improved bias correction techniques for hydrological simulations of climate change, *J. Hydrometeorol.*, 16(6), 2421–2442, doi:10.1175/JHM-D-14-0236.1, 2015.
- Prakash, S., Mitra, A. K., Pai, D. S. and AghaKouchak, A.: From TRMM to GPM: How well can heavy rainfall be detected from space?, *Adv. Water Resour.*, 88(December 2014), 1–7, doi:10.1016/j.advwatres.2015.11.008, 2016.
- Prakash, S., Mitra, A. K., AghaKouchak, A., Liu, Z., Norouzi, H. and Pai, D. S.: A preliminary assessment of GPM-based multi-satellite precipitation estimates over a monsoon dominated region, *J. Hydrol.*, 556(February 2014), 865–876, doi:10.1016/j.jhydrol.2016.01.029, 2018.
- Raje, D., Priya, P. and Krishnan, R.: Macroscale hydrological modelling approach for study of large scale hydrologic impacts under climate change in Indian river basins, *Hydrol. Process.*, 28(4), 1874–1889, doi:10.1002/hyp.9731, 2014.
- Rajeevan, M., Bhate, J., Kale, J. D. and Lal, B.: High resolution daily gridded rainfall data for the Indian region: Analysis of break and active monsoon spells, *Curr. Sci.*, 91(3), 296–306, 2006.
- Rajeevan, M., Bhate, J. and Jaswal, A. K.: Analysis of variability and trends of extreme rainfall events over India using 104 years of gridded daily rainfall data, *Geophys. Res. Lett.*, 35(18), 1–6, doi:10.1029/2008GL035143, 2008.
- Rajendran, K., Surendran, S., Varghese, S. J. and Sathyanath, A.: Simulation of Indian summer monsoon rainfall, interannual variability and teleconnections: evaluation of CMIP6 models, Springer Berlin Heidelberg., 2021.
- Rawls, W. J., Gimenez, D. and Grossman, R.: Use of soil texture, bulk density, and slope of the water retention curve to predict saturated hydraulic conductivity, *Trans. ASAE*, 41(4), 983, 1998.
- Refsgaard, J. C., Alley, W. M. and Vuglinskiĭ, V. S.: Methodology for distinguishing between man's influence and climatic effects on the hydrological cycle, 1989.
- Reynolds, C. A., Jackson, T. J. and Rawls, W. J.: Estimating soil water-holding capacities by linking the Food and Agriculture Organization soil map of the world with global pedon databases and continuous pedotransfer functions, *Water Resour. Res.*, 36(12), 3653–3662, 2000.
- Rickards, N., Thomas, T., Kaelin, A., Houghton-Carr, H., Jain, S. K., Mishra, P. K., Nema, M. K., Dixon, H., Rahman, M. M., Horan, R., Jenkins, A. and Rees, G.: Understanding future water challenges in a highly regulated indian river basin-modelling the impact of climate change on the hydrology of the upper Narmada, *Water (Switzerland)*, 12(6), doi:10.3390/w12061762, 2020.

2020.

Rodell, M., Houser, P. R., Berg, A. A. and Famiglietti, J. S.: Evaluation of 10 methods for initializing a land surface model, *J. Hydrometeorol.*, 6(2), 146–155, doi:10.1175/JHM414.1, 2005.

Rodriguez, D. A. and Tomasella, J.: On the ability of large-scale hydrological models to simulate land use and land cover change impacts in Amazonian basins, *Hydrol. Sci. J.*, 61(10), 1831–1846, doi:10.1080/02626667.2015.1051979, 2016.

Rodríguez, E., Sánchez, I., Duque, N., Arboleda, P., Vega, C., Zamora, D., López, P., Kaune, A., Werner, M., García, C. and Burke, S.: Combined Use of Local and Global Hydro Meteorological Data with Hydrological Models for Water Resources Management in the Magdalena - Cauca Macro Basin – Colombia, *Water Resour. Manag.*, 34(7), 2179–2199, doi:10.1007/s11269-019-02236-5, 2020.

Rogger, M., Agnoletti, M., Alaoui, A., Bathurst, J. C., Bodner, G., Borga, M., Chaplot, V., Gallart, F., Glatzel, G., Hall, J., Holden, J., Holko, L., Horn, R., Kiss, A., Quinton, J. N., Leitinger, G., Lennartz, B., Parajka, J., Peth, S., Robinson, M., Salinas, J. L., Santoro, A., Szolgay, J., Tron, S. and Viglione, A.: *Water Resources Research*, (June 2013), 5209–5219, doi:10.1002/2017WR020723. Received, 2016.

Rosenberg, E. A., Clark, E. A., Steinemann, A. C. and Lettenmaier, D. P.: On the contribution of groundwater storage to interannual streamflow anomalies in the Colorado River basin, *Hydrol. Earth Syst. Sci.*, 17(4), 1475–1491, doi:10.5194/hess-17-1475-2013, 2013.

Rosolem, R., Gupta, H. V., Shuttleworth, W. J., Zeng, X. and De Gonçalves, L. G. G.: A fully multiple-criteria implementation of the Sobol' method for parameter sensitivity analysis, *J. Geophys. Res. Atmos.*, 117(7), 1–18, doi:10.1029/2011JD016355, 2012.

Rost, S., Gerten, D. and Heyder, U.: Human alterations of the terrestrial water cycle through land management, *Adv. Geosci.*, 18, 43–50, doi:10.5194/adgeo-18-43-2008, 2008.

Roy, P. S., Roy, A., Joshi, P. K., Kale, M. P., Srivastava, V. K., Srivastava, S. K., Dwevidi, R. S., Joshi, C., Behera, M. D., Meiyappan, P., Sharma, Y., Jain, A. K., Singh, J. S., Palchowdhuri, Y., Ramachandran, R. M., Pinjarla, B., Chakravarthi, V., Babu, N., Gowsalya, M. S., Thiruvengadam, P., Kotteeswaran, M., Priya, V., Yelishetty, K. M. V. N., Maithani, S., Talukdar, G., Mondal, I., Rajan, K. S., Narendra, P. S., Biswal, S., Chakraborty, A., Padalia, H., Chavan, M., Pardeshi, S. N., Chaudhari, S. A., Anand, A., Vyas, A., Reddy, M. K., Ramalingam, M., Manonmani, R., Behera, P., Das, P., Tripathi, P., Matin, S., Khan, M. L., Tripathi, O. P., Deka, J., Kumar, P. and Kushwaha, D.: Development of decadal (1985-1995-2005) land use and land cover database for India, *Remote Sens.*, 7(3), 2401–2430, doi:10.3390/rs70302401, 2015.

Rupa Kumar, K., Sahai, A. K., Krishna Kumar, K., Patwardhan, S. K., Mishra, P. K., Revadekar, J. V., Kamala, K. and Pant, G. B.: High-resolution climate change scenarios for India for the 21st century, *Curr. Sci.*, 90(3), 334–345, 2006.

Saha, A., Ghosh, S., Sahana, A. S. and Rao, E. P.: Failure of CMIP5 climate models in simulating post-1950 decreasing trend of Indian monsoon, *Geophys. Res. Lett.*, 41(20), 7323–7330, doi:10.1002/2014GL061573, 2014.

Saleth, R. M.: Pénurie d'eau et changement climatique en Inde: Nécessité d'une gestion de la demande et de l'offre en eau, *Hydrol. Sci. J.*, 56(4), 671–686, doi:10.1080/02626667.2011.572074, 2011.

Saltelli, A., Ratto, M., Andres, T., Campolongo, F., Cariboni, J., Gatelli, D., Saisana, M. and Tarantola, S.: *Global sensitivity analysis: the primer*, John Wiley & Sons., 2008.

Sarrazin, F., Pianosi, F. and Wagener, T.: Global Sensitivity Analysis of environmental models: Convergence and validation, *Environ. Model. Softw.*, 79, 135–152, doi:10.1016/j.envsoft.2016.02.005, 2016.

Sarrazin, F., Hartmann, A., Pianosi, F., Rosolem, R. and Wagener, T.: V2Karst V1.1: A parsimonious large-scale integrated vegetation-recharge model to simulate the impact of climate and land cover change in karst regions., 2018.

Scheidegger, J. M., Jackson, C. R., Muddu, S., Tomer, S. K. and Filgueira, R.: Integration of 2D lateral groundwater flow into the variable infiltration capacity (VIC) model and effects on simulated fluxes for different grid resolutions and aquifer diffusivities, *Water (Switzerland)*, 13(5), doi:10.3390/w13050663, 2021.

Seibert, J. and van Meerveld, H. J. I.: Hydrological change modeling: Challenges and opportunities, *Hydrol. Process.*, 30(26), 4966–4971, doi:10.1002/hyp.10999, 2016.

Shah, R. and Mishra, V.: Evaluation of the Reanalysis Products for the Monsoon Season Droughts in India, *J. Hydrometeorol.*, 15(4), 1575–1591, doi:10.1175/jhm-d-13-0103.1, 2014a.

Shah, R. and Mishra, V.: Evaluation of the Reanalysis Products for the Monsoon Season Droughts in India, *J. Hydrometeorol.*, 15(4), 1575–1591, doi:10.1175/jhm-d-13-0103.1, 2014b.

Sharifi, E., Steinacker, R. and Saghafian, B.: Assessment of GPM-IMERG and other precipitation products against gauge data under different topographic and climatic conditions in Iran: Preliminary results, *Remote Sens.*, 8(2), doi:10.3390/rs8020135, 2016.

Sharmila, S., Joseph, S., Sahai, A. K., Abhilash, S. and Chattopadhyay, R.: Future projection of Indian summer monsoon variability under climate change scenario: An assessment from CMIP5 climate models, *Glob. Planet. Change*, 124, 62–78, doi:10.1016/j.gloplacha.2014.11.004, 2015.

Sheffield, J., Wood, E. F., Chaney, N., Guan, K., Sadri, S., Yuan, X., Olang, L., Amani, A., Ali, A., Demuth, S. and Ogallo, L.: A drought monitoring and forecasting system for sub-sahara african water resources and food security, *Bull. Am. Meteorol. Soc.*, 95(6), 861–882, doi:10.1175/BAMS-D-12-00124.1, 2014.

Shepard, D.: A two-dimensional interpolation function for irregularly-spaced data, *Proc. 1968 23rd ACM Natl. Conf. ACM 1968*, 517–524, doi:10.1145/800186.810616, 1968.

Singh, L. and Saravanan, S.: Impact of climate change on hydrology components using CORDEX South Asia climate model in Wunna, Bharathpuzha, and Mahanadi, India, *Environ. Monit. Assess.*, 192(11), doi:10.1007/s10661-020-08637-z, 2020.

Singh, R., Wagener, T., Crane, R., Mann, M. E. and Ning, L.: A vulnerability driven approach to identify adverse climate and land use change combinations for critical hydrologic indicator thresholds: Application to a watershed in Pennsylvania, USA, *Water Resour. Res.*, 50(4), 3409–3427, doi:10.1002/2013WR014988, 2014.

Singh, R. B.: Environmental consequences of agricultural development: A case study from the green revolution state of Haryana, India, *Agric. Ecosyst. Environ.*, 82(1–3), 97–103, doi:10.1016/S0167-8809(00)00219-X, 2000.

Sivapalan, M., Blöschl, G., Zhang, L. and Vertessy, R.: Downward approach to hydrological prediction, *Hydrol. Process.*, 17(11), 2101–2111, doi:10.1002/hyp.1425, 2003.

Sivasena Reddy, A. and Janga Reddy, M.: Evaluating the influence of spatial resolutions of DEM on watershed runoff and sediment yield using SWAT, *J. Earth Syst. Sci.*, 124(7), 1517–1529, 2015.

Sridhar, V., Billah, M. M. and Hildreth, J. W.: Coupled Surface and Groundwater Hydrological Modeling in a Changing Climate, *Groundwater*, 56(4), 618–635, doi:10.1111/gwat.12610, 2018.

Srivastava, A. K., Rajeevan, M. and Kshirsagar, S. R.: Development of a high resolution daily gridded temperature data set (1969–2005) for the Indian region, *Atmos. Sci. Lett.*, 10(4), 249–254, 2009.

Sterling, S. M., Ducharme, A. and Polcher, J.: The impact of global land-cover change on the terrestrial water cycle, *Nat. Clim. Chang.*, 3(4), 385–390, doi:10.1038/nclimate1690, 2013.

Stoffel, M., Tiranti, D. and Huggel, C.: Climate change impacts on mass movements - Case studies from the European Alps, *Sci. Total Environ.*, 493, 1255–1266, doi:10.1016/j.scitotenv.2014.02.102, 2014.

Strömqvist, J., Dahne, J., Donnelly, C., Lindström, G., Rosberg, J., Pers, C., Yang, W. and Arheimer, B.: Using recently developed global data sets for hydrological predictions, *IAHS-AISH Publ.*, 333(September), 121–127, 2009.

Sungmin, O., Foelsche, U., Kirchengast, G., Fuchsberger, J., Tan, J. and Petersen, W. A.: Evaluation of GPM IMERG Early, Late, and Final rainfall estimates using WegenerNet gauge data in southeastern Austria, *Hydrol. Earth Syst. Sci.*, 21(12), 6559–6572, doi:10.5194/hess-21-6559-2017, 2017.

Tang, G., Clark, M. P., Papalexiou, S. M., Ma, Z. and Hong, Y.: Have satellite precipitation products improved over last two decades? A comprehensive comparison of GPM IMERG with nine satellite and reanalysis datasets, *Remote Sens. Environ.*, 240(September 2019), 111697, doi:10.1016/j.rse.2020.111697, 2020.

Tang, Y., Reed, P., Wagener, T. and Van Werkhoven, K.: Comparing sensitivity analysis methods to advance lumped watershed model identification and evaluation, *Hydrol. Earth Syst. Sci.*, 11(2), 793–817, doi:10.5194/hess-11-793-2007, 2007.

Tarawneh, E., Bridge, J. and Macdonald, N.: A pre-calibration approach to select optimum inputs for hydrological models in data-scarce regions, *Hydrol. Earth Syst. Sci.*, 20(10), 4391–4407, doi:10.5194/hess-20-4391-2016, 2016.

Taylor, K. E., Stouffer, R. J. and Meehl, G. A.: An overview of CMIP5 and the experiment design, *Bull. Am. Meteorol. Soc.*, 93(4), 485–498, doi:10.1175/BAMS-D-11-00094.1, 2012.

Tekleab, S., Mohamed, Y., Uhlenbrook, S. and Wenninger, J.: Hydrologic responses to land cover change: The case of Jedeb mesoscale catchment, Abay/Upper Blue Nile Basin, Ethiopia, *Hydrol. Process.*, 28(20), 5149–5161, doi:10.1002/hyp.9998, 2014.

Tesemma, Z. K., Wei, Y., Peel, M. C. and Western, A. W.: The effect of year-to-year variability of leaf area index on Variable Infiltration Capacity model performance and simulation of runoff, *Adv. Water Resour.*, 83, 310–322, doi:10.1016/j.advwatres.2015.07.002, 2015.

- Thanapakpawin, P., Richey, J., Thomas, D., Rodda, S., Campbell, B. and Logsdon, M.: Effects of landuse change on the hydrologic regime of the Mae Chaem river basin, NW Thailand, *J. Hydrol.*, 334(1–2), 215–230, doi:10.1016/j.jhydrol.2006.10.012, 2007.
- Thokchom, B.: Water-related problem with special reference to global climate change in India, Elsevier Inc., 2020.
- Tsarouchi, G. and Buytaert, W.: Land-use change may exacerbate climate change impacts on water resources in the Ganges basin, *Hydrol. Earth Syst. Sci.*, 22(2), 1411–1435, doi:10.5194/hess-22-1411-2018, 2018.
- Vanrolleghem, P. A., Mannina, G., Cosenza, A. and Neumann, M. B.: Global sensitivity analysis for urban water quality modelling: Terminology, convergence and comparison of different methods, *J. Hydrol.*, 522, 339–352, doi:10.1016/j.jhydrol.2014.12.056, 2015.
- Vanuytrecht, E., Raes, D. and Willems, P.: Global sensitivity analysis of yield output from the water productivity model, *Environ. Model. Softw.*, 51, 323–332, doi:10.1016/j.envsoft.2013.10.017, 2014.
- Viglione, A., Merz, B., Viet Dung, N., Parajka, J., Nester, T. and Blöschl, G.: Attribution of regional flood changes based on scaling fingerprints, *Water Resour. Res.*, 52(7), 5322–5340, 2016.
- Viola, M. R., Mello, C. R., Beskow, S. and Norton, L. D.: Impacts of Land-use Changes on the Hydrology of the Grande River Basin Headwaters, Southeastern Brazil, *Water Resour. Manag.*, 28(13), 4537–4550, doi:10.1007/s11269-014-0749-1, 2014.
- Voisin, N., Wood, A. W. and Lettenmaier, D. P.: Evaluation of precipitation products for global hydrological prediction, *J. Hydrometeorol.*, 9(3), 388–407, doi:10.1175/2007JHM938.1, 2008.
- van Vuuren, D. P., Edmonds, J., Kainuma, M., Riahi, K., Thomson, A., Hibbard, K., Hurtt, G. C., Kram, T., Krey, V., Lamarque, J. F., Masui, T., Meinshausen, M., Nakicenovic, N., Smith, S. J. and Rose, S. K.: The representative concentration pathways: An overview, *Clim. Change*, 109(1), 5–31, doi:10.1007/s10584-011-0148-z, 2011.
- van Vuuren, D. P., Kriegler, E., O’Neill, B. C., Ebi, K. L., Riahi, K., Carter, T. R., Edmonds, J., Hallegatte, S., Kram, T., Mathur, R. and Winkler, H.: A new scenario framework for Climate Change Research: Scenario matrix architecture, *Clim. Change*, 122(3), 373–386, doi:10.1007/s10584-013-0906-1, 2014.
- Wagner, P. D., Kumar, S. and Schneider, K.: An assessment of land use change impacts on the water resources of the Mula and Mutha Rivers catchment upstream of Pune, India, *Hydrol. Earth Syst. Sci.*, 17(6), 2233–2246, doi:10.5194/hess-17-2233-2013, 2013.
- Wang, A. and Solomatine, D. P.: Practical experience of sensitivity analysis: Comparing six methods, on three hydrological models, with three performance criteria, *Water (Switzerland)*, 11(5), 1–26, doi:10.3390/w11051062, 2019.
- Wang, A., Li, K. Y. and Lettenmaier, D. P.: Integration of the variable infiltration capacity model soil hydrology scheme into the community land model, *J. Geophys. Res. Atmos.*, 113(9), 1–15, doi:10.1029/2007JD009246, 2008.
- Wang, Z., Zhong, R., Lai, C., Zeng, Z., Lian, Y. and Bai, X.: Climate change enhances the severity and variability of drought in the Pearl River Basin in South China in the 21st century, *Agric. For. Meteorol.*, 249(September 2017), 149–162, doi:10.1016/j.agrformet.2017.12.077, 2018.

- Whitehead, P., Jin, L., Macadam, I., Janes, T., Sarkar, S., Rodda, H. J. E., Sinha, R. and Nicholls, R. J.: Corrigendum to “Modelling Impacts of Climate Change and Socio-Economic Change on the Ganga, Brahmaputra, Meghna, Hooghly and Mahanadi River Systems in India and Bangladesh” [Stoten 636 (2018) 1362–1372] (Science of the Total Environment (2018) 636 (1362–1, Sci. Total Environ., 644, 1651–1652, doi:10.1016/j.scitotenv.2018.07.180, 2018.
- Whitehead, P. G., Sarkar, S., Jin, L., Futter, M. N., Caesar, J., Barbour, E., Butterfield, D., Sinha, R., Nicholls, R., Hutton, C. and Leckie, H. D.: Dynamic modeling of the Ganga river system: Impacts of future climate and socio-economic change on flows and nitrogen fluxes in India and Bangladesh, *Environ. Sci. Process. Impacts*, 17(6), 1082–1097, doi:10.1039/c4em00616j, 2015.
- Wilby, R. L. and Harris, I.: A framework for assessing uncertainties in climate change impacts: Low-flow scenarios for the River Thames, UK, *Water Resour. Res.*, 42(2), 1–10, doi:10.1029/2005WR004065, 2006.
- Wilk, J. and Hughes, D. A.: Simulating the impacts of land-use and climate change on water resource availability for a large south Indian catchment, *Hydrol. Sci. J.*, 47(1), 19–30, 2002.
- Woldesenbet, T. A., Elagib, N. A., Ribbe, L. and Heinrich, J.: Hydrological responses to land use/cover changes in the source region of the Upper Blue Nile Basin, Ethiopia, *Sci. Total Environ.*, 575, 724–741, doi:10.1016/j.scitotenv.2016.09.124, 2017.
- Wood, A. W., Leung, L. R., Sridhar, V. and Lettenmaier, D. P.: Hydrologic implications of dynamical and statistical approaches to downscaling climate model outputs, *Clim. Change*, 62(1–3), 189–216, doi:10.1023/B:CLIM.0000013685.99609.9e, 2004.
- Wood, E. F., Roundy, J. K., Troy, T. J., Van Beek, L. P. H., Bierkens, M. F. P., Blyth, E., de Roo, A., Döll, P., Ek, M., Famiglietti, J. and others: Hyperresolution global land surface modeling: Meeting a grand challenge for monitoring Earth’s terrestrial water, *Water Resour. Res.*, 47(5), 2011.
- Wootten, A., Terando, A., Reich, B. J., Boyles, R. P. and Semazzi, F.: Characterizing sources of uncertainty from global climate models and downscaling techniques, *J. Appl. Meteorol. Climatol.*, 56(12), 3245–3262, doi:10.1175/JAMC-D-17-0087.1, 2017.
- Wu, Y., Liu, S., Sohl, T. L. and Young, C. J.: Projecting the land cover change and its environmental impacts in the Cedar River Basin in the Midwestern United States, *Environ. Res. Lett.*, 8(2), doi:10.1088/1748-9326/8/2/024025, 2013.
- Xie, Z., Yuan, F., Duan, Q., Zheng, J., Liang, M. and Chen, F.: Regional parameter estimation of the VIC land surface model: Methodology and application to river basins in China, *J. Hydrometeorol.*, 8(3), 447–468, doi:10.1175/JHM568.1, 2007.
- Xu, C. Y., Widén, E. and Halldin, S.: Modelling hydrological consequences of climate change - Progress and challenges, *Adv. Atmos. Sci.*, 22(6), 789–797, doi:10.1007/BF02918679, 2005.
- Yaduvanshi, A., Zaroug, M., Bendapudi, R. and New, M.: Impacts of 1.5°C and 2°C global warming on regional rainfall and temperature change across India, *Environ. Res. Commun.*, 1(12), 0–14, doi:10.1088/2515-7620/ab4ee2, 2019.
- Yang, J.: Convergence and uncertainty analyses in Monte-Carlo based sensitivity analysis, *Environ. Model. Softw.*, 26(4), 444–457, doi:10.1016/j.envsoft.2010.10.007, 2011.
- Yang, X. L., Ren, L. L., Liu, Y., Jiao, D. L. and Jiang, S. H.: Hydrological response to land use and

- land cover changes in a sub-watershed of West Liaohe River Basin, China, *J. Arid Land*, 6(6), 678–689, doi:10.1007/s40333-014-0026-4, 2014.
- Yanto, Livneh, B., Rajagopalan, B. and Kasprzyk, J.: Hydrological model application under data scarcity for multiple watersheds, Java Island, Indonesia, *J. Hydrol. Reg. Stud.*, 9, 127–139, doi:10.1016/j.ejrh.2016.09.007, 2017.
- Yeste, P., García-Valdecasas Ojeda, M., Gámiz-Fortis, S. R., Castro-Díez, Y. and Jesús Esteban-Parra, M.: Integrated Sensitivity Analysis of a Macroscale Hydrologic Model in the North of the Iberian Peninsula, *J. Hydrol.*, 590(September 2019), 125230, doi:10.1016/j.jhydrol.2020.125230, 2020.
- Zeng, X.: Global Vegetation Root Distribution for Land Modeling, *J. Hydrometeorol.*, 2(5), 525–530, doi:10.1175/1525-7541(2001)002<0525:gvrdf>2.0.co;2, 2002.
- Zhang, T., Zhang, X., Xia, D. and Liu, Y.: An analysis of land use change dynamics and its impacts on hydrological processes in the Jialing River Basin, *Water (Switzerland)*, 6(12), 3758–3782, doi:10.3390/w6123758, 2014.
- Zhao, F., Chiew, F. H. S., Zhang, L., Vaze, J., Perraud, J. M. and Li, M.: Application of a macroscale hydrologic model to estimate streamflow across Southeast Australia, *J. Hydrometeorol.*, 13(4), 1233–1250, doi:10.1175/JHM-D-11-0114.1, 2012.
- Zhao, R. J., Zhang, Y. L., Fang, L. R., Liu, X. R. and Zhang, Q. S.: The Xinanjiang model Hydrological Forecasting Proceedings Oxford Symposium, IASH, 1980.
- Zubieta, R., Getirana, A., Espinoza, J. C., Lavado-Casimiro, W. and Aragon, L.: Hydrological modeling of the Peruvian-Ecuadorian Amazon basin using GPM-IMERG satellite-based precipitation dataset, *Hydrol. Earth Syst. Sci. Discuss.*, 1–21, doi:10.5194/hess-2016-656, 2016.

Appendix A – Supporting information for chapter 6

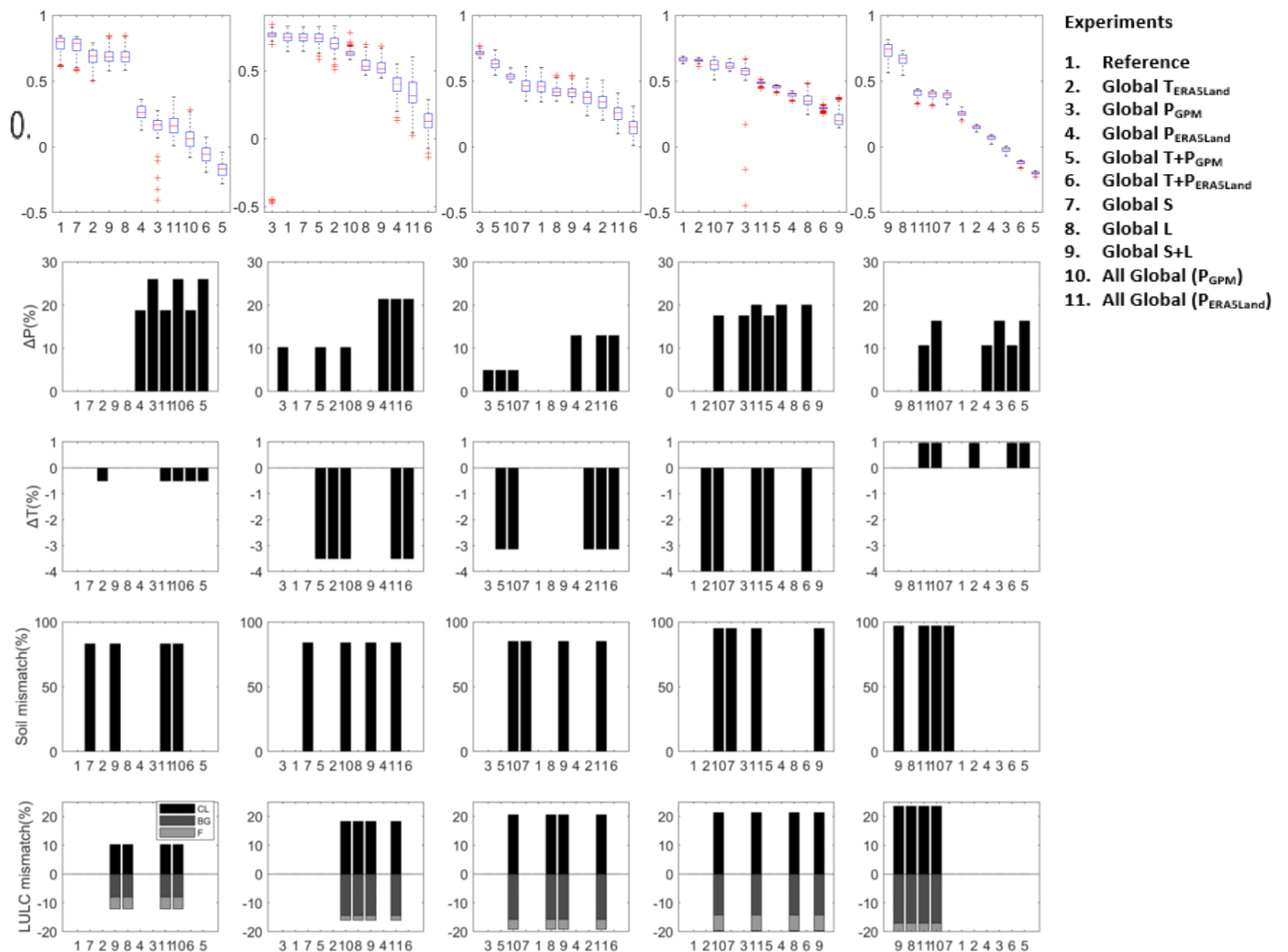
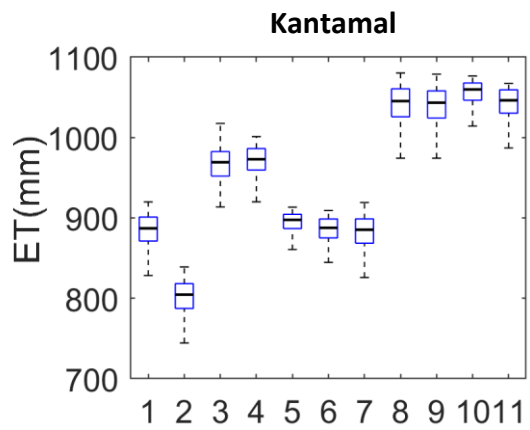
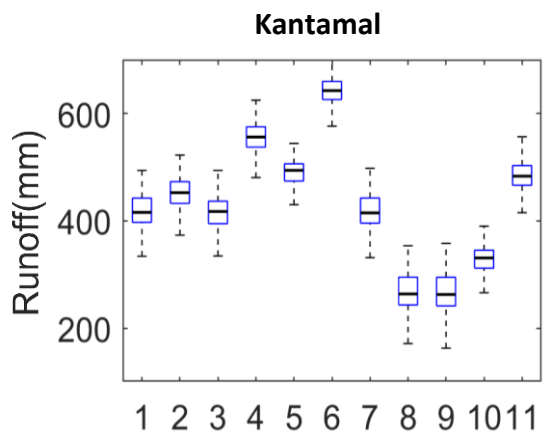


Figure A.1: (top) Values of KGE calculated for prediction of discharge of all experiments, ranked in order of their performance, at all subbasins. Boxplot of KGE values represents 250 behavioural models, meaning the uncertainties stemming from 250 model parameters sets (b) Bar charts representing the corresponding percent changes in datasets (precipitation, temperature, soil and land cover) obtained from global sources with respect to that of datasets from local source. In the legend, T, P, S and L are temperature, precipitation, soil and LULC respectively.



- Experiments**
1. Reference
 2. Global $T_{ERASLand}$
 3. Global P_{GPM}
 4. Global $P_{ERASLand}$
 5. Global $T+P_{GPM}$
 6. Global $T+P_{ERASLand}$
 7. Global S
 8. Global L
 9. Global S+L
 10. All Global (P_{GPM})
 11. All Global ($P_{ERASLand}$)

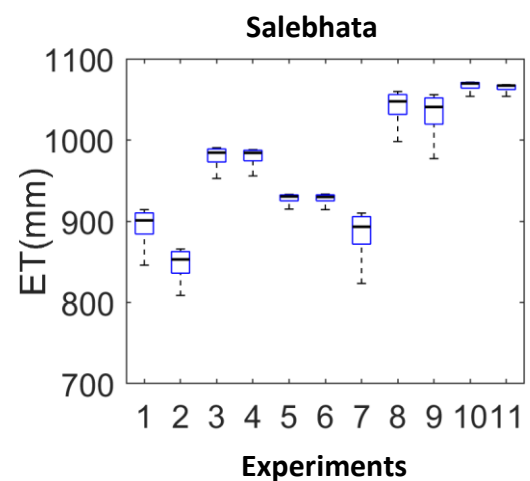
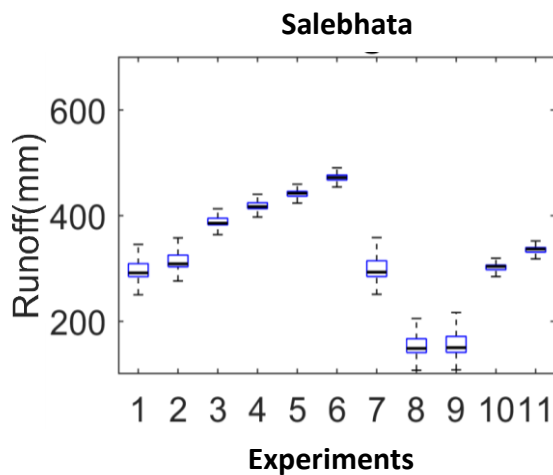
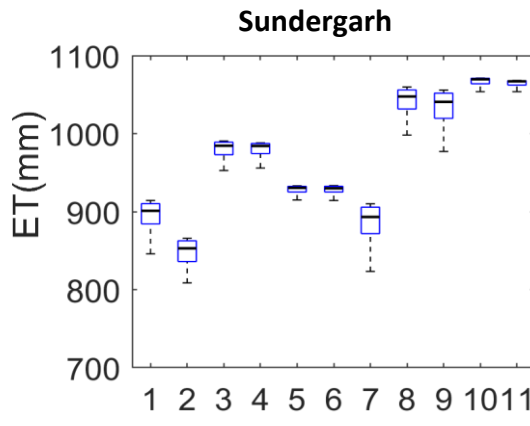
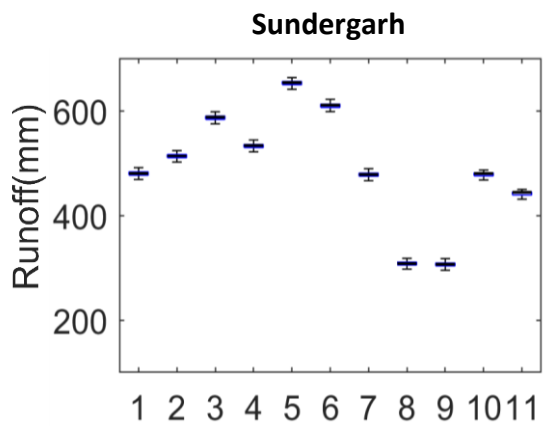
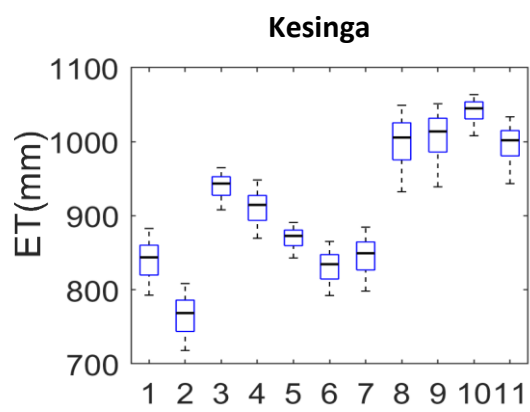
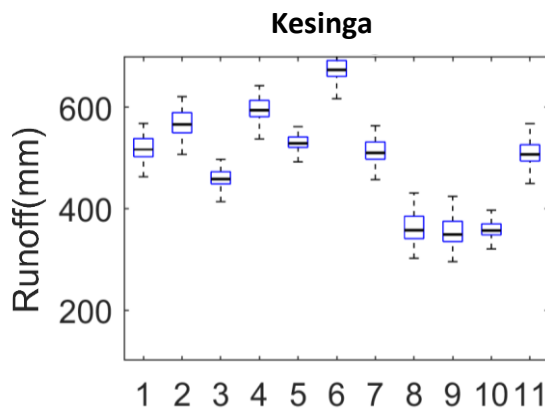
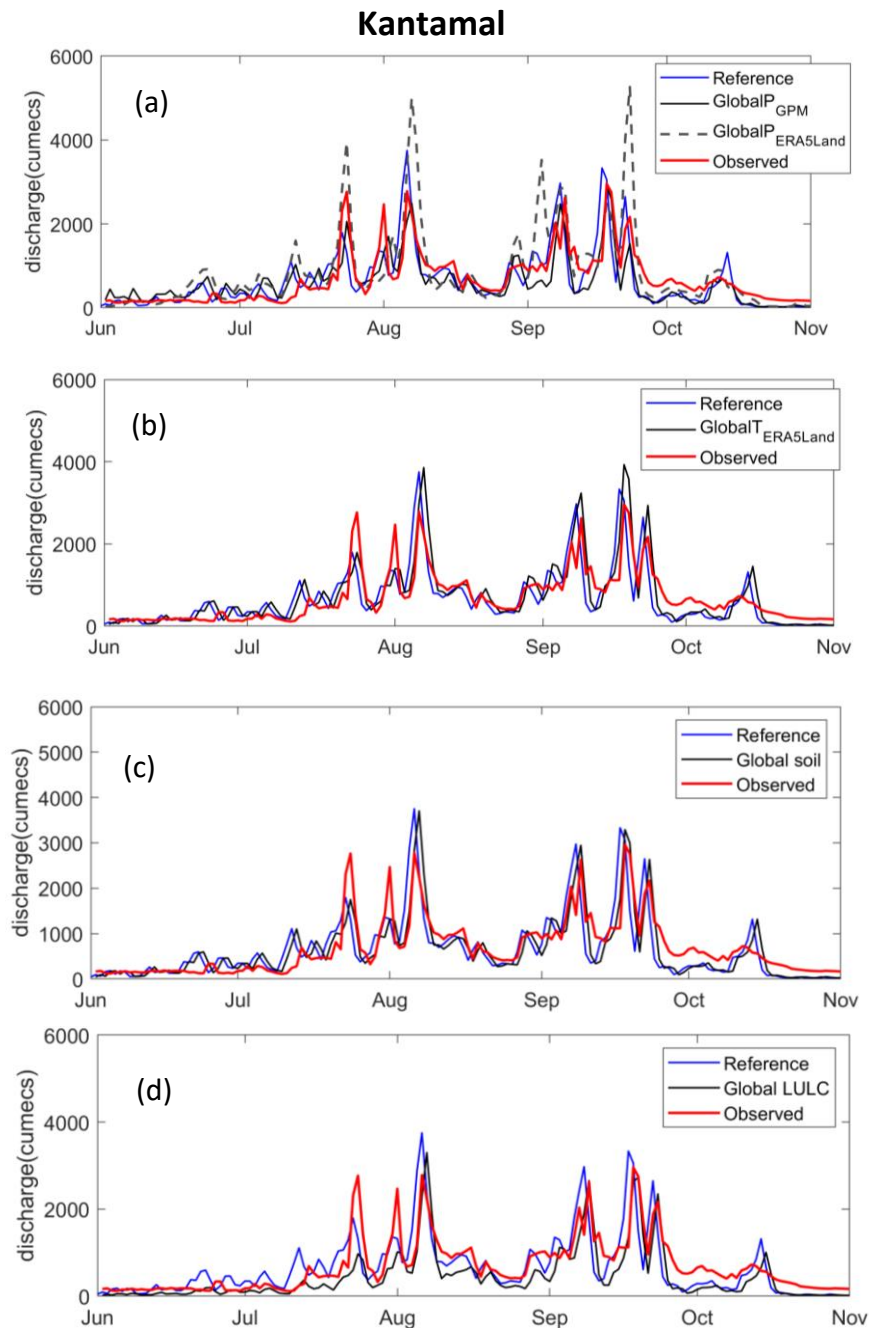
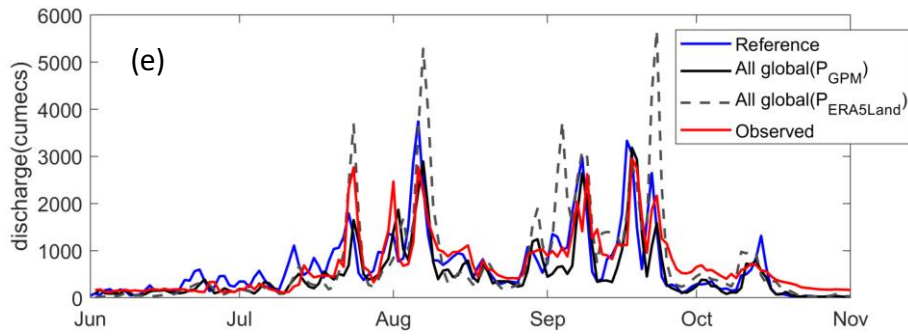
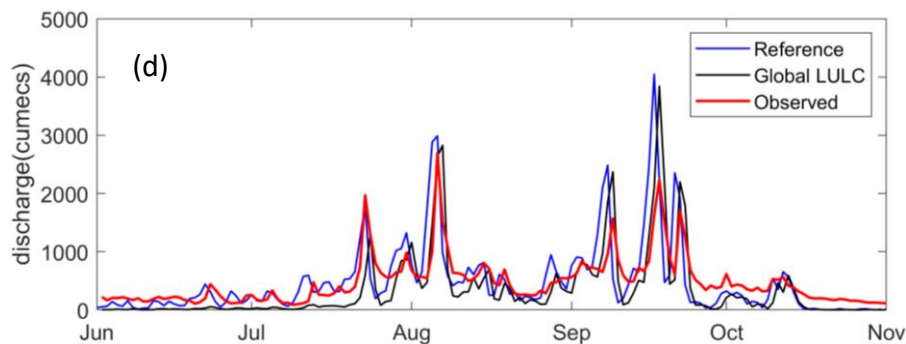
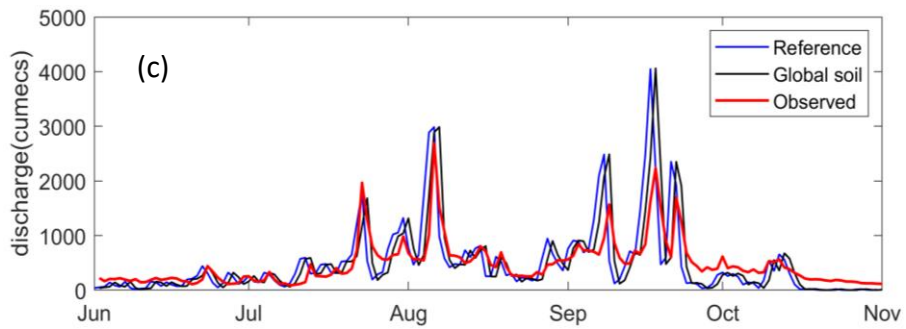
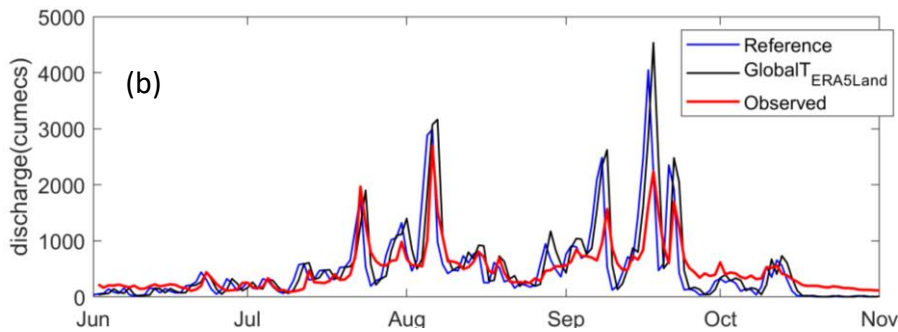
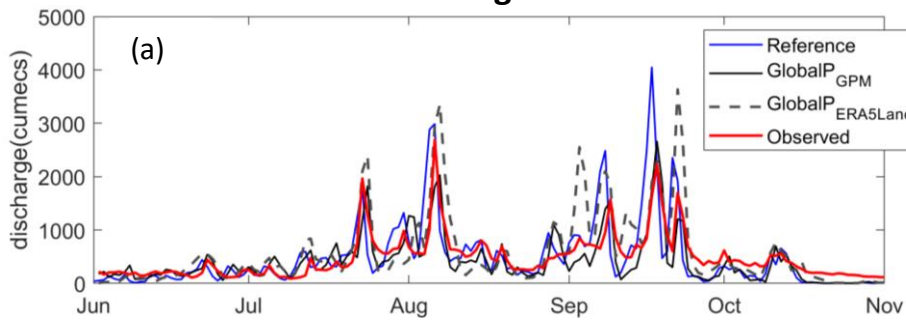


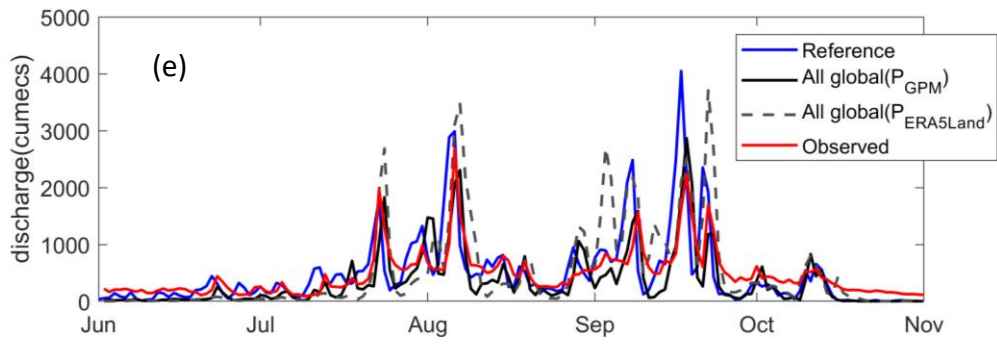
Figure A.2: Annual average of runoff and evapotranspiration at Kantamal, Kesinga, Sundergarh and Salebhata, for all experiments. In the legend, T, P, S and L are temperature, precipitation, soil and LULC respectively. Please note that the precipitation varies across experiments.



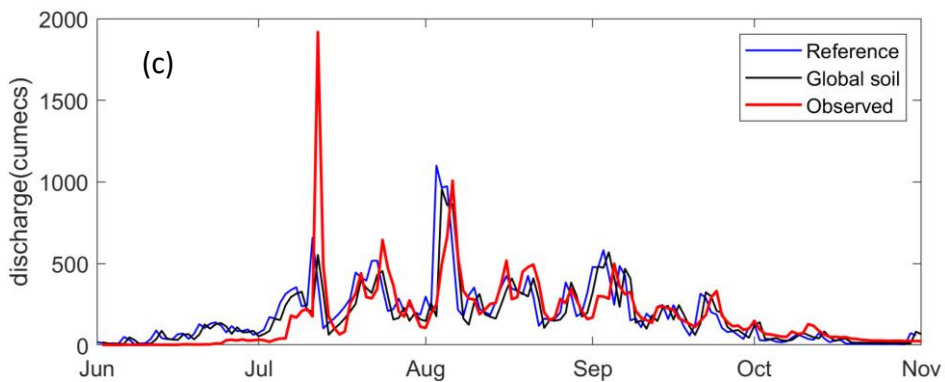
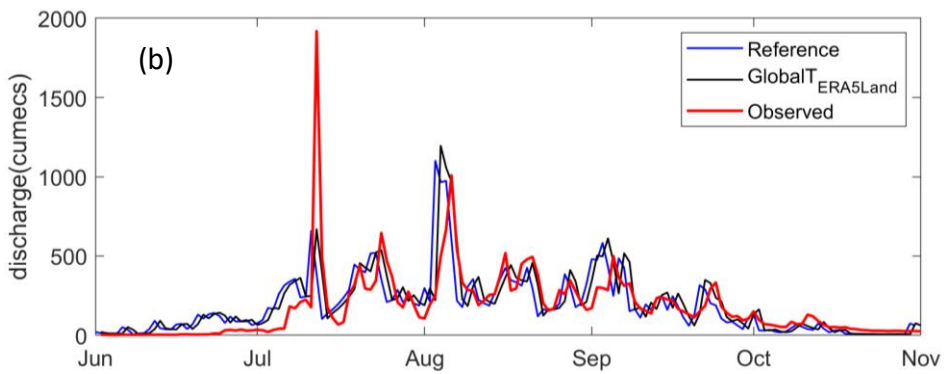
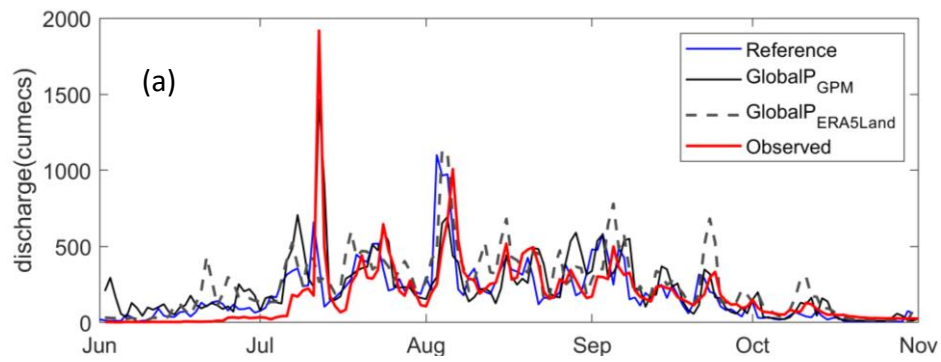


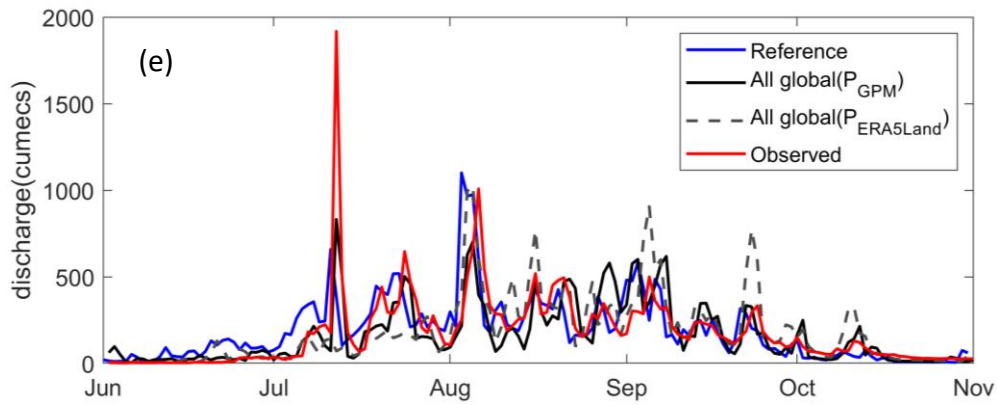
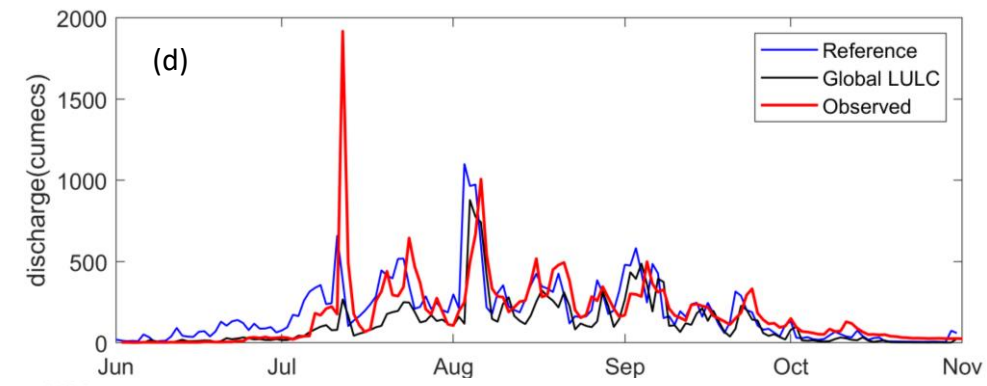
Kesinga



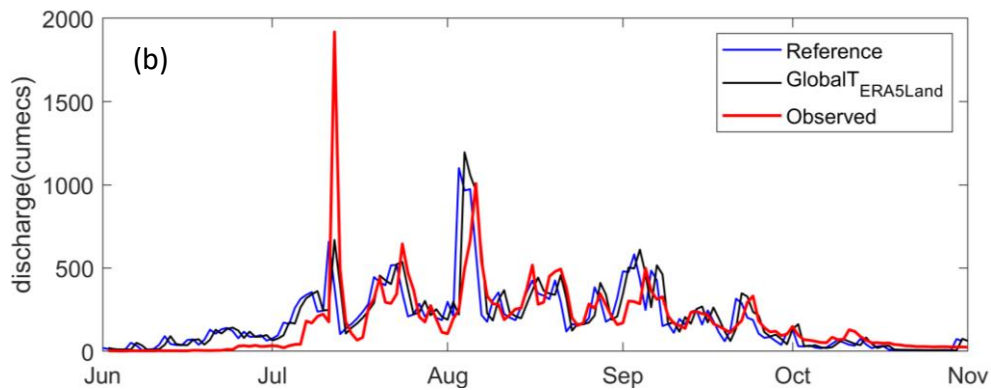
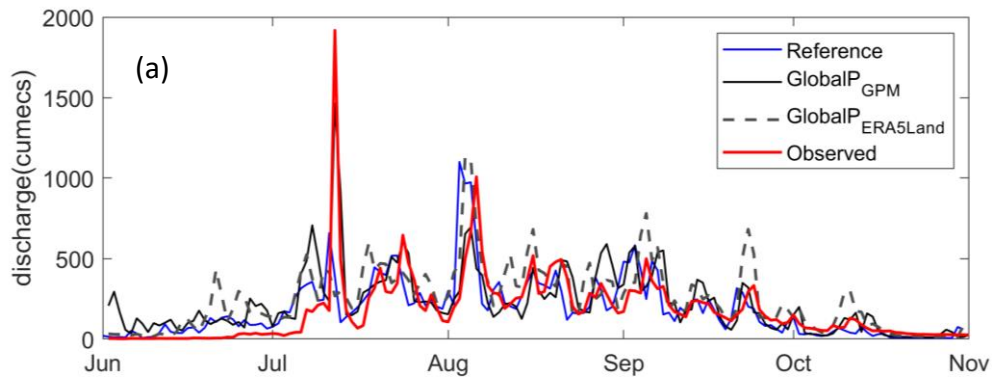


Sundergarh





Salebhata



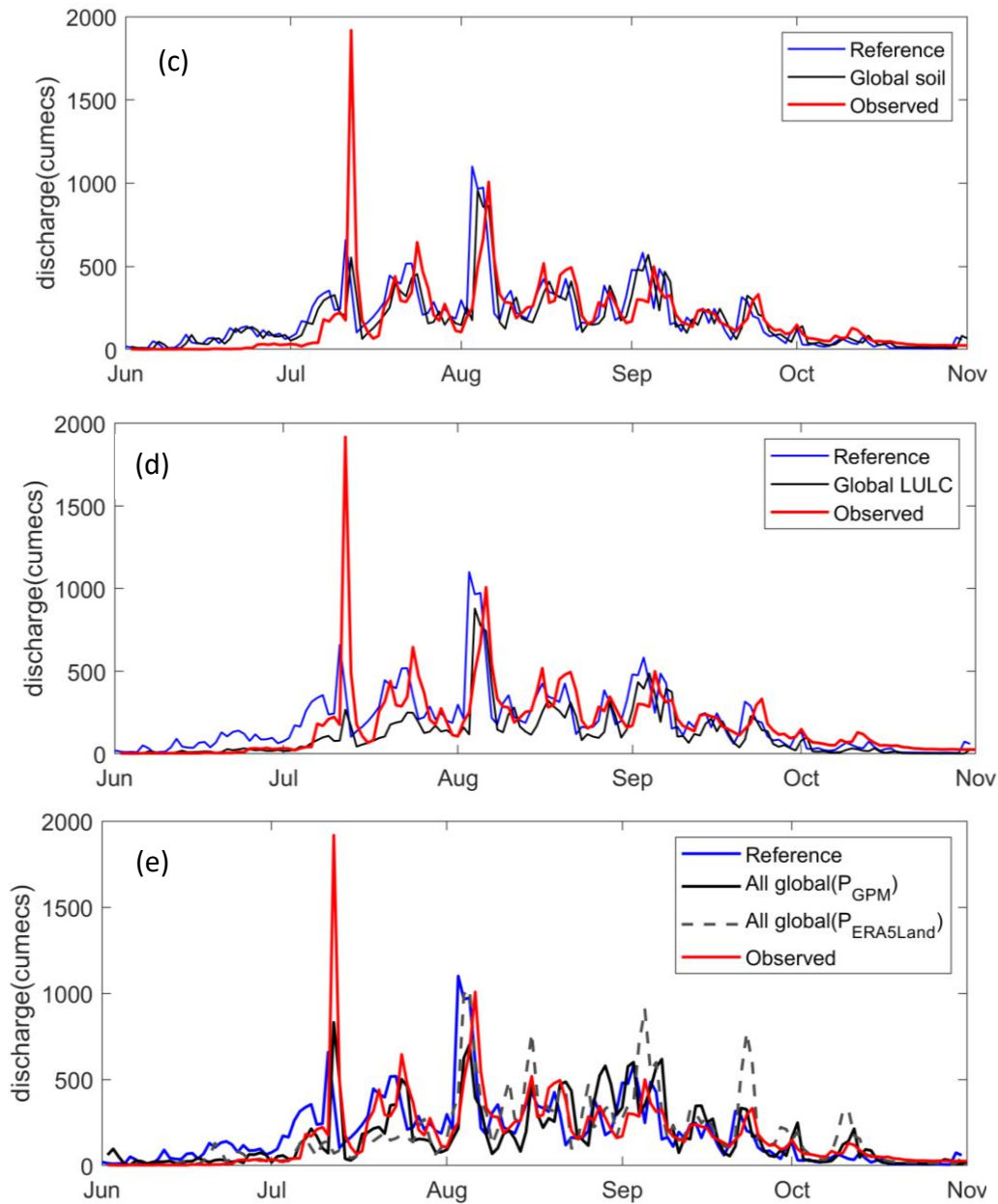


Figure A.3. Comparison of daily observed discharge and ensemble mean of simulated discharge of experiments at Kantamal, Kesinga, Sundergarh and Salebhata using (a) precipitation from GPM, ERA5-land and IMD (reference) (b) temperature from ERA5-Land and IMD (reference) (c) soil from SoilGrids and local soil (reference) (d) LULC from ESA CCI and local LULC (reference) (e) all global datasets and all local datasets (reference), averaged for the years (2014-2016). In order to show the details of the hydrographs, they are zoomed in to the monsoon (wet) months.

Appendix B – Supporting information for chapter 7

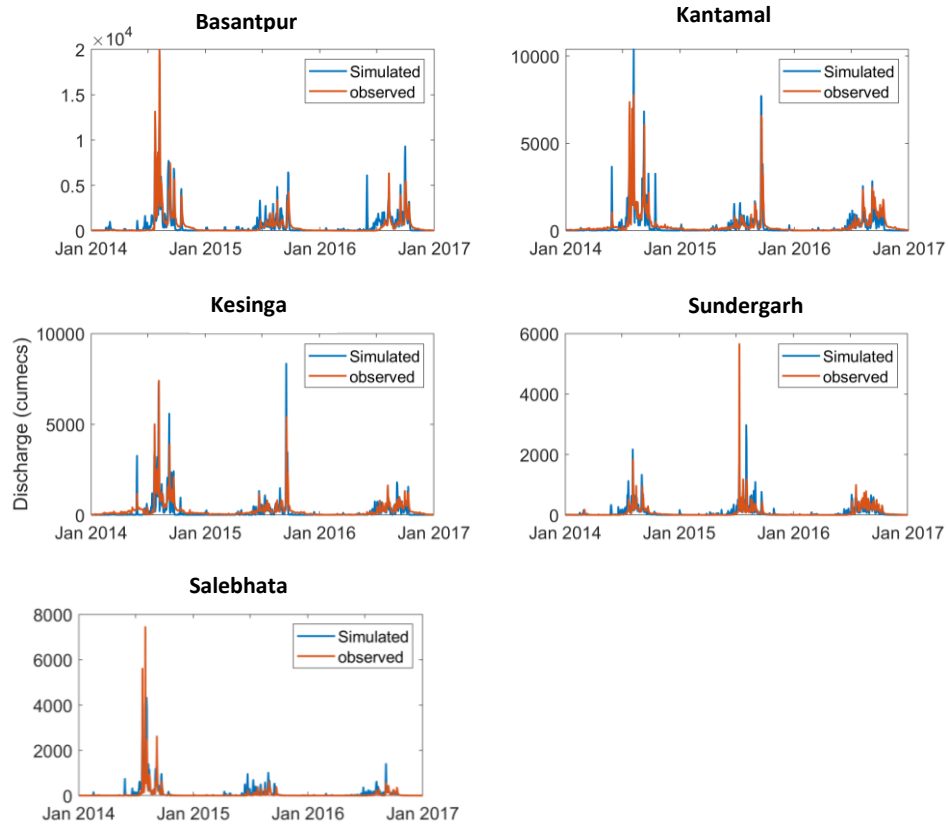


Figure B.1 Comparison of daily observed discharge and ensemble mean of simulated discharge at Basantpur, Kantamal, Kesinga, Sundergarh and Salebhata for the years 2014-2016.

Curriculum Vitae

SHAINI NAHA

Hodgkin house, 3-7 Meridian Place, Clifton, Bristol, BS81JG

██████████ | shaini.naha@bristol.ac.uk

www.linkedin.com/in/shaini-naha-691059116

Education

PhD Civil Engineering (Hydrology) Water and Environmental Research Group, Department of Civil Engineering, University of Bristol **2017- 2021**

Thesis “Modelling hydrological changes of a largescale river basin in India”.

Supervisor Dr Miguel Rico Ramirez and Dr Rafael Rosolem

Research highlights

- Setting up and implementation of a distributed hydrological model on a flood prone river basin in India
- Model Parameter Sensitivity Analysis, Calibration and Uncertainty assessment
- Investigating the impacts of Land Use and Land Cover changes (LULC) and climate changes on hydrology
- Evaluating model performance by replacing local data with global data as model inputs in a data scarce region

MTech, Remote Sensing & GIS (Application in Water Resources), Indian Institute of Remote Sensing, Indian Space Research Organisation **2014-2016**

Final year dissertation Data Assimilation and Ensemble prediction for Hydrological Modelling in snow-fed River Basin in India

Relevant courses Photogrammetry and Remote Sensing, Digital Image Processing, Geographical Information System, Remote Sensing Applications in water resource assessment, development, and management

- CGPA: 8.2 (Distinction)

BTech, Civil Engineering, West Bengal University of Technology (WBUT), India **2010-2014**

Final year dissertation Design of an industrial shed

Relevant courses Water Resources Engineering, Hydraulics, Environmental engineering

Industrial internship experience study of steel plant, study of structures of Unit Type Baily bridges, Railway wagons, Railway bridge plate girder, bunk houses, Pile and Shallow Foundation, Pile load test, mix design, Sieve Analysis (Certificates available)

- CGPA: 8.48 (Distinction)

Computing and Modelling skills

Environments

Linux, Windows, and MacOS

Programming Languages

Proficient in MATLAB, Working knowledge of R, Python and Fortran.

Software tools

ArcGIS (ArcMap 10.6), ERDAS IMAGINE, Envi, QGIS, Google Earth Engine

Hydrological and Land Surface Models

Proficient in Variable Infiltration Model (VIC), Soil and Water Assessment Tool (SWAT), Snowmelt Runoff Model (WinSRM), HEC-Ras, HEC HMS

Miscellaneous

Proficient in many Microsoft Office packages (Word, Excel, PowerPoint), Overleaf, Mendeley

Academic Activities

Training and Meetings

- 30-Sept 2020: **Historic Droughts: Using the past to inform the future**, Institution of Civil Engineers, London
- 24-June 2019: **Celebrating Hydrometry**, Institution of Civil Engineers, London
- 11 Oct 2017: **Introduction to Linux**, University of Bristol

Conferences

- **National Symposium on Geomatics for Digital India**, Jaipur, 2015

Talk Energy balanced based snowmelt runoff estimation and snow cover data assimilation of hydrological modelling of Beas river basin

- **XXIII International Society of Photogrammetry and Remote Sensing (ISPRS) Congress**, Prague-2016

Talk Hydrological modelling and data assimilation of satellite-based snow cover area using a variable infiltration capacity macro scale land surface model

- **European Geosciences Union (EGU)**, 2018, Vienna, Austria

Poster Talk Mahanadi river basin model calibration and parameter sensitivity analysis for flood forecasting (**Abstract and Poster published online**)

- **American Geosciences Union (AGU)**, 2019, San Francisco, California

Poster Talk Role of Land Use Land Cover changes on the hydrological regime of a flood prone river basin in India (**Abstract and Poster published online**)

- **American Geosciences Union (AGU)**, 2020, Online

Poster Talk Hydrological responses to various land use, soil, and meteorological inputs in a largescale river basin in India (**Abstract and Poster published online**)

Reviewer for Publications

Journal of Hydroinformatics

Publications

- Hydrological modelling and data assimilation of satellite-based snow cover area using a variable infiltration capacity macro scale land surface model

Naha, S., Thakur, P. K., & Aggarwal, S. P. (2016). Int. Arch. Photogramm. Remote Sens. Spatial Inf. Sci., XLI-B8, 353-360, doi: 10.5194/isprs-archives-XLI-B8-353-2016, 2016.

- Quantifying the impact of land cover changes on hydrological responses in Mahanadi river basin India (Accepted for publication)

Naha, S., Rico-Ramirez, M. A., & Rosolem, R. (2021). Quantifying the impact of land cover changes on hydrological responses in India. Hydrology and Earth System Sciences Discussions, 1-35.

- Assessing the impacts of local versus global datasets on hydrological responses

(Manuscript ready for submission to a journal)

Honours, Awards, and scholarship

- University of Bristol Deans scholarship for Postgraduate studies: 2017-2020 (PhD)
- University of Bristol alumni travel grant to AGU 2019, San Francisco
- The ISPRS Foundation and Congress Travel Grant to attend ISPRS conference, Prague, 2016

- Appointed as session chair for session ‘Water Resources 2’ in ISPRS congress, 2016, Prague, Czech Republic.
- Received honorarium for instructing a group of Water Resource engineers in Karnataka, India using GIS applications for efficient water resources planning and development.
- Ranked 1st in Bachelor’s 8th semester within the institute batch.

Work Experience

Research

Junior Research Fellow – National Institute of Hydrology (NIH), Ministry of Jal Shakti, Department of Water Resources, India **July 2016-Feb 2017**

Project: **Hydrological modelling of Alaknanda river basin (in India) and assessment of climate change** sponsored by the agency, National Mission for Sustaining the Himalayan Ecosystem (NMSHE), one of the eight missions under the National Action Plan on Climate Change (NAPCC).

Research Assistant – Interdisciplinary Centre for Water Research, (ICWAR), Indian Institute of Science, Bangalore, India **Feb 2017-Aug 2017**

Project: **Assessments of climate change impacts on precipitation and streamflow in Tungabhadra river basin**

Collaboration: Advanced centre for Integrated Water Resources Management (ACIWRM), Karnataka, India

Hydrological-Hydrochemical modeller – The James Hutton Institute, Aberdeen Oct,2021- Present

Teaching

Teaching Assistant – University of Bristol, UK **Jan-2018 - 2021**

Subjects assisted **Fluid mechanics, Hydraulics and Water resources, Terrestrial Hydrometeorology.**

Duties assisting in lectures, delivering lectures, lab demonstrations, conducting tutorials, providing both formative and summative assessments and feedback e.g., lab reports, problem sheets, class tests.

